Development of a human non-alcoholic fatty liver disease (NAFLD) model using organ-on-chip technology

Lisa Morisseau

Par **Lisa MORISSEAU**

Development of a human non-alcoholic fatty lliver disease (NAFLD) model using organ-on-chip technology

Thèse présentée
pour l'obtention du grade
de Docteur de l'UTC

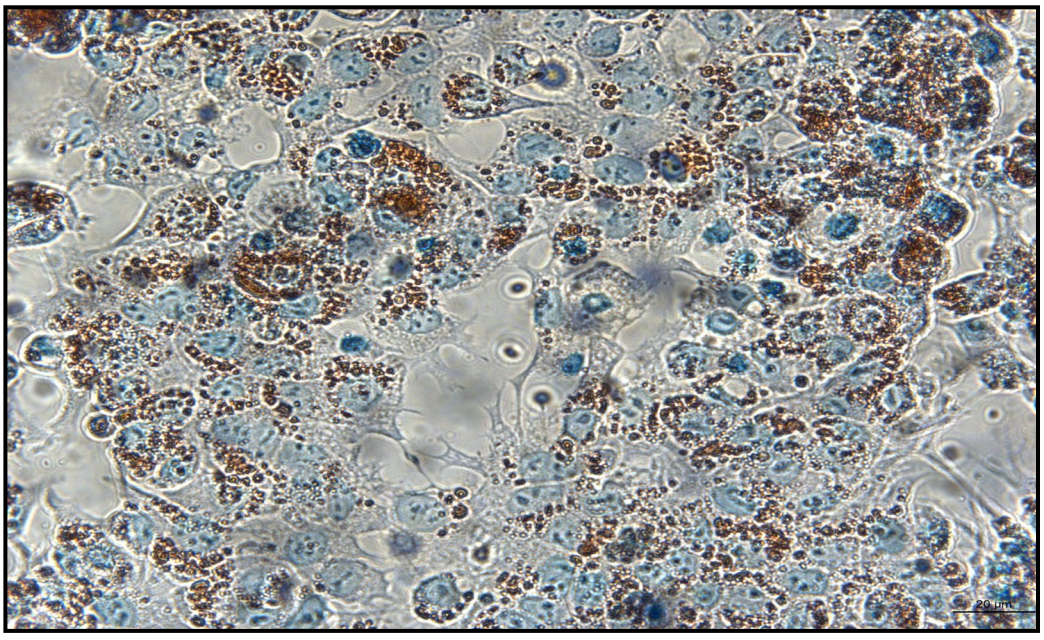

Soutenue le 18 décembre 2023
Spécialité : Bioingénierie : Unité de Recherche en Biomécanique et Bioingénierie (UMR-7338)
D2787

Thèse de doctorat de l'Université de Technologie de Compiègne

École doctorale : **n° 71 - Sciences pour l'ingénieur**
Unité de recherche : **BMBI CNRS UMR 7338**

Spécialité : Bioingénierie

Directeurs de thèse : Dr. Eric Leclerc et Pr. Yasuyuki Sakai

Development of a human non-alcoholic fatty liver disease (NAFLD) model using organ-on-chip technology

---

Soutenue le

18 décembre 2023

&

Présenté par

Lisa Morisseau

Membres du jury :

Muriel Vayssade	Professeur, UMR CNRS 7338	Président
Fabienne Foufelle Fabrice	Directeur de recherche, Inserm U1158	Rapporteur
Soncin	Directeur de recherche, INSERM/LIMMS/CNRS IRL2820	Rapporteur
Gloria Gallego-Ferrer	Professor, CBIT, Polytechnic University of Valencia	Examinateur
Petr Sláma	Professor, AgriSciences, Mendel University	Examinateur
Rachid Jellali	PhD, Ingénieur de Recherche, UMR CNRS 7338	Membre invité
Amar Abderrahmani	Professeur, UMR CNRS 8520	Membre invité

Acknowledgements

First of all, I would like to acknowledge the Ministry of Higher Education and Research providing financial support without which this research would not have been possible. I am grateful to the committee members for dedicating their time, expertise, and valuable insights to evaluate my doctoral thesis. Special thanks to Dr. Fabienne Foufelle and Dr. Frabrice Soncin for their thoughtful examination, and to Pr. Gloria Gallego-Ferrer and Pr. Petr Sláma for their expertise, advice, and jury participation.

I would like to deeply acknowledge my supervisors and advisors Dr. Eric Leclerc, Pr. Yasuyuki Sakai, Dr. Rachid Jellali and Pr. Cecile Legallais for their unwavering support, guidance, and mentorship throughout my doctoral journey. Your expertise and encouragement have been pivotal in shaping my academic and research capabilities. Special thanks to Dr. Rachid Jellali for his invaluable advice, patience and assistance at every stage of the research project. I express my gratitude to the Biomechanics and Bioengineering lab (BMBI) and Pr. Cecile Legallais for providing the resources, academic environment, and opportunities that enabled me to undertake this research and reach this significant milestone in my academic career. I would like to deeply thank all the members of the lab and particularly the CBB team for their sympathy, kindness and for all the good and bad times. Special thanks to Dr. Taha Messelmani whose role in my doctoral journey have been significant, and I am truly happy to have worked alongside him.

I would like to thank my family for their support even if they still don't know exactly what I am "searching" for. A special thought to my dad, who had to endure my absence for 2 years. A huge thank to my best friend Charis, for supporting me and visiting me since the start of my postgraduate studies. As well as Morel, for pushing me again and again since my high school graduation. Last but not least, I would like to thank from the bottom of my heart my loving Stephan for believing in me from the beginning and for his unwavering support during this journey. Thank you all for being a part of this important chapter in my personal and professional life. It was tough but guess what? We did it!

Abstract

Non-Alcoholic Fatty Liver Disease (NAFLD) is a growing global health concern, closely linked to the rise in obesity and metabolic syndrome. It encompasses a range of liver conditions, from simple fat accumulation (steatosis) to more severe forms like non-alcoholic steatohepatitis (NASH) and fibrosis, leading to cirrhosis and hepatocellular carcinoma. Despite its widespread impact and potential for severe health consequences, effective treatments for NAFLD remain elusive due to its complex and multifaceted dynamics. Indeed, the multifactorial nature of NAFLD involves several interactions among genetics, diet, lifestyle, and metabolic processes, making it difficult to solve. This challenge is exacerbated by the limitations of traditional research models, both *in vitro* and *in vivo*. These models often fall short when it comes to capturing the intricate dynamics of this disease with other health condition such as diabetes, hindering our ability to decipher its underlying mechanisms and develop targeted therapies. In this context, emerging technologies like organ-on-chip models offer new hope. By replicating the features of the microenvironment of the liver, these platforms can provide deeper insights into NAFLD pathogenesis and facilitating drug development. Therefore, this thesis tackles the need for a more physiologically relevant NAFLD model by harnessing the potential of organ-on-chip technology. The objective is to create a human NAFLD model that faithfully replicates the liver's microenvironment, including cellular interactions, fluid dynamics, and metabolic processes. First, experiments with HepG2/C3A cells were conducted to determine the most effective treatment for inducing liver steatosis, by analyzing mRNA levels and the expression of hepatic markers. Subsequently, we studied metabolomic profiles of the different conditions and correlated them with specific metabolic pathways. We also expanded the liver-on-chip model by incorporating hepatocyte-like cells (HLC) derived from hiPSCs, demonstrating the feasibility of HLCs for investigating steatosis and lipid accumulation.

Keywords: NAFLD, steatosis, organ-on-chip, liver-on-chip, fatty acids, metabolomics

Résumé

La stéatose hépatique non alcoolique (NAFLD) est une maladie chronique étroitement liée à l'augmentation de l'obésité et du syndrome métabolique. Elle englobe toute une gamme de troubles du foie, allant de l'accumulation simple de graisse (stéatose) à des formes plus graves telles que la stéato-hépatite non alcoolique (NASH) et la fibrose, qui conduisent à la cirrhose et au carcinome hépatocellulaire. Malgré son impact généralisé sur la santé, il n'existe pour l'instant aucun traitement médicamenteux approuvé de la NAFLD en raison de la dynamique complexe et multifactorielle de la pathologie ainsi que les limites des modèles de recherche *in vitro* et *in vivo* traditionnels. Dans ce contexte, les technologies émergentes tels que les modèles d'organes-sur-puce offrent un nouvel espoir. En reproduisant les caractéristiques du microenvironnement du foie, ces plateformes peuvent fournir des informations plus approfondies sur la pathogenèse de la NAFLD et faciliter le développement traitement médicamenteux. Par conséquent, cette thèse répond au besoin d'un modèle de NAFLD physiologiquement pertinent en exploitant le potentiel de la technologie des organes-sur-puce. L'objectif est de créer un modèle de NAFLD humain qui reproduit fidèlement le microenvironnement du foie, y compris les interactions cellulaires, la dynamique des fluides et les processus métaboliques. Tout d'abord, des expériences avec les cellules HepG2/C3A ont été menées pour déterminer le traitement le plus efficace pour induire la stéatose hépatique, en analysant les niveaux d'ARNm et l'expression des marqueurs hépatiques. Ensuite, nous avons étudié les profils métabolomiques des différentes conditions et les avons corrélés à des voies métaboliques spécifiques. Nous avons également amélioré le modèle de foie-sur-puce en incorporant des cellules hépatiques dérivées de cellules souches pluripotentes induites (hiPSC), démontrant la faisabilité de ces cellules pour l'étude de la stéatose non alcoolique.

Mots clés : NAFLD, stéatose, organe-sur-puce, foie-sur-puce, acide gras, métabolomique

Table of contents

List of figures

List of tables

Abbreviations

ALB: Albumin

ANOVA: Analysis of Variance

ATCC: American Type Culture Collection

BSA: Bovine Serum Albumin

CDH1/ E-cadherin: Cadherin-1/Epithelial Cadherin

CTRL: Control

Cyp3A4: Cytochrome P3A4

DNL: *De novo* Lipogenesis

ECM: Extracellular matrix

ELISA: Enzyme-Linked Immunosorbent Assay

ER: Endoplasmic reticulum

FA/ FFA: Fatty acid/Free Fatty Acid

FDR: False Discovery Rate

FASN: Fatty Acid Synthase

GC-MS: Gas Chromatography – Mass Spectrometry

GCG: Glucagon

GCK: Glucokinase

GLP1: Glucagon-like peptide-1

GLP1R: Glucagon-like peptide-1 Receptor

GLUT2: Glucose Transporter 2

HEPES: hydroxyethyl-piperazineethane-sulfonic acid

HCC: Hepatocellular Carcinoma

hiPSCs/ IPSCs: human induced Pluripotent Stem Cells

HLC: Hepatocyte-like Cells

IDCCM: Integrated Dynamic Cell Culture in Microsystems

INS: Insulin

INSR: Insulin Receptor

INSRA: Insulin Receptor A gene

INSRB: Insulin Receptor B gene

IR: Insulin Resistance

MEM: Minimum Essential Medium

MetS: Metabolic Syndrome

MOoC: Multi-organ-on-chip

mRNA: messenger Ribonucleic Acid

NAFL: Non-alcoholic Fatty Liver (steatosis)

NAFLD: Non-alcoholic Fatty Liver Disease

NASH: Non-alcoholic Steatohepatitis

NPCs: Non-Parenchymal cells

OA: Oleic acid

OA/PA: Oleic acid/palmitic acid mix

OoC: Organ-on-chip

PA: Palmitic acid

PDMS: Polydimethylsiloxane

PHH: Primary Human Hepatocytes

PLS-DA: Partial Least-Squares Discriminant Analysis

ROS: Reactive Oxygen Species

RPMI-1640: Roswell Park Memorial Institute 1640

RT-qPCR : Reverse Transcription-quantitative Polymerase Chain Reaction

SD: Standard Deviation

SREBP-1: Sterol Regulatory Element Binding Protein 1

T2DM: Type 2 Diabete Mellitus

TAG: Triacylglycerol

WAT: White adipose tissue

General introduction

Non-Alcoholic Fatty Liver Disease (NAFLD) has emerged as a global health epidemic, closely paralleling the increasing prevalence of obesity and metabolic syndrome. As a spectrum of liver disorders ranging from simple steatosis to non-alcoholic steatohepatitis (NASH) and fibrosis, NAFLD poses significant health risks, including the progression to cirrhosis and hepatocellular carcinoma. Nowadays, NAFLD is the most common cause of chronic liver disease worldwide and also the most rapidly growing cause of HCC patient listed for liver transplantation. Recently, an international expert panel recommended renaming non-alcoholic fatty liver disease (NAFLD) to metabolic-dysfunction associated steatotic liver disease (MASLD) to accurately reflect the pathogenesis of the disease and its strong association with cardiometabolic risk factors. Although traditional *in vitro* and 2D *in vivo* models have provided valuable insights into NAFLD pathophysiology, they often fall short in capturing the dynamic and multicellular/multiorgan nature of the disease, making it challenging to unravel the underlying mechanisms, reliable biomarkers and develop targeted therapies.

This thesis embarks on a journey to address the pressing need for a more physiologically relevant model of NAFLD. Leveraging the power of organ-on-chip technology, we aim to develop a human NAFLD model that faithfully mimics the liver's microenvironment. By recapitulating the intricate cellular interactions, fluid flow dynamics, and metabolic processes within the liver, this model offers new insights into the pathogenesis of NAFLD and provides the basis for drug screening platform. In the following chapters, we will delve into the development of our HepG2/C3A-based NAFL-on-a-chip model, exploring its potential applications, advantages, and limitations. We will present data on its ability to recapitulate key features of NAFLD such as hepatic lipid accumulation, while investigating specific biomarkers and metabolic pathway of the disease. Then, as a perspective, we will propose an advanced model of our NAFL-on-chip by using human induced pluripotent stem cell as hepatocytes source and consider a co-culture with pancreatic cells (beta cells).

The first chapter of the manuscript will be dedicated to the state-of-the-art of NAFLD and liver-on-chip technology. We will contextualize the project by describing the liver

physiology, the known pathophysiology of NAFLD and its intricate link with type 2 diabetes mellitus. We will expose the current *in vitro* models used to mimic and study the disease, including the liver-on-chip technology, their advantages and limitations. Furthermore, a section of this chapter will highlight the use of metabolomic analysis for NAFD detection and monitoring.

The second chapter will present the entire materials and methods used for this project. We will describe the HepG2/C3A cell culture process in the microfluidic biochip and the fatty acids exposure. We will also display the differentiation protocol of human induced pluripotent stem cells into hepatocyte-like cells and beta-like cells. The different methods of analysis performed will be described (ELISA, staining, gas chromatography and mass spectrometry, etc.).

In the third chapter, we will explore the potential of the HepG2/C3A-based liver-on-chip to recapitulate the features of NAFLD. For this purpose, we will analyse the physiologically and functionality relevance of the model when exposed to different free fatty acids (oleic acid, palmitic acid and their mixture).

The exploration of the metabolome of our model using gas chromatography and mass spectrometry, will be described in the fourth chapter. We will attempt to identify specific biomarkers and determine the metabolic dysregulations associated with the disease through metabolomic profiling.

Finally, the fifth chapter will describe the perspective of the project. We will expose the first steps of the development of a liver-pancreas-on-chip model exposed to pro-NAFLD fatty acid. We will attempt to develop an advanced model of NAFL-on-chip by using hepatocytes derived from human induced pluripotent stem cell. In the other hand, we will explore the differentiation of induced pluripotent into pancreatic β-cells by using a combination between static and dynamic cell culture. We will investigate cell maturity and functionality for cell types.

Ultimately, this research aims to contribute to a deeper understanding of NAFLD and provide a transformative tool for accelerating therapeutic discoveries in the battle against this burgeoning global health crisis.

Chapter I:

State-of-the-art

This chapter provides an overview of the state-of-the-art of liver-on-chip technology and its use as model to mimic metabolic disease. First, the liver and pancreas anatomy and their physiology are introduced. Then, the physiopathology of the Metabolic Syndrome, including symptoms and treatment, and is correlation with Non-alcoholic fatty liver disease (NAFLD) and Type 2 diabetes mellitus (T2DM) is highlighted. Finally, liver-on-chip technology for NAFLD modelling is reviewed by outlining the different materials, cells sources and approaches currently in use.

1.1 Mechanism of glycaemic regulation

1.1.1 Liver anatomy and physiology

The liver is the largest organ in humans and accounts approximately 2% to 5% of the total body mass. It is located in the upper right part of the abdomen and is partly protected by the rib cage. It is surrounded by a connective envelope, called Glisson capsule, whose invaginations allow the delimitation of two main lobes, the right and left lobes, as well as two annexed lobes, the caudate lobe and the quadrate lobe. The liver is vascularised by two major blood vessels, the portal vein which contributes 25% to 30% of the blood supply and the hepatic artery which is responsible for the remaining 70% to 75%[1] . The hepatic artery brings oxygen-rich blood to the liver, while the portal vein drains blood that is poor in oxygen but rich in various substances (nutrients and xenobiotics) from the digestive tract. These two afferent vessels divide and subdivide to supply the different parts of the liver, making it a highly vascularised organ. Once filtered, the blood returns to the heart via the hepatic veins, which drain into the inferior vena cava. The liver is also crossed by numerous bile ducts which collect the secreted bile and lead it into the hepatic duct to drain out of the organ[2] (Figure 1.1).

The liver is composed of structural units called hepatic lobules. These are polyhedral in shape, organised around the central vein and surrounded by portal triads comprising a branch of the hepatic artery, a branch of the portal vein and the bile ducts. Thus, the blood flow is from the periphery to the centre of the liver lobules. The parenchymal cells, mainly hepatocytes, represent 60% of the cell population of the liver and are organised in trabeculae separated by the hepatic sinusoids (blood capillaries of the liver). Hepatocytes are responsible for the specific metabolic functions of synthesis, catabolism and storage of many compounds and nutrients. Indeed, they are responsible for the metabolism of plasma proteins (albumin and coagulation factors), carbohydrates (glucose and glycogen) and lipids (cholesterol). Another of its main functions is the detoxification of the blood of all toxic molecules (xenobiotics and harmful endogenous metabolites) before it passages into the general circulation. The non-parenchymal cells (NPC) compose the remaining 40% of the cell population and play a significant role in tissue architecture and in mediating responses of the tissue to metabolic and toxic stimuli, as well as supporting the hepatocyte function. These cells

types include liver sinusoidal endothelial cells (LSECs), Kupffer cells (KCs), hepatic stellate cells (HSCs), and pit cells (natural killer cells, NKs). Furthermore, this structural organisation of the liver generates gradients of oxygen, nutrients and xenobiotics within the hepatic lobule: it is the phenomenon of zonation. Consequently, hepatic lobules present three zones with distinct metabolic functions: the periportal region, the mid-lobular region and the perivenous (pericentral) region (Figure 1.2).

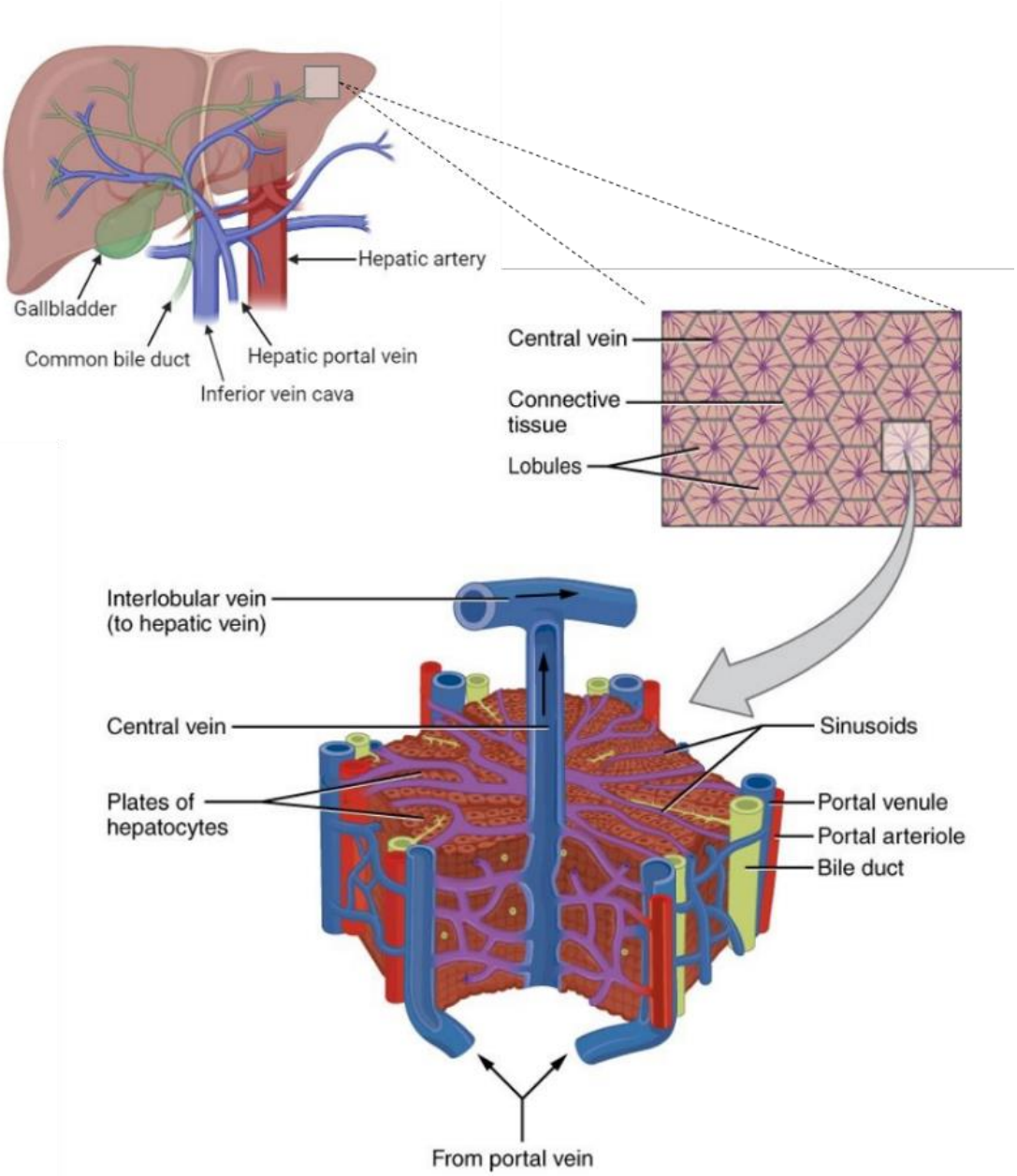

Figure 1. 1: *Overview of the liver structure and functional subunits (adapted from the book Anatomy and Physiology by Lindsay M. Biga et al.,2019 and created in BioRender.com).*

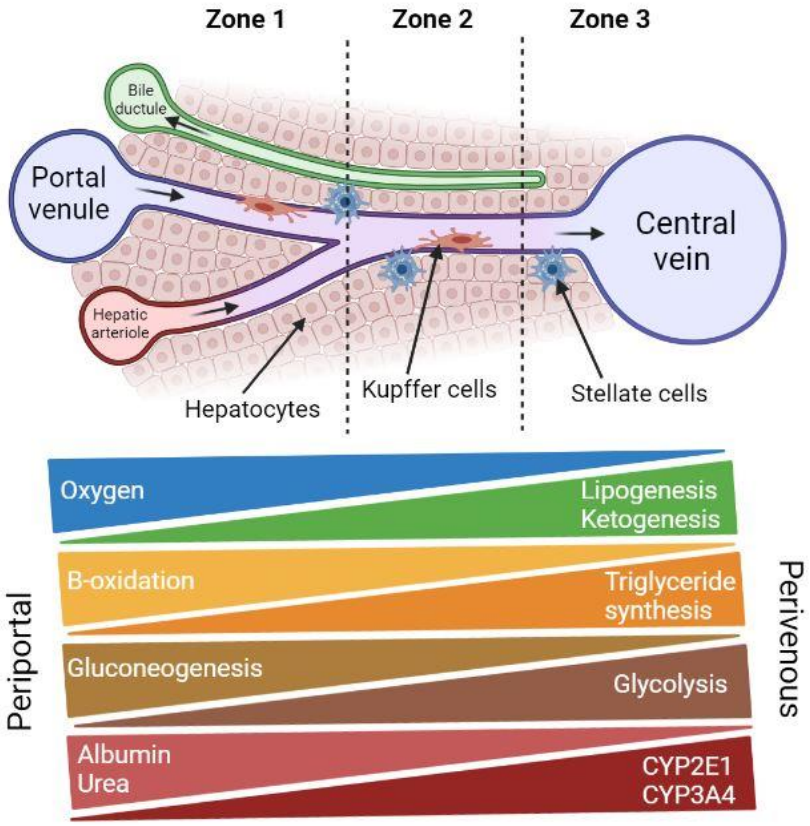

Figure 1. 2: *Metabolic zonation along the portal-perivenous axis of the hepatic lobule (created in Biorender.com).*

1.1.2 Regulation of blood glucose level

Liver and pancreas play an essential role for the blood glucose levels homeostasis maintenance (Table 1.1). Insulin is a polypeptide hormone mainly secreted by β-cells in the islets of Langerhans of the pancreas, which regulates glucose level in the bloodstream and induces glucose storage in the liver, muscles and adipose tissue. Biosynthesis and secretion of insulin are controlled by circulating glucose levels. In postprandial period, there is an increase in insulin/glucagon ratio to bring glucose serum levels back to normal (0.7 - 1g/L)[3].

Glucose enters β-cells through the glucose transporter GLUT2. Following glucose uptake, the rate-limiting glucokinase enzyme (GCK) generates glucose-6-phosphate, which is metabolized during glycolysis to generate pyruvate, NADH and ATP. In the mitochondria, pyruvate and NADH fuel the production of cytosolic ATP via the tricarboxylic acid (TCA) cycle and oxidative phosphorylation[4]. Previous work demonstrates that in the β-cells, this increase in ATP/ADP ratio causes closure of K-ATP channels and depolarization of the cellular

membrane, opening voltage-gated calcium channels to increase intracellular $Ca^{2+,}$ promoting fusion of insulin granules with the plasma membrane for hormone release into the circulation[5]. It has been reported, that insulin secretion is carried out in a pulsatile manner with a first phase corresponding to a rapid increase in the rate of secretion, followed by a decrease of the insulin rate and, a second stable or gradually increasing phase which lasts as long as the glucose simulation is applied[6]. After secretion and circulation through the body, insulin binds to insulin receptors (IR) on target cell membranes (liver, skeletal muscles and adipose tissue) inducing the phosphorylation of insulin receptor substrate (IRS) on tyrosine residues. This results in the activation of phosphoinositide 3-kinase (PI3K)/protein kinase B (Akt) pathway and the mitogen-activated protein kinase (MAPK) pathway which are essential for cell functions and energy metabolism regulation (Figure 1.3). In the liver, insulin stimulates glycogenesis and glycolysis resulting in increased glucose uptake and *de novo* lipogenesis (DNL) and suppressing glycogenolysis and gluconeogenesis.

On the other hand, during fasting, glucagon activates the production of glucose by releasing stored hepatic glycogen (glycogenolysis) and transforming non-carbohydrate substrates via the gluconeogenic pathway. Major non-carbohydrate precursors for gluconeogenesis are lactate, which is transported from peripheral tissues such as skeletal muscles or red blood cells, and glycerol, which is released from the adipose tissues via enhanced lipolysis during fasting[7].

Table 1. 1: *Biochemical effects of insulin and glucagon (adapted from Kalra and Gupta, 2016).*

Process	***Insulin***	***Glucagon***	***Organs***
Glycogenesis	Increased	Inhibited	Liver and muscles
Glycogenolysis	Inhibited	Increased	Liver and muscles
Glycolysis	Increased		All tissue
Gluconeogenesis	Inhibited	Increased	Liver
Ketogenesis	Inhibited		Liver
Lipogenesis	Increased	Decreased	Liver and adipose tissue
Lipolysis	Inhibited		Adipose tissue

Protein synthesis	Decreased protein degradation	Increased amino acid uptake	Liver and muscles

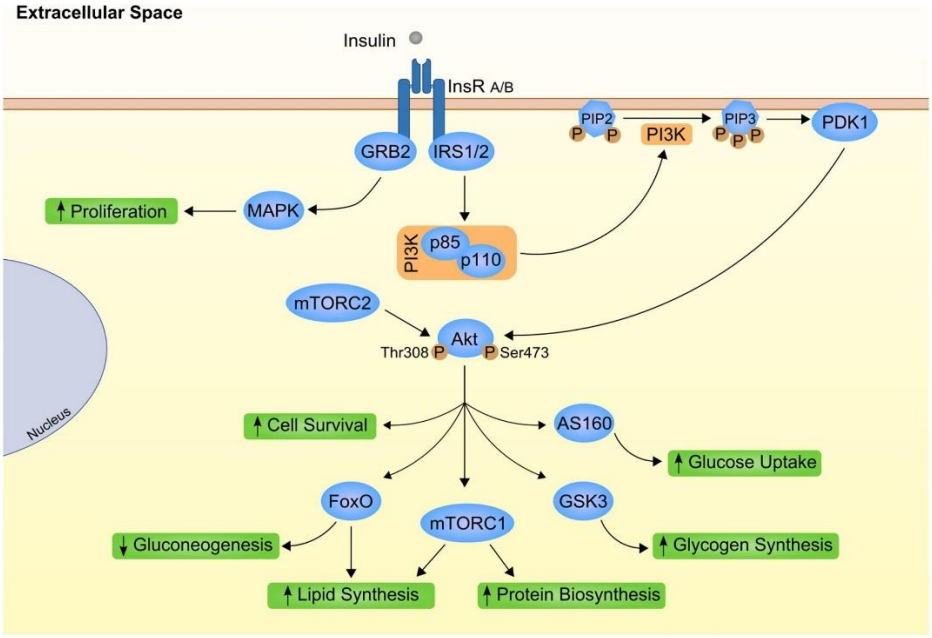

Figure 1. 3: *Insulin signaling cascade (Pina et al., 2020).*

1.1.3 Lipid metabolism pathway in the liver

Lipids are a group of hydrophobic or amphiphilic molecules which essentially have an energetic, structural or informational role in the organism. The liver plays a central role in lipid metabolism. It is involved in *de novo* lipogenesis (DNL), cholesterol synthesis, triacylglycerol (TAG) and cholesterol packaging for transport in the body, fatty acids (FA) and cholesterol uptake, and FA oxidation[8].

1.1.3.1 *De novo* lipogenesis

De novo lipogenesis (DNL) is the synthesis of FA from two-carbon precursors derived from glucose, fructose, and amino acids[8]. It occurs in the cytosol and it is affected by the amount of fats and carbohydrates in the diet and increased by high- carbohydrate diet, particularly the type that is high in simple sugars. DNL is mainly dependent on insulin and the concentration of carbohydrate metabolites. Sterol regulatory element-binding proteins (SREBPs) are a family of transcription factors involved in DNL but also the biogenesis of cholesterol and triglycerides. The SREBP family is composed of three members, two of which

are mainly expressed in the liver. SREBF-1 gene encodes for SREBP-1c which is expressed in the liver, white adipose tissue and skeletal muscle whereas SREBP-1a which is expressed in liver cell lines, spleen and intestinal tissue. Insulin stimulates the expression and transcriptional activity of SREBP-1c while SREBP-1a is not controlled by insulin signalling. Another transcription factor, carbohydrate-responsive element-binding protein (ChREBP), is involved in the regulation of the DNL pathway. Unlike SREBP-1c, ChREBP expression and action is stimulated by glucose-6-phosphate[9] (Figure 1.4). These transcription factors increase the expression of genes whose protein products are involved in the FA synthesis pathway, including acetyl-CoA carboxylase (ACC), fatty acid synthase (FAS), stearoyl-CoA desaturase 1 (SCD1) and mitochondrial glycerol 3-phosphate acyltransferase (GPAT)[10].Therefore, overexpression of SREBP1 and ChREBP significantly increases the expression of genes involved in cholesterol synthesis and FAS, and causes a corresponding accumulation of both cholesterol and TAG[11].

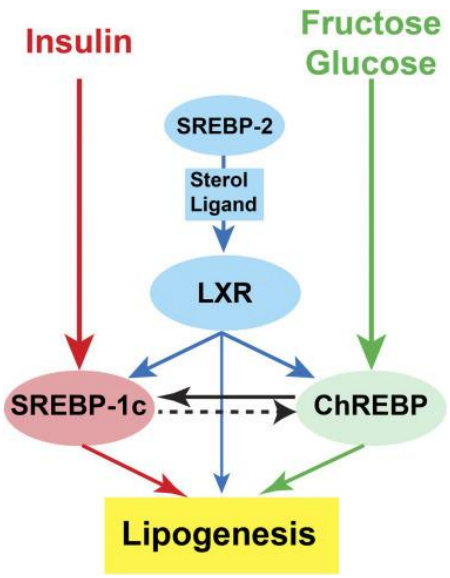

Figure 1. 4: *Simplified schema of the regulation of hepatic DNL (reproduced from G. Linden et al., 2018).*

1.1.3.2 Fatty acid oxidation and ketogenesis

The fatty acid oxidation pathway can occur in the mitochondria (β-oxidation), peroxisome (β-oxidation) or by cytochrome 450 CYP4A (ω-oxidation) and consists of a spiral of reactions, with the substrate reducing in size until the final set of reactions liberates two acetyl-CoA molecules[12]. During fasting, TAG stored in white adipose tissue (WAT) is hydrolysed

by a cascade of lipases (adipose triglyceride lipase, hormone-sensitive lipase, monoacylglycerol lipase) to produce free fatty acids (FFA) and glycerol: this process is called lipolysis. The FFA released from lipolysis is transported to the liver by serum albumin and enters hepatocytes by both diffusion and fatty acid transporters such as fatty acid transport protein (FATP), fatty acid translocase (FAT)/CD36 and fatty acid binding protein (FABP). Within the hepatocytes, fatty acid oxidation begins in the cytoplasm where long-chain fatty acids are converted to fatty acyl-coenzyme A (CoA) esters by acyl-CoA synthetases. These fatty acyl-CoA esters combine with carnitine to form fatty acyl carnitine molecules, which help to transport the fatty acid across the mitochondrial membrane. Once inside the mitochondrial matrix, the fatty acyl carnitine molecules are converted back to fatty acyl-CoA and then to acetyl-CoA that enters the Krebs cycle[12,13]. This process generates an abundance of ATP and reducing equivalents to support the conversion of pyruvate and other anaplerotic substrates to glucose via gluconeogenesis. Under conditions where acetyl-CoA production from β-oxidation exceeds the oxidative capacity of the Krebs cycle, the excess acetyl-CoA is diverted to ketone body synthesis. Ketogenesis is directly controlled by carnitine palmitoyltransferase I (CPT-1), which is activated by low insulin levels, and directly by the activity of the key mitochondrial regulatory enzyme 3-hydroxy-3-methylglutaryl-CoA (HMG-CoA) synthase. Synthesised ketone bodies can serve as a fuel source when glucose levels are too low in the body (e.g., during prolonged starvation) or in uncontrolled diabetics, where most of the circulating glucose cannot be utilised[14].

1.1.3.3 Triacylglycerol biosynthesis and transport

When carbohydrates or fats are ingested in excess of the body's requirements, the excess is stored mainly in the adipose tissue as TAG. The other tissue capable of storing TAG under conditions of excess fat is the liver. TAG is synthesised in the endoplasmic reticulum (ER) and consists of three fatty acyl molecules esterified to a glycerol backbone. In the liver, the glycerol backbone, glycerol-3-phosphate (G3P), is derived from glycerol by the action of glycerol kinase or the glycolytic intermediate dihydroxyacetone phosphate (DHAP) in a reaction catalysed by the cytosolic NAD-linked glycerol-3-phosphate dehydrogenase. Then, fatty acid, in order to be attached to a glycerol backbone, has to be activated into fatty acyl CoA. This activation process is catalysed by the enzyme fatty acyl-CoA synthetase, which is

located in the lumen of the ER, in the mitochondrial outer membrane and matrix, and also in the membrane of peroxisomes. After activation, the first fatty acyl-CoA molecule is acylated to G3P by the enzyme glycerol 3-phosphate acyltransferase which is the point of regulation in TAG synthesis[12].

1.2 Metabolic Syndrome: mechanism underlying the disorder

1.2.1 Definition and prevalence

As the liver is a key organ in the metabolism, any disturbance of its balance leads to consequences such as fatty infiltration, elevated fasting plasma glucose, high serum triglycerides. Large evidence supports the hypothesis of liver and pancreas dysmetabolism as both causes and consequences of the Metabolic Syndrome[15]. Primary characteristics of Mets includes the clustering of abdominal obesity, insulin resistance, dyslipidemia and hypertension. Thus, the World Health Organization (WHO) defined this disorder as a cluster of interconnected factors that increase the risk of cardiovascular diseases and type 2 diabetes mellitus (T2DM)[16]. As the metabolic syndrome has several definitions, the prevalence estimate depends on the definition that is used to determine inclusion as well as the composition (e.g., sex, age, race, and ethnicity) of the population being studied. Moreover, lifestyle habits and socio- economic status (SES) appear to influence prevalence across sex, age, and race/ethnicity cohorts. Despite the differences in design and variables considered in these studies, some inferences can be made. Indeed, consistent result shows that the prevalence of metabolic syndrome is strongly dependent on age and sex. In a study conducted by Azizi's team, it was found that the prevalence is less than 10% for both men and women in the 20–29-year age- group, rising to 38% and 67%, respectively, in the 60–69-year age-group[17]. However, it seems that the increase in obesity rates in children leads to a parallel increase in the prevalence of MetS and T2DM in this group[18]. Moreover, some studies shown an influenced of the ethnicity on the MetS prevalence[19]. Worldwide, the available evidence indicates that in most countries between 20% and 30% of the adult population can be characterized as having the metabolic syndrome, a rate that is currently increasing.

1.2.2 Physiopathology

1.2.2.1 Obesity

The World Health Organization (WHO) defined obesity as abnormal or excessive fat accumulation and a body mass index (BMI) equal or greater than 30. It is considered as an early stage of insulin resistance (IR) and cardiovascular disease. Indeed, visceral adipose tissue secretes a variety of bioactive substances called adipo-cytokines, such as adiponectin, leptin, resistin, tumour necrosis factor a (TNFα), interleukin-6 (IL-6), and angiotensin II which are associated with IR, as well as plasminogen activator inhibitor 1 (PAI-1), which is implicated in thrombogenic vascular disease. Adiponectin is directly associated with insulin sensitivity by activating AMP-activated protein kinase (AMPK) and thus protects against the development of IR, T2DM, and atherosclerotic vascular diseases. Studies showed a decrease in adiponectin level in individuals with visceral fat accumulation[20,21]. Therefore, adipokines are potential causes of insulin resistance and reflect the role visceral obesity plays as a causal factor in metabolic and vascular disease. Visceral fat accumulation also promotes lipolysis in obese individuals due to decreased expression of adipocyte lipid droplet proteins such as perilipin (PLIN) and Cide proteins. This results in an increase in the release of FFAs into the bloodstream, leading to FFA deposition in insulin-sensitive non-adipose tissues resulting in lipotoxicity. Lipotoxicity is an important cause of insulin resistance as well as chronic inflammation and oxidative stress[20,22].

1.2.2.2 Insulin signalling mechanism and Insulin Resistance (IR)

As we previously mentioned, insulin is a pancreatic pleiotropic molecule regulating glucose metabolism through its action on skeletal muscle, liver and adipose tissue[4]. In order to understand the mechanisms that might be responsible for the development of insulin resistance, it is necessary to review the molecular pathways involved in insulin action.

After food intake, insulin is released by pancreatic β-cells to the bloodstream in response to high glucose level. Circulating insulin binds to the extracellular domain of the insulin receptor (INSR) which trigger a conformational change in the intracellular domain of the protein leading to the tyrosine phosphorylation of insulin receptor substrate (IRS) and the activation of multiple proteins including phosphatidylinositol 3-kinase (PI3K). Activation of

PI3K result in activation of which is responsible for propagation of insulin signal to one of the most important downstream effectors, Akt. After fully activation by PDK1 and mammalian target of rapamycin complex (mTORC) 2 protein, Akt can interact with different proteins, eliciting different effects as stimulation of glucose uptake and glycogen synthesis by Akt substrate 160 (AS160) and glycogen synthase kinase 3 (GSK3), respectively[23,24].In obese individuals, lipotoxicity caused inflammation resulting in elevated level of proinflammatory cytokines such as TNF-α and IL-6. These inflammatory factors can directly inhibit insulin signaling through competitive inhibition of tyrosine phosphorylation of IRS and inhibition of the IRS1/PI3K/Akt signaling pathway (Figure 1.5). In addition, inflammatory factors decrease the expression of peroxidase proliferator-activated receptor-gamma (PPAR-γ), leading to an increase in circulating FFA levels via the promotion of lipolysis. These circulating FFAs activate Toll-like receptor 4 (TLR-4) which promotes serine phosphorylation of IRS and leads to altered insulin signaling.

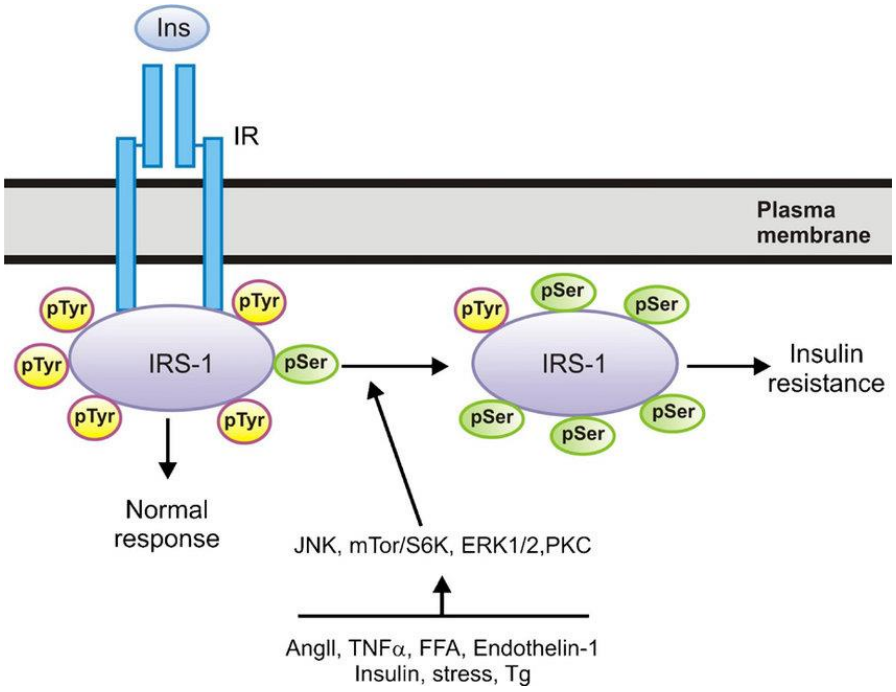

Figure 1. 5: *Impaired IRS phosphorylation causes insulin resistance. (J. Alberto Olivares-Reyes et al., 2009)*

Thus, insulin resistance (IR) is characterized by a reduced action of insulin despite increased insulin secretions from pancreatic β-cells. In the skeletal muscle, IR is due to impaired phosphorylation of AS160 with subsequent defects in GLUT4 translocation, glucose

uptake and glycogen synthesis. In the adipose tissue, IR is associated with a decrease of fat storage and an increase level of circulating FFA due to lipolysis, that further inhibit the antilipolytic effect of insulin. In the liver, Foxo1 is a transcription factor that increases the expression of key enzymes of gluconeogenesis, hence its upregulation results in the increased conversion of incoming substrates to the liver to glucose. Under normal condition, insulin causes phosphorylation and suppression of Foxo1 function through the action of the protein kinase AKT, leading to a down-regulation of gluconeogenic activities[22,23]. Therefore, insulin resistance condition result in hyperglycemia. Insulin also promote lipogenesis by activating the transcription factor SREBP-1C, involved in triacylglycerol synthesis, through the action of Akt activation of the mTORC1 protein kinase complex. While elevated insulin concentrations (hyperinsulinemia) may be needed to regulate gluconeogenesis, insulin-responsive lipogenesis mechanisms have no resistance and are hyper-activated, resulting in increased very low-density lipoprotein (VLDL) and reduced high density lipoprotein (HDL) particle production, manifesting by hypertriglyceridemia and low plasma HDL-cholesterol concentration[25] (Figure 1.6). Insulin resistance-mediated increase in circulating FFAsis believed to play a pivotal role in the pathogenesis of MetS[26].

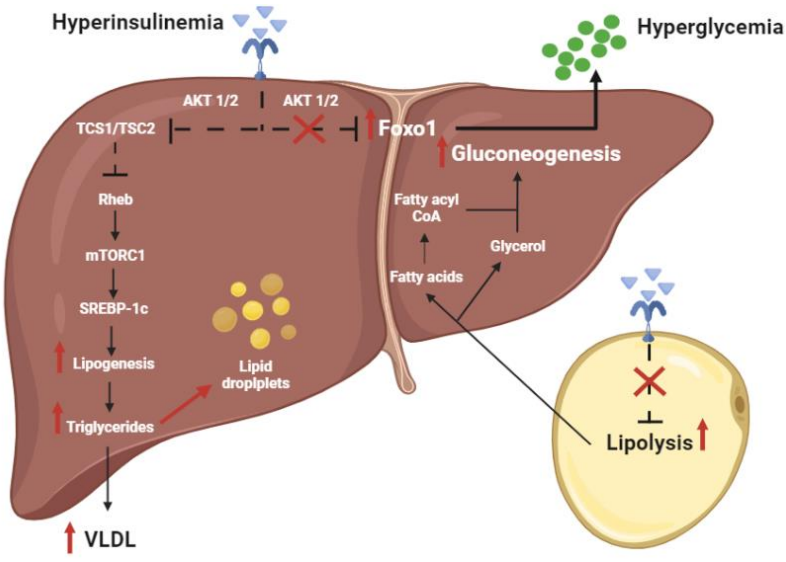

Figure 1. 6: *Hepatic hyperinsulinemia leading to hypertriglyceridemia under high-fat diet/obesity (adapted from Czech 2017 and created in Biorender.com).*

1.3 Obesity-related metabolic complications: Type 2 diabetes mellitus (T2DM)

Diabetes mellitus (DM) is the most significant dysfunction of the pancreas. According to the World Health Organization (WHO) definition, DM is a chronic disease occurring when the pancreas does not produce enough insulin, or none at all, or when the body cannot use the insulin secreted[27,28]. In the most recent report (Diabetes Atlas 2019) published by the International Diabetes Foundation (IDF), it was estimated that approximately 537 million people (1 in 10 adults) have diabetes worldwide and, worryingly, that 700 million will be affected by 2030 and 2045, respectively[29,30]. Diabetes is now one of the largest global health concerns. In 2021, the IDF estimated that 6.7 million deaths among adults (20–79 -years) can be attributed to diabetes[29,31]. The World Health Organization (WHO) ranked diabetes among the top ten causes of death in 2019[28]. Diabetes is also associated with multiple complications, such as blindness, kidney failure, cardiovascular diseases, sexual dysfunction, neuropathy, lower limb amputations and peripheral vascular disease[32–34]. The annual healthcare cost of diabetes was estimated at approximately 760 billion USD in 2019 and is predicted to reach 845 billion USD by 2045[29,34]. DM can be classified into four categories: type 1 DM (T1DM), type 2 DM (T2DM), gestational diabetes mellitus (GDM), and a fourth category which includes specific types of diabetes due to other causes such as genetic mutations, diseases of the exocrine pancreas and drug exposure[35]. T1DM and T2DM alone account for 90% to 95% of all diagnosed cases worldwide[36]. Nevertheless, T2DM is the most common form of diabetes, affecting approximately 90% of total diabetic patients, particularly adults aged 20-79 years[29]. It is named the disease of the century because its prevalence has increased exponentially in recent decades.

1.3.1 Definition of T2DM

Type 2 Diabetes Mellitus is a complex pathology caused by insulin resistance and impaired insulin secretion[37]. Insulin resistance is present in the majority of people with the MetS and associates with a number of its other factors. Thus, suffer from MetS is associated with a 5-fold increase risk of developing T2DM in adults[15]. T2DM occurs when the pancreas fails to adapt to increased blood glucose levels which leading to glucolipotoxicity[36–38]. Several factors play a part in increasing the risk of developing T2DM: genetic factors, age, obesity,

unhealthy lifestyles and lack of physical activity[34,37]. Therefore, patients with T2DM are mostly characterized by a MetS related to obesity or higher body fat percentage, localised predominantly in the abdominal region. In this condition, adipose tissue promotes IR through various inflammatory mechanisms, including increased free fatty acid (FFA) release and adipokine deregulation[39]. The response of the pancreatic islets to this new environment may include inflammatory stress, ER stress, metabolic and oxidative stress (e.g., glucotoxicity, lipotoxicity, and glucolipotoxicity) and amyloid stress. The increase of these interdependent stress factors will promote β-cell dysfunction, followed by dedifferentiation and/or loss of β-cell mass and finally to the loss of islet integrity marking the onset of T2DM[39,40].

1.3.2 Beta-cell dysfunction leading to T2DM

Beta-cells failure is central to the development and progression of T2DM. In response to a high glucose levels, β-cells synthetize and secrete around 1 million insulin molecules/minute, which require highly functional ER. Excess of saturated FFA and hyperglycemia due to IR can induce ER stress through the activation of the apoptotic unfolded protein response (UPR) pathways[39,41]. The UPR pathway activation may follow several mechanisms including inhibition of the sarco-endoplasmic reticulum Ca^{2+} ATPase (SERCA) responsible for ER Ca^{2+} mobilization; activation of IP3 receptors or direct impairment of ER homeostasis.

In addition, hyperglycemia increase proinsulin biosynthesis and islet amyloid polypeptides (IAAP) in β-cells, leading to the accumulation of misfolded insulin and IAAP and increasing the production of oxidative protein folding-mediated reactive oxygen species (ROS)[39,42]. Moreover, since β-cells lack certain antioxidant enzymes that remove ROS, increased production of ROS may promote dysfunction (Figure 1.7). These effects alter physiological ER Ca^{2+} mobilization and promotes proapoptotic signals, proinsulin mRNA degradation and induce interleukin-1β (IL-1β) release that recruit macrophages and enhances local islet inflammation[40,43].

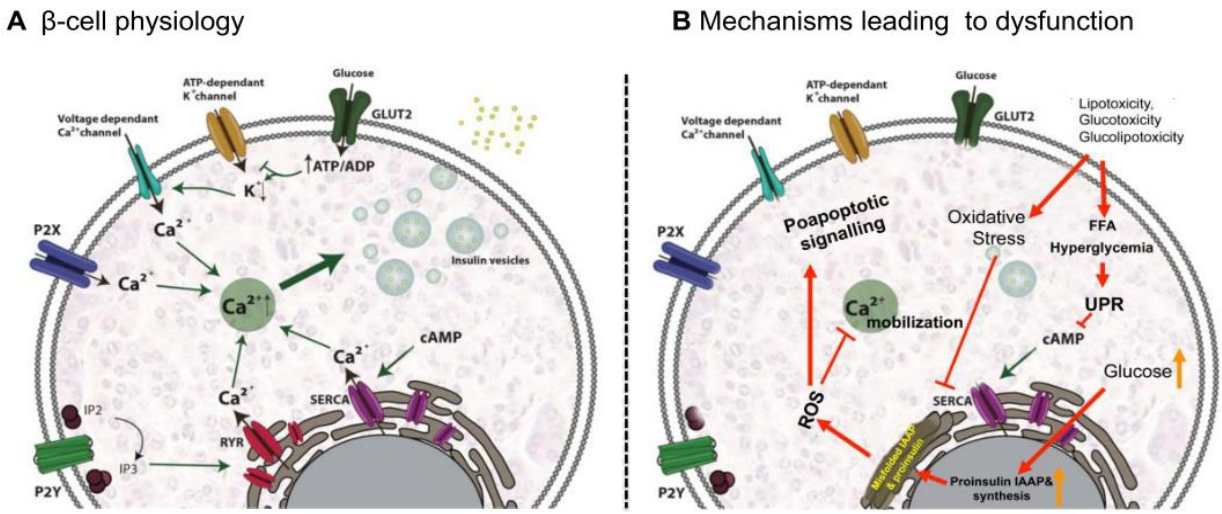

Figure 1. 7: *Signaling pathways of insulin secretion in β-cells (A) in physiological condition (B) in hyperglycemia and hyperlipidemia condition (Galicia-Garcia et al., 2020).*

Therefore, it is possible to postulate that the progression of T2DM occurs in three phases. As insulin resistance increases, β-cells initially compensate by increasing insulin production (phase 1). Prolonged insulin resistance and increase islet inflammation due to oxidative stress lead to β-cell decompensation leading to impaired glucoses tolerance and prediabetes (phase 2). Ongoing hyperglycemia and hyperlipidemia lead to a decline of functional β-cell mass due to dedifferentiation and/or β -cell death leading to T2DM (phase 3) [39,44]. Arguments are developed that the loss of β-cell function found in T2DM are strongly correlated with increased glucose levels than with non-esterified fatty acids (NEFA) levels, thus supporting the importance of glucotoxicity [45] (Figure 1.8).

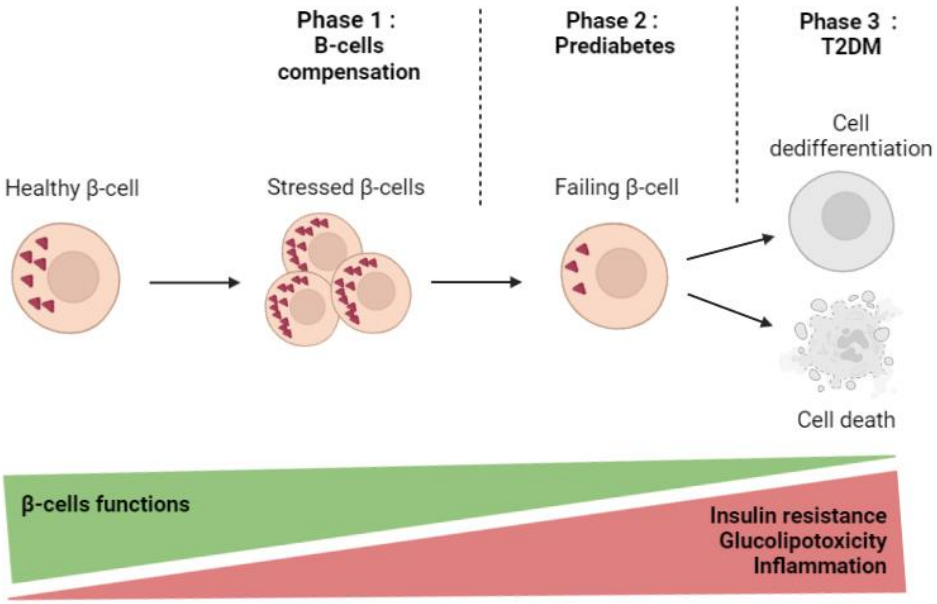

Figure 1. 8: *Schematic representation of T2DM progression (inspired from Christensen and Gannon 2019).*

During the past several years, a new hypothesis has been challenged the idea that insulin resistance precedes β-cells dysfunction. Indeed, there is a growing appreciation that the contribution of islet β-cells hyperresponsiveness is a primary event in the development hyperinsulinemia and leads the other components of the metabolic syndrome[46]. As discussed, β cell response to physiologic and pathophysiologic states of nutrient excess can occur through several mechanisms, including adaptive changes in β cell mass and function that may occur both prior to and in response to MetS[47].

1.3.3 Treatment

Nonpharmacological treatment such as reduced caloric intake and increased physical activity represent the basis of treatment of insulin resistance in type 2 diabetic patients. Nevertheless, this nonpharmacological treatment is not sufficient for most patient (75% patients with 3 years old duration of diabetes) for whom the use of a drug treatment is necessary.

Currently, there are 12, non-insulin, classes of drug treatments for type 2 diabetes[48–51] (Table 1.2). One major mechanism of action to increase insulin sensitivity is reducing the deleterious effects of chronic hyperglycaemia on insulin action and insulin secretion[50].

Table 1. 2: *Current hypoglycaemic drugs and their major metabolic effects to treat T2DM (in USA).*

Drug Class	Current available drugs	Main metabolic effects
1st and 2nd generation Sulfonylureas	Tolazamide, Tolbutamide, Glyburide, Glimepiride, Gliclazide	Glucose independent stimulation of insulin secretion
Meglitinides	Repaglinide, Nateglinide	
DDP4 inhibitors	Alogliptin, Linagliptin, Sitagliptin, Saxagliptin, Vildagliptin	Glucose independent stimulation of insulin secretion/ inhibition of glucagon secretion
GLP-1 receptor agonist	Exanatide, Liraglutide, Albiglutide, Dulaglutide, Lixisenatide, Semaglutide	
Biguanides	Metformin, Glucophage XR	Insulin sensitization
Thiazolidinediones	Rosiglitazone, Pioglitazone	
α-glucosidase inhibitors	Aacrbose, Miglitol, Voglibose	Inhibition of glucose liberation from carbohydrates
Bile acid sequestrant	Colesevelam	Increase incretin secretion/improve β-cell function
Dopamine agonist	Bromocriptine	Increase low hypothalamic dopamine levels/ inhibition of hepatic glucose production
SGLT2 inhibitors	Canagliflozin, Dapagliflozin, Empagliflozin, Ertuglifozin	Renal glucose excretion

Amylin mimetic	Pramlintide	Slowing of gastric emptying/ inhibition of glucagon secretion
GLP-1 receptor and GIP receptor agonists	Tirzepatide	1st and 2nd phase insulin secretion stimulation/ glucagon levels reduction

1.3.3.1 Biguanides: Metformin hydrochloride

Metformin hydrochloride, a biguanide oral drug, is the first-line therapy for T2DM. The mechanism of action of metformin is complex. In brief, the drug appears to reduce mitochondrial energy production via inhibition of Complex 1. The higher AMP to ATP ratio lead to phosphorylation and activation of the energy sensor AMPK (AMP kinase). Activation of AMPK results in reduced gluconeogenesis (in both fasting and postprandial periods), increased insulin sensitivity, and enhanced peripheral glucose uptake[50,52,53]. Metformin also have downstream effects on decreasing fatty acid and triglyceride production. Moreover, as metformin does not stimulate endogenous insulin production, it does not cause hypoglycemia, which is an adverse effect that is associated with several antidiabetic medication. As a result, metformin is efficacious when paired with other glucose lowering medication such as sulfonylureas and GLP-1 inhibitors[54].

1.3.3.2 Incretins-based therapy: GLP-1 and DPP4

Incretins are a relatively new group of injectable drugs for treatment of type 2 diabetes. Glucagon-like peptide-1 (GLP-1) is a product of proglucagon cleavage synthesized in L cells in the intestinal mucosa, α-cells in the pancreatic islet, and neurons in the nucleus of the solitary tract. The glucose-dependent postprandial release of GLP-1 induces insulin secretion by pancreatic β-cells and suppresses glucagon secretion from pancreatic α-cells, which regulates glycaemia. Moreover, GLP-1 modulates appetite by slowing gastric emptying and inducing satiety. However, these effects are short-lived because circulating GLP-1 is quickly degraded by dipeptidyl peptidase-4 (DPP4) and has a half-life greater or equal to 5 min in circulation. Thus, analogue peptide of GLP-1, called GLP-1 receptor agonists (GLP-1RAs), were developed as glucose-lowering agents to treat patients with T2DM. Few clinical research

studies also highlight the benefice of GLP1-RAs in losing weight when used in combination with diet and exercise. Furthermore, DPP4 inhibitors represent another approach to treat T2DM by prolonging the half-life of endogenous GLP-1.

1.3.3.3 SGLT-2 inhibitors

Sodium-glucose co-transporter 2 (SGLT2) is located on the luminal side of the first segment of the proximal tubule in the kidney and it is responsible for the reabsorption of approximately 90% of all filtered glucose[55]. Thus, SGLT2 inhibitors are drugs that inhibiting glucose and sodium reabsorption in the kidneys leading to glycosuria. Their effects consequently include reductions in HbA1c, plasma glucose levels and blood pressure, but also reductions in body weight and adiposity [56].

1.3.3.4 Insulin-based therapy

Insulin was for many years the only treatment for diabetes. It is still the most effective treatment to reduce both glucose and glycated haemoglobin (HbA1C) concentration. As T2DM is characterised by a progressive loss of glycaemic control, most patients require treatment with basal insulin[57]. Nowadays, a multitude of short-acting and long-acting insulin analogues are currently available for the treatment of DM, which mimic physiological insulin secretion better than human insulins. For instance, ultra-rapid insulin analogues can significantly reduce postprandial glucose increases while long-acting insulin analogues can reduce the rate of hypoglycemia, especially nocturnal hypoglycaemia. These novel insulin formulations can also be used in combination with another agent, such as GLP-1RAs, DPP4 inhibitors, and SGLT-2 inhibitors, to achieve recommended glycaemic targets and reduce insulin doses, weight gain, and hypoglycaemic episodes[58,59].

1.4 Obesity-related metabolic complications: Non-alcoholic fatty liver disease (NAFLD)

1.4.1 Definition and prevalence of NAFLD

The term non-alcoholic fatty liver disease (NAFLD) comprises a spectrum of increasingly harmful conditions ranging from steatosis to non-alcoholic steatohepatitis (NASH), which is associated with progressive liver fibrosis leading to cirrhosis and end-stage

hepatocellular carcinoma (HCC)[60]. NAFLD represents the hepatic manifestation of MetS and it is characterized by enhanced fatty infiltration in more than 5% of hepatocytes in the absence of alcohol or drug consumption, virus hepatitis and autoimmunity disease. Its physiopathology involves several mechanisms, such as, glucose intolerance, insulin resistance (IR), enhanced lipogenesis and lipotoxicity, hepatic and systemic inflammation, and oxidative stress.

Nowadays, it is estimated that about 25% of the world population has NAFLD[61]. For instance, the prevalence of NAFLD in the United States is reported to be between 25% and 40%, with similar rates reported from Europe and Asia[62,63]. Due to the spread of the obesity and T2DM epidemic, NAFLD is becoming the most common chronic liver disease and one of the principal indications for liver transplantation. In fact, prevalence of NAFLD is significant in patients with MetS. For instance, NAFLD has been reported in over 70% of T2DM patients and over 90% of severely obese patients undergoing bariatric surgery[62,64]. In addition to MetS and T2DM, other factors may also contribute to the prevalence and outcomes of NAFLD, such as genetic factors. Indeed, a high prevalence of a polymorphism in the gene encoding patatin-like phospholipase domain containing three genes (*PNPLA3*; rs738409 C/G, M148I) have been related to the prevalence of NAFLD.

1.4.2 Physiopathology and evolution

1.4.2.1 Physiopathology: mechanism of fat accumulation in the liver

The mechanism of steatosis development as well as the liver damage resulting in NASH remain incompletely understood. Nevertheless, retention of various lipids seems to be a prerequisite for the development of NAFLD. In fact, alterations in the equilibrium of several mechanisms may lead to a fatty liver: (1) increased free fatty acids (FFAs) supply due to increased lipolysis from both visceral/subcutaneous adipose tissue and/or increased intake of dietary fat; (2) decreased free fatty oxidation; (3) increased de novo lipogenesis (DNL) and (4) decreased hepatic very low-density lipoprotein–triglyceride secretion[65].

Circulating FFAs provide the substrate for triacylglycerol formation in the liver. In hepatic steatosis, progressive triacylglycerol deposition exceeds the livers capacity to export very low-density lipoprotein particles (VLDL) and β-oxidation of FFAs. The most abundant and well-studied FFAs in the context of NAFLD are palmitic acid, a 16-carbon length saturated fatty

acid (C16:0) and oleic acid, an 18-carbon length monounsaturated fatty acid (C18:1). Due to their hydrophobic properties FFAs can diffuse across cell membrane but they can also be transported by fatty acid transport proteins (FATP) or the fatty acid transporter, CD36[66]. FFAs can originate from increased lipolysis in adipose tissue. Indeed, studies in individuals with obesity have demonstrated that ~60% of liver triglyceride content is derived from free fatty acids from adipose tissue, which highlighting the dominance of the lipolysis pathway in NAFLD pathogenesis and provides a strong link between the comorbidities of obesity, insulin resistance and NAFLD. On the other hand, it is estimated that 15-20% of the triglyceride content of the liver comes directly from dietary fatty acids and the remaining 20% from the DNL mechanism[62]. Although many studies assert the negative effect of triglyceride accumulation in the liver, recent evidence indicates that triglycerides may have a protective function. In fact, Yamaguchi *et al.* demonstrated a protective role of TGs accumulation in the liver by showing that inhibition of DAG acetyltransferase 2, the final catalyst in hepatocyte TG synthesis, generated increased necroinflammation and increased peroxidation and oxidative stress. In summary, triglyceride synthesis seems to be an adaptive, beneficial response in situations where hepatocytes are exposed to potentially toxic non-triglyceride metabolites.

Furthermore, elevated peripheral FFAs and DNL can lead to ectopic accumulation of non-triglyceride toxic metabolites, such as lysophosphatidylcholine (LPC) which is responsible for lipotoxicity and lipoapoptosis. Indeed, LPCs seem to be a key mediator of FFAs cytotoxicity by causing an endoplasmic reticulum (ER) stress and inducing apoptotic pathways downstream of the activation of Jun terminal kinase (JNK). These processes lead to an upregulation of proapoptotic proteins Bim and Bax which trigger the mitochondrial apoptotic pathway[66,67]. In addition to mitochondrial dysfunction, lysosomal permeabilization has an important role in apoptotic cell. LPCs also upregulate genes involved in cholesterol biosynthesis and downregulate genes involved in hepatic fatty acid oxidation leading in oxidative stress and inflammatory responses.

In the liver, the breakdown of cholesterol homeostasis contributes to its accumulation in hepatocytes and within organelles. High intracellular free cholesterol leads to liver damage through the activation of Kupffer cells and hepatic stellate cells, which mediate inflammation and fibrosis. In addition, free cholesterol can accumulate in liver mitochondria leading to

mitochondrial dysfunction, which results in increasing generation of ROS and in activation of the unfolded protein response (UPR) in the endoplasmic reticulum (ER), resulting in ER stress and hepatocyte apoptosis. These events contribute to the maintenance of steatosis and promote ongoing hepatocyte death and liver injury[65,68].

Numerous studies well established the major risk factors for hepatic steatosis and hepatic fibrosis in NAFLD: age >50 years, obesity, insulin resistance, T2DM, increased ferritin levels and the patatin-like phospholipase domain-containing 3 (PNPLA3) I148M polymorphism. PNPLA3 encodes a triacylglycerol lipase that mediates triacylglycerol hydrolysis in adipocytes. I148M gene variant has been associated with lower plasma triacylglycerol profile, increased liver fat content and concentrations of serum aspartate aminotransferase[69,70]. This supports the notion that this gene variant inhibits intra-hepatocellular lipolysis rather than stimulates hepatic triacylglycerol synthesis. However, further work is required to establish the precise function of PNPLA3 in the pathogenesis of liver disease progression in NAFLD.

1.4.2.2 Steatosis to Non-alcoholic Steatohepatitis (NASH): the "multiple-hit" hypothesis

Steatohepatitis is defined strictly by the presence of hepatocellular ballooning with or without Mallory-Denk bodies and accompanying inflammation in the presence of macrovesicular steatosis[60]. Originally, the progression of NAFLD from simple steatosis to NASH was conceptualised as a "two hits" model[71,72]. It was suggested that the first hit, defined as fat accumulation, sensitises the liver and trigger the second hit, an inflammatory process that results in steatohepatitis and fibrosis. Nevertheless, the "multi-parallel hits" hypothesis is the most accepted for understanding the pathogenesis of NASH and its progression to fibrosis. This hypothesis proposes that many simultaneous hits such as mitochondrial dysfunction, ER stress, inflammatory cytokines (principally TNF-α and IL-6), adipokines and gut-derived endotoxin may promote inflammation and liver injury [65,73] (Figure 1.9).

Lipotoxicity and insulin resistance are major mechanisms underlying hepatocyte dysfunction leading to steatosis progression in NASH. As previously described (section 3.2.1), lipotoxic injury appears to occur in the setting of excess FFA traffic, especially saturated fatty

acids, rather than due to simple triglyceride accumulation. The increased lipid flux may alter mitochondrial or peroxisomal function leading to respiratory oxidation collapse with impairment of fat homeostasis, generation of lipid-derived toxic metabolites and overproduction of ROS leading to chronic inflammation[66,74]. Increased hepatic expression of CYP2E1, an enzyme present into the mitochondria, promotes oxidative stress by hydrolyses FFA and ketones into free radicals that alter mitochondrial respiratory chain and promotes hepatic inflammation. Moreover, high lipid flux induced endoplasmic reticulum stress with UPR activation leading to chronic hepatic inflammation through NF-κB and JNK pathways activation and ROS overproduction[72,74,75]. Thus, there is a mutual and bidirectional interaction between ROS production by mitochondria and ER stress in the progression from steatosis to steatohepatitis. Hepatic iron is also suggested as source of oxidative stress and therefore hepatocyte dysfunction by catalysing the conversion of hydrogen peroxide to hydroxyl radical. However, its role in the progression of NASH remains controversial[74,76].

Obesity-related adipocyte hypertrophy and/or insulin resistance result in an imbalance of adipokines that may profoundly affect not only the adipose tissue itself but also the liver. Adiponectin is an anti-inflammatory adipocytokine and increases insulin sensitivity. The anti-inflammatory and hepato-protective activities of adiponectin are achieved through blocking the activation of NF-κB, secreting anti-inflammatory cytokines, inhibiting pro-inflammatory cytokines such as TNF-α and IL-6. In contrast, leptin has a proinflammatory action by activating hepatic stellate cells and stimulating Kupffer cells to produce TGF-β1. Insulin appears to stimulate leptin production via PI3K/AKT and the activation of the transcription factors SREBP1, C/EBP-α and Sp1. Therefore, in obese patients, reduced adiponectin and increased leptin levels may result in hepatic steatosis and activation of inflammation and fibrogenesis[65,72,73].

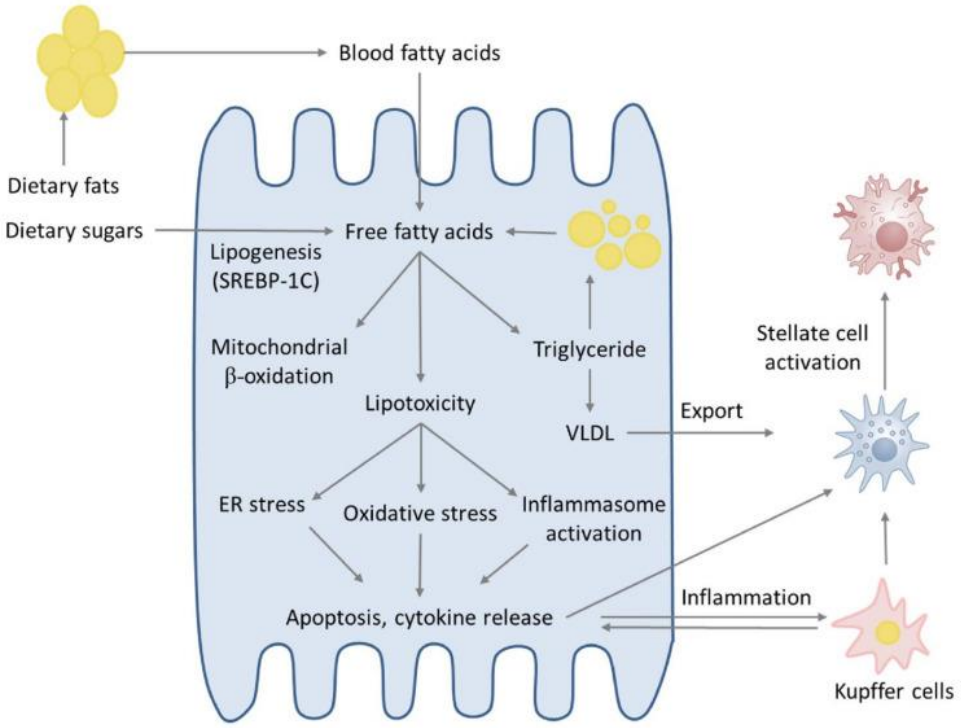

Figure 1. 9: *Schema of the processes involved in NASH development (Berardo et al., 2020).*

It is increasingly recognized that the gut microbiome is implicated in the pathogenesis and progression of steatosis through the so-called gut-liver axis. High diet-induced dysbiosis is associated with increased production of short-chains fatty acids (SCFAs) which may induce DNL and cholesterol synthesis, alter glucose homeostasis and promote hepatic fat accumulation. Moreover, patients with steatosis have significantly increased gut permeability (due to tight junction disruption) which promote the passage of lipopolysaccharide (LPS), a key constituent of many bacteria presents in the microbiota, into the portal circulation. Lipopolysaccharidemia induce a consequent activation of the inflammatory cascade via Tool-Like receptors (TLRs) and different cells type such as Kupffer cells and hepatic stellate cells. Therefore, high LPS level plasma have demonstrated effects on insulin resistance, obesity, hepatic fat accumulation and NASH development and progression[73,75,77]. On the molecular level, LPS is recognized by the specific pattern recognition receptor, called Toll-like receptor 4 (TLR4) and its co-receptors, LPS binding protein (LBP) and CD14. Activation of TLR4 triggers down-stream inflammatory cascade, involving, depending on the context, NF-κB, AP-1, and IRF3 activation. TLR can also be activated via inflammasomes, a multiprotein complex localized in the cytoplasm. Inflammasome activation, by either exogenous pathogen-associated

molecular patterns (PAMPS) (e.g. saturated fatty acids) or internal host damage-associated molecular patterns (DAMPS) (e.g. products from gut microbiota), lead to a cascade of reactions that results in the secretion of IL-1 et IL-18 which have pro-inflammatory and pro-fibrotic effects[75,77,78]. Furthermore, perturbations in gut microbiota levels and community composition are very likely to affect the bile acid pool, by increasing their production, especially deoxycholic acid (DCA). Thus, bile acids are potential carcinogens whose alterations may contribute to NAFLD development and progression and have also been linked to HCC [79,80] (Figure 1.10).

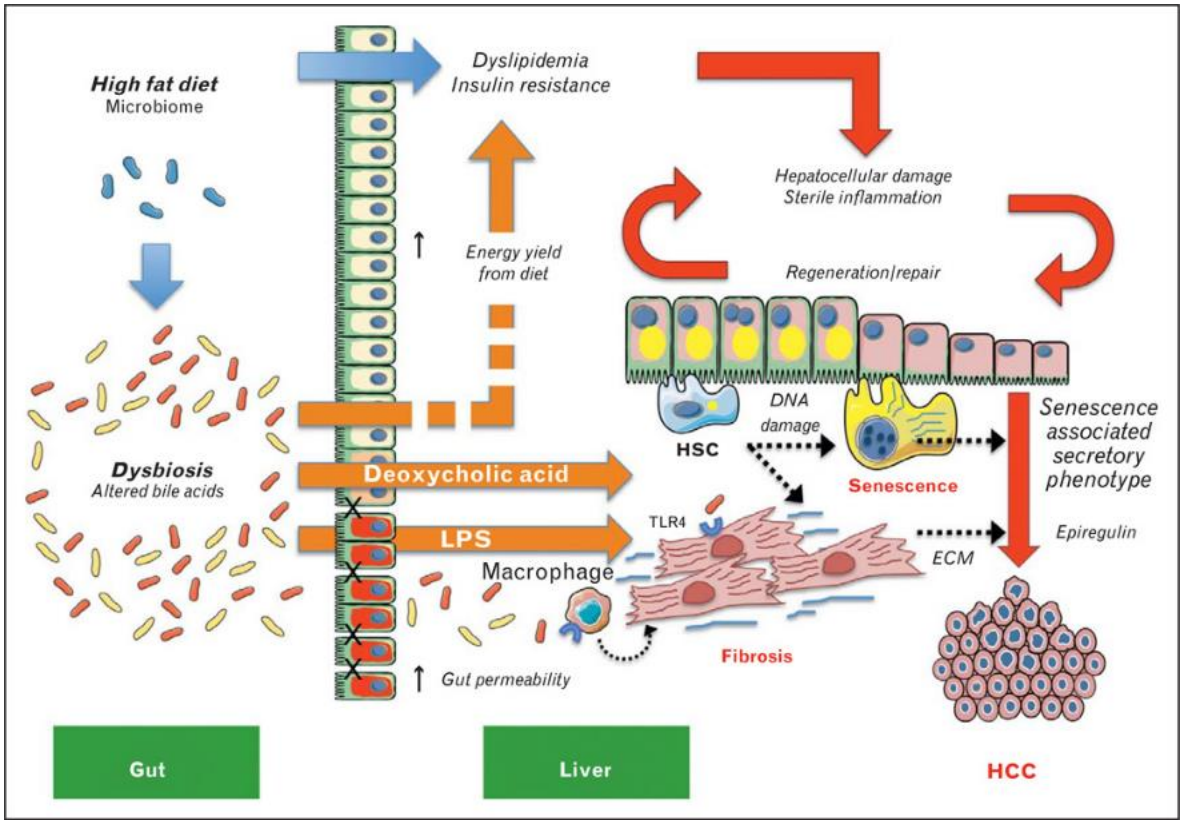

Figure 1. 10: *Contributions of diet and dysbiosis in promoting NAFLD progression to NASH, hepatic fibrosis and HCC (Lade et al., 2014).*

1.4.2.3 Progressive NASH: From inflammation to Fibrosis

Hepatic fibrosis is the natural consequence of iterative injury in chronic liver disease that is usually mediated by chronic inflammation. Fibrosis is defined by the excessive accumulation of ECM, mostly in the form of collagen, and goes hand in hand with altered angiogenesis. Fibrogenesis is driven by signaling from stressed or injured hepatocytes and activated Kupffer cells, leading to activation of resident hepatic stellate cells or/and (portal

and perivascular) fibroblasts into myofibroblasts to produce matrix proteins faster than they are degraded[78,80]. On the other hand, bone marrow-derived myofibroblasts differentiate from pluripotent stem cells can also migrate to the damaged liver but they are currently believed to contribute little to the ECM production in liver injury[74]. Another NASH-specific pathway is through the PNPLA3-I148M variant's effects directly on stellate cell fibrogenesis (Figure 1.11). Advanced fibrosis results in liver failure and portal hypertension with its associated complications of ascites and life-threatening variceal bleeding, as well as an increased risk of HCC[81].

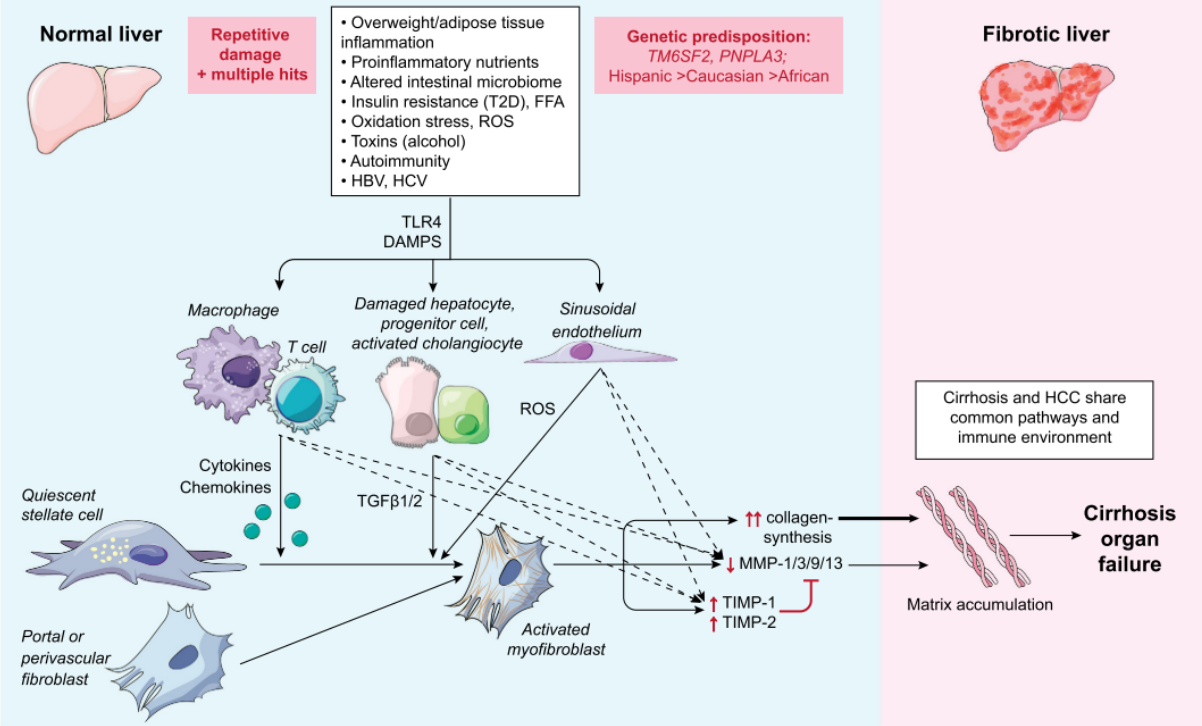

Figure 1. 11: *Mechanisms of fibrosis progression in NASH (Schuppan et al., 2018).*

1.4.3 Diagnostic and treatment

Since the exact molecular mechanisms underlying NAFLD pathogenesis and progression need to be further elucidated; it is not yet possible to diagnose NAFLD solely on the basis of routine blood tests and tissue biomarkers or by ultrasound imaging. Indeed, an expensive, invasive and potentially dangerous liver biopsy still represents the gold standard for the diagnosis and staging of NAFLD. Thus, in the vast majority of cases, the diagnosis of NAFLD are based on the presence of hepatic steatosis on imaging, chronic cytolysis,

hyperferritinemia, with a dysmetabolic context. Nevertheless, it is necessary to look for other reliable, accurate and non-invasive biomarkers.

1.4.3.1 Physical approach in suspected NAFLD: imaging study

In clinical practice, radiological imaging techniques (ultrasound, computed tomography or magnetic resonance-based elastography) are considered the first-line method for evaluating steatosis in any patient suspected with NAFLD[82]. Typically, liver fatty infiltration is observed and appears "bright" on ultrasound, since acoustic interfaces are increased in hepatic lipid accumulation, but only when >20% of liver steatosis is present[83]. Furthermore, liver stiffness stage can be determinate using ultrasound based transient elastography (TE) which measures the velocity of a low-frequency elastic shear wave propagation through the liver[84,85]. The sensitivity of the method increases as the degree of steatosis increases but is decreased for morbid obese patients and patients with ascites. This weakness can be bypass by using magnetic resonance elastography (MRE). MRE uses radio waves and magnets to produce detailed images of the entire liver. However, it is an expensive, time consuming, that cannot be used in routine practice and cannot be performed in livers patients with iron overload (because of signal-to-noise limitations) and metal implants[84].

1.4.3.2 Biological approach in suspected NAFLD: current biological biomarkers

Liver enzymes, especially alanine and aspartate aminotransferases (ALT, AST) are the first laboratory tests every clinician will consider worth evaluating in a patient with suspected NAFLD. Several steatosis scores based on serum biomarkers have been proposed for diagnosing or grading steatosis or staging fibrosis. The most validated steatosis scores for fibrosis in NAFLD are the NAFLD Fibrosis Score (NFS, variables: age, body mass index, hyperglycaemia/diabetes, AST, ALT, platelets, albumin) and FIB4 (age, AST, ALT, platelets)[84]. NFS and FIB-4 are free tests that are interpreted with two diagnostic thresholds. The lower threshold of these tests (NFS < -1.455, FIB4 < 1.30) excludes advanced liver fibrosis (stage 3 and 4) with more than 90% accuracy. The upper threshold (CBC > 0.676, FIB4 > 2.67) is less effective: only 67% of positive patients actually have advanced liver fibrosis. Between the two thresholds, there is a grey zone (about 30% of patients) in which the diagnosis remains undetermined[86,87]. Nevertheless, it has been evaluated than patients with an intermediate or

high probability of advanced liver fibrosis had a significantly higher glucose and a higher AST/ALT ratio at the end of follow-up compared to those with a low probability of advanced liver fibrosis[88]. Moreover, they present a higher plasma level of cytokeratin 18 (CK18) fragment levels, a marker of hepatocyte apoptosis. Although useful, liver enzymes per se are not reliable and accurate predictors. Indeed, while abnormal liver enzymes are frequently reported in patients with NAFLD, liver enzymes may be normal in up to 80% of cases[89].

1.4.3.3 Liver biopsy in suspected NASH and Fibrosis patients

The key issues in NAFLD patients are the differentiation of NASH from simple steatosis and identification of advanced hepatic fibrosis. Until now, liver biopsy is the gold standard for identifying these two critical end points, but has well-known limitations, including invasiveness; rare but potentially life-threatening complications, inter-/intra-observer variability and cost. Liver biopsy is principally performed for NAFLD patients showing increased risk of NASH or advanced fibrosis as well as discordant non-invasive scores results (Figure 1.12). Several systems of histopathological biopsy analysis allow to grade and stage NAFLD. The NAFLD Activity Score (NAS) scoring systems, is mostly used by clinician for grading steatosis by analyzing hepatocellular vesicular steatosis (macrovesicular steatosis and microvesicular steatosis separately), hepatocellular hypertrophy and inflammatory cell aggregate[90,91]. Since the last decade, new scoring systems have emerged and allowed to bypass the limitations of NAS. Indeed, Steatosis Activity and Fibrosis (SAF), a score system allowing to distinguish steatosis from inflammation and fibrosis, have showed a better reproducibility and accuracy than NAS. On the other hand, the Fatty Liver Inhibition of progression algorithm (FLIP), used for NASH severity assessment, have decreased inter-observer variability and enhanced the characterisation of hepatocellular ballooning and fibrosis[82,90].

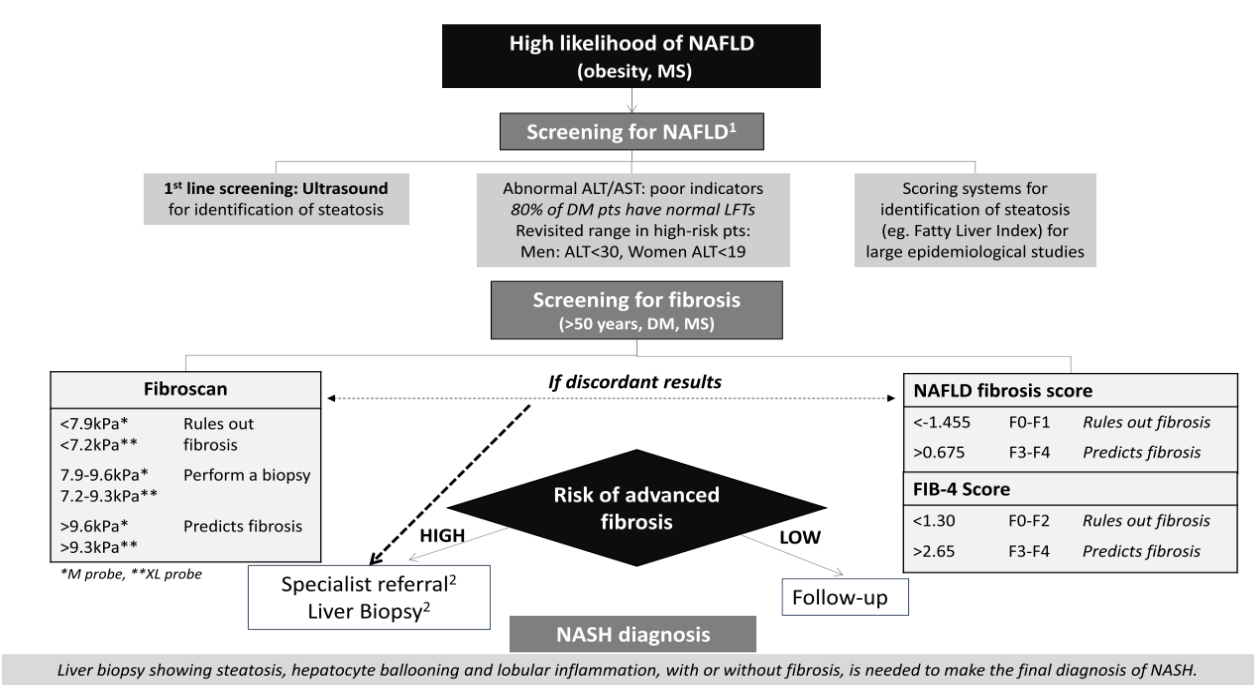

Figure 1. 12: *Algorithm for current diagnostic approach in NAFLD (Papatheodoridi and Cholongitas, 2019).*

1.4.4 Treatment of NAFLD

Because of the increasing prevalence and association with a significant number of comorbidities and mortality, it is essential to treat NAFLD patient as soon as the diagnosis is made. Currently, there are no specific pharmacological therapies or surgical procedures that directly treat NAFLD, although over 25 medications are undergoing clinical trials (phase 2 or 3)[92]. Therapeutic approaches focus on the management of the disease through reducing related risk factors, including obesity, insulin resistance, hyperglycemia, dyslipidemia, inflammation and oxidative stress. Lifestyle interventions, including weight loss and exercise, remain the first-line treatment. Dietary strategies including Palaeolithic, ketogenic, low-carbohydrate, and intermittent fasting diets have become increasingly popular due to their purported benefits at slowing the development and progression of steatosis/NASH[93]. Indeed, several studies have shown that reducing body weight by 7-10% with hypocaloric diets is the most efficacious in the treatment of NAFLD/NASH and fibrosis[94–96]. Moreover, weight loss ≥10% have been associated with the highest rates of NAFLD/NASH resolution and fibrosis regression[94].

Pharmacotherapy studies have investigated the efficacy of several drugs including - weight reducing drugs, lipid lowering agents, antioxidants, bile salts and co-factors increasing the mitochondrial transport of fatty acids are being considered. Insulin resistance, as a major driving force for excessive fat accumulation in the liver and initiation and progression of steatohepatitis and fibrosis, several pharmacological agents used as NAFLD treatment are insulin sensitizers. Metformin is currently the recommended first-line agent for the management of T2DM and tends to lower blood glucose through a number of mechanisms that may be beneficial in patients with steatosis, however it is not recommended for the treatment of NASH as there is no proof of its efficacy on hepatic histology[97]. Thiazolidinediones (TZD), another insulin sensitizer, show great potential in patients with NAFLD because they promote the differentiation of insulin-resistant large pre-adipocytes into small, proliferative, insulin-sensitive adipocytes preadipocyte. Furthermore, TZD may induce a redistribution of lipid from visceral sites such as liver and muscle to peripheral subcutaneous adipose tissue, increase circulating adiponectin levels, and improve insulin sensitivity[92].On the other hand, vitamin E, an antioxidant, have shown great efficacy in patient without TD2M by improving steatosis, inflammation and ballooning, and inducing resolution of NASH[97,98]. Therefore, it is the first-line therapy for biopsy-proven NASH without diabetes and cirrhosis[99].

Bariatric surgery may be an option for reducing weigh and metabolic complications associated in patients with obesity who are unresponsive to lifestyle changes and pharmacotherapy. A prospective study of 180 severely obese patients with biopsy-proven NASH, defined by the NASH clinical research network histologic scores highlighted resolution of NASH in liver samples from 84% of patients 5 years after the procedure. Furthermore, the progressive reduction of fibrosis has been observed during the first year until the fifth years[100]. However, rapid weight loss induce by bariatric surgery can increases the risk of developing hepatic failure especially in cirrhotic patients[101].

In recent years, novel mechanisms in the pathogenesis of NAFLD have been revealed, and created novel therapeutic possibilities for NAFLD treatment. Two promising drugs, farnesoid X receptor (FXR) agonists (Obeticholic acid) and CCR2/CCR5 inhibitor (Cenicriviroc) are currently in phase 3 trials[97,99,101–104].Unfortunately, PPAR-α and -δ agonists (Elafibranor)

and Selonsertib (ASK1 inhibitors), two other drugs candidates in phase 3 trials, had shown no significant effect in patients suffering from NASH[105].

1.4.5 NAFLD and T2DM: an intricate correlation

We have seen that metabolic syndrome included important disorders bridging liver and pancreas. The NAFLD and TD2M are strongly related as illustrated by several studies[46,106–109]. However, given the complex and bi-directional relationships between NAFLD, insulin resistance and chronic hyperglycaemia, it is extremely difficult to distinguish whether NAFLD is a cause or a consequence of insulin resistance and type 2 diabetes. Nevertheless, the crosstalk between the liver and pancreas and the interdependence of their pathologies depend, at the molecular level, on differentially regulated branches of the insulin signalling pathway. Meta- analysis demonstrated that patients diagnosed with non-alcoholic fatty liver present a risk to develop T2DM and MetS over a median 5-year follow period[110,111]. Indeed, insulin resistance compensatory hyperinsulinemia and visceral obesity contribute to the development of NAFLD first; in return, the insulin resistant fatty liver overproduces glucose and VLDL thus boosting the mechanisms that lead to with progressive exhaustion of pancreatic β-cell reserve, leading to T2DM development at later stages of life. This finding suggests that the magnitude of risk of TD2M development parallels the severity of NAFLD and particularly the severity of liver fibrosis[70]. However, many aspects of the crosstalk between NAFLD and IR/T2DM are not yet fully elucidated, as genetic risk factors for increased hepatic fat content have revealed that excess hepatic fat is associated with progressive liver disease, but does not always increase the risk of developing T2DM[108].

As discussed previously, many agents that are currently prescribed for hyperglycaemia have yielded positive results on NAFLD. As NAFLD linked to T2DM and contribute to CVD, which is the leading cause of mortality in patient with liver chronic disease, metabolic-targeted therapies would represent the most effective NAFLD-treatment as it might also reduce cardiometabolic risk factors[106,107]. However, for the development of such treatment further research is needed to define the crosstalk between liver and pancreas as well as assessing the impact of newer anti-diabetic treatments and identification of additional novel targets. To this end, it is essential to develop reliable experimental models representing the synergy of both NAFLD and T2DM[106].

1.5 Current *in vitro* models for NAFLD research

Investigating the mechanism that underlie steatosis and the hepatocellular consequences of triglyceride accumulation is important for understanding the development and progression of the pathology and allowing the development of novel therapy. While significant advances in pathophysiology have been made using genetically modified and diet-induced animal models, our manuscript focuses on *in vitro* models. This choice is motivated by our commitment to developing an alternative to animal testing and addressing significant species-species differences in metabolism. However, it will be essential to compare our results with those from animal models and available clinical patient data to assess the relevance of *in vitro* models.

1.5.1 Potential cell source for NAFLD research

1.5.1.1 Primary Human Hepatocytes

Primary human hepatocytes (PHH) are considered the gold standard for the study of liver biology and are widely used in various domains such as drug discovery, safety studies and disease modelling. They are isolated from human liver with benign pathologies, i.e. not affecting hepatocytes. Although PHHs are the cell type most likely to give functional liver responses, their monolayer culture leads to rapid dedifferentiation with a decline in CYP activity after 48 hours and loss of other liver functions after one week[112,113]. Indeed, PHH are complex metabolic cells whose function depends on their microenvironment, which consists not only of direct cell-cell and cell-matrix interactions, but also of a myriad of diffusible factors secreted by nearby non-parenchymal cells (NPCs)[112]. In addition to their limited lifespan and unstable phenotype, PHH are not easily available for practical and ethical reasons. Nevertheless, they can be of value to experimental liver steatosis research[114,115].

1.5.1.2 Cell lines

Human liver cell lines represent a promising *in vitro* study model due to their proliferative capacity, stable metabolism and simplicity to standardize[113]. There are many human liver cell lines listed by the American Type Culture Collection (ATCC). Among the most

commonly used cell lines, we can find HepG2/C3A which are derived from HepG2 cell line and generate hepatocytes that retain CYP activity and display accumulation of TGs after exposure to oleic acid either alone or together with palmitic acid. This also holds true for Huh-7 cells, a well-differentiated HCC cell line [116]. HepaRG cell line can differentiate into hepatocyte-like and biliary-like cells. HLC-derived HepaRG cells express major liver-specific functions, including CYP activity, are functionally stable at confluency and have an indefinite growth potential[117]. This cell line represents a great potential in *in vitro* liver steatosis research, as they accumulate lipid droplets following exposure to many FAs[118,119].

1.5.1.3 Pluripotent stem cell

Pluripotent stem cells are defined as cells that are capable of self-renewal and differentiation into mature cells of a tissue type. They include both embryonic stem cells (ESC) and induced pluripotent stem cells (iPSC). To date, many research teams have established protocols for differentiating ESCs and iPSCs into hepatocyte-like cells (HLCs) in 2D and 3D culture[120–122]. These approaches are generally based on mimicking embryonic liver development by adding the different growth factors required for each stage of development. Activin A and Wnt3a are the most important cytokines for the commitment of pluripotent cells to differentiate into definitive endoderm[123], although fibroblast growth factor 2 (FGF2) and bone morphogenetic protein 4 (BMP4) also play important roles[124]. Hepatocyte growth factor (HGF) and oncostatin M (OSM) are the most commonly used cytokines for liver maturation[125]. In recent years, the differentiation of iPSCs into HLC has provided a versatile platform for the functional study of various lipid disorders associated with insulin resistance or non-alcoholic fatty liver disease[126–128]. However, as the differentiation remains complicated and not fully efficient, differentiation protocols are constantly under development and optimization to improve the quality and reproducibility of HLCs[126].

1.5.2 Co-culture strategy for NAFLD exploration

In vitro models are considered as important tools for the investigation of the molecular mechanisms involved in the pathogenesis of NAFLD. However, simplistic set up, such as mono-culture, is a limit when investigating NAFLD/NASH progression. In the complex architecture of *in vivo* hepatic tissue, the interaction between the different cells type is a common phenomenon. Therefore, a major limiting factor in the development of new NAFLD therapies

is the absence of models that capture the unique cellular structure of the liver microenvironment and recapitulate the complexities of steatosis progression to NASH. Indeed, Kupffer cells (KC) contribute to hepatic inflammation and promote fibrosis through the activation of hepatic stellate cells (HSC). Thus, co-culture of hepatocytes with HSCs or/and Kupffer cells allows a better maintenance of specific liver functions and reproduces more accurately the biochemical response to fat accumulation with an elevation of inflammatory and profibrotic markers[129–132]. Nevertheless, very few models of co-culture between the liver and organs involved in metabolic syndrome have been developed. Thus, there is a real need to create these systemic models that the emergence of engineering techniques will help to fill.

1.5.3 3D static engineering strategies for NAFLD exploration

In vitro models represent the most pertinent alternative for studying NAFLD as a result of increasing sophistication and the ability to recapitulate several hallmarks of the disease. A systematic review indicated that researchers predominantly favoured 2D monocultures (59.4%) to more complex models (2D co-cultures (14%), spheroids (9.7%), organoids (7.3%), liver-on-a-chip (7.8%), collagen gel sandwiches (1.2%), and micropatterned cultures (0.6%). However, they observed an increasing trend in the publication of 3D *in vitro* models, specifically in on-chip cultures suggesting that 3D culture systems are more relevant in this field[133].

1.5.3.1 Collagen-gel sandwich culture

Hepatocytes sandwich culture is a 3D culture model in which cells are seeded between two layers of collagen gel. This configuration better mimics the *in vivo* conditions, as demonstrated by reorganization of the cytoskeleton, improved morphology and polarity, and enhanced expression of liver-specific functions compared with monolayer cultures[133,134]. A key strength of sandwich cultures is their formation of bile canaliculi network, which opens possibilities to study biliary transport and excretion[135,136]. This model can also be used for co-culture. For instance, Bale *et al.*[137] mimicked the liver lobular architecture by combining hepatocytes with LSEC, and showed stable secretion and metabolic activity for up to 4 weeks[137]. Nevertheless, collagen gel sandwich presented limitations such as cell dedifferentiation when using PHH, lower sensitivity to long-term exposure to hepatotoxic

compounds and cell-cell interactions perturbance due to the collagen thickness. Thereby, this model is rarely used to investigate NAFLD[138].

1.5.3.2 Spheroids/ organoids

As an alternative to sandwich cultures, hepatocytes can be cultured as spheroids and organoids. These models have become the most commonly 3D *in vitro* models used for investigate NAFLD.

Hepatic spheroids are aggregates of hepatocytes formed by spontaneous self-aggregation in the presence or absence of an ECM. In this configuration hepatocytes retain their cell-cell contacts, viability and mature phenotype. Moreover, compared to conventional 2D culture, PHH spheroids does not result in cell dedifferentiation and significant alterations of metabolic activity and signaling pathways even after 5 weeks of cultivation[139]. Hepatic spheroids can be cocultured with NPCs, including Kupffer, stellate and endothelial cells to form liver spheroids organoids. Such coculture was shown to enhance hepatic functions, as indicated by increased expression of albumin, apolipoprotein B, CYP3A4[140] and allows mimicking pathologies that involve a dysfunctional interplay between cell types, such as NAFLD[141,142]. We can conclude that the 3D spheroid system is metabolically stable and constitutes a suitable model for *in vitro* studies of long-term.

Organoids are new research tools, which are defined as a 3D structure capable of self-organisation which must mimic the functionality and architecture of an organ[143]. Liver organoids are obtained through isolation and expansion of stem and progenitor cells from hepatic stem cell niches to form small self-organizing 3D structures which able to recapitulate functional and structural features of the native liver[144]. In addition, organoids can undergo extensive expansion and culture and maintain their genomics stability, making long-term storage and high-throughput screening possible. Thus, they can provide a more accurate model of human development and disease than animal models do[143]. However, cell differentiation remains sometimes incomplete, and cell organization is random, which leads to a lack of reproducibility. Methods and techniques still need further improvement to reach a complete differentiation and a standardized architecture of the organoids. Despite this, several papers have demonstrated the usefulness of organoids for the study of NAFLD[145–147].

For instance, to mimic steatosis Ramli *et al.*[46] incubated the mature organoids with a cocktail of FFA. After 4 days, the FFA-organoids readily built up lipid droplets that are evident by staining[146].

1.5.3.3 Scaffold-based strategy

Biomaterials-based scaffolds have many different functions in the field of tissue engineering. They are applied as space filling agents, as delivery vehicles for bioactive molecules, and also as 3D structures that allow cell organization and differentiation[148].

Hydrogels are an appealing biomaterial because they are structurally similar to the extracellular matrix of many tissues[149]. Hydrogel can be used to encapsulate liver cells to form the bioink required for 3D bioprinting. Indeed, this emerging technology allows cells to be manipulated and assembled into a specific structure using biomaterials[150]. By forming scaffolds, cell behaviour and functions can be studied and cell-cell or cell-matrix interactions can be investigated. In addition, bioinks have been developed to ensure the long-term maintenance of cell viability and functions such as albumin[151].

On the other hand, hydrogels allow structural support to create an appropriate environment for cell loading and tissue development, ultimately promoting liver regeneration. In this idea, Kumar *et al.*[152] have developed a liver model for NASH and fibrosis using a defined hydrogel microenvironment, termed hepatocyte maturation (HepMat) gel, that supports maturation and maintenance of Hepatocytes like-cells and NPC-like cells for at least one month[152]. Despite the advantages of scaffold-based culture, problems with controlling pore size and porosity, large batch-to-batch variations upon isolation from biological tissues and poor biomechanical strength have been observed.

1.5.4 Limitations

Despite their potential for modelling the disease, the 3D *in vitro* models currently used to mimic NAFLD do not provide a representative model. One of the major drawbacks of the static 3D culture is the lack of representation of the liver microenvironment. Indeed, hepatocytes zonation in the liver may play an important role in NAFLD development and progression, as lipids have been shown to have distinct zonal distributions[153] which may become dysregulated in NASH[154]. However, hepatocyte zonation is difficult to mimic under

static condition, as a medium flow is required to create a nutrient and gas gradient[155]. Furthermore, as we know NAFLD is strongly correlate with IR/T2DM, thus, is essential to develop multi-organ system mimicking both liver and pancreas in order to highlight the kinetic crosstalk and identify novel companion biomarkers of NAFLD progression or regression. Thus, organ-on-a-chip technology could overcome these drawbacks to obtain reliable *in-vitro* models of NAFLD.

1.6 Organ-on-chip technology for NAFLD and T2DM exploration

Organ-on-chip (OoC) is defined by Bathia and Ingber as a microfluidic device dedicated to living cell cultures in continuously perfused micro-chambers in order to reproduce the behaviours and microenvironment of *in vivo* tissues and organs. An OoC system is composed of three essentials elements: i) a microfluidic device, most commonly based on glass or polymeric material, with microchannels for medium perfusion and microchambers for cell culture; ii) living cells or tissues; iii) microfluidic flow providing culture medium for the cells/tissues.

1.6.1 Liver-on-chip model for NAFLD exploration

Despite their considerable advantages over traditional 2D culture models, a major drawback of static 3D culture model is the lack of several key features such as shear stress, zonation, nutrient/gas exchange, waste/toxins removal and multiple cell/organ co-culture. For overcoming these limitations, organ-on-chip approaches have been adopted to model the liver microenvironment. Furthermore, microfluidic devices also represent a solid support from live cell microscopy, high-content analysis (HCA), and computational modeling, which constitute powerful tools for cell analysis.

In this context, Leclerc *et al.*, have developed a PDMS based liver on-chip system composed of cell culture microchambers interconnected by microchannels. Liver functions and metabolism studies were performed on perfusion cultures of human liver cell lines, primary human cells or hiPSC. These models revealed the presence of liver zonation markers and an improved metabolic profile, particularly in terms of albumin production and EMX activity, compared to static culture models. Moreover, they allowed to predict human

hepatotoxicity by identifying biomarkers and metabolic signatures in response to xenobiotics such as paracetamol and pesticides[156–158].

In the last decade, a considerable number of liver-on-a-chip models have been developed. Among the first models developed for study NAFLD, the one by Gori and his colleagues stands out[159]. They attempted to mimic the architecture and microvasculature of the liver by growing HepG2 cells in parallel microchannels mimicking the endothelial barrier. The chip enabled gradual and lower intracellular lipid accumulation, higher hepatic cell viability and minimal oxidative stress in microfluidic dynamic vs 2D static cultures, thus mimicking the chronic condition of steatosis observed *in vivo* more closely. More recently, Jellali *et al.*, studied pesticide-induced steatosis profiles using a rat liver-on-a-chip system[160]. Cells were expose with low or high concentration of dichlorodiphenyltrichloroethane (DDT) and permethrin (PMT), two pesticides highly prevalent in the environment which have been associated to dysregulation of liver lipids and glucose metabolisms during 24h. The transcriptomic and metabolomic results suggested a dose-dependent effect of the two pesticides and reflected liver inflammation, steatosis, necrosis, PPAR signaling and fatty acid metabolism.

Furthermore, coculture liver-on-chip have been developed to explore the evolution of steatosis. For instance, Freag *et al*., describe a NASH-on-a-chip platform[161]. They cocultured under microfluidic dynamics four main types of human primary liver cells: PHH, Kupffer cells, LSEC, and hepatic stellate cells (HSCs). Their model successfully recapitulated a functional liver cellular microenvironment with stable albumin and urea secretion for at least 2 weeks. Cell exposure to lipotoxic environment led to gradual development of NASH phenotypic characteristics, including intracellular lipid accumulation, hepatocellular ballooning, HSC activation, and elevation of inflammatory and profibrotic markers. Moreover, the model has also shown capabilities for drug screening.

1.6.2 Microfluidics system for T2DM exploration

Although OoC technology generates a suitable microenvironment that reproduces endocrine function, there is less development of the technology for the pancreas than for other tissues or organs, such as the liver, lung, kidney, gut, and heart[34,162]. Pancreas-on-chip

applications for diabetes research can be classified in three groups: islet evaluation, drug research, and the study of islet physiology and function[163]. To mimic the *in vivo* physiology and functionality of native islets as much as possible, pancreas-on-chip models are developed using cultures of islets, or cells aggregated into spheroids (pseudo-islets). The pseudo-islet approach makes it possible to engineer uniform, small-sized spheroids (< 150 µm), which enhance oxygen and nutrients diffusion, viability and functionality when compared to native islets (heterogenous size 50-400 µm)[164,165]. Pseudo-islets can be engineered by aggregating β-cells line, iPSC-derived β-cells or primary β-cells obtained after islet dissociation[166]. To maintain the islets/pseudo-islets under flow inside the microfluidic biochip, trapping microstructures fabricated in the microchambers of the device are use. Micro-wells with different geometries (flat, pyramidal and concave) are the most commonly used designs for islets trapping[164,167–169]. Islets can also be immobilised using crescent-shaped structures[170], mesh systems[171], nozzle systems, or channel reduction[172–174], and other constructions involving hydrodynamic trapping principles[162,175].

In this framework, Essaouiba et *al.,* developed a microfluidic biochip composed of 600 micro-wells for assessment of rat islets and showed that biochip culture improves the viability and expression of pancreatic genes[176]. To improve their results, Essaouiba *et al., d*eveloped another microfluidic biochip composed of crescent-shapes structure allowing to culture β-cells spheroids derived from hiPSC. Those pseudo-islets were created by using the honeycomb technology developed by Shinohara *et al*., which is a 24-well plate containing 8000 polygons made of PDMS and with the geometric characteristics of 126µm width and 129µm depth. After 4 days of culture in the honeycombs, the formed spheroids were collected and seeded in biochips. Results shown that microfluidic culture contributed to increasing pancreatic maturation by improving C-peptide and insulin secretion levels when compared to 2D culture[170]. In a different strategy, islets were cocultured with mesenchymal stem cells (MSCs) to investigate the viability and preservation of islet functions. MSCs have been shown to secrete several paracrine molecules, which mediate trophic effects on neighbouring cells[177].

1.6.3 Multi-organ-on-chip

As previously described (section 2.3) there is an intricate correlation between T2DM and NAFLD. Thus, to understand the biological processes and develop therapeutic strategies

for NAFLD and T2DM, scientists conventionally used *in vivo* models because of the complexity and integrated multi-organ responses they confer[133]. However, these models tended to fail due to the phylogenetic distance between humans and animals, and their use has been limited for ethical reasons[34,178]. Different researchers have been focused on this subject and have tried to develop culture systems that combine different organs to reproduce NAFLD[152,179,180] (Figure 1.13). The most recent innovation is to use organ-on-chip technology to reproduce the behaviour of a group of organs. The idea is to combine different cell types in different culture compartments (each compartment mimicking a specific microphysiological condition) and connect them through microfluidic channels to mimic and ensure the cross-talk between two or more organs[181]. Most of the time, multi-organ-on-chip tries to faithfully emulate the *in vivo* environment and interactions between organs. The implied signalling pathways create synergic effects on cells which enhance their functions compared to monocultured cells[182].

Nowadays only a few studies have focused on the liver and its interactions with the pancreas to produce a liver-pancreas multi-organ-on-chip. Recent works have demonstrated the potential for OoC technology to ensure pancreatic islet-liver crosstalk. Bauer *et al.,* designed a two-organ-chip system to ensure the dynamic culture of human pancreatic islets and liver spheroids composed of the HepaRG cell line and primary human stellate cells[183]. The aim of their study was to develop a reliable human T2DM model. They observed an increase and a conservation of insulin secretion which supported stabilisation of the homeostatic state when comparing the co-culture condition with the monoculture. In addition, they confirmed that islet microtissues lose their function after being subjected to prolonged hyperglycaemia. In another approach, Essaouiba *et al.,* used a perfusion loop with two biochips hosting primary hepatocytes and rat islet to investigate the interaction between the organs compared with monoculture conditions[184] . They proved that co-culturing pancreatic cells with hepatocytes helped to recover hepatic functions (compared to the hepatic monoculture without insulin) and modified the expression of the genes involved in insulin/glucagon homeostasis.

Integrating MOoC has always been a challenging goal because of the optimisations that must be taken into consideration to allow optimal culture of all the cell types involved in the system. Lee *et al.* developed a pancreas-muscle-liver OoC, given the relation that links these 3 organs[185]. Indeed, *in vivo*, the muscle is responsible for the most important glucose uptake

of the body. As a consequence, signalling pathways are activated in the pancreas to produce glucagon, and start glucose production in the liver (gluconeogenesis and glycogenolysis) and the clearance of insulin[186]. In addition to the experimental results obtained from glucose metabolism stimulation, the combination of the multi-organ-on-chip led to the construction of a mathematical model describing time-dependent concentration changes in glucose and insulin. In the same idea, Casas *et al.*,[187] developed an integrated experimental-computational approach to analyse a liver-islet MOoC. They co-cultured liver spheroids and pancreatic islets using the HUMIMC Chip2 from TissUse® then investigated the behavior of the system under hypoglycemia and hyperglycemia. Their computational model was able to translate the experimental results to humans when comparing with published data of the glucose response to a meal in healthy subjects. Thus, they created a model allowing to integrate and quantitatively analyse experimental data in order to improve their mechanistic interpretation, generate model predictions and, ultimately, extrapolate the results from *in vitro* to *in vivo*[187].

Despite the potential that these approaches offer for reproducing the multi-organ interactions implied in T2DM and NAFLD, several limitations are encountered in reference to the optimisations needed to ensure the optimal culture of the different cells, vascularisation of the organs, which has not yet been mastered, and standardisation of the materials and cells in the models used which causes variabilities that could impact results[188].

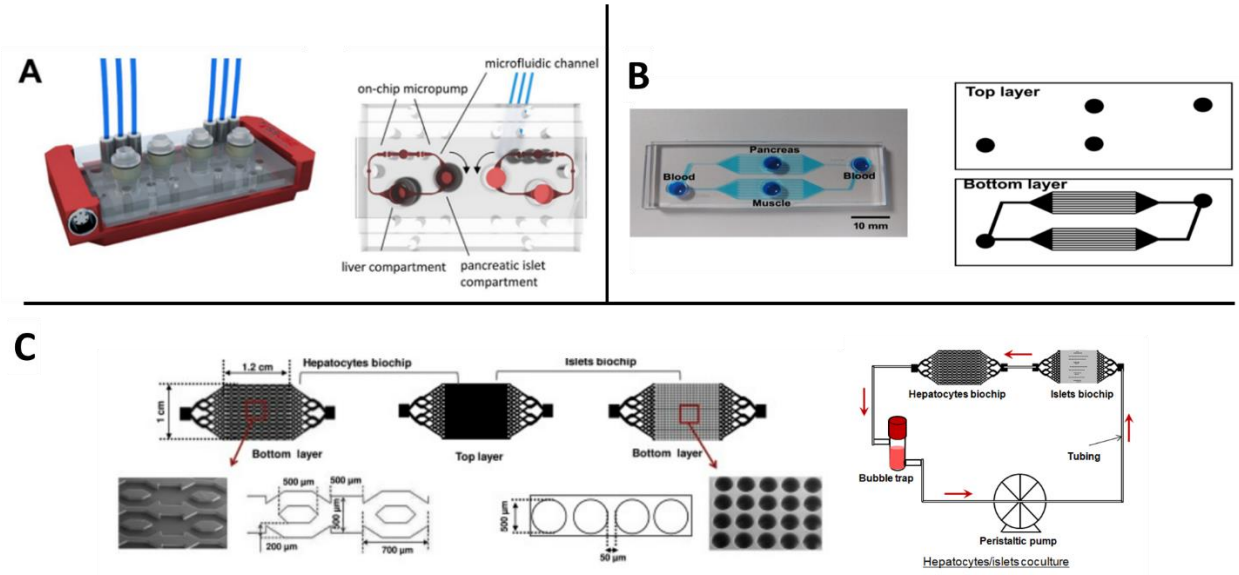

Figure 1. 13: *Multi-organ-on-chip systems developed to study T2DM (**A**: Bauer et al.,2017; **B:** D. W. Lee et al.,2019; **C**: Essaouiba et al.,2020).*

1.7 Metabolomic analysis in NAFLD investigation

Metabolomics, a pivotal discipline within omics sciences, is dedicated to the comprehensive study of small molecules, known as metabolites, present in biological systems. This approach allows for the deciphering of the metabolic profile of a given biological sample (such as serum and urine), providing a detailed insight into the metabolic state of an organism, cell, or tissue[189].

1.7.1 Principle of metabolomics

Current metabolomics research can be divided into two complementary methodologies: targeted and untargeted approaches. The targeted approach concentrates on examining particular groups of metabolites linked to specific metabolic pathways or classes of compounds. In contrast, the untargeted approach involves a comprehensive analysis of metabolic alterations in response to factors such as disease, environmental factors, or genetic disruptions. Typically, the untargeted approach is used for hypothesis generation, which is subsequently followed by targeted profiling to ensure more precise quantification of relevant metabolites[190].

To conduct metabolomic analysis, a series of sophisticated analytical techniques are employed. Among the most commonly used methods are mass spectrometry (MS) and nuclear magnetic resonance (NMR). MS accurately measures the mass of metabolites and identifies their molecular structure, while NMR provides information on the structure and concentration of metabolites based on their magnetic properties. These techniques are complemented by separation methods such as liquid or gas chromatography coupled with mass spectrometry (LC-MS and GC-MS), which isolate complex metabolites in biological samples[190,191]. Once the samples have been processed, the raw data is generated using bioinformatics analysis. Various algorithms and software tools are employed to process this raw data, transforming it into a two-dimensional data matrix that encompasses measurements of different metabolites present in the samples. Following the processing of raw data and the acquisition of the data matrix, various statistical analyses are conducted to identify metabolites that exhibit significant differences between the groups under comparison. In many cases, the determination of statistical significance relies on the p-value.

Therefore, by combining analytical and bioinformatics approaches, metabolomics offers a unique window into metabolism, paving the way for the discovery of biomarkers, understanding metabolic responses to stimuli and diseases, and significant applications in personalized medicine, biomedical research, and systems biology[192].

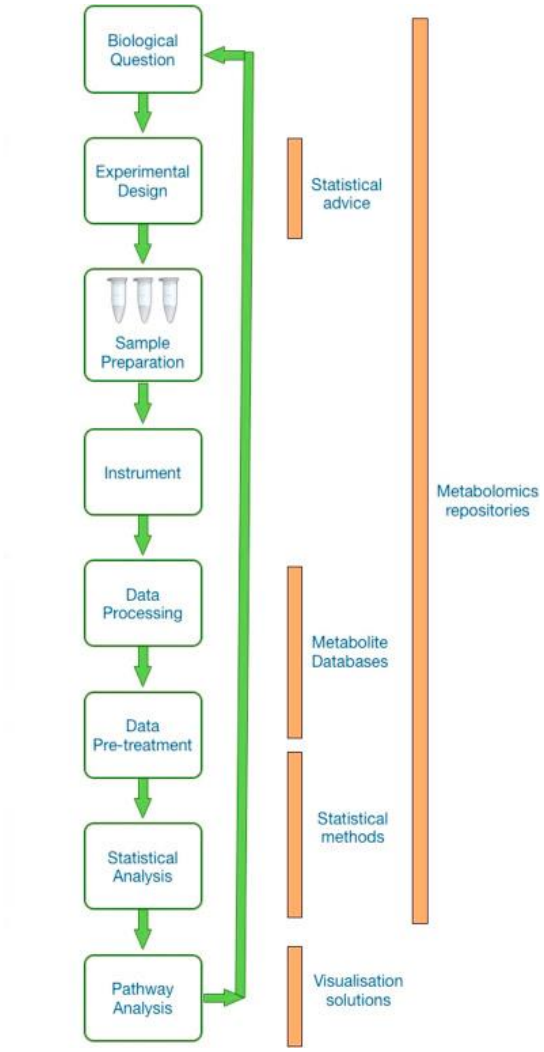

Figure 1. 14: *Metabolomic experimental workflow (adapted from Dayalan et al., 2019).*

1.7.2 Metabolomics research for NAFLD investigations

Perturbations in metabolism are a key characteristic feature of fatty liver disorder. Therefore, several studies have been conducted to explore the circulating biomarkers following NAFLD. Thus, an efficient way to identify the metabolites altered in the circulation is by using the metabolomics approach[193]. Most of the studies relies on metabolomics or lipidomics on serum, urine and saliva although their objectives are not similar. Indeed, considerable interest now lies in the discovery and development of novel non-invasive

biomarkers of NAFLD. Gaggini *et al.,* and Grzych *et al*., highlighted the importance of circulating amino acids, especially branched-chain amino acids (BCAA) and aromatic amino acids (AAA), as non-invasive biomarkers for assessing NAFLD severity[194–196].

Lack of effective early diagnostic tools for NAFLD is a problem for proper therapy. Therefore, metabolomics has been introduced as a way to perform early detection[197]. In a study by Zhou *et al*.,[198] a prediction model was developed and validated, consisting of aspartate aminotransferase (AST), insulin, and patatin-like phospholipase domain-containing-3 (PNPLA3) genotype, achieving an area under the ROC curve (AUROC) of 0.778 for the identification of NASH (NASH Clinical Score). This model then incorporated metabolomics-based markers such as glutamate, glycine, isoleucine, lysophosphatidylcholine (LysoPC 16:0), and phosphatidylethanolamine (PE 40:6), resulting in the NASH ClinLipMet Score model, which showed improved differentiation between NASH and non-NASH, with an AUROC of 0.866, a sensitivity of 85%, and a specificity of 72%[198]. Other studies have also developed diagnostic algorithms based on metabolites, including serum triglycerides and amino acids, to differentiate NASH from NAFL. Indeed, Caussy *et al*., explored plasma eicosanoids in relation to liver fibrosis, as well as metabolomics models to diagnose NASH and/or fibrosis[199]. As NAFLD progression lead to cirrhosis then hepatocellular carcinoma (HCC), investigations of these late stages were performed on serum, biopsies and faeces. Few studies suggested that the cirrhotic liver has an impaired ability to metabolize both protein and d-amino acids and gut flora alteration highlighted by an increase of major lysophosphatidylcholine (16:0, 18:0, 18:1, 18:2)[200]. Moreover, Cassim *et al.,* identified that an increase expression of glycolytic and hypoxia signaling pathway was associated with decreased survival in HCC patients[201].

In the last 20 years, NAFLD became the fastest growing indication for liver transplantation. Unfortunately, patient with NAFLD present a higher risk of failure of donor graft and mortality[202]. Some reports have shown benefits of using metabolic approaches after a transplantation. Serkova et *al.,* identified six metabolites, on 48 analysed metabolites, as consistent markers of a non-functional liver graft. Importantly, this distinctive metabolic profile was present as early as two hours after transplantation when no other variable or conventional laboratory tests indicated poor graft function[203]. Therefore, metabolomics profiling can be an additional tool in clinical decision making[204].

1.7.3 Metabolomics analyses for *in-vitro* models

Most of metabolomics studies which related to biological and health research have been conducted on body fluids, especially plasma, serum and urine. Nevertheless, it is important to highlight that not all biological inquiries can be fully addressed through the analysis of body fluids. Indeed, factors like diet, body mass index (BMI), age, and gender, can introduce confounding variables that might contribute to noise rather than enhancing the clarity of metabolic signatures. In such cases, additional metabolomics applications, such as those involving *in-vitro* experiments, can serve as valuable complements to data obtained from biological fluids[205]. Thus, metabolomics in cultured cells represents an advantage for elucidating mechanisms in many areas of research such as pharmacology, toxicology, stem cell research, oncology and systems biology. Nevertheless, in order to obtain reliable and reproducible results some aspects should be taken into consideration[206].

An adequate metabolomic study in cultured cells involves the following steps: (i) study design, (ii) cell culture growth with cell treatment, (iii) quenching of cell metabolism and extraction of the metabolites, (iv) metabolomics measurement, and (v) data processing and analyses[205]. Standardization of every step of this process is mandatory in order to avoid significant variations in outcomes. According to the biological question the endo-metabolome, the exo-metabolome, or both (endo and exo-metabolome) can be studied. The endo-metabolome is defined as all the metabolites within the cells while the exo-metabolome is the result of an interchange of metabolites between the cells and the culture medium. Therefore, its composition reflects the metabolic activity of cells and varies in response to perturbations without cells disruption.

Studying the exo-metabolome allows to monitoring metabolic changes over time and provide valuable insights into cell physiology, cell-cell communication, and the broader ecosystem. Intercellular communication is a complex network whose elucidation is essential to understand disease onset and progression in heterogenous tissue. Thus, characterization of signalling molecules in co-culture system using metabolomic approaches have been achieved in multiple studies. For instance, Chen *et al*., explored the influence of drug-resistant cells on drug-sensitive by measuring cellular exo-metabolites in a direct and indirect co-culture system[207]. In the other hand, metabolomic has received an increasing attention for drug and

chemical toxicity. As the liver is the metabolic and biotransformation centre of the human body, several studies have been conducted on drug-induced liver injury (DILI) using metabolomics. In this purpose, Ramirez *et al.*, predicted the liver toxicity of 35 substances using metabolomic in HepG2-based system[208]. Furthermore, metabolomics approaches have been recently used for the detection of early disease-related biomarkers and altered metabolic pathways, especially in liver disease[209]. Kozyra *et al.,* investigated steatosis and insulin resistance using lipidomic analyses on a PHH 3D spheroids model and highlighted an upregulation of the diglycerides, the free fatty acids as well as the triglycerides pathway[210].

1.8 References

1 S. R. Z. Abdel-Misih, M. Bloomston and H. Bismuth, *Surg Clin North Am*. 2010, **90(4)**, 643-53.

2 A. Kalra, E. Yetiskul, C. J. Wehrle and F. Tuma, *Physiology, Liver*, StatPearls, 2023.

3 S. Kalra and Y. Gupta, *Diabetes Therapy*, 2016, **7**, 1–9.

4 C. Berger, D. Zdzieblo*, Pflugers Arch*, 2020, **472(9)**, 1249-1272.

5 M. Komatsu, M. Takei, H. Ishii and Y. Sato, *J Diabetes Investig*, 2013, **4**, 511–516.

6 Y. Wang, J. F. Lo, J. E. Mendoza-Elias, A. F. Adewola, T. A. Harvat, K. P. Kinzer, D. Lee, M. Qi, D. T. Eddington and J. Oberholzer, *Bioanalysis*, 2010, **2**, 1729–1744.

7 H. S. Han, G. Kang, J. S. Kim, B. H. Choi and S. H. Koo, *Exp Mol Med*, 2016, **48**, e218.

8 C. Y. Park and S. N. Han, in *The Molecular Nutrition of Fats*, ed. V.B. Patel, Elsevier Inc, 2028, chapter 8, 103-116.

9 A. G. Linden, S. Li, H. Y. Choi, F. Fang, M. Fukasawa, K. Uyeda, R. E. Hammer, J. D. Horton, L. J. Engelking and G. Liang, *J Lipid Res*, 2018, **59**, 475–487.

10 J. D. Horton, J. L. Goldstein and M. S. Brown, *J Clin Invest*, 2002, **109**, 1125.

11 F. Ameer, L. Scandiuzzi, S. Hasnain, H. Kalbacher and N. Zaidi, *Metabolism*, 2014, **63**, 895–902.

12 P. Nguyen, V. Leray, M. Diez, S. Serisier, J. Le Bloc'H, B. Siliart and H. Dumon, *J Anim Physiol Anim Nutr (Berl)*, 2008, **92**, 272–283.

13 S.M Houten, S. Violante, F.V Venture, R.J.A Wanders, *Annual Review of Physiology*, 2016, **78**, 23-44.

14 E.S. Selen, J. Choi, M.J Wolfgang, *JCI Insight*, 2021, **6(2)**, e135626.

15 R. Catanzaro, B. Cuffari, A. Italia and F. Marotta, *World J Gastroenterol*, 2016, **22**, 7660.

16 K. G. M. M. Alberti and P. Z. Zimmet, *Diabetic Medicine*, 1998, **15**, 539–553.

17 F. Azizi, P. Salehi, A. Etemadi and S. Zahedi-Asl, *Diabetes Res Clin Pract*, 2003, **61**, 29–37.

18 E. RH, G. SM and Z. PZ, *Lancet*, 2005, **365**, 1415–1428.

19 M.-A. Cornier, D. Dabelea, T. L. Hernandez, R. C. Lindstrom, A. J. Steig, N. R. Stob, R. E. Van Pelt, H. Wang and R. H. Eckel, 2008, **29(7)**, 777-822.

20 E. Kassi, P. Pervanidou, G. Kaltsas and G. Chrousos, *BMC Med*, 2011, **9**, 48.

21 G. A. and G. V., *Biosci Trends*, 2010, **4**, 204–212.

22 M. P. Czech, *Nat Med*, 2017, **23**, 804–814.

23 H. E. Lebovitz, *Experimental and Clinical Endocrinology & Diabetes*, 2001, **109**, 135–148.

24 A. F. Pina, D. O. Borges, M. J. Meneses, P. Branco, R. Birne, A. Vilasi and M. P. Macedo, *Front Cell Dev Biol*, 2020, **8**, 519.

25 A. Ighbariya and R. Weiss, *J Clin Res Pediatr Endocrinol*, 2017, **9**, 49.

26 Y. Rochlani, N. V. Pothineni, S. Kovelamudi and J. L. Mehta, *Ther Adv Cardiovasc Dis*, 2017, **11**, 215.

27 E. Maillard and S. Sigrist, in *Biomaterials for Organ and Tissue Regeneration*, Elsevier, 2020, 299–333.

28 World Health Oorganization (WHO) Official Web Site.

29 IDF Diabetes Atlas 9th edition 2019, https://www.diabetesatlas.org/en/, (accessed 22 May 2021).

30 P. Saeedi, I. Petersohn, P. Salpea, B. Malanda, S. Karuranga, N. Unwin, S. Colagiuri, L. Guariguata, A. A. Motala, K. Ogurtsova, J. E. Shaw, D. Bright and R. Williams, *Diabetes Res Clin Pract*, 2019, **157**, 107843.

31 P. Saeedi, P. Salpea, S. Karuranga, I. Petersohn, B. Malanda, E. W. Gregg, N. Unwin, S. H. Wild and R. Williams, *Diabetes Res Clin Pract*, 2020, **162**, 108086.

32 K. Papatheodorou, M. Banach, E. Bekiari, M. Rizzo and M. Edmonds, *J Diabetes Res*, 2018.

33 J. L. Harding, M. E. Pavkov, D. J. Magliano, J. E. Shaw and E. W. Gregg, *Diabetologia,* 2019, **62**, 3–16.

34 J. Rogal, A. Zbinden, K. Schenke-Layland and P. Loskill, *Adv Drug Deliv Rev*, 2019, **140**, 101–128.

35 Z. Punthakee, R. Goldenberg and P. Katz, *Can J Diabetes*, 2018, **42**, S10–S15.

36 S. Szunerits, S. Melinte, A. Barras, Q. Pagneux, A. Voronova, A. Abderrahmani and R. Boukherroub, *Chem Soc Rev*, 2021, **50**, 2102–2146.

37 R. A. DeFronzo, E. Ferrannini, L. Groop, R. R. Henry, W. H. Herman, J. J. Holst, F. B. Hu, C. R. Kahn, I. Raz, G. I. Shulman, D. C. Simonson, M. A. Testa and R. Weiss, *Nat Rev Dis Primers*, 2015, **1**, 1–22.

38 D. Tripathy and A. O. Chavez, *Curr Diab Rep*, 2010, **10**, 184–191.

39 U. Galicia-Garcia, A. Benito-Vicente, S. Jebari, A. Larrea-Sebal, H. Siddiqi, K. B. Uribe, H. Ostolaza and C. Martín, *Int J Mol Sci*, 2020, **21**, 1–34.

40 P. A. Halban, K. S. Polonsky, D. W. Bowden, M. A. Hawkins, C. Ling, K. J. Mather, A. C. Powers, C. J. Rhodes, L. Sussel and G. C. Weir, *Diabetes Care*, 2014, **37**, 1751–1758.

41 F. Engin, *J Investig Med*, 2016, **64**, 2.

42 D. Raleigh, X. Zhang, B. Hastoy and A. Clark, *J Mol Endocrinol*, 2017, **59**, R121–R140.

43 A. F. Adewola, Y. Wang, T. Harvat, D. T. Eddington, D. Lee and J. Oberholzer, *Journal of Visualized Experiments*, 2010, **35**, e1649.

44 A. A. Christensen and M. Gannon, *Curr Diab Rep*, 2019, **19(9)**, 81.

45 G.C. Weir, D.R. Laybutt, H. Kaneto, S. Bonner-Weir and A. Sharma, *Diabetes*, 2001, **50**.

46 C. J. Nolan and M. Prentki, *Diab Vasc Dis Res*, 2019, **16**, 118–127.

47 L. I. Hudish, J. E. B. Reusch and L. Sussel, *J Clin Invest*, 2019, **129**, 4001.

48 R. A. DeFronzo, *Diabetes Care*, 2011, **34**, 789–794.

49 J. Osório, *Nature Reviews Endocrinology 2012 8:3*, 2012, **8**, 128–128.

50 H. Staiger, E. Schaeffeler, M. Schwab and H. U. Häring, *Review of Diabetic Studies*, 2015, **12**, 363–376.

51 Feingold KR, Anawalt B, Blackman MR, Boyce A, Chrousos G, Corpas E, de Herder WW, Dhatariya K, Dungan K, Hofland J, Kalra S, Kaltsas G, Kapoor N, Koch C, Kopp P, Korbonits M, Kovacs CS, Kuohung W, Laferrère B, Levy M, McGee EA, McLachlan R, New M, Purnell J, Sahay R, Shah AS, Singer F, Sperling MA, Stratakis CA, Trence DL, Wilson DP, editors, *Endotext* [Internet] .

52 S. Srinivasan, S. W. Yee and K. M. Giacomini, *Pharmacogenetics of Antidiabetic Drugs*, 2018, **83**, 361-389.

53 M. Foretz and B. Viollet, *J Hepatol*, 2011, **54**, 827–829.

54 E. Sanchez-Rangel and S. E. Inzucchi, *Diabetologia 2017 60:9*, 2017, **60**, 1586–1593.

55 C. C. J. Dekkers, R. T. Gansevoort and H. J. L. Heerspink, *Curr Diab Rep*, 2018, **18(5)**, 27.

56 M. J. Pereira and J. W. Eriksson, *Drugs*, 2019, **79**, 219–230.

57 D. Raccah, *Diabetes Metab*, 2017, **43**, 110–124.

58 A. Cahn, R. Miccoli, A. Dardano and S. Del Prato, *Lancet Diabetes Endocrinol*, 2015, **3**, 638–652.

59 Pablo Aschner, *US Endocrinol*, 2013, **9**, 6–12.

60 P. K. Santhekadur, D. P. Kumar and A. J. Sanyal, *J Hepatol*, 2018, **68**, 230–237.

61 Z. M. Younossi, *J Hepatol*, 2019, **70**, 531–544.

62 R. C. R. Meex and M. J. Watt, *Nature Reviews Endocrinology 2017 13:9*, 2017, **13**, 509–520.

63 M. C. S. Wong, J. L. W. Huang, J. George, J. Huang, C. Leung, M. Eslam, H. L. Y. Chan and S. C. Ng, *Nat Rev Gastroenterol Hepatol*, 2019, **16**, 57–73.

64 Z. Younossi, F. Tacke, M. Arrese, B. Chander Sharma, I. Mostafa, E. Bugianesi, V. Wai-Sun Wong, Y. Yilmaz, J. George, J. Fan and M. B. Vos, *Hepatology*, 2019, **69**, 2672–2682.

65 H. Tilg and A. R. Moschen, *Hepatology*, 2010, **52**, 1836–1846.

66 H. Malhi and G. J. Gores, *Semin Liver Dis*, 2008, **28**, 360.

67 B. A. Neuschwander-Tetri, *Hepatology*, 2010, **52**, 774–788.

68 N. Mendez-Sanchez, V. C. Cruz-Ramon, O. L. Ramirez-Perez, J. P. Hwang, B. Barranco-Fragoso and J. Cordova-Gallardo, *Int J Mol Sci*, 2018, **19(7)**, 2034.

69 C. D. Byrne and G. Targher, *J Hepatol*, 2015, **62**, S47–S64.

70 G. Targher, K. E. Corey, C. D. Byrne and M. Roden, *Nature Reviews Gastroenterology & Hepatology 2021 18:9*, 2021, **18**, 599–612.

71 C. P. Day and O. F. W. James, *Gastroenterology*, 1998, **114**, 842–845.

72 J. K. Dowman, J. W. Tomlinson and P. N. Newsome, *Qjm*, 2009, **103**, 71–83.

73 E. Buzzetti, M. Pinzani and E. A. Tsochatzis, *Metabolism*, 2016, **65**, 1038–1048.

74 W. Peverill, L. W. Powell and R. Skoien, *International Journal of Molecular Sciences 2014, Vol. 15, Pages 8591-8638*, 2014, **15**, 8591–8638.

75 I. Pierantonelli and G. Svegliati-Baroni, *Transplantation*, 2019, **103**, E1–E13.

76 C. P. Day, *Bailliere's Best Practice and Research in Clinical Gastroenterology*, 2002, **16**, 663–678.

77 A. A. Kolodziejczyk, D. Zheng, O. Shibolet and E. Elinav, *EMBO Mol Med*, 2019, **11**, 1–13.

78 S. L. Friedman, B. A. Neuschwander-Tetri, M. Rinella and A. J. Sanyal, *Mechanisms of NAFLD development and therapeutic strategies*, 2018, **24**.

79 X. Wang, X. Fu, C. Van Ness, Z. Meng, X. Ma and W. Huang, *Curr Pathobiol Rep*, 2013, **1**, 29–35.

80 A. Lade, L. A. Noon and S. L. Friedman, *Curr Opin Oncol*, 2014, **26**, 100.

81 D. Schuppan, R. Surabattula and X. Y. Wang, *J Hepatol*, 2018, **68**, 238–250.

82 M. Papatheodoridi and E. Cholongitas, *Curr Pharm Des*, 2019, **24**, 4574–4586.

83 J. Maurice and P. Manousou, *Clinical Medicine*, 2018, **18**, 245.

84 L. Castera, H. L. Yuen Chan, M. Arrese, N. Afdhal, P. Bedossa, M. Friedrich-Rust, K. H. Han and M. Pinzani, *J Hepatol*, 2015, **63**, 237–264.

85 S. Mueller and L. Sandrin, *Hepat Med*, 2010, **2**, 49.

86 H. Xiao, M. Shi, Y. Xie and X. Chi, *PLoS One*, 2017, **12**, 1–14.

87 L. Castera, M. Friedrich-Rust and R. Loomba, *Gastroenterology*, 2019, **156**, 1264-1281.e4.

88 S. Treeprasertsuk, E. Björnsson, F. Enders, S. Suwanwalaikorn and K. D. Lindor, *World Journal of Gastroenterology: WJG*, 2013, **19**, 1219.

89 V. A. Piazzolla and A. Mangia, *Cells*, 2020, **9(4)**, 1005.

90 K. Lee, E. S. Jung, E. Yu, Y. K. Kang, M. Y. Cho, J. M. Kim, W. S. Moon, J. S. Jeong, C. K. Park, J. B. Park, D. Y. Kang, J. H. Sohn and S. Y. Jin, *J Pathol Transl Med*, 2020, **54**, 228.

91 W. Liang, A. L. Menke, A. Driessen, G. H. Koek, J. H. Lindeman, R. Stoop, L. M. Havekes, R. Kleemann. and A. M. Van Den Hoek, *PLoS One*, 2014**, 9(12)**, e115922.

92 M. S. Mundi, S. Velapati, J. Patel, T. A. Kellogg, B. K. Abu Dayyeh and R. T. Hurt, *Nutrition in Clinical Practice*, 2020, **35**, 72–84.

93 M. P. Moore, R. P. Cunningham, R. J. Dashek, J. M. Mucinski and R. S. Rector, *Obesity (Silver Spring)*, 2020, **28**, 1843.

94 K. Promrat, D. E. Kleiner, H. M. Niemeier, E. Jackvony, M. Kearns, J. R. Wands, J. L. Fava and R. R. Wing, *Hepatology*, 2010, **51**, 121–129.

95 E. Vilar-Gomez, Y. Martinez-Perez, L. Calzadilla-Bertot, A. Torres-Gonzalez, B. Gra-Oramas, L. Gonzalez-Fabian, S. L. Friedman, M. Diago and M. Romero-Gomez, *Gastroenterology*, 2015, **149**, 367-378.e5.

96 V. W. S. Wong, R. S. M. Chan, G. L. H. Wong, B. H. K. Cheung, W. C. W. Chu, D. K. W. Yeung, A. M. L. Chim, J. W. Y. Lai, L. S. Li, M. M. M. Sea, F. K. L. Chan, J. J. Y. Sung, J. Woo and H. L. Y. Chan, *J Hepatol*, 2013, **59**, 536–542.

97 S. Raza, S. Rajak, A. Upadhyay, A. Tewari and R. A. Sinha, *Front Biosci (Landmark Ed)*, 2021, **26**, 206.

98 J. S. Soden, M. W. Devereaux, J. E. Haas, E. Gumpricht, R. Dahl, J. Gralla, M. G. Traber and R. J. Sokol, *Hepatology*, 2007, **46**, 485–495.

99 Y. Sumida and M. Yoneda, *J Gastroenterol*, 2018, **53**, 362.

100 G. Lassailly, R. Caiazzo, L. C. Ntandja-Wandji, V. Gnemmi, G. Baud, H. Verkindt, M. Ningarhari, A. Louvet, E. Leteurtre, V. Raverdy, S. Dharancy, F. Pattou and P. Mathurin, *Gastroenterology*, 2020, **159**, 1290-1301.e5.

101 S. Singh, N. A. Osna and K. K. Kharbanda, *World J Gastroenterol*, 2017, **23**, 6549.

102 Q. M. Anstee, B. A. Neuschwander-Tetri, V. W. S. Wong, M. F. Abdelmalek, Z. M. Younossi, J. Yuan, M. L. Pecoraro, S. Seyedkazemi, L. Fischer, P. Bedossa, Z. Goodman, N. Alkhouri, F. Tacke and A. Sanyal, *Contemp Clin Trials*, 2020, **89**, 105922.

103 R. A. Shah and K. V. Kowdley, *Expert Rev Gastroenterol Hepatol*, 2020, **14**, 311–321.

104 R. W. Chapman and K. D. Lynch, *Br Med Bull*, 2020, **133**, 95–104.

105 S. A. Harrison, V. W. S. Wong, T. Okanoue, N. Bzowej, R. Vuppalanchi, Z. Younes, A. Kohli, S. Sarin, S. H. Caldwell, N. Alkhouri, M. L. Shiffman, M. Camargo, G. Li, K. Kersey, C. Jia, Y. Zhu, C. S. Djedjos, G. M. Subramanian, R. P. Myers, N. Gunn, A. Sheikh, Q. M. Anstee, M. Romero-Gomez, M. Trauner, Z. Goodman, E. J. Lawitz and Z. Younossi, *J Hepatol*, 2020, **73**, 26–39.

106 J. M. Hazlehurst, C. Woods, T. Marjot, J. F. Cobbold and J. W. Tomlinson, *Metabolism*, 2016, **65**, 1096.

107 D. Ferguson and B. N. Finck, *Nat Rev Endocrinol*, 2021, **17**, 484.

108 L. Valenti, E. Bugianesi, U. Pajvani and G. Targher, *Liver International*, 2016, **36**, 1563–1579.

109 A. Bovolini, J. Garcia, M. A. Andrade and J. A. Duarte, *Int J Sports Med*, 2021, **42**, 199–214.

110 A. E. Morrison, F. Zaccardi, K. Khunti and M. J. Davies, *Liver International*, 2019, **39**, 557–567.

111 S. Ballestri, S. Zona, G. Targher, D. Romagnoli, E. Baldelli, F. Nascimbeni, A. Roverato, G. Guaraldi and A. Lonardo, *J Gastroenterol Hepatol*, 2016, **31**, 936–944.

112 R. Malik, C. Selden and H. Hodgson, *Semin Cell Dev Biol*, 2002, **13(6)**, 425-431.

113 K. Zeilinger, N. Freyer, G. Damm, D. Seehofer and F. Knöspel, *Exp Biol Med*, 2016, **241**, 1684–1698.

114 N. Hasui, K. Sakaguchi, T. Ogawa, Y. Sakamoto and T. Shimizu, *Sci Rep*, 2022, **12(1)**, 5341.

115 T. Hurrell, V. Kastrinou-Lampou, A. Fardellas, D. F. G. Hendriks, Å. Nordling, I. Johansson, A. Baze, C. Parmentier, L. Richert and M. Ingelman-Sundberg, *Cells*, 2020, **9(4)**, 964.

116 J. Willebrords, I. V. A. Pereira, M. Maes, S. Crespo Yanguas, I. Colle, B. van den Bossche, T. C. da Silva, C. P. M. S. de Oliveira, W. Andraus, M. Vinken, V. A. Alves and B. Cogliati, *Prog Lipid Res*, 2015, **59**, 106.

117 T. B. Andersson, K. P. Kanebratt and J. G. Kenna, *Expert Opin Drug Metab Toxicol*, 2012 **8(7)**, 909-20.

118 S. di Cocco, L. Belloni, A. D. G. Nunn, D. Salerno, S. Piconese, M. Levrero and N. Pediconi, *J Vis Exp*, 2019, **18(149)**.

119 J. Allard, S. Bucher, J. Massart, P. J. Ferron, D. le Guillou, R. Loyant, Y. Daniel, Y. Launay, N. Buron, K. Begriche, A. Borgne-Sanchez and B. Fromenty, *Cell Biol Toxicol*, 2021, **37**, 151–175.

120 T. Pan, N. Wang, J. Zhang, F. Yang, Y. Chen, Y. Zhuang, Y. Xu, J. Fang, K. You, X. Lin, Y. Li, S. Li, K. Liang, Y. Li and Y. Gao, *Stem Cell Res Ther*, 2022, **13**, 159.

121 S. J. Mun, J. S. Ryu, M. O. Lee, Y. S. Son, S. J. Oh, H. S. Cho, M. Y. Son, D. S. Kim, S. J. Kim, H. J. Yoo, H. J. Lee, J. Kim, C. R. Jung, K. S. Chung and M. J. Son, *J Hepatol*, 2019, **71**, 970–985.

122 M. Danoy, M. L. Bernier, K. Kimura, S. Poulain, S. Kato, D. Mori, T. Kido, C. Plessy, H. Kusuhara, A. Miyajima, Y. Sakai and E. Leclerc, *Biotechnol Bioeng*, 2019, **116**, 1762–1776.

123 D. C. Hay, J. Fletcher, C. Payne, J. D. Terrace, R. C. J. Gallagher, J. Snoeys, J. R. Black, D. Wojtacha, K. Samuel, Z. Hannoun, A. Pryde, C. Filippi, I. S. Currie, S. J. Forbes, J. A. Ross, P. N. Newsome and J. P. Iredale, *Proc Natl Acad Sci U S A*, 2008, **105**, 12301–12306.

124 T. Touboul, N. R. F. Hannan, S. Corbineau, A. Martinez, C. Martinet, S. Branchereau, S. Mainot, H. Strick-Marchand, R. Pedersen, J. di Santo, A. Weber and L. Vallier, *Hepatology*, 2010, **51**, 1754–1765.

125 E. Luce, Hépatocytes différenciés à partir de cellules souches pluripotentes induites : modèle pour la thérapie cellulaire et génique autologue de l ' hémophilie B et modèle préclinique chez le primate, Thèse de doctorat, Physiopathologie, 2017.

126 L. E. Larsen, M. A. Smith, D. Abbey, A. Korn, L. F. Reeskamp, N. J. Hand and A. G. Holleboom, *Atherosclerosis*, 2020, **303**, 8–14.

127 N. Graffmann, S. Ring, M. A. Kawala, W. Wruck, A. Ncube, H. I. Trompeter and J. Adjaye, *Stem Cells Dev*, 2016, **25**, 1119–1133.

128 M. N. bin Ramli, Y. S. Lim, C. T. Koe, D. Demircioglu, W. Tng, K. A. U. Gonzales, C. P. Tan, I. Szczerbinska, H. Liang, E. L. Soe, Z. Lu, C. Ariyachet, K. M. Yu, S. H. Koh, L. P. Yaw, N. H. B. Jumat, J. S. Y. Lim, G. Wright, A. Shabbir, Y. Y. Dan, H. H. Ng and Y. S. Chan, *Gastroenterology*, 2020, **159**, 1471-1486.e12.

129 I. Mannaerts, N. Eysackers, E. Anne van Os, S. Verhulst, T. Roosens, A. Smout, A. Hierlemann, O. Frey, S. B. Leite and L. A. van Grunsven, *Biomaterials*, 2020, **261**, 120335.

130 G. Wei, J. Wang, Q. Lv, M. Liu, H. Xu, H. Zhang, L. Jin, J. Yu and X. Wang, *J Biomed Mater Res A*, 2018, **106**, 2171–2180.

131 H. Nagai, K. Terada, G. Watanabe, Y. Ueno, N. Aiba, T. Shibuya, M. Kawagoe, T. Kameda, M. Sato, H. Senoo and T. Sugiyama, *Biochem Biophys Res Commun*, 2002, **293**, 1420–1425.

132 R. E. Feaver, B. K. Cole, M. J. Lawson, S. A. Hoang, S. Marukian, B. R. Blackman, R. A. Figler, A. J. Sanyal, B. R. Wamhoff and A. Dash, *JCI Insight*,2016, **1(20)**, e90954.

133 M. J. Ramos, L. Bandiera, F. Menolascina and J. A. Fallowfield, *iScience*, 2022, **25(1)**, 103549.

134 R. M. Ezzell, M. Toner, K. Hendricks, J. C. Y. Dunn, R. G. Tompkins and M. L. Yarmush, *Exp Cell Res*, 1993, **208**, 442–452.

135 T. L. Marion, C. H. Perry, R. L. st. Claire and K. L. R. Brouwer, *Toxicol Appl Pharmacol*, 2012, **261**, 1.

136 S. Youhanna, A. M. Kemas, L. Preiss, Y. Zhou, J. X. Shen, S. D. Caka, F. S. Paqualini, S. K. Goparaju, R. Z. Shafagh, J. U. Lind, C. M. Sellgren and V. M. Lauschke, *Pharmacol Rev*, 2022, **74**, 141–206.

137 S. S. Bale, I. Golberg, R. Jindal, W. J. McCarty, M. Luitje, M. Hegde, A. Bhushan, O. B. Usta and M. L. Yarmush, *Tissue Eng Part C Methods*, 2015, **21**, 413–422.

138 P. A. Soret, J. Magusto, C. Housset and J. Gautheron, *J Clin Med*, 2021, **10**, 1–18.

139 C. C. Bell, D. F. G. Hendriks, S. M. L. Moro, E. Ellis, J. Walsh, A. Renblom, L. Fredriksson Puigvert, A. C. A. Dankers, F. Jacobs, J. Snoeys, R. L. Sison-Young, R. E. Jenkins, Å. Nordling, S. Mkrtchian, B. K. Park, N. R. Kitteringham, C. E. P. Goldring, V. M. Lauschke and M. Ingelman-Sundberg, *Sci Rep*, 2016, **6**, 25187.

140 A. Baze, C. Parmentier, D. F. G. Hendriks, T. Hurrell, B. Heyd, P. Bachellier, C. Schuster, M. Ingelman-Sundberg and L. Richert, *Tissue Engineering Part C: Methods*, 2018, **24 (9)**, 534–545.

141 C. A. E. Suurmond, S. Lasli, F. W. van den Dolder, A. Ung, H. J. Kim, P. Bandaru, K. J. Lee, H. J. Cho, S. Ahadian, N. Ashammakhi, M. R. Dokmeci, J. Lee and A. Khademhosseini, *Adv Healthc Mater*,2019, **8(24)**, 1901379.

142 M. Kozyra, I. Johansson, Å. Nordling, S. Ullah, V. M. Lauschke and M. Ingelman-Sundberg, *Scientific Reports 2018 8:1*, 2018, **8**, 1–12.

143 J. Kim, B. K. Koo and J. A. Knoblich, *Nat Rev Mol Cell Biol*, 2020, **21**, 1.

144 L. J. Wu, Z. Y. Chen, Y. Wang, J. G. Zhao, X. Z. Xie and G. Chen, *World J Gastroenterol*, 2019, **25**, 1913.

145 N. Prior, P. Inacio and M. Huch, *Gut*, 2019, **68**, 2228.

146 M. N. bin Ramli, Y. S. Lim, C. T. Koe, D. Demircioglu, W. Tng, K. A. U. Gonzales, C. P. Tan, I. Szczerbinska, H. Liang, E. L. Soe, Z. Lu, C. Ariyachet, K. M. Yu, S. H. Koh, L. P. Yaw, N. H. B. Jumat, J. S. Y. Lim, G. Wright, A. Shabbir, Y. Y. Dan, H. H. Ng and Y. S. Chan, *Gastroenterology*, 2020, **159**, 1471-1486.e12.

147 H. S. Kruitwagen, L. A. Oosterhoff, I. G. W. H. Vernooij, I. M. Schrall, M. E. van Wolferen, F. Bannink, C. Roesch, L. van Uden, M. R. Molenaar, J. B. Helms, G. C. M. Grinwis, M. M. A. Verstegen, L. J. W. van der Laan, M. Huch, N. Geijsen, R. G. Vries, H. Clevers, J. Rothuizen, B. A. Schotanus, L. C. Penning and B. Spee, *Stem Cell Reports*, 2017, **8**, 822.

148 M. S. Shoichet, *Macromolecules*, 2010, **43**, 581–591.

149 J. L. Drury and D. J. Mooney, *Biomaterials*, 2003, **24**, 4337–4351.

150 D. Kim, M. Kim, J. Lee and J. Jang, *Front Bioeng Biotechnol*, 2022, **10**, 764682.

151 R. Taymour, D. Kilian, T. Ahlfeld, M. Gelinsky and A. Lode, *Sci Rep*, 2021, **11**, 5130.

152 M. Kumar, B. Toprakhisar, M. van Haele, A. Antoranz, R. Boon, F. Chesnais, J. de Smedt, T. I. Idoype, M. Canella, P. Tilliole, J. de Boeck, T. Tricot, M. Bajaj, A. Ranga, F. M. Bosisio, T. Roskams, L. A. van Grunsven and C. M. Verfaillie, *Biomaterials*, 2020, **276**.

153 J. Schleicher, C. Tokarski, E. Marbach, M. Matz-Soja, S. Zellmer, R. Gebhardt and S. Schuster, *Biochim Biophys Acta*, 2015, **1851**, 641–656.

154 C. J. Green, S. A. Parry, P. J. Gunn, C. D. L. Ceresa, F. Rosqvist, M. E. Piché and L. Hodson, *Horm Mol Biol Clin Investig*,2018, **41(1)**, 38.

155 G. Janani and B. B. Mandal, *ACS Appl Mater Interfaces*, 2021, **13(21**), 24401-24421.

156 E. Leclerc, J. Hamon, I. Claude, R. Jellali, M. Naudot and F. Bois, *Cell Biol Toxicol*, 2015, **31**, 173–185.

157 R. Jellali, P. Zeller, F. Gilard, A. Legendre, M. J. Fleury, S. Jacques, G. Tcherkez and E. Leclerc, *Environ Toxicol Pharmacol*, 2018, **59**, 1–12.

158 R. Jellali, F. Gilard, V. Pandolfi, A. Legendre, M. J. Fleury, P. Paullier, C. Legallais and E. Leclerc, *Journal of Applied Toxicology*, 2018, **38**, 1121–1134.

159 M. Gori, M. C. Simonelli, S. M. Giannitelli, L. Businaro, M. Trombetta and A. Rainer, *PLoS One*, 2016, **11(7)**.

160 R. Jellali, S. Jacques, A. Essaouiba, F. Gilard, F. Letourneur, B. Gakière, C. Legallais and E. Leclerc, *Food and Chemical Toxicology*, 2021, **152**, 112155.

161 M. S. Freag, B. Namgung, M. E. Reyna Fernandez, E. Gherardi, S. Sengupta and H. L. Jang, *Hepatol Commun*, 2021, **5**, 217.

162 A. Zbinden, J. Marzi, K. Schlünder, C. Probst, M. Urbanczyk, S. Black, E. M. Brauchle, S. L. Layland, U. Kraushaar, G. Duffy, K. Schenke-Layland and P. Loskill, *Matrix Biology*, 2020, **85–86**, 205–220.

163 S. Abadpour, A. Aizenshtadt, P. A. Olsen, K. Shoji, S. R. Wilson, S. Krauss and H. Scholz, *Curr Diab Rep*, 2020, **20**, 1–13.

164 Y. Jun, J. S. Lee, S. Choi, J. H. Yang, M. Sander, S. Chung and S. H. Lee, *Sci Adv*, 2019, **5**, 4520–4547.

165 Y. Yu, A. Gamble, R. Pawlick, A. R. Pepper, B. Salama, D. Toms, G. Razian, C. Ellis, A. Bruni, B. Gala-Lopez, J. (Lulu) Lu, H. Vovko, C. Chiu, S. Abdo, T. Kin, G. Korbutt, A. M. J. Shapiro and M. Ungrin, *Diabetologia*, 2018, **61**, 2016–2029.

166 P. L. Lewis and J. M. Wells, *Stem Cells*, 2021, **39**, 522-535.

167 J. S. Mohammed, Y. Wang, T. A. Harvat, J. Oberholzer and D. T. Eddington, *Lab Chip*, 2009, **9**, 97–106.

168 T. Schulze, K. Mattern, E. Früh, L. Hecht, I. Rustenbeck and A. Dietzel, *Biomed Microdevices*, 2017, **19**, 1–11.

169 T. Schulze, K. Mattern, P. Erfle, D. Brüning, S. Scherneck, A. Dietzel and I. Rustenbeck, *Front Bioeng Biotechnol*, 2021, **9**, 158.

170 A. Essaouiba, R. Jellali, M. Shinohara, B. Scheidecker, C. Legallais, Y. Sakai and E. Leclerc, *J Biotechnol*, 2021, **330**, 45–56.

171 T. Hori, K. Yamane, T. Anazawa, O. Kurosawa and H. Iwata, *Biomed Microdevices*, 2019, **21**, 1–9.

172 K. S. Sankar, B. J. Green, A. R. Crocker, J. E. Verity, S. M. Altamentova and J. v. Rocheleau, *PLoS One*, 2011, **6**, 24904.

173 P. N. Silva, B. J. Green, S. M. Altamentova and J. v. Rocheleau, *Lab Chip*, 2013, **13**, 4374–4384.

174 A. L. Glieberman, B. D. Pope, J. F. Zimmerman, Q. Liu, J. P. Ferrier, J. H. R. Kenty, A. M. Schrell, N. Mukhitov, K. L. Shores, A. B. Tepole, D. A. Melton, M. G. Roper and K. K. Parker, *Lab Chip*, 2019, **19**, 2993–3010.

175 M. Nourmohammadzadeh, Y. Xing, J. W. Lee, M. A. Bochenek, J. E. Mendoza-Elias, J. J. McGarrigle, E. Marchese, Y. Chun-Chieh, D. T. Eddington, J. Oberholzer and Y. Wang, *Lab Chip*, 2016, **16**, 1466–1472.

176 A. Essaouiba, T. Okitsu, R. Jellali, M. Shinohara, M. Danoy, Y. Tauran, C. Legallais, Y. Sakai and E. Leclerc, *Mol Cell Endocrinol*, 2020, **514**, 110892.

177 K. S. Park, Y. S. Kim, J. H. Kim, B. K. Choi, S. H. Kim, S. H. Oh, Y. R. Ahn, M. S. Lee, M. K. Lee, J. B. Park, C. H. Kwon, J. W. Joh, K. W. Kim and S. J. Kim, *Transplant Proc*, 2009, **41**, 3813–3818.

178 J. Bailey, M. Thew and M. Balls, *ATLA Alternatives to Laboratory Animals*, 2013, **41**, 335–350.

179 M. J. Hsu, M. Christ and B. Christ, *Methods Mol Biol*, 2021, **2269**, 151–165.

180 G. R. Romualdo, T. C. da Silva, M. F. de Albuquerque Landi, J. Á. Morais, L. F. Barbisan, M. Vinken, C. P. Oliveira and B. Cogliati, *Environ Toxicol*, 2021, **36**, 168–176.

181 N. Picollet-D'hahan, A. Zuchowska, I. Lemeunier and S. Le Gac, *Trends Biotechnol*, 2021, **39(8)**, 788-810.

182 Y. Zhao, R. K. Kankala, S. Bin Wang and A. Z. Chen, *Molecules*, 2019, 24, 675.

183 S. Bauer, C. Wennberg Huldt, K. P. Kanebratt, I. Durieux, D. Gunne, S. Andersson, L. Ewart, W. G. Haynes, I. Maschmeyer, A. Winter, C. Ämmälä, U. Marx and T. B. Andersson, *Sci Rep*, 2017, **7**, 1–11.

184 A. Essaouiba, T. Okitsu, R. Kinoshita, R. Jellali, M. Shinohara, M. Danoy, C. Legallais, Y. Sakai and E. Leclerc, *Biochem Eng J*, 2020, **164**, 107783.

185 D. W. Lee, S. H. Lee, N. Choi and J. H. Sung, *Biotechnol Bioeng*, 2019, **116**, 3433–3445.

186 O. Pivovarova, W. Bernigau, T. Bobbert, F. Isken, M. Möhlig, J. Spranger, M. O. Weickert, M. Osterhoff, A. F. H. Pfeiffer and N. Rudovich, *Diabetes Care*, 2013, **36**, 3779–3785.

187 B. Casas, L. Vilén, S. Bauer, K. Kanebratt, C. W. Huldt, L. Magnusson, U. Marx, T. B. Andersson, P. Gennemark and G. Cedersund, *bioRxiv*, 2021.

188 Q. Wu, J. Liu, X. Wang, L. Feng, J. Wu, X. Zhu, W. Wen and X. Gong, *Biomed Eng Online*, 2020, **19**, 1–19.

189 S. Qiu, Y. Cai, H. Yao, C. Lin, Y. Xie, S. Tang and A. Zhang, *Front.Microbiol*, 2023, **14**.

190 J. F. Xiao, B. Zhou and H. W. Ressom, *TrAC Trends in Analytical Chemistry*, 2012, **32**, 1–14.

191 S. Dayalan, J. Xia, R. A. Spicer, R. Salek and U. Roessner, *Encyclopedia of Bioinformatics and Computational Biology: ABC of Bioinformatics*, 2019, **1–3**, 396–409.

192 N. R. Anwardeen, I. Diboun, Y. Mokrab, A. A. Althani and M. A. Elrayess, *BMC Bioinformatics 2023 24:1*, 2023, **24**, 1–18.

193 H. Y. Kim, *Clin Mol Hepatol*, 2021, **27**, 553–559.

194 M. Gaggini, M. Morelli, E. Buzzigoli, R. A. DeFronzo, E. Bugianesi and A. Gastaldelli, *Nutrients 2013, Vol. 5, Pages 1544-1560*, 2013, **5**, 1544–1560.

195 M. Gaggini, F. Carli, C. Rosso, E. Buzzigoli, M. Marietti, V. Della Latta, D. Ciociaro, M. L. Abate, R. Gambino, M. Cassader, E. Bugianesi and A. Gastaldelli, *Hepatology*, 2018, **67**, 145–158.

196 G. Grzych, L. Vonghia, M. A. Bout, J. Weyler, A. Verrijken, E. Dirinck, M. J. C. Curt, L. Van Gaal, R. Paumelle, S. Francque, A. Tailleux, J. T. Haas and B. Staels, *J Clin Endocrinol Metab*, 2020, **105**, 2311–2321.

197 A. Safaei, A. A. Oskouie, S. R. Mohebbi, M. Rezaei-Tavirani, M. Mahboubi, M. Peyvandi, F. Okhovatian and M. Zamanian-Azodi, *Gastroenterol Hepatol Bed Bench*, 2016, **9**, 158.

198 Y. Zhou, M. Orešič, M. Leivonen, P. Gopalacharyulu, J. Hyysalo, J. Arola, A. Verrijken, S. Francque, L. Van Gaal, T. Hyötyläinen and H. Yki-Järvinen, *Clinical Gastroenterology and Hepatology*, 2016, **14**, 1463-1472.e6.

199 C. Caussy, J. C. Chuang, A. Billin, T. Hu, Y. Wang, G. M. Subramanian, C. S. Djedjos, R. P. Myers, E. A. Dennis and R. Loomba, *Therap Adv Gastroenterol*, 2020, **13**.

200 D. Beyoğlu and J. R. Idle, *J Hepatol*, 2013, **59**, 842–858.

201 S. Cassim, V.-A. Raymond, B. Lacoste, P. Lapierre, M. Bilodeau, S. Cassim, V.-A. Raymond, B. Lacoste, P. Lapierre and M. Bilodeau, *Oncotarget*, 2018, **9**, 26868–26883.

202 P. Burra, C. Becchetti and G. Germani, *JHEP Reports*, 2020, **2**, 100192.

203 N. J. Serkova, Y. Zhang, J. L. Coatney, L. Hunter, M. E. Wachs, C. U. Niemann and M. S. Mandell, *Transplantation*, 2007, **83**, 517–521.

204 R. Amathieu, M. N. Triba, C. Goossens, N. Bouchemal, P. Nahon, P. Savarin and L. Le Moyec, *World J Gastroenterol*, 2016, **22**, 417–426.

205 A. Artati and J. Tokarz, *Metabolomics for Biomedical Research*, 2020, 137–157.

206 S. J. Harrison, *Encyclopedia of Cell Biology*, 2016, **4**, 199–210.

207 X. Chen, Z. Peng and Z. Yang, *Chem Sci*, 2022, **13**, 6687–6695.

208 T. Ramirez, A. Strigun, A. Verlohner, H. A. Huener, E. Peter, M. Herold, N. Bordag, W. Mellert, T. Walk, M. Spitzer, X. Jiang, S. Sperber, T. Hofmann, T. Hartung, H. Kamp and B. van Ravenzwaay, *Arch Toxicol*, 2018, **92**, 893–906.

209 M. Yu, Y. Zhu, Q. Cong and C. Wu, *Can J Gastroenterol Hepatol*, 2017.

210 M. Kozyra, I. Johansson, Å. Nordling, S. Ullah, V. M. Lauschke and M. Ingelman-Sundberg, *Scientific Reports 2018 8:1*, 2018, **8**, 1–12.

Chapter II:

Materials & Methods

This chapter presents in detail the experimental protocols and materials that were used during this project, laying the foundation for a thorough analysis of the results and findings. First, we presented the design and the manufacturing process of the different microsystems and also the platform that were used for the dynamic culture. Then, we explained the different cell culture procedures implemented in this project. Finally, we presented the analysis methods used to characterise our cell models.

2.1 Biochip manufacturing

Both liver and pancreas biochips were manufactured using a replica moulding process. Photolithography was performed to created mould master of the both layers that composed the biochip using SU-8 photosensitive resin. Then polydimethylsiloxane (PDMS) (Sylgard 184 kit, Dow Corning) was mixed with a crosslinking agent at 10:1(w/w) and poured on moulds. After degassing PDMS under vacuum bell, moulds were heated in an oven for 2h at 70°C. Once the PDMS cross-linked, layers were unmoulded. The top layer was then perforated with a 2mm puncher to create the inlet and the outlet of the biochip. Then, the two replicas were irreversible sealed together after a reactive air plasma treatment for 1min. The biochip was cut with a custom-made puncher to obtain their specific shape. Finally, silicone tubes with a polypropylene connector (Luer, diameter 1.6mm, Cole Farmer) were inserted in the inlet and outlet holes of the top layer. They were sealed to the biochip with PDMS. The microsystem was then placed in the oven at 70°C for solidification.

2.1.1 Liver-on-chip design

The liver-on-chip was designed by Eric Leclerc (Patent n° WO2010149567) and consists of a large cell culture chamber which is manufactured with two PDMS layers (Figure 2.1). The bottom PDMS layer is used as a support for cell attachment. The microstructures of the bottom layer consist of series of microchambers (520 µm × 520 µm × 100 µm) interconnected by microchannels (720 µm × 220 µm × 100 µm) and its specific geometry makes a uniform flow field possible above the microstructures. The upper PDMS layer is composed of a reservoir with a depth of 100 µm for culture medium perfusion. After closing the biochip with the upper PDMS layer the total resulting depth and volume of the assembled cell culture chamber is 200 µm and 40 µl respectively, with a cell growth surface area of 2 cm^2.

2.1.2 Pancreas-on-chip design

In the pancreas-on-chip model, the micro-structured bottom layer, used to trap islets, was composed of crests measuring 300 µm height and 600 µm wide each (Figure 2.2). The second PDMS layer, with a reservoir with a depth of 100 µm, was placed on top of the first layer and included an inlet and outlet for culture medium perfusion. A microchannels network placed at the inlet and outlet of each layer made it possible to distribute the culture medium homogenously in the biochip.

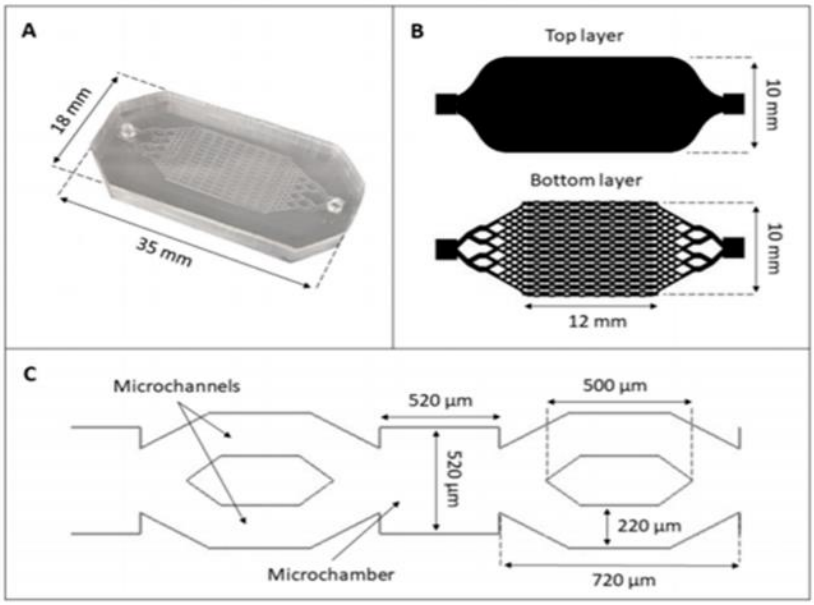

Figure 2. 1: *Design of the liver biochip.* ***(A)*** *External dimension of the biochip.* ***(B)*** *Dimension of the effective surface.* ***(C)*** *Geometry and dimension of the microstructure (adapted from Messelmani, 2023).*

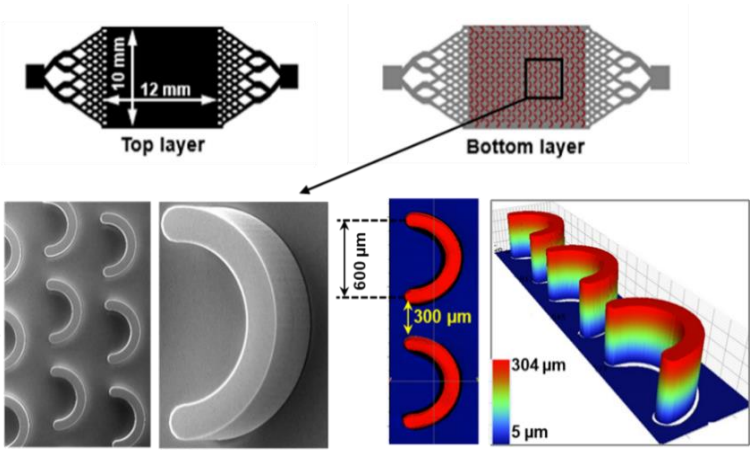

Figure 2. 2: *Design of the microstructure of the pancreas biochip (adapted from Essaouiba, 2020).*

2.2 Cells sources

2.2.1 HepG2/C3A cell line

The HepG2/C3A cell line (ATCC, CRL-10741) is a clonal derivative of HepG2, a human hepatocyte cell line coming from a hepatocellular carcinoma. This cell line has the ability to produce albumin, alpha fetoprotein (AFP) and to grow in a glucose deficient medium. Moreover, HepG2/C3A exhibit a strong epithelial-like morphology.

2.2.2 Hepatocytes-like cells derived from hiPSC

Hepatocytes-like cells have been differentiated from Cellartis human iPS cell line 22 (ChiPSC22). Cellartis human iPS cell lines were delivered with the Cellartis DEF-CS™ 100 Culture System which is a complete system for efficient cell expansion.

2.2.3 Beta -cells derived from hiPSC

Beta-cells have been differentiated from Cellartis hiPS beta cells ChiPSC12 lines using hiPS beta cell media kit (Cat. N° Y10108, Takara Bio, Europe). Manufacturer's instructions recommended daily or every two days medium renewal and to use the cells within 16 days post-thaw.

2.3 Perfusion system for cell culture

2.3.1 Perfusion circuit with the IDCCM platform

In order to parallelize culture biochips and test multiple conditions Leclerc *et al.*, (Patent n° WO2011107519) developed the Integrated Dynamic Cell Culture Microchip (IDCCM) platform. Inspired from a 24-well plate and fabricated by heat press of polycarbonate to form 24 wells, the IDCCM can host 12 independent biochips. The platform is composed of 2 parts: a top and a bottom layer. The bottom layer corresponding to the 24 culture reservoirs with the biochips plugged via the two polypropylene connectors at the bottom of each couple of reservoirs (2 ml of culture medium per well). The top layer is the interface with the perfusion circuit. Indeed, to each couple reservoir a perfusion circuit is associated ensuring the culture medium circulation. The perfusion circuit is composed of silicone (ID=0.63mm, ISMATEC) and PTFE tubing (ID = 0.56 mm, Adtech) that are squeezed through the peristaltic pump (ISM949, ISMATEC) actuators forcing the circulation of the culture medium from a reservoir to another through the biochip. The two layers are sealed with a silicon joint and the

whole system is quenched with a clamping system. A plexiglass support is designed to hold the IDCCM on the peristaltic pump. The different components of the IDCCM was sterilized by autoclaving before each experiment. The IDCCM can either ensures the culture of independent biochips, or the culture reservoirs can be connected to study the interactions of serial biochips to understand the organs interactions.

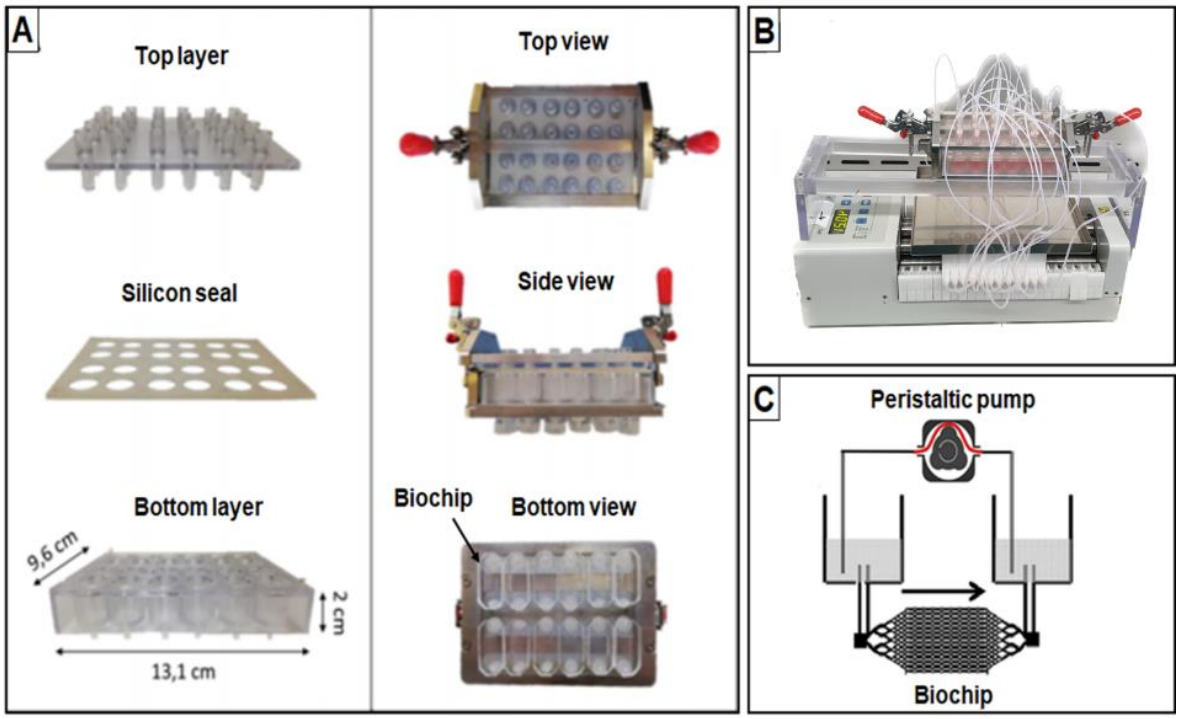

Figure 2. 3: *Design of the Integrated Dynamic Cell Culture Microchip (IDCCM) platform.* ***(A)*** *Different compartments of the IDCCM platform.* ***(B)*** *The IDCCM connected to a peristaltic pump.* ***(C)*** *Schematic representation of the IDCCM and perfusion culture operating mode (adapted from Messelmani, 2023).*

2.3.2 Perfusion circuit with bubble trap

The bubble trap system (MEDICOLAB) was a cylindrical glass reservoir with a volume of 2 ml. It is composed of an inlet at the mid-height and an outlet at the bottom. The bubble trap system was connected to a biochip and to the peristaltic pump using silicone (ID=0.63mm, ISMATEC) and PFTE tubing (ID = 0.56mm, Adtech). Each microchip was independently connected to one bubble trap with its proper perfusion loop. The culture medium flowed from the top to the bottom to avoid any air bubbles in the biochip. The system is maintained in an upright position thanks to a homemade PDMS support. Before each experiment, the perfusion circuit (biochip, tubing and bubble trap) was sterilized by autoclaving.

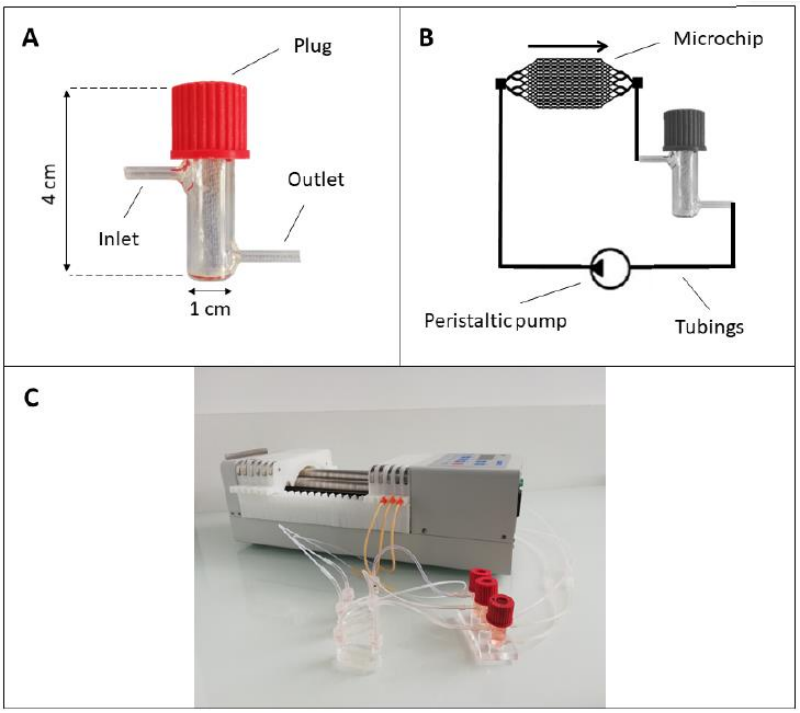

Figure 2. 4: *Design of the dynamic culture system using bubble traps.* ***(A)*** *Design of a bubble trap.* ***(B)*** *Schematic representation of the perfusion culture with bubble traps.* ***(C)*** *Set up for the perfusion culture in biochips using bubble traps (Essaouiba, 2020).*

2.4 Cell culture experimental procedures

2.4.1 Preparation of the fatty acid solutions

Oleic acid (C18:1) and palmitic acid (C16:0) are the most abundant dietary FFAs and represent 31% and 27%, respectively, of total plasma FFAs. The oleic acid (OA, Sigma-Aldrich), was dissolved in EtOH 99% at 500 mM. Palmitic acid (PA, Sigma-Aldrich), provided as sodium salts, was prepared in stock solution of EtOH 50% at 150 mM. A 10% BSA stock solution was prepared in sterile water. Fatty acids mixtures were prepared according to the following percentages:

- OA mixture consisted of 0.13% of OA stock solution, 4.4% of stock BSA solution and 95.47% of MEM.
- PA mixture consisted of 0.2% of PA stock solution, 4.4% of the stock BSA solution and 95.4% of MEM.

This resulted to an OA concentration of 0.5 mM and a PA concentration of 0.33 mM in mixture with BSA (1:20 final ratio) per total of 15 ml. The control experiments were performed with the vehicle that consisted of 4.4% of the stock BSA solution and 95.4% of MEM.

2.4.2 HepG2/C3A as model for human liver steatosis model

2.4.2.1 Cell maintenance

HepG2/C3A cell line (ATCC-CRL-10741, France) was used as hepatocyte model for the proof of concept of the NAFL liver-on-chip model. The HepG2/C3A cell line was cultivated in a T75 cm² flask with treated surface. Cells were cultured in Minimal Essential Medium (MEM) with phenol red (Life Technologies, Grand Island, NY). The culture medium was supplemented with 10% decomplemented fetal bovine serum (FBS; Life Technologies, Grand Island, NY), 2 mM L-glutamine, 0.1 mM nonessential amino acids (NEAA), 1 mM sodium pyruvate (all supplements are from PAN Biotech, Aidenbach), 100 U/ml streptomycin/penicillin (Life Technologies, Grand Island, NY) and was renewed every 2 days. At confluence, the cells were detached using 0.25% trypsin-EDTA (Life Technologies, Grand Island, NY) for 5 min at 37°C and were seeded at a density of 13,000 cell/cm².

2.4.2.2 Dynamic cell culture setup

HepG2/C3A cells were detached from the T75 flask using 0.25% trypsin-EDTA (Life Technologies, Grand Island, NY) and 75,000 cell/cm² were injected into the biochips. The seeded biochips were then placed in a 5% CO_2 and 37°C incubator overnight for cell adhesion. After the adhesion step, the biochips were plugged into the IDCCM and each well were loaded with 2 ml of fresh MEM supplemented medium (4 ml/biochips). The IDCCM were then connected to the peristaltic pump through the perfusion circuit and the flow rate was set at 15 µL/min. The whole system was placed in a humidified incubator at 5% CO_2 and 37°C. After 4 days of dynamic culture we started the fatty acids treatment. The culture medium was prepared with the different fatty acids treatments: (i) Oleic acid (0.66 mM); (ii) Palmitic acid (0.33 mM); (iii) Oleic acid/Palmitic acid (2:1). The culture medium was renewed every 2 days. At every culture medium changing, samples are saved for quantification analyses. After 2 days and 7 days of fatty acids treatment biochips were detached from the circuit and the cells were fixed for staining. At the 18th day of culture, the perfusion was stopped, the biochips were detached and the whole system was rinsed in bleach then in Milli-Q® water.

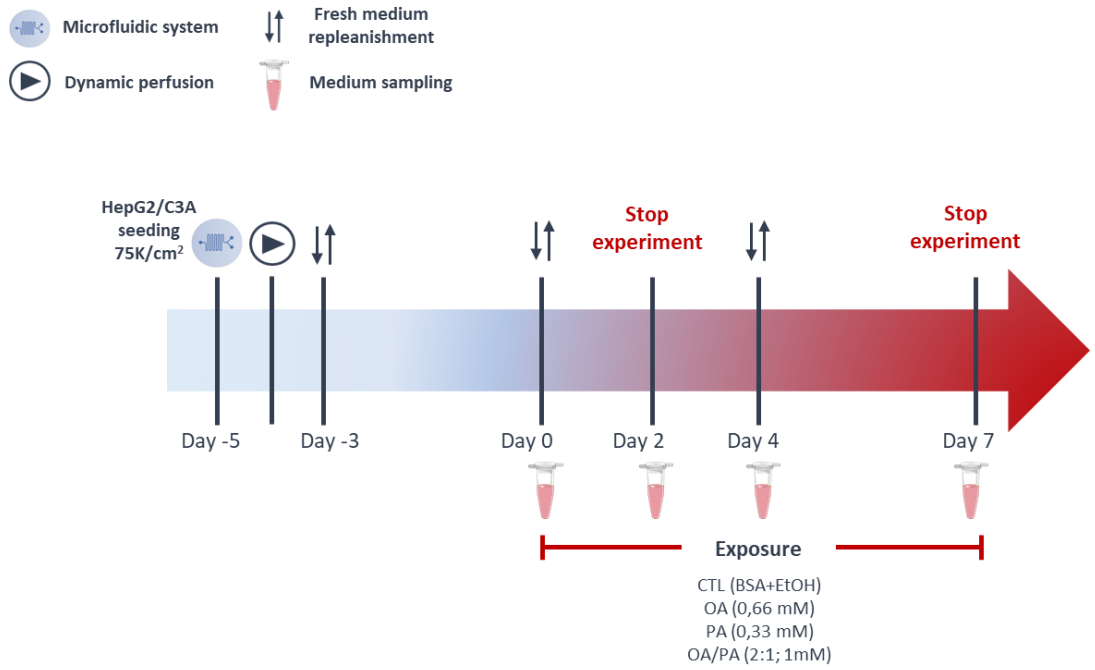

Figure 2. 5: *Experimental procedure used for the NAFL liver-on-chip.*

2.4.3 HLC differentiated from hiPSC as model for human liver steatosis

2.4.3.1 Cell thawing and plating

Cellartis human iPS cell line 22 (ChiPSC22) were thawed following the manufacturer's instructions. ChiPSC22 were seeded at 10,000 cells/cm^2 in a coated 6-well plate and maintained using Cellartis DEF-CS 100 Culture System (Cat. N° Y30020, Takara Bio, Europe) in an incubator at 37°C, 5% CO_2 and >90% humidity. Cells were cultured until 30% confluence with daily medium changes.

2.4.3.2 Protocol of hiPSC differentiation into HLC under static conditions

The differentiation protocol was composed of four steps (S1, S2, S3 and S4) during which media composition and atmospheric condition were specifically defined. From S1 to S3, cells were culture in RPMI 1640 (Sigma, Saint-Louis, MO) supplemented with 2% B-27 (Life Technologies, Grand Island, NY) to promote cell survival and media was renewed every day. First step (S1; 5 days, 37°C, 20% O2, 5% CO_2), corresponding to hiPSC differentiation in definitive endoderm (DE) cells, was divided in two sub-steps:

(i) S1.1 medium was supplemented with CHIR99021 (Stemcell Technologies, Grenoble, FRANCE) at 2µM and Activin A (R&D Systems, Minneapolis, MN) at 100 ng/ml during 2 days

(ii) S1.2 medium was supplemented with Activin A (R&D Systems, Minneapolis, MN) at 100 ng/ml during 3 days

Then, DE cells entered S2 (5 days, 37°C, 5% O2, 5% CO2) and were cultured in medium supplemented with β-FGF (Peprotech, Cranbury, NJ) at 10 ng/ml and BMP-4 (Proteintech, Rosemont, IL) at 20 ng/ml to engage differentiation into hepatoblast-like cell. In order to reach the immature hepatocyte commitment, cells were cultured in medium supplemented with HGF (Peprotech, Cranbury, NJ) at 20 ng/ml. During this third step that last 10 days, cells were cultured in 37°C, 5% O_2, 5% CO_2 as in S2.

2.4.3.3 Protocol of hiPSC differentiation into HLC under fluidic conditions

Sterilised biochips were coated with 20 mg/ml Matrigel solution (Corning, Europe) in order to promote cell adhesion. At the end of S3, cells were detached with TrypLE (Life Technologies, Grand Island, NY) from Petri dishes and transferred in biochips. After 48h of cell adhesion, Step 4 of the differentiation process was initiated and applied to 28 days using a 10 µl/min perfusion rate. For this last step, cells were cultured in DMEM/Ham's F-12 medium (Fujifilm Wako, Osaka) supplemented with 10% decomplemented FBS (Life Technologies, Grand Island, NY), 1% N-2 (Life Technologies, Bleiswijk), 1% insulin transferrin sodium (Life Technologies, Bleiswijk), 100 U/ml streptomycin/penicillin (Life Technologies, Grand Island, NY), 2 mM L-glutamine (PAN Biotech, Aidenbach), 0.1 mM NEAA (PAN Biotech, Aidenbach), 20 ng/ml HGF (Peprotech, Cranbury, NJ), 10 ng/ml EGF (Peprotech, Cranbury, NJ), 1 mM Ascorbic Acid (Sigma, Saint-Louis, MO), 10 mM Nicotinamide (Sigma, Saint-Louis, MO), 0.2 µm Dexamethasone (Sigma, Saint-Louis, MO), 5 µM Rock Inhibitor (Stemcell technologies, Grenoble), 5 µM A8301 (Stemcell Technologies, Grenoble), 0.2 mM N-acetylcysteine (Sigma, Saint-Louis, MO) for hepatic maturation. To induce steatosis, cells were exposed to oleic acid at 0.5mM during the last 14 days of S4. Perfusion culture was performed with the bubble trap set up at 37°C under 20% O_2 and 5% CO_2 and medium were renewed every two days.

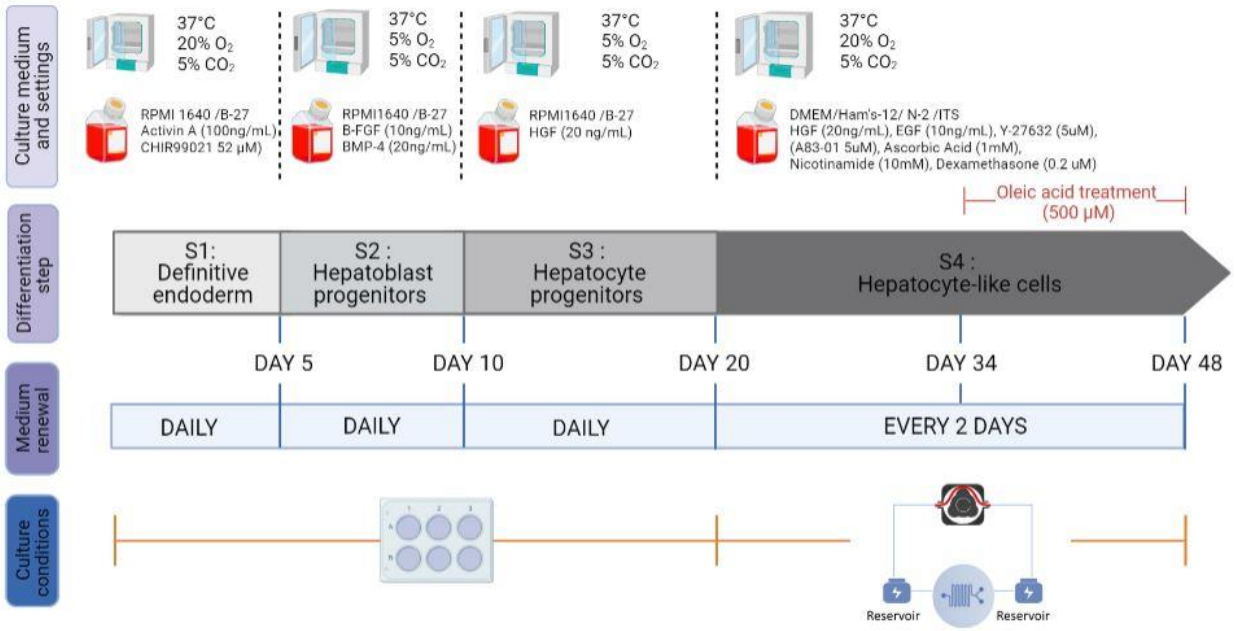

Figure 2. 6: *Schema of the hiPSC differentiation protocol.*

2.5 Experimental setup for human pancreas model

2.5.1 hiPSC as model for human pancreas: 3D spheroids formation and culture using honeycomb technology

2.5.1.1 Honeycombs technology

In order to form 3D spheroids, we used the honeycomb technology developed by Shinohara *et al.*[1,2]. Briefly, this culture system corresponds to polygons made of PDMS with geometric characteristics of 126 µm width and 129 µm depth. The 8000 PDMS honeycombs sheet is set on a bottomless 24 well plate in order to promote gas exchange.

To prevent cell adhesion, the plate was coated with a Pluronic-PBS solution (Pluronic® F-127; Life Technologies, Grand Island, NY) overnight at 37°C. Then, the plate is rinsed three time with PBS (Life Technologies, Grand Island, NY) and sterilised by ultraviolet (UV) for 3 h. Finally, honeycombs sheet was rinsed and filled with 500 µL of maintenance culture medium.

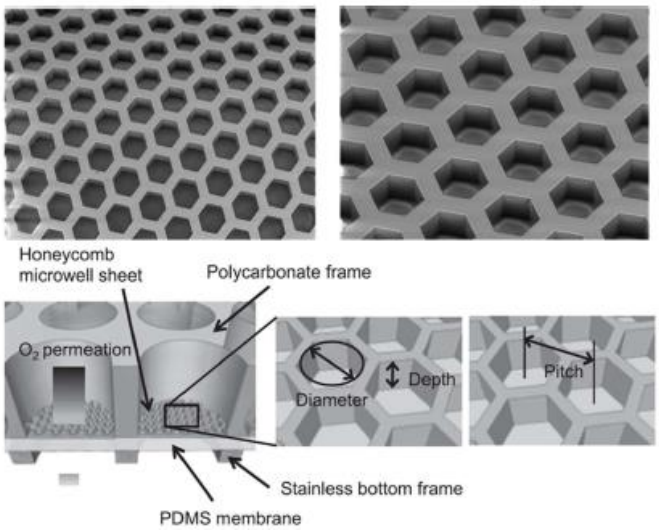

Figure 2. 7: *Design and structure of the honeycombs microwells plate (adapted from Essaouiba et al.,2021).*

2.5.1.2 Cell thawing and seeding

Cellartis hiPS Beta cell (ChiPSC12) were thawed following manufacturer's instructions. After thawing, five wells (filled with 500 µl of culture medium) were seeded at $6x10^5$ cells/wells and incubated in a humidified incubator at 5% CO_2 and 37°C. After 24h, culture medium was adjusted at 1 ml. Maintenance culture medium was changed daily by replacing only 600 µl of culture medium with fresh medium in order to avoid spheroids being aspirated. On day 4, β-cells spheroids were formed and two wells were used to seed the biochips while the other two were used to seed six new wells. The culture medium was renewed according to the manufacturer's recommendations and culture were maintained until day 16. Then, islet-like spheroids were harvested and fixed for staining. Finally, the wells were cleaned with sodium dodecyl sulfate 2% (SDS; Life Technologies, Grand Island, NY) and rinsed with Milli-Q® water.

2.5.2 Dynamic culture in biochip

After sterilisation, biochips and tubing were filled with maintenance culture medium in order to remove air bubbles. The bubble traps were filled with 2 ml of culture medium. After 4 days of culture, the spheroids, formed in the honeycombs, were suspended by gently aspirating and discharging the medium using wide orifice pipette tips with low binding. Then, 100 µl of cell solution were collected from the well and seeded in biochips. One well of the honeycomb plate allows three biochips to be seeded. After spheroids seeding, the biochips were incubated at 37°C in a 5% CO_2 supplied incubator for 1 h to allow spheroid trapping by

the crests. Then, the biochips were connected to the perfusion circuits and peristaltic pump, and the perfusion started at 15 µl/min. The entire setup was continuously incubated at 37°C in a 5% CO_2 supplied incubator. The culture medium was renewed according to the manufacturer's recommendations. At every culture medium changing, samples are saved for quantification analyses. On the 18th day of culture, the perfusion was stopped and biochips were detached from the circuit. Islet-like spheroids were harvested and fixed for staining. The biochips were cleaned with SDS 2% (Life Technologies, Grand Island, NY) while the circuit system was cleaned with bleach. Then, the whole system was rinsed with Milli-Q® water.

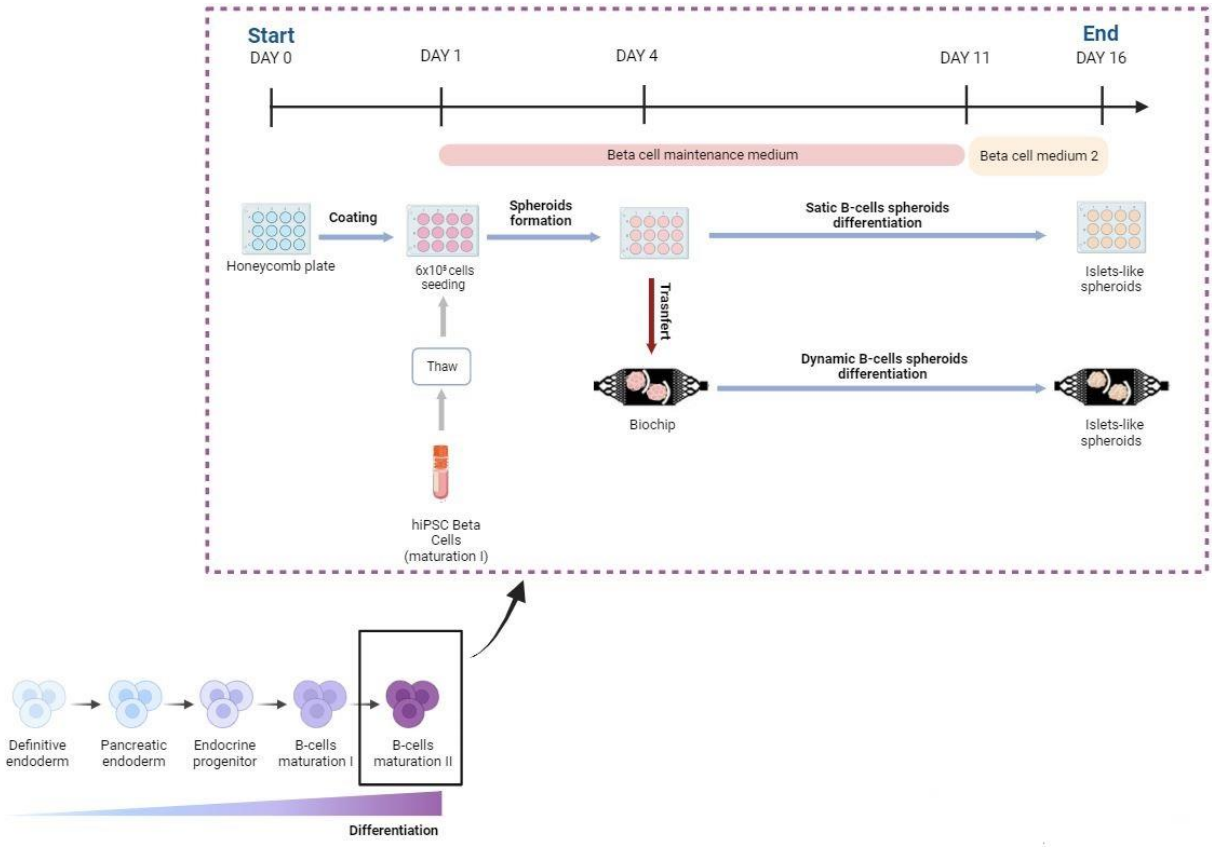

Figure 2. 8: *Schematic representation of the differentiation procedure of Cellartis® hiPSC beta-cells (created in Biorender.com).*

2.6 Staining and immunostaining process

2.6.1 Liver-on-chip models staining process

Concerning both liver-on-chip models (hiPSC and HepG2/C3A) cells were washed with phosphate buffer saline solution (PBS) and fixed with paraformaldehyde 4% (PFA, MP biomedicals) at room temperature (RT) during 30 min. PFA is then washed with PBS and the samples are stored in PBS until staining. In order to perform the immunohistochemistry staining, the samples were permeabilized with 0.5% Triton X-100 solution for 30 min at room temperature. Then the unspecific binding sites were blocked with PBS/1% BSA (Life Technologies, Grand Island, NY) solution for 30 min. The primary antibodies are diluted in the blocking solution (following the manufacturer recommendations) and incubated with the samples overnight at 4°C.

After washing three times with PBS, the secondary antibody's solution diluted in PBS/1% BSA solution is introduced and samples are incubated at 4°C overnight. Then, nuclei were stained using DAPI (4',6-diamidino-2-phenylindole, D1306, Invitrogen) at 10 µg/ml for 30 min at RT. Finally, the staining solution is washed three times and samples are stored in PBS until observation. The primary and secondary antibodies used are presented in Table 2.1.

All observations were made with a confocal microscope (Zeiss LSM 710). Samples were mounted in a coverslip with a drop of PBS to prevent them from drying out during the acquisitions.

Table 2. 1: *Primary and secondary antibodies used for hepatocytes immunostaining.*

Immunostaining / Function	**Primary antibody**	**Secondary antibody**
Albumin Liver specific protein	Goat anti-human albumin (a80-129A, **Bethyl)**	Donkey anti-Goat IgG Alexa fluor®488 (ab150129, **Abcam)**
CYP3A4 Enzyme involved in oxidation reactions of various compounds	Rabbit anti-CYP3A4 (ab3572, **Abcam**)	Donkey anti-Rabbit IgG Alexa Fluor® 568 (A10042, **Invitrogen**)

E-cadherin Mediator for cell-cell adhesion	Mouse anti-E-cadherin (BDB610181, **BD Biosciences**)	Donkey anti-Mouse Alexa Fluor® 647 (ab150107, **Abcam**)
BSEP (ABCB11) The ATP-dependent secretion of bile salts into the canaliculus of hepatocytes	Rabbit anti-Human ABCB11/BSEP (ab155421, **Abcam**)	Donkey anti-Rabbit IgG Alexa Fluor® 568 (A10042, **Invitrogen**)
PECAM (CD31) Platelet endothelial cell adhesion molecule	Mouse anti- Human PECAM/CD31 (ab24590, **Abcam**)	Donkey anti-Mouse Alexa Fluor® 647 (ab150107, **Abcam**)

2.6.2 Pancreas-on-chip model staining process

Islet-like spheroids were harvested in an untreated TCPS24 wells plate after for staining. Islet-like spheroids were washed with PBS and fixed in paraformaldehyde 4% at 4 °C overnight. Then, islet-like spheroids were permeabilized with 1% Triton X100 in PBS for 3 h at 4 °C and wash three times with PBS for 30 min under oscillation. Non-specific binding sites were blocked a 3% BSA solution for 24 h at 4 °C. Primary antibodies were diluted in a 3% BSA solution (following the manufacturer recommendations) and incubated for 48 h at 4 °C. After a wash step, secondary antibodies were incubated in a 3% BSA solution at 4 °C for 24 h. Then, islet-like spheroids were washed and nuclei were stained with DAPI (4',6-diamidino-2-phenylindole, D1306, Invitrogen) at 10 µg/ml for 30 min at RT. Finally, the staining solution is washed and samples are stored in PBS until observation. The primary and secondary antibodies used are presented in Table 2.2. All observations were made with a confocal microscope (Zeiss LSM 710). Samples were mounted in a coverslip with a drop of PBS to prevent them from drying out during the acquisitions.

Table 2. 2: *Primary and secondary antibodies used for islets immunostaining.*

Immunostaining / Function	Primary antibody	Secondary antibody
Insulin	Rabbit anti-Insulin (ab181547, **Abcam)**	anti-Rabbit IgG Alexa Fluor® 568
Glucagon	Mouse anti-Glucagon (G2654, **Sigma-Aldrich**)	anti-Mouse IgG Alexa Fluor® 488

2.6.3 Lipid droplet and total collagen staining

Lipid droplet accumulation within hepatocytes were stained using Oil Red O of the Hepatic steatosis kit (Life Technologies, Grand Island). The cells were fixed as previously described (section **5.1.1**) and the staining process was followed according the manufacturer's instructions. Samples were immediately observed under a light microscope. The lipid droplets appeared in red while the nuclei appeared in blue.

Total collagen was stained using the dye combination of the Sirius Red/Fast Green collagen staining kit (Chondrex, Woodinville, WA). After fixation (section **5.1.1)**, the cells were stained according the manufacturer's instructions. Under a light microscope, total collagen appeared in purple while non-collagenous proteins appeared in green.

2.7 Albumin and urea measurement by ELISA sandwich

Albumin, secreted by the hepatocytes, is a major component of the human serum. Albumin concentration was determined using the Human Serum Albumin DuoSet ELISA kit (R&D Systems, Minneapolis, MN) according to the manufacturer's guidelines. First, a flat-bottom 96 well microplates was coated with diluted mouse anti-human serum albumin capture antibody (2 µg/ml) overnight at RT After a wash step, non-specific bindings were blocked with a PBS/1% BSA solution during 1 h at RT. The standard curve was created by serial dilution of the recombinant human serum albumin standard (160 ng/ml) in the PBS/1% BSA solution. Diluted standards and samples were then distributed in duplicate in the coated 96-well microplates and incubated for 2 h at RT. After the incubation, excess solutions were washed away and biotinylated mouse anti-human serum albumin antibody (125 ng/ml) was added in each well and incubated for 2 h at RT. After a wash step, streptavidin conjugated to

horsedish-peroxidase is incubated in the dark for 20 min at RT. The reaction was revealed with a 1:1 (v/v) mix of two reagents (hydrogen peroxide and tetramethylbenzidine) in the dark for 20 min at RT. Finally, the reaction was stopped with a 2N sulfuric acid solution and absorbance was measured with a microplate reader at 450 and 540 nm (Spark 10M, TECAN).

2.7.1 Urea measurement by colorimetric method

The production of urea, a chemical compound produced in the liver, was measured directly from the culture medium by an improved Jung method using the Urea Assay Kit (QuantiChrom DIUR100; BioAssay Systems, Hayward, CA). The reaction consists of the condensation of o-phthalaldehyde (OPA) with urea to form a colored complex. First, the two reagents A and B are mixed 1:1 (v/v). Then, in a 96-well plate with a transparent bottom, the samples, standard and blank were introduced in duplicate together with the reagent mixture A and B and incubated for 50 min at room temperature. Finally, the optical density was measured at 430 nm with a microplate reader (Spark 10M, TECAN).

2.8 RNA extraction and RT-qPCR analysis

All RT-qPCR analysis were performed at the IEMN laboratory (UMR 8520) of the Université de Lille. Total RNA was extracted and precipitated from cells by adding TRIzol (Invitrogen™, ThermoFisher) and chloroform: isoamyl alcohol (4 %). Concentration and purity of RNAs were determined using NanoDrop ™ One © Spectrophotometer (Life Technologies, Europe). RNA was transcribed into cDNA using 1 µg total RNA as a template, 1µl of random hexamers (Roche Diagnostics, Germany) and M-MLV (Moloney Murine Leukaemia Virus) reverse transcriptase (Life Technologies, Europe). Then, real-time quantitative reverse transcription polymerase chain reaction was performed using SsoAdvanced Universal SYBR® Green Supermix (Biorad, Hercules, CA) on an AriaMx Real-time PCR System (Agilent, USA). The 20 µl reaction volume included 2 µl of cDNA, 10 µl of SsoAdvanced Universal SYBR® Green Supermix, and 1 µl of primers (forward and reverse, 100 nM each). Each sample was analyzed in triplicate. Gene expression analysis was normalized against 60S acidic ribosomal protein P0 (RPLP0). The primer sequences are available in the Table 2.3 and Table 2.4. The mixture was incubated in AriaMx Real-time PCR thermal cycler at 95°C for 5 s, 59°C for 20 s and 72°C for 5 s for 40 cycles.

Table 2. 3: *Primers used in RT-qPCR of hepatic cells.*

Genes	Sequences
ALB	f_TGCTTGAATGTGCTGATGACAGG
	r_AAGGCAAGTCAGCAGGCATCTCATC
Cyp3A4	f_CCAAGCTATGCTCTTCACCG
	r_TCAGGCTCCACTTACGGTGC
INSRA	f_TTTTCGTCCCCAGGCCATC
	r_GTCACATTCCCAACATCGCC
INSRB	f_CCCCAGAAAAACCTCTTCAGG
	r_GTCACATTCCCAACATCGCC
GLUT2	f_TACATTGCGGACTTCTGTGG
	r_AGACTTTCCTTTGGTTTCTGG
P16	f_CTCGTGCTGATGCTACTGAGGA
	r_GGTCGGCGCAGTTGGGCTCC
P21	f_AGGTGGACCTGGAGACTCTCAG
	r_TCCTCTTGGAGAAGATCAGCCG
FASN	f_AGCCCTGTGCTGTTCCAG
	r_AACTCCAGGTTGTCCCTG
SREBP1	f_TCAGCGAGGCGGCTTTGGA
	r_GACTTCACCTTCGATGTCGGTCAG
RPLP0	f_ ACCTCCTTTTTCCAGGCTTT
	r_ CCCACTTTGTCTCCAGTCTTG

2.9 Metabolomic analysis

The culture medium was collected for the different conditions of each experiment and the samples were frozen in liquid nitrogen until analysis.

2.9.1 Samples preparation

The metabolomic analysis was performed on the culture media collected at the end of the experiments. For each culture condition, 6 samples from 3 independent experiments were used for 2 days of exposures, 5 samples from 3 independent experiments were used for 4 days of exposures; and 5 samples from 3 independent experiments were used for 7 days of exposures.

The procedure for sample preparation and metabolite extraction followed our previously published method[3]. In brief, 250 µL of culture medium was combined with 500 µL of an extraction solution (-20 °C) consisting of water, acetonitrile, and isopropanol in a ratio of 2:3:3. This solution also contained 4 mg/L of ribitol and 2.75 mg/L of α-aminobutyric acid (αABA). The mixture was stirred in an Eppendorf thermomixer (1500 rpm) for 10 min at 4 °C. After that, insoluble materials were removed through two centrifugation steps at 14000 rpm for 15 min. Subsequently, the samples were dried for 4 h at 35 °C in a speed-vac system and stored at -80 °C until further analysis.

Before injection into the gas chromatograph-mass spectrometer (GC-MS), the samples were dried again for 2 h, and 10 µL of a methoxyamine solution in pyridine (20 mg/mL) was added. Following 90 min at 30 °C, 90 µL of N-methyl-N-trimethylsilyl-trifluoroacetamide (MSTFA) was added, and the reaction continued for 30 min at 37 °C. Finally, 100 µL of the resulting solution was transferred to an Agilent vial for injection.

The GC-MS analysis was performed using an Agilent 7890B gas chromatograph coupled to an Agilent 5977A quadrupole mass spectrometer. The column used was a Rxi-5SilMS from Restek. For quantification of saturated compounds, a split mode with a ratio of 1:30 was used for injection. The oven temperature ramp ranged from 60 °C for 1 min, then increased at a rate of 10 °C/min to 325 °C for 10 min. Helium was used as the carrier gas with a constant flow of 1.1 mL/min. The temperatures for the injector, transfer line, source, and quadrupole were set at 250 °C, 290 °C, 230 °C, and 150 °C, respectively. The mass spectrometer was turned on

after a solvent delay of 5.90 min, and data was collected in the range of 50-600 u. External retention index calibration was performed using a fatty acid methyl ester mix (C8, C9, C10, C12, C14, C16, C18, C20, C22, C24, C26, C28, C30).

Raw data files obtained from Agilent were analyzed using AMDIS software (www.amdis.net). Metabolite identifications were conducted using the Agilent Fiehn GC/MS Metabolomics RTL Library (version June 2008). Peak areas were determined using Agilent Masshunter Quantitative Analysis in both splitless and split 30 modes. To ensure accuracy, automated peak integration was verified manually for each compound, and peak areas were normalized to ribitol. Metabolite contents were expressed in arbitrary units, representing semi-quantitative determinations.

Finally, OA and PA contents in the samples were normalised by the OA and PA contents detected in the blank culture medium (medium not exposed to the cells).

2.9.2 Metabolomic statistical analysis

The metabolomic multivariate data analysis was performed using MetaboAnalyst 5.0[4]. The data were auto-scaled (mean-centered and divided by the standard deviation of each metabolite).

Firstly, we performed an ANOVA to clarify if we could detect difference between the treatments for each time points. Then, supervised partial least squares-discriminant analysis (PLS-DA, comparison of more than two groups) were applied to get the maximum separation between control and treated groups, and to explore the variables that contributed to this separation. The quality of PLS-DA model was evaluated by the R2Y (fitting degree) and Q2 (prediction parameter) values. To determine the best discriminators metabolites, the adjusted p_value < 0.05 was used from the ANOVA analysis (FDR < 0.05). Heatmap and hierarchical clustering were performed using the normalized data (auto-scale features, Euclidean distance measure, and ward clustering method on the ANOVA analysis). Finally, pathway enrichment analysis was performed with MetaboAnalyst using the selected significant metabolites. Then, a similar analysis was performed to extract the difference between the time points on each treatment.

2.10 Statistical analysis

The data are expressed as the mean ± SD. A Student's t-test was used for statistically evaluating pairs of groups. Two-way ANOVA and post-Tukey's multiple comparison test were used to compare groups of three or more. The significance level was set at $p < 0.05$ and calculated on GraphPad Prism version 3.01.

2.11 References

1 M. Shinohara, K. Komori, T. Fujii and Y. Sakai, *Biomed Phys Eng Express*, 2017, **3**, 045016.

2 M. Shinohara, H. Kimura, K. Montagne, K. Komori, T. Fujii and Y. Sakai, *Biotechnol Prog*, 2014, **30**, 178–187.

3 R. Jellali, P. Zeller, F. Gilard, A. Legendre, M. J. Fleury, S. Jacques, G. Tcherkez and E. Leclerc, *Environ Toxicol Pharmacol*, 2018, **59**, 1–12.

4 Z. Pang, J. Chong, G. Zhou, D. A. De Lima Morais, L. Chang, M. Barrette, C. Gauthier, P. É. Jacques, S. Li and J. Xia, *Nucleic Acids Res*, 2021, **49**, W388–W396.

Chapter III:

Development of a NAFL-on-chip using a HepG2/C3A-based liver-on-chip

In this chapter, we investigated the effect of several fatty acids in order to develop a relevant NAFL liver-on-chip model. We used HepG2/C3A cell line as hepatocyte model for study acute and chronic exposure to fatty acids. After exposure, HepG2/C3A cells were analysed structurally and functionally in order to highlight (i) if our liver-on-chip can reproduce the NAFL behaviour (ii) what fatty acids treatment is the more relevant to mimic NAFL (iii) advantages of NAFL liver-on-chip model. This chapter is partially extracted from the article "Investigation of the lipotoxicity of oleic acid, palmitic acid and their mixture on human hepatocarcinoma in a 3D dynamic micro environment".

3.1 Introduction

The deleterious effects of non-alcoholic fatty liver disease (NAFLD) are becoming a growing challenge for public health as a direct effect of the increasing prevalence of diabetes and obesity worldwide. NAFLD is the most common chronic liver disease in the Western world notably. As defined in Chapter I, NAFLD is characterized by hepatic steatosis when no other causes for secondary hepatic fat accumulation (e.g., excessive alcohol consumption) can be identified. NAFLD ranges to benign steatosis (NAFL; 80%) without evidence of inflammation to Non-Alcoholic Steato-Hepatitis (NASH; 20%) which is associated with lobular inflammation and apoptosis that can lead to fibrosis, cirrhosis and Hepato-Cellular Carcinoma (HCC)[1,2]. Moreover, the risk of a cardiovascular disease is significantly increased in patients affected by NAFLD and their complications[2]. Since NAFLD is strongly associated with obesity and diabetes, the disease has been recently redefined as metabolic (dysfunction)-associated fatty liver disease (MAFLD)[3]. Nevertheless, the consideration of this new terminology is still on going. In the past 70 years, research has been conducted on rodent models of obesity (high fat diet; high cholesterol diet; *db/db* mice (diabete mice); *ob/ob* mice (obese mice) in order to investigate the pathophysiology of NAFLD and led to the "two-hit hypothesis"[2,4]. According to this, the first hit refers to hepatic accumulation of lipids secondary to sedentary lifestyle, high fat diet, obesity and insulin resistance. Then, the "second hit" activates inflammatory cascades, mitochondrial dysfunction, oxidative stress promoting disease progression toward fibrogenesis[5]. However, progress in the last decade demonstrated that this hypothesis cannot fully explain the heterogeneity of the pathophysiology, leaving room for the "multiple-hit hypothesis"[6]. Indeed, NAFLD involved metabolic dysfunctions resulting from organs interactions, dietary habits, gut microbiota, genetic and environmental factors[7,8].

In terms of diagnostic, the most precise test to NAFLD detection is histology analysis of liver biopsy despite a non-uniformly distribution of the disease in the liver. Although this test is the gold standard, non-invasive tests are privileged for NAFLD detection. Indeed, numerous non-invasive scores based on abdominal ultrasound (AUS), Magnetic Resonance Imaging (MRI) and/or Magnetic Resonance Spectroscopy (MRS) and serum biomarkers allowed to determine presence, but not severity of liver steatosis[9]. Even though several international guidelines have been published the past few years, inconsistent attitudes are

still noticed in screening and detection strategies due to non-uniformity but above all to sample and inter-observer variations causing inappropriate management of patient[10,11]. Currently, there are no specific drug therapies for the treatment of NAFLD. Changes in diet and lifestyle are recognize as the first strategies while drug therapy mainly focused on glucose and lipid metabolism regulation and anti-inflammation[8]. Indeed, progress in developing pharmacologic therapies for NAFLD has been hampered by several challenges, including a high screening failure rate and the reliance on an invasive gold standard that could be unclear and accompanied by high and variable placebo responses[12]. Thus, it is necessary to develop new biomarkers to enable concrete non-invasive diagnosis of the patient, prognosis and propose NAFLD-specific therapy. Moreover, reliable biomarkers would allow to identify subpopulation of patient according to disease severity and to treat them with adjust therapy[12,13]. Thus, the progression and development of new technologies in NAFLD diagnostics and therapy is crucial to find a unified position for NAFLD management.

Lately, several emerging technologies, developed for the need of the toxicology and pharmacology fields, have created opportunities for a more modern approach to liver disease study including steatosis using 3D hepatic cultures in spheroids and organoids[14–16]. Of those technologies, organ-on-chip is a strong candidate to replace the traditional animal-based model[17]. They also have the potential to efficiently replace 2D primary cell cultures in which the cell physiological properties and regulations are often lost. The liver-on-chip approach is hence based on the conviction that the reconstitution of the physiological microenvironment of the organ is key in obtaining *in vivo*-like cell cooperation and responses and will provide a detailed unravelling of the cellular and molecular events underlying a specific pathophysiological condition[18,19]. Our group, among very few others, has developed successful liver-on-chip solutions allowing to gain new insights in liver metabolism[20], biomarkers identification and predictive toxicology[21,22]. This innovative technology was also used to investigate the development of liver steatosis and the key aspects of NAFLD progression[23–25]. Among them, our team, initially focused on pesticide actions, have already validated the possibility of recapitulating steatosis via the use of our human primary hepatocytes integrated to a liver-on-chip approach[26].

In order to extend the investigations on NAFL using organ-on-chip we propose to characterize the effect of several free fatty acids using our HepG2/C3A based liver-on-chip[22,27,28]. We selected oleic acid (OA), palmitic acid (PA) and a mixture of oleic and palmitic acids (OA/PA) as far as they are common dietary products with strong impact on human's health, including obesity and NAFLD[29–31]. The objective is to confirm whether our hepatic organ-on-chip can reproduce such behaviour and if so, to highlight new pathophysiological processes and to extract potential biomarkers by studying cell morphologies and functions.

3.2 Pathophysiological characterization of the NAFL liver-on-chip based on HepG2/C3A cell line

As described in Chapter II, we perfused HepG2/C3A cells with high concentration of FFAs (0.66 mM OA, 0.33 mM PA or 1 mM OA/PA (2:1)) for 2 or 7 days. First, we analysed qualitatively the cell proliferation rate for each condition, then we observe the development of intracellular lipid accumulation which is a NAFL hallmark.

3.2.1 Morphological observation reveals noticeable difference between the different FFAs treatments

HepG2/C3A cells were inoculated into coated biochips and were incubated overnight at 37 °C for cell adhesion. Observation at phase contrast microscopy before microfluidic perfusion demonstrated the successful cellular adhesion as cells were elongated and homogenously dispersed inside the microsystem (Figure 3.1).

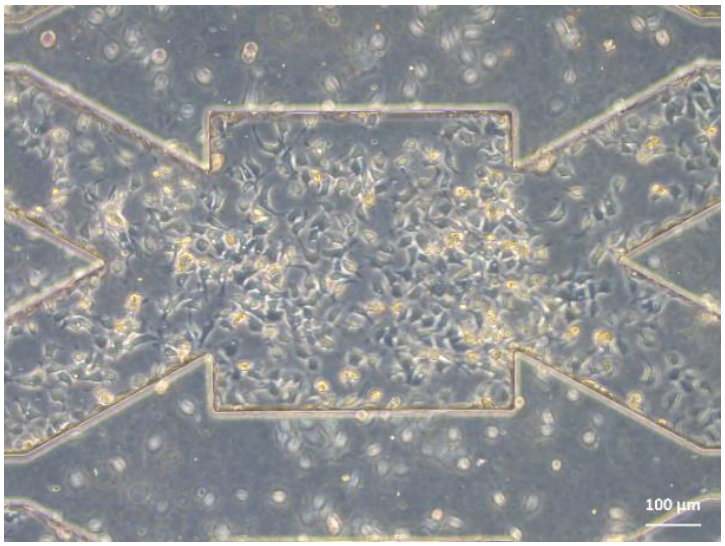

Figure 3. 1: *Cells morphology after 24 h after seeding.*

After 7 days of exposure to FFAs, we observed a multilayer cell proliferation inside the biochips while after 2 days this proliferation was less important for all experiments. Nevertheless, when compared to control, OA and OA/PA experiments, PA experiments showed a weaker cell density particularly after 7 days of exposure as shown in Figure 3.2B. Indeed, numerous biochips presented degraded tissues in which cells have detached from the biochips. Cell counting at the end of experiment, showed a similar proliferation of the HepG2/C3A in all conditions at day 2. Then, between day 2 and day 7, we measured an increase of the cell proliferation in control and OA experiments (proliferations between D2 vs D7 for control and OA have a p-value < 0.05), whereas any statistic difference in the proliferation between for PA and OA/PA treatments was detected (Figure 2C). Nevertheless, PA ($4.7\pm1.6\text{x}10^6$ cells) treated biochips showed a two-fold decrease of cell numbers compared to OA ($9.1\pm2.1\text{x}10^6$ cells) treated biochip after 7 days of exposure.

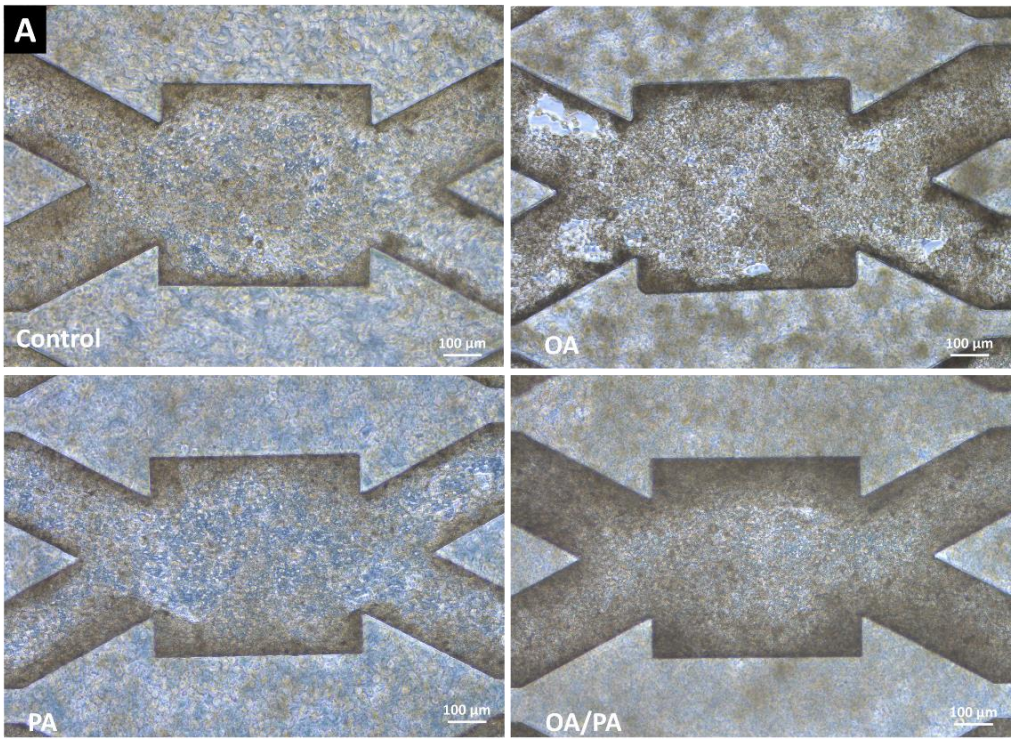
A
Control
100 µm
OA
100 µm
PA
100 µm
OA/PA
100 µm

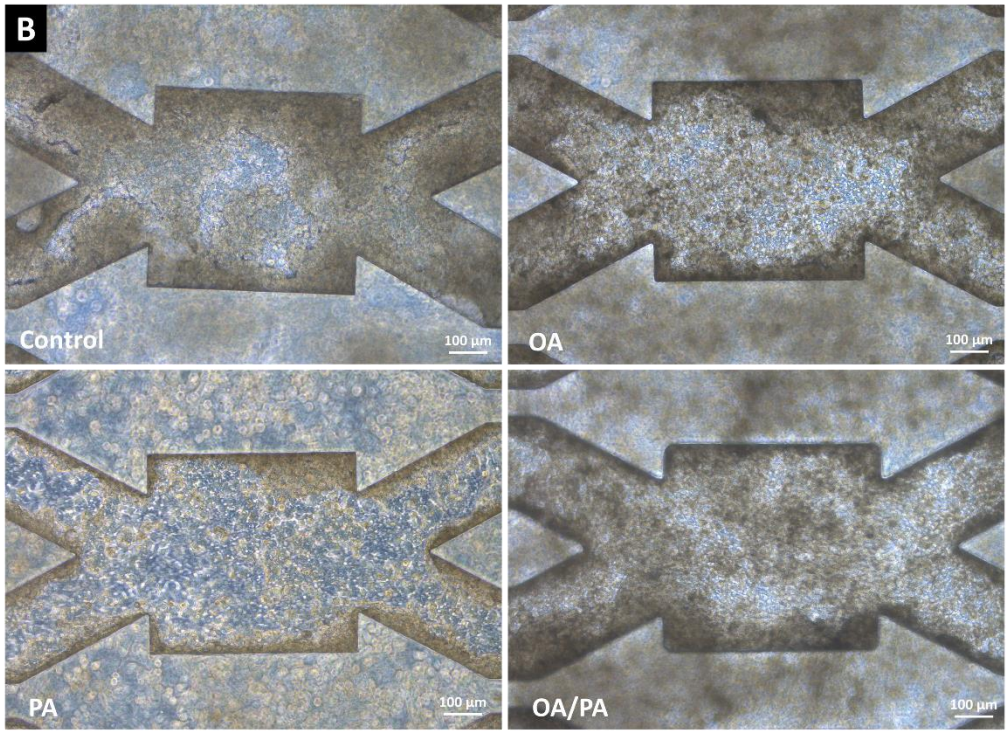
B
Control
100 µm
OA
100 µm
PA
100 µm
OA/PA
100 µm

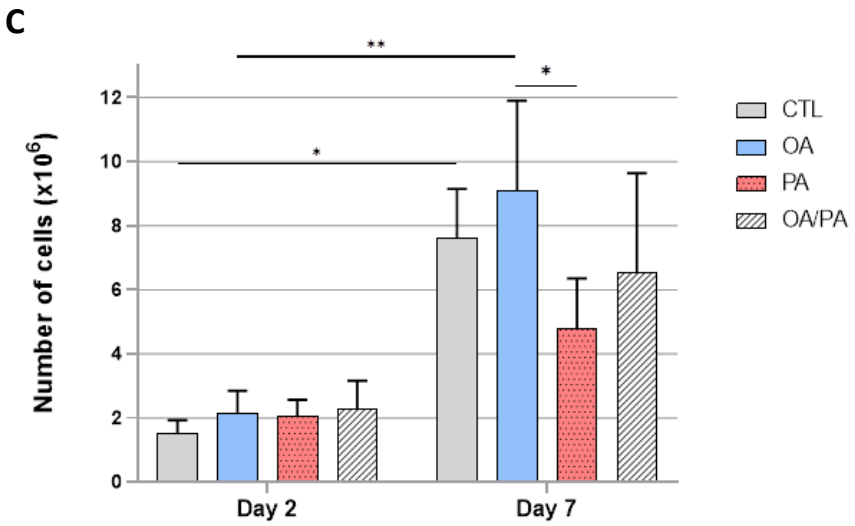

Figure 3. 2: *Morphological and functional analysis of HepG2-C3A.* ***(A)*** *Cell morphology at the end of the 2 days and* ***(B)*** *7 days exposure experiment.* ***(C)*** *Collected cell number in control and treated samples after 2 and 7 days of culture. Statistically analysed by ANOVA test with *p<0.05; **p<0.01. n=3.*

3.2.2 NAFL was successfully induced on HepG2/C3A based liver-on-chip

As we know that the exposure of cell to high concentration of FFAS led to lipid accumulation of neural lipids we assessed lipid droplet accumulation using Oil Red O as shown in Figure 3.3. Firstly, we observed an absence of lipid accumulation in the control situations after two days of exposure. In parallel, the analysis revealed a slight accumulation of lipid in OA conditions when compared control situation (Figure 3.3A). Conversely, on the PA and OA/PA tissues, we did not observe such clear accumulation. After 7 days of FFA exposures, we found, as for the 2 days FFAs exposure, an absence of lipid accumulation in control tissue. On the OA treated tissues we observed a larger lipid droplet accumulation when compared to the 2 days exposure situations (Figure 3.3B). We did not observe any change in lipid accumulation for PA and OA/PA tissues when compared to 2 days exposure tissues.

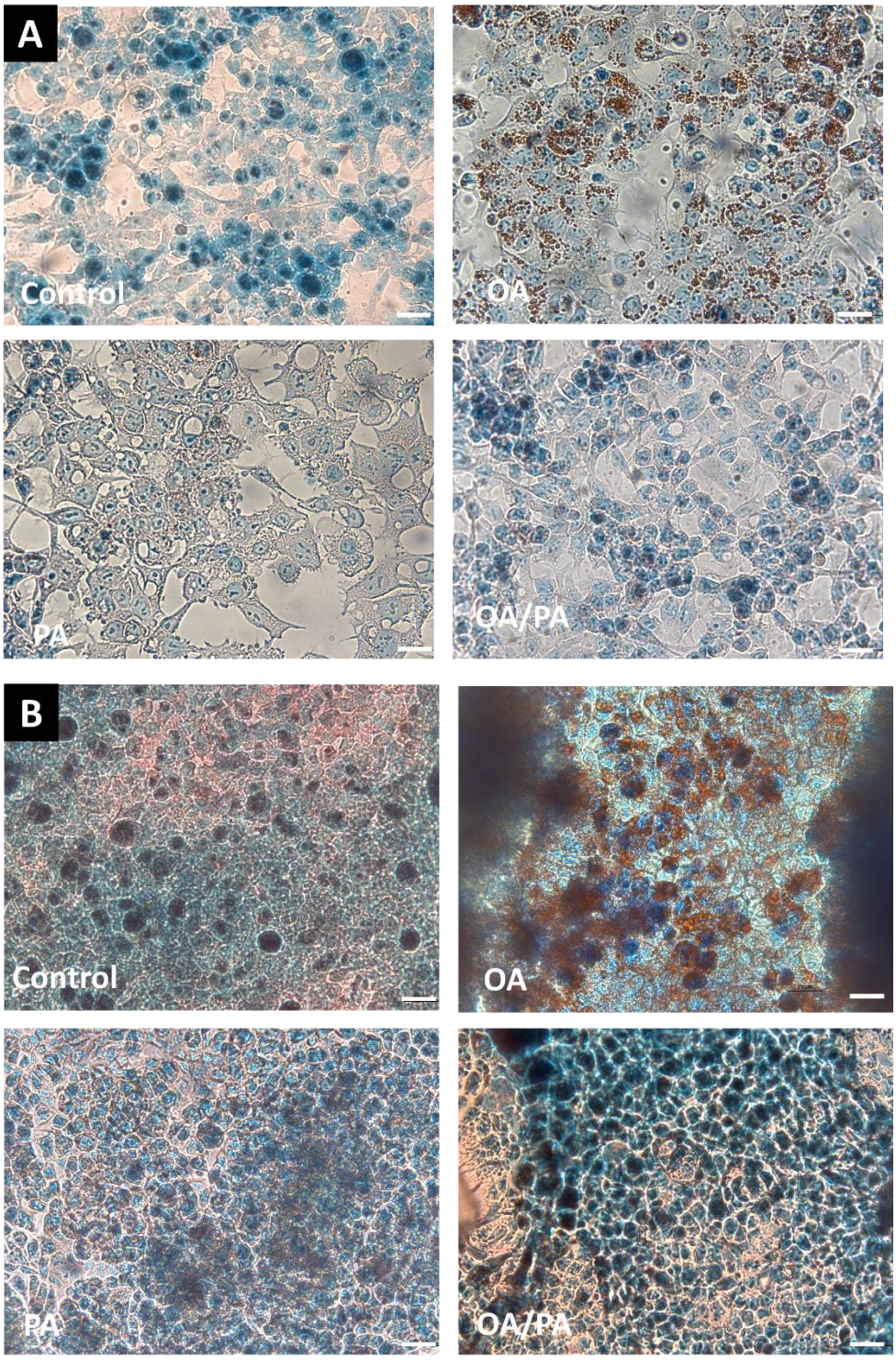

Figure 3. 3: *Intracellular lipid droplet staining using Oil Red O* ***(A)*** *after 2 days and* ***(B)*** *7 days of FFAs exposure. Scale bar: 20 µm.*

3.2.3 ROS investigation reveals the toxic action PA treatment

As we know that FFAs can generate Reactive Oxygen Species (ROS), we assessed ROS generation using a fluorogenic dye, 2',7'- dichlorofluorescin diacetate (DCFDA). Fluorescence microscopic observation shown no notable difference between the experiments after 2 days of exposure (Figure 3.4A) while intense green fluorescence in OA and OA/PA experiments have been observed after 7 days of exposure (Figure 3.4B). Indeed, fluorescence intensity assessment demonstrated a decrease in green fluorescence for PA experiment when compared to OA and OA/PA experiments (Figure 3.4C).

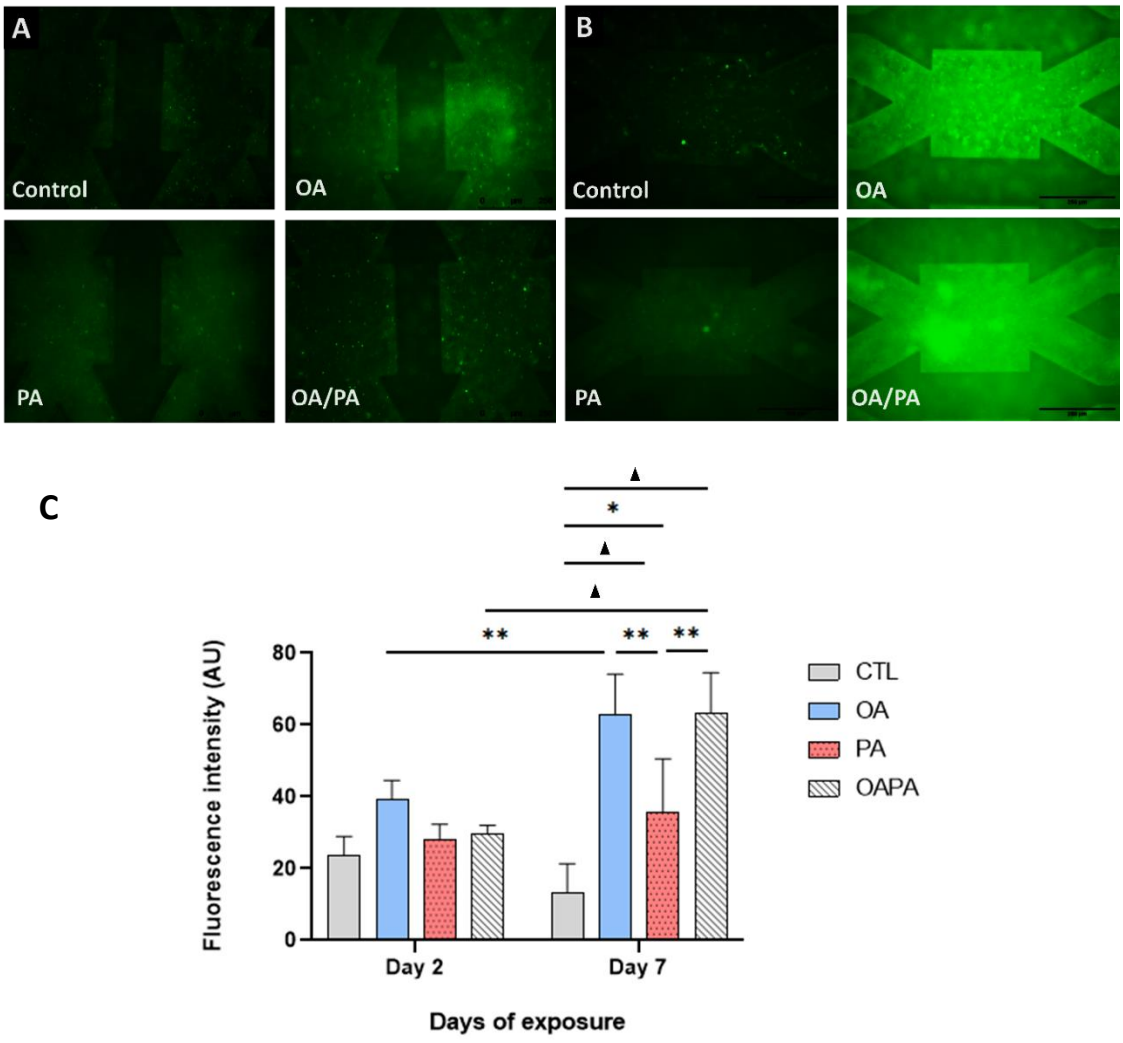

Figure 3. 4: *ROS detection using DCFDA staining on control and samples treated for* ***(A)*** *2 days and* ***(B)*** *7 days.* ***(C)*** *Fluorescence intensity assessment of ROS staining. Statistically analysed by ANOVA test with *p<0.05, ** p<0.005, ▲p<0.0001. n≥3.*

3.3 Functional characterization of the NAFL liver-on-chip based on HepG2/C3A cell line

3.3.1 Albumin and CDH1 assessment reveals decreased in albumin secretion and dedifferentiation following exposures

Assessment of albumin secretion is commonly used as a liver function test to indicate potential liver injury and pathology. First, we investigated albumin secretion by immunostaining. We observed a fluorescent signal for all experiments for both end points. However, the fluorescent signal for treated cells was weaker compared to healthy cells after 2 days of exposure, especially for PA experiments when compared to OA and OA/PA. (Figure 3.5A). This tendency was still observable at day 7. Indeed, albumin expression seemed to be weaker for PA condition when compared to CTRL, OA and PA condition (Figure 3.5B). Nevertheless, there was no obvious difference between CTRL, OA and OA/PA albumin expression. We also evaluated CDH1 (E-cadherin) for all conditions. The exposure to FFA, particularly PA and OA/PA mixture, contributed to reduce the intensity of the CDH1 signal for both end point with a more significant effect observed after 2 days of exposure.

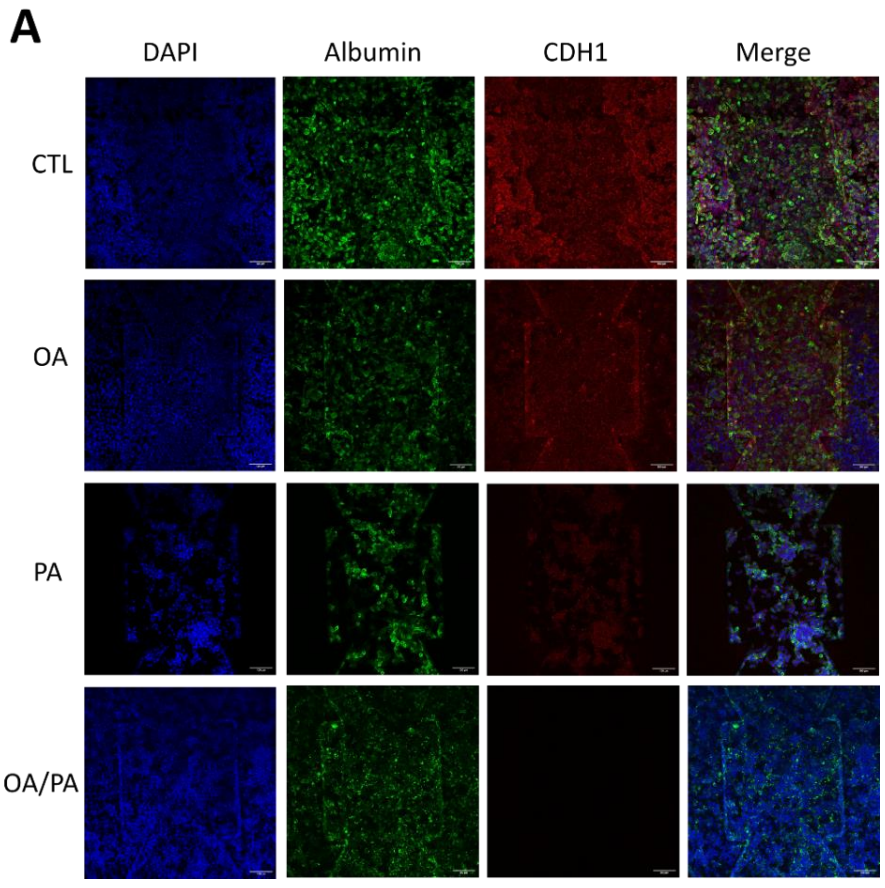

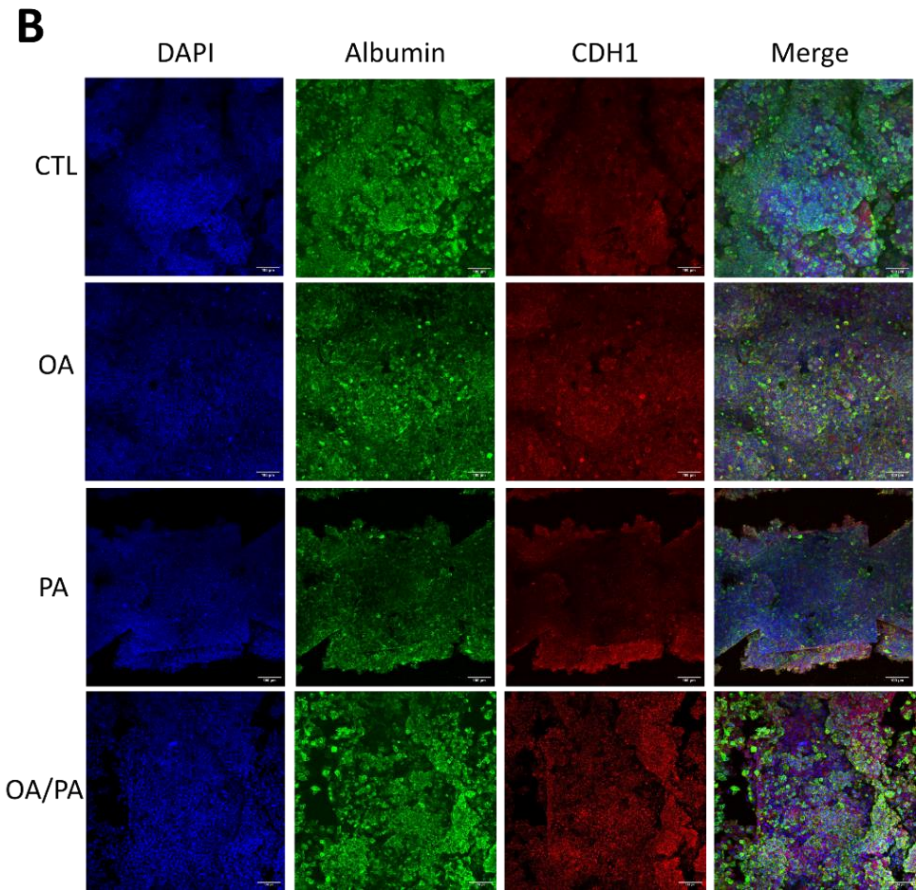

Figure 3. 5: *Immunostaining of control and treated samples after* ***(A)*** *2 days and* ***(B)*** *7 days of FFAs exposure. Scale bar: 100 µm.*

Then, we performed measurement of albumin secretion in culture media samples. We noticed a significant decrease of the albumin secretion for the treated cells after 2 days of exposure. Indeed, healthy cells albumin secretion reached 109.62±20.3 ng/day/10^6 cells while treated cells did not reached 32 ng/day/10^6 cells. Then, we established that, after 7 days of exposure, the cells produced about 81.21±15.34 ng/day/10^6 cells, 52.45±21.24 ng/day/10^6 cells, 128.98±31.33 ng/day/10^6 cells and 84.9±25.68 ng/day/10^6 cells in control, OA, PA and OA/PA conditions, respectively. We observed a significant higher albumin secretion in PA when compared to control OA, PA and OA/PA condition.

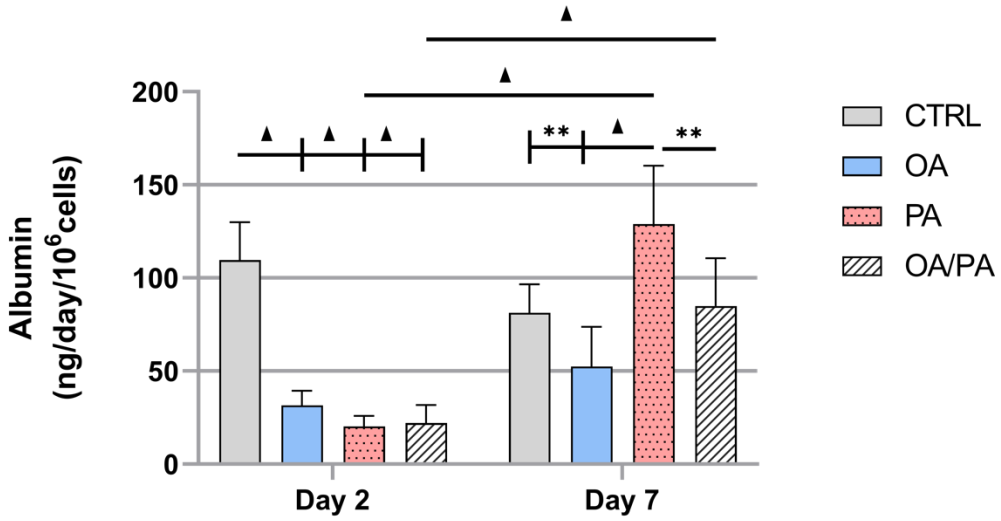

Figure 3. 6: *Albumin secretion in control and treated samples after 2 and 7 days of culture. Statistically analysed by ANOVA test with *p<0.05; **p<0.01; ▲ p<0.0001. n=5.*

3.3.2 RT-qPCR analysis highlights disruption in the expression of key genes involved in liver function and lipid metabolism in 7 days- treated samples

The comparison of the mRNA levels by RT-qPCR demonstrated that any (or only a weak) perturbation of the mRNA expressions of ALB, CYP3A4 (hepatic differentiation), INSRA, INSRB, FASN, SREBP1 (lipid metabolism), GLUT2 (glucose transport), p16, p21 (cell cycle, senescence related genes) after 2 days of cultures in OA, PA and OA/PA treated conditions when compared to the controls. Nevertheless, a weak upregulation of INSRA, INSRB, p16 and p21, was observed in OA/PA samples (Figure 3.6).

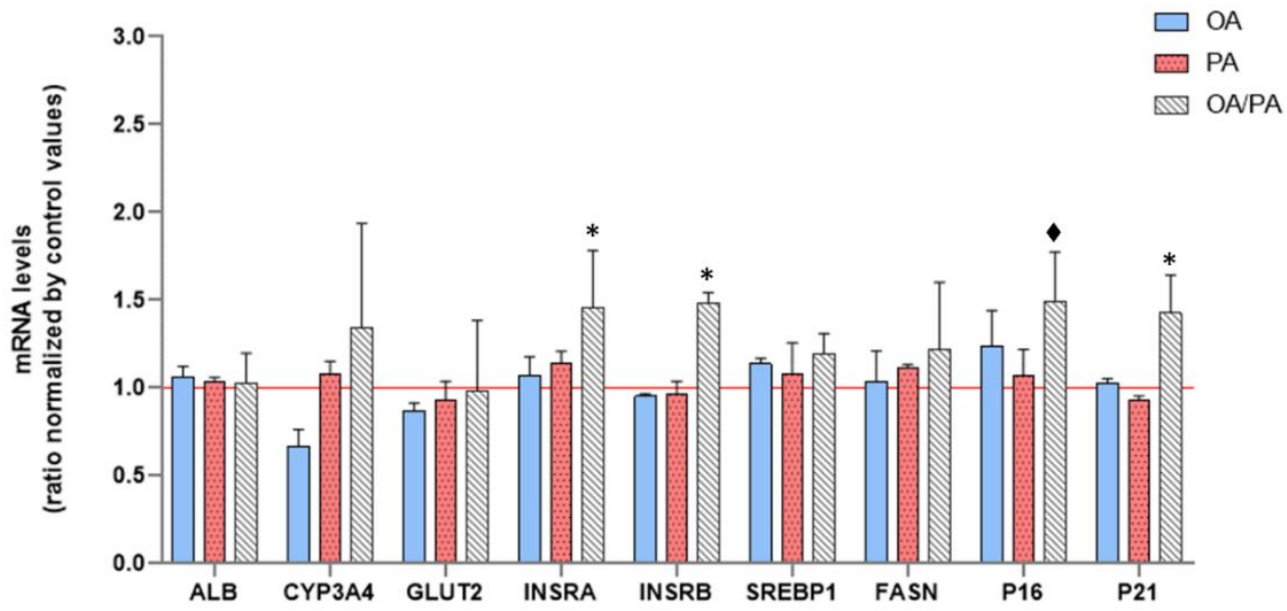

Figure 3. 7: *mRNA expression (RT-qPCR) of some key genes involved in liver function, lipid metabolism and senescence after 2 days treatment. Statistically analysed by ANOVA test with *p<0.05; ♦ p<0.005;▲ p<0.0001. n=12.*

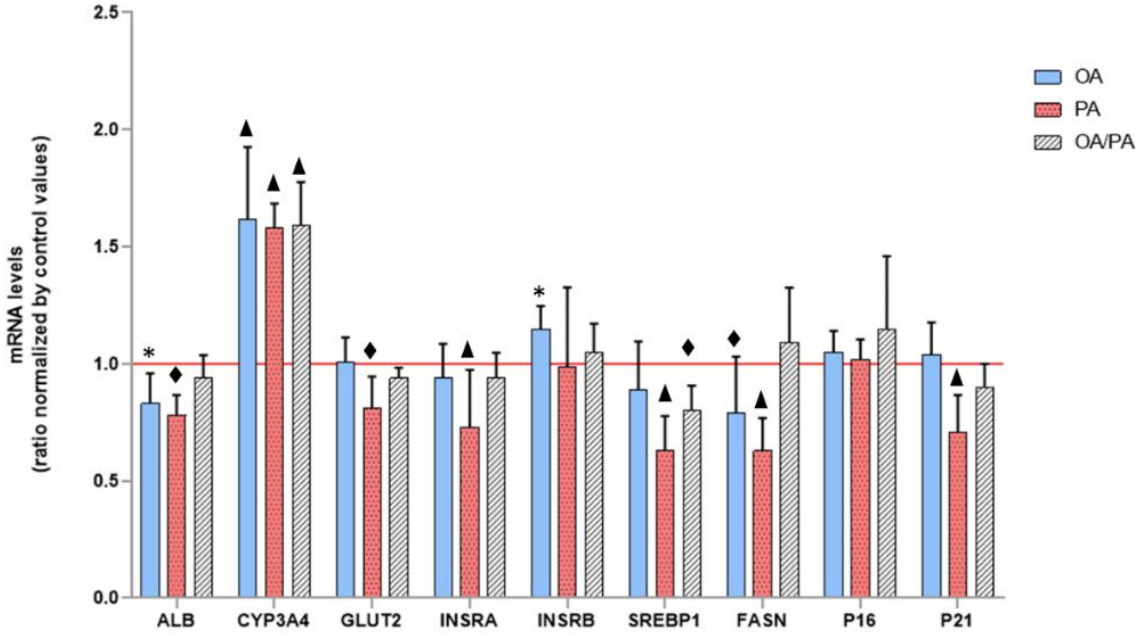

Figure 3. 8: *mRNA expression (RT-qPCR) of some key genes involved in liver function, lipid metabolism and senescence after 7 days treatment. Statistically analysed by ANOVA test with *p<0,05; ♦ p<0,005; ▲p<0,0001. n=12.*

After 7 days of culture (Figure 3.7), we found that all fatty acid treatments induced an upregulation of the CYP3A4 mRNA when compared to controls. Then OA and PA led to the reduction of ALB mRNA whereas OA/PA appeared to restore control levels. OA and OA/PA treatments did not modulate the mRNA expression of FASN, GLUT2, INSRA in our biochip experiments. Conversely, PA treatments contributed to downregulate those genes when compared to control, OA and OA/PA conditions. SREBP1 was downregulated in both PA and OA/PA conditions. The p21 gene appeared downregulated in PA treatments and only a weak upregulation was detected on the p16 gene in OA/PA conditions.

3.4 Discussion

We have compared the HepG2/C3A response cultivated inside a microfluidic biochip to three FFA treatments. The literature largely reported the hepatoprotective effect of oleic acid to palmitic acid injury[32,33]. This effect was partially observed in our biochip model after 7 days of exposure as we will discuss in the following paragraphs.

A reduction of the viability, in dose and time dependent manner under PA, OA, OA/PA was observed in 2D culture of HepG2[32]. Furthermore, OA hepatoprotective effect under PA treatment due to OA/PA exposure was reported by Zeng *et al.*[32]. In our data, we observed any perturbation of the proliferation at after 2 days of exposure between all conditions. Then, after 7 days of exposure, we even measured a significant proliferation in control and OA treatments (when compared to 2 days situation). As, the increase of the proliferation was not significant in PA and OA/PA treatments, this result may tend to demonstrate a negative effect of the PA on the proliferation. However, the hepatoprotective effect of OA on PA in OA/PA was not highlighted by the proliferation assay. When compared to conventional 2D well plates cultures, our biochip provided a dynamic and 3D micro environment that is suitable for dense and large HepG2/C3A proliferation[28,34,35]. Such environment is therefore more suitable for cell growth when compared to 2D models leading to difference with literature observations.

Regarding the carbohydrates and lipid metabolisms, GLUT2, a glucose transporter, is induced in OA[36] and PA treated HepG2[37]. In other studies, using HepG2 cells, PA was also associated with down regulation of insulin receptor[38] and with the reduction of the glucose

uptake[39]. In the present analysis, we found down regulation of GLUT2 and INSRA only in PA treatments but not in OA and OA/PA illustrating the probable restoration by OA to the PA negative effect for both mRNA levels. We also found the downregulation of FASN, SREBP1 by PA and the partial recovery of those mRNA levels due to OA in the OA/PA treatments. Our 3D results appeared different from 2D recent literature that reported that FASN and SREBP1 mRNA levels are (i) not modulated by OA, (ii) induced by PA, (iii) and then restored to control levels in AO/PA treatments after 24 h of exposure in HepG2[32]. Furthermore, SREBP1 protein is also reported to increase in HepG2 with 24 h PA treatments[40]. However, SREPB1 upregulation was PA dose dependent and did not occur at 0,66 mM after 24 h of treatment in HepG2[41]. After 2 days of FFA exposure, we did not detect OA and PA effect on FASN and SREBP1. Although we observed a recovery like-effect by OA in OA/PA condition after 7 days of treatments at the mRNA level, additional investigations are required to refine the understanding of those complex tendencies.

Then, we found that all FFA treatments led to modify the hepatic classical differentiation markers consistently with the literature. We measured an over expression of the mRNA of CYP3A4 mRNA levels after 7 days of exposure. This finding is consistent with HepG2 reports in which CYP3A4 was reported to be upregulated under oleic acid via AMPK-, PKC-, and NF-κB–dependent pathways, and under the palmitic acid via probably the PKC-dependent pathway[42]. In parallel, the albumin secretion and the albumin immunostaining demonstrated a clear reduction of the albumin level in FFA treated condition (when comparing the controls of the 2 days of treatments), which appeared consistent with several literature reports (in rat hepatocytes after 24 h of exposure [33,43] and after 72 h in AML12 cells[43]). Although we detected a downregulation of the ALB mRNA levels at day 7, we observed that the albumin secretion was not significantly modulated anymore after 7 days of exposure in OA and OA/PA conditions (when compared to the controls). We furthermore detected an increase of the albumin cell secretion in PA conditions. It was reported that FFA did not affect mRNA levels after day 7 of treatment in HepG2/C3A spheroids[44]. In addition, albumin protein is used to transport FFA[45], as an antioxidant[46] and therefore to detoxify FFA accumulation. Finally, as HepG2/C3A are tumoral cells, abnormal behavior cannot be excluded. Additional analysis would be required to fully understand this mechanism.

At the immunostaining level we also confirmed a reduction of CDH1 intracellular expression after 2 days of exposure. CDH1 is a marker of epithelial specification and its expression is reduced during hepatic dedifferentiation[47]. Consistently, a reduction of CDH1 mRNA levels in HepG2 has been documented after 48h and 72h of OA/PA exposures[44]. In parallel, CDH2 protein (CDH1 reduction and CDH2 increase is hallmark of epithelial to mesenchymal transition and dedifferentiation[47]) is reported to increase during OA/PA exposure in parallel to TGFα activation in HepG2 spheroids[44]. Then, we did not detect any clear alteration by FFA of CDH1 after 7 days of treatments in our experiments (immunostaining data). Interestingly, at longer time of culture, it was also reported that the OA/PA treatment did not affect CDH1 mRNA levels after day 7 of treatment in HepG2 spheroids[44] which was also consistent with our immunostaining data finding.

Then, we investigated lipid accumulation and characterized reactive oxygen species production in our model. We observed lipid accumulation only in OA treatments. This accumulation increased with the time of exposure. Long term FFA exposition gradually led to a steatosis and is well characterized by the hepatic ballooning (illustrated by the lipid droplet accumulation, Takahashi *et al.*[48]. Consistently literature reported higher lipid accumulation of OA when compared to PA in HepG2 cells[49]. Interestingly, our finding indicated that the PA co-exposure to OA led to reduce this lipid accumulation. In fact, in HepG2, PA treatment resulted in a significant decrease in the OXPHOS complex assembly and in their faster degradation, a weaker ATP production which could explain the lower ROS production in our PA conditions[50]. Furthermore, we detected an intense ROS expression in OA and OA/PA treatments whereas PA treatment led to weaker ROS secretion. In fact, in HepG2, PA resulted in a significant decrease in the OXPHOS complex assembly and in their faster degradation, a weaker ATP production[50] which could explain the lower ROS production in our PA conditions.

Finally, FFA are often associated with senescence and modification of cell cycle[51]. Senescence was characterized by the increases of the p21 and p16 genes in HepG2 which in turn contribute to promote pro NASH's signallings[52]. In our data set, the p21 mRNA was downregulated only in PA conditions (whereas the p16 mRNA was weakly up regulated in OA/PA). As result we were not able to particularly conclude on the status of the senescence process within our biochip. In fact, we hypothesis that the liver cell model (HepG2/C3A) used

in this study promote 3D organization of the tissue within the biochip and contribute to enhance continuous cellular multi-layer proliferation.

3.5 Conclusion

We have used a liver-on-chip technology to investigate the effect of free fatty acids on HepG2/C3A cells. We observed that the FFA treatments did not modify significantly the HepG2/C3A proliferation after 2 days of exposure. All FFA treatments led to the upregulation of CYP3A4 mRNA levels after 7 days of exposures. We found that palmitic acid treatment led to a lipid metabolism perturbation that was characterized by the important downregulation of GLUT2, INSRA, FASN and SREBP1 mRNA levels after 7 days of exposure. However, the co-exposure of oleic acid with palmitic acid restored the mRNA levels of GLUT2, INSRA, FASN and partially of SREBP1. Oleic acid exposure was associated with a lipid accumulation in the cells that was not observed in PA and suppressed in OA/PA conditions. Finally, the oleic acid exposure and oleic/palmitic acids co-exposure led to higher ROS productions when compared to control and palmitic acid treated conditions.

3.6 References

1 K. C. Lee, P. S. Wu and H. C. Lin, *Clin Mol Hepatol*, 2023, **29**, 77.

2 S. L. Friedman, B. A. Neuschwander-Tetri, M. Rinella and A. J. Sanyal, *Nat Med*, 2018, **24**, 908.

3 C. Gofton, Y. Upendran, M.-H. Zheng and J. George, *Clin Mol Hepatol*, 2023, **29**, S17–S31.

4 Y. R. Im, H. Hunter, D. de Gracia Hahn, A. Duret, Q. Cheah, J. Dong, M. Fairey, C. Hjalmarsson, A. Li, H. K. Lim, L. McKeown, C. G. Mitrofan, R. Rao, M. Utukuri, I. A. Rowe and J. P. Mann, *Hepatology*, 2021, **74**, 1884–1901.

5 P. Paschos and K. Paletas, *Hippokratia*, 2009, **13**, 128.

6 H. Tilg, T. E. Adolph and A. R. Moschen, *Hepatology*, 2021, **73**, 833–842.

7 E. Buzzetti, M. Pinzani and E. A. Tsochatzis, *Metabolism*, 2016, **65**, 1038–1048.

8 L. Rong, J. Zou, W. Ran, X. Qi, Y. Chen, H. Cui and J. Guo, *Front Endocrinol*,2022, **13**.

9 S. Pouwels, N. Sakran, Y. Graham, A. Leal, T. Pintar, W. Yang, R. Kassir, R. Singhal, K. Mahawar and D. Ramnarain, *BMC Endocr Disord*, 2022, **22(1)**, 63.

10 N. Chalasani, Z. Younossi, J. E. Lavine, A. M. Diehl, E. M. Brunt, K. Cusi, M. Charlton and A. J. Sanyal, *Hepatology*, 2012, **55**, 2005–2023.

11 European Association for the Study of the Liver (EASL), *Diabetologia*, 2016, **59**, 1121–1140.

12 Z. Gluvic, R. Tomasevic, K. Bojovic, M. Obradovic and E. R. Isenovic, *Emergency and Critical Care Medicine*, 2022, **2**, 12–22.

13 D. G. K. Rasmussen, Q. M. Anstee, R. Torstenson, B. Golding, S. D. Patterson, C. Brass, P. Thakker, S. Harrison, A. N. Billin, D. Schuppan, J. F. Dufour, A. Andersson, I. Wigley, E. Shumbayawonda, A. Dennis, C. Schoelch, V. Ratziu, C. Yunis, P. Bossuyt and M. A. Karsdal, *J Hepatol*, 2023, **78**, 852–865.

14 P. Pingitore, K. Sasidharan, M. Ekstrand, S. Prill, D. Lindén and S. Romeo, *Int J Mol Sci*, 2019, **20(7)**, 1629.

15 M. Kozyra, I. Johansson, Å. Nordling, S. Ullah, V. M. Lauschke and M. Ingelman-Sundberg, *Sci Rep*, 2018, **8**, 14297.

16 M. Duriez, A. Jacquet, L. Hoet, S. Roche, M. D. Bock, C. Rocher, G. Haussy, X. Vigé, Z. Bocskei, T. Slavnic, V. Martin, J. C. Guillemot, M. Didier, A. Kannt, C. Orsini, V. Mikol and A. C. Le Fèvre, *J Clin Transl Hepatol*, 2020, **8(4)**, 359–370.

17 E. W. Esch, A. Bahinski and D. Huh, *Nat Rev Drug Discov*, 2015, **14**, 248–260.

18 E. Moradi, S. Jalili-Firoozinezhad and M. Solati-Hashjin, *Acta Biomater*, 2020, **116**, 67–83.

19 P. Dalsbecker, C. B. Adiels and M. Goksör, *Am J Physiol Gastrointest Liver Physiol*, 2022, **323**, G188–G204.

20 R. Jellali, T. Bricks, S. Jacques, M. J. Fleury, P. Paullier, F. Merlier and E. Leclerc, *Biopharm Drug Dispos*, 2016, **37**, 264–275.

21 E. Leclerc, J. Hamon, I. Claude, R. Jellali, M. Naudot and F. Bois, *Cell Biol Toxicol*, 2015, **31**, 173–185.

22 J. M. Prot, A. S. Briffaut, F. Letourneur, P. Chafey, F. Merlier, Y. Grandvalet, C. Legallais and E. Leclerc, *PLoS One*, 2011, **6**, e21268.

23 T. Kostrzewski, P. Maraver, L. Ouro-Gnao, A. Levi, S. Snow, A. Miedzik, K. Rombouts and D. Hughes, *Hepatol Commun*, 2020, **4**, 77–91.

24 T. Kostrzewski, S. Snow, A. L. Battle, S. Peel, Z. Ahmad, J. Basak, M. Surakala, A. Bornot, J. Lindgren, M. Ryaboshapkina, M. Clausen, D. Lindén, C. Maass, L. M. Young, A. Corrigan, L. Ewart and D. Hughes, *Communications Biology 2021 4:1*, 2021, **4**, 1–15.

25 M. S. Freag, B. Namgung, M. E. Reyna Fernandez, E. Gherardi, S. Sengupta and H. L. Jang, *Hepatol Commun*, 2021, **5**, 217–233.

26 R. Jellali, S. Jacques, A. Essaouiba, F. Gilard, F. Letourneur, B. Gakière, C. Legallais and E. Leclerc, *Food and Chemical Toxicology*, 2021, **152**, 112155.

27 J. M. Prot, A. Bunescu, B. Elena-Herrmann, C. Aninat, L. C. Snouber, L. Griscom, F. Razan, F. Y. Bois, C. Legallais, C. Brochot, A. Corlu, M. E. Dumas and E. Leclerc, *Toxicol Appl Pharmacol*, 2012, **259**, 270–280.

28 R. Baudoin, L. Griscom, J. M. Prot, C. Legallais and E. Leclerc, *Biochem Eng J*, 2011, **53**, 172–181.

29 C. L. Kien, J. Y. Bunn, R. Stevens, J. Bain, O. Ikayeva, K. Crain, T. R. Koves and D. M. Muoio, *Am J Clin Nutr*, 2014, **99**, 436–445.

30 X. Palomer, J. Pizarro-Delgado, E. Barroso and M. Vázquez-Carrera, *Trends Endocrinol Metab*, 2018, **29**, 178–190.

31 H. Zhou, C. J. Urso and V. Jadeja, *J Inflamm Res*, 2020, **13**, 1–14.

32 X. Zeng, M. Zhu, X. Liu, X. Chen, Y. Yuan, L. Li, J. Liu, Y. Lu, J. Cheng and Y. Chen, *Nutr Metab (Lond)*,2020, **17**, 11.

33 A. Moravcová, Z. Červinková, O. Kučera, V. Mezera, D. Rychtrmoc and H. Lotková, *Physiol Res*, 2015, **64**, S627–S636.

34 J. M. Prot, C. Aninat, L. Griscom, F. Razan, C. Brochot, C. G. Guillouzo, C. Legallais, A. Corlu and E. Leclerc, *Biotechnol Bioeng*, 2011, **108**, 1704–1715.

35 J. M. Prot, A. Bunescu, B. Elena-Herrmann, C. Aninat, L. C. Snouber, L. Griscom, F. Razan, F. Y. Bois, C. Legallais, C. Brochot, A. Corlu, M. E. Dumas and E. Leclerc, *Toxicol Appl Pharmacol*, 2012, **259**, 270–280.

36 Y. Okamoto, S. Tanaka and Y. Haga, *Hepatology Research*, 2002, **23**, 138–144.

37 Y. Zang, L. Fan, J. Chen, R. Huang and H. Qin, *J Agric Food Chem*, 2018, **66**, 6772–6781.

38 M. Ishii, A. Maeda, S. Tani and M. Akagawa, *Arch Biochem Biophys*, 2015, **566**, 26–35.

39 L. Zhang Shengli Zhang, T. J. Biol, L. Zhang and S. Zhang, *Turkish Journal of Biology*, 2022, **46**, 298–306.

40 A. U. Nissar, L. Sharma and S. A. Tasduq, *Toxicol Res (Camb)*, 2015, **4**, 1344–1358.

41 M. Ricchi, M. R. Odoardi, L. Carulli, C. Anzivino, S. Ballestri, A. Pinetti, L. I. Fantoni, F. Marra, M. Bertolotti, S. Banni, A. Lonardo, N. Carulli and P. Loria, *J Gastroenterol Hepatol*, 2009, **24**, 830–840.

42 N. Hu, M. Hu, R. Duan, C. Liu, H. Guo, M. Zhang, Y. Yu, X. Wang, L. Liu and X. Liu, *J Pharmacol Sci*, 2014, **124**, 433–444.

43 F. De Chiara, A. Ferret-Miñana, J. M. Fernández-Costa, A. Senni, R. Jalan and J. Ramón-Azcón, *Biomedicines*, 2022, **10(5)**, 958.

44 H. S. Frandsen, J. M. Vej-Nielsen, L. E. Smith, L. Sun, K. L. Mikkelsen, A. P. Thulesen, C. E. Hagensen, F. Yang and A. Rogowska-Wrzesinska, *Cells*, 2022, **11**, 3216.

45 G. J. van der Vusse, *Drug Metab Pharmacokinet*, 2009, **24**, 300–307.

46 G. De Simone, A. Di Masi and P. Ascenzi, *Int J Mol Sci*, 2021, **22(18)**, 10086.

47 G. Giannelli, P. Koudelkova, F. Dituri and W. Mikulits, *J Hepatol*, 2016, **65**, 798–808.

48 Y. Takahashi and T. Fukusato, *World Journal of Gastroenterology: WJG*, 2014, **20**, 15539.

49 A. Eynaudi, F. Díaz-Castro, J. C. Bórquez, R. Bravo-Sagua, V. Parra and R. Troncoso, *Front Nutr*, 2021, **8**, 775382.

50 I. García-Ruiz, P. Solís-Muñoz, D. Fernández-Moreira, T. Muñoz-Yagüe and J. A. Solís-Herruzo, *DMM Disease Models and Mechanisms*, 2015, **8**, 183–191.

51 A. S. Meijnikman, H. Herrema, T. P. M. Scheithauer, J. Kroon, M. Nieuwdorp and A. K. Groen, *JHEP Reports*, 2021, **3**, 100301.

52 L. Bonnet, I. Alexandersson, R. K. Baboota, T. Kroon, J. Oscarsson, U. Smith and J. Boucher, *Front Endocrinol (Lausanne)*, 2022, **13**, 957616.

Chapter IV:

NAFL-on-chip model: Investigation of the metabolomic profiles of the exposed HepG2/C3A cells

In this chapter, we studied the metabolic signatures of oleic acid, palmitic acid and their mixture on our HepG2/C3A-based liver-on-chip. We aim to investigate the metabolic perturbation associated to the different treatments and extract potential biomarkers of NAFL and liver injury. Furthermore, the results in this chapter allowed us to better define the range of relevance of our model.

4.1 Introduction

We recently introduced “metabolomics-on-a-chip” approach to our group to better investigate the metabolic changes in our biological systems. Metabolomics is a cutting-edge field in the realm of omics sciences that focuses on the comprehensive study of small molecules (< 1500 Da), known as metabolites, within biological systems[1]. These metabolites serve as the functional readouts of cellular processes, reflecting the dynamic interplay between genes, proteins, and environmental factors. By employing advanced analytical techniques such as mass spectrometry (MS) and nuclear magnetic resonance (NMR) spectroscopy, metabolomics can be used to identify and quantify a wide range of metabolites present in biological samples, including blood, urine, and tissues[2]. One of the key advantages of metabolomics is its ability to provide a real-time snapshot of an organism's metabolic state, making it a powerful tool in various fields such as biomarker discovery, drug development, and personalized medicine[3]. Additionally, metabolomics can be used to uncover subtle metabolic perturbations associated with diseases, offering valuable insights into disease mechanisms and progression but also potential therapeutic targets[4]. We previously investigated the effects of various molecules (e.g., drugs, solvents, pesticides) on liver metabolism using our liver-on-chip models and metabolomic analysis[5–9]. Since the past years, several study in NAFLD started to adopt metabolomic analysis on biological samples to investigate the pathophysiologic role of the metabolome in patients with NAFLD and extract disease-specific biomarkers for improved diagnosis[10–16] .

In this same approach, we proposed to investigate the perturbation of the metabolomic profile due to the effects of free fatty acids using our HepG2/C3A-based liver-on-chip. For that purpose, we have selected the oleic acid (OA), palmitic acid (PA), and a mixture of OA and PA (OA/PA). Indeed, we previously demonstrated the potential of our HepG2/C3A-based liver-on-chip to mimic NAFL when exposing the cells to fatty acids, in Chapter 3. HepG2/C3A cells were found to exhibit different dysregulations in their functions (including ROS production lipid accumulation and albumin secretion decrease) depending on the fatty acid to which they were exposed. We aim now to characterize the pathophysiologic metabolic network resulting from those FFA exposures in order to extract potential biomarkers.

4.2 Morphological analysis still reveals a weaker cell density for PA treatment

HepG2/C3A cells were exposed, under dynamic condition, to OA, PA and OA/PA for 2 and 7 days. Cells morphology at the end of experiment is presented in Figure 4.1. As in Chapter 3.2.1, we observed after 2 days of exposure a massive cell proliferation inside all the biochips for all condition unless for PA condition. Indeed, the cell density seems to be weaker when compared to other treatment and control condition (Figure 4.1A). We noticed, an increase in cell density for all condition after 7 days of exposure. Nevertheless, we still observed a less dense multilayer tissue for the PA condition (Figure 4.1B).

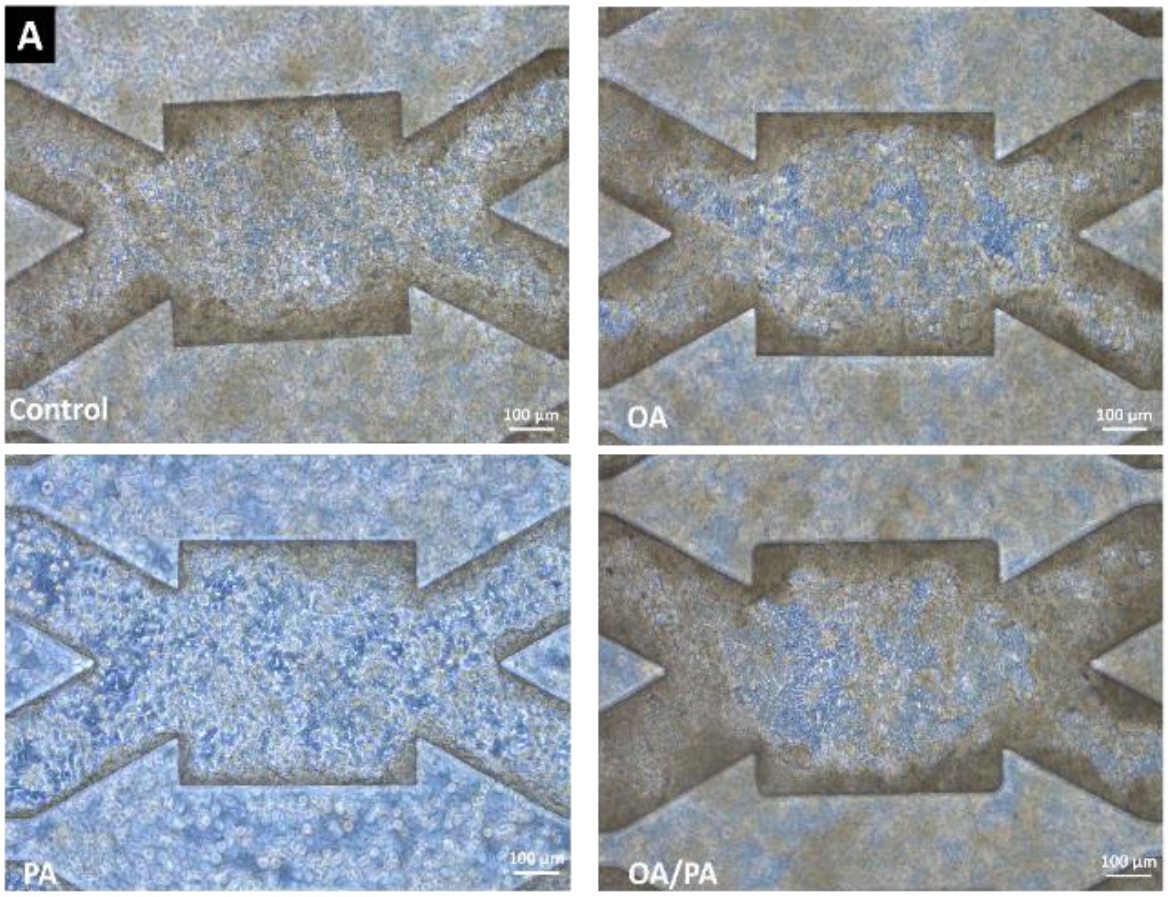

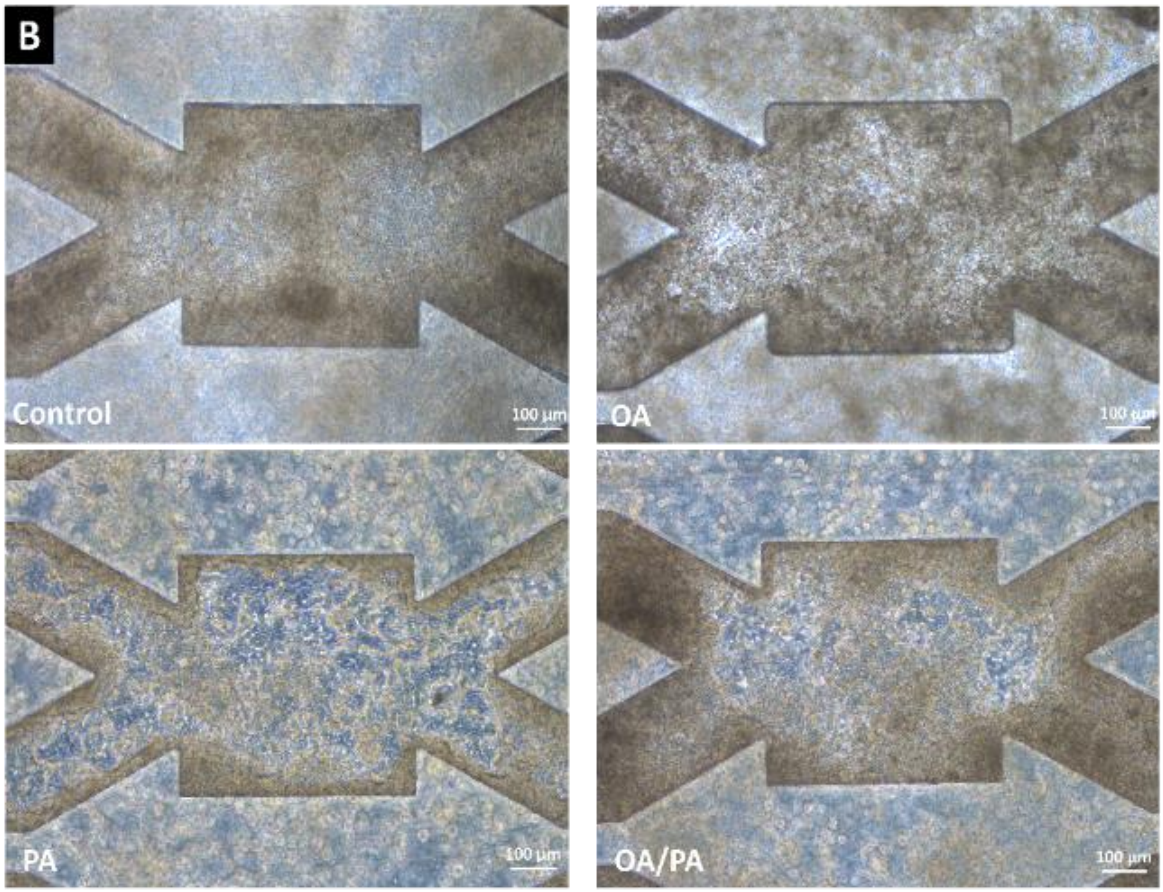

Figure 4. 1: (A) *Cell morphology at the end of the 2 days and* ***(B)*** *7 days of exposure experiments.*

4.3 Oleic acid and palmitic acid basal productions are complementation dependent

The footprint of the oleic acid and palmitic acid confirmed the presence of those compounds in their respective medium. In addition, we found that HepG2/C3A were able to produce very low levels of palmitic acid under control conditions (Figure 4.2B). OA treated cells were secreting PA after 4 days and 7 days of exposure but consumed OA. Similarly, PA treated cells consumed PA and led to a weak secretion of OA. Finally, cells treated with OA/PA treatments reduced the levels of OA and PA in the culture medium leading to their consumptions when compared to controls.

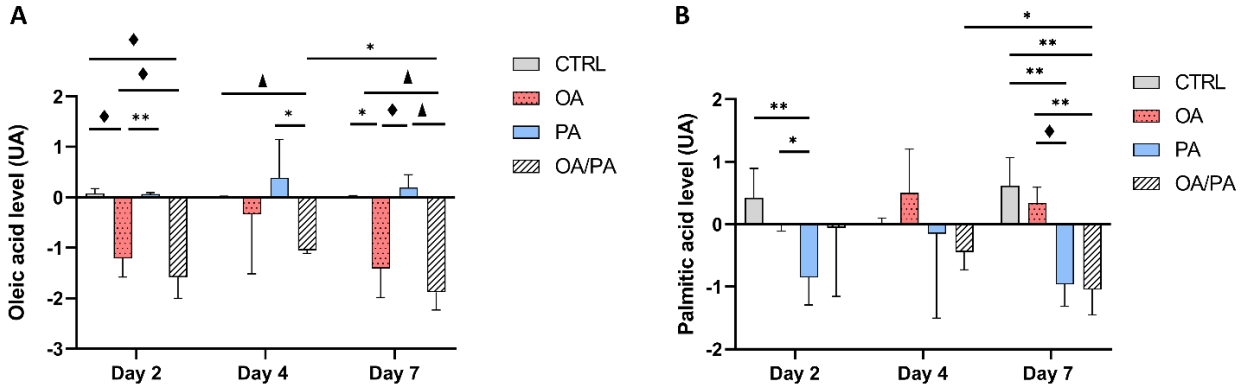

Figure 4. 2: (A) *Oleic acid and* ***(B)*** *palmitic acid level obtained by metabolomic analysis at day 2, day 4 and day 7. Statistically analysed by Kruskal-Wallis test with * p<0.05; **p<0.005;* ♦ *p<0.0005;* ▲ *p<0.0001.*

4.4 Overall metabolomic profiling demonstrated a metabolic kinetic due to FFA treatment

To identify the metabolomic signature of each condition, we performed a multivariate analysis to compare the exo-metabolome of exposed HepG2/C3A cells on day 2, day 4 and day 7. At day 2, the PLS-DA score plots showed (Figure 4.3A) that the different groups are mixed illustrating a poor discrimination between the conditions. At day 4, we observed the populations started to separate although the CTRL and OA conditions were still superimposed (Figure 4.3B). At day 7, PA condition cluster is clearly separated from CTRL and OA condition clusters that are still superimposed, indicating its distinct metabolic profile. Regarding OA/PA condition, its metabolic profile was between OA and PA conditions, representing the mixture of both FFA (Figure 4.3C).

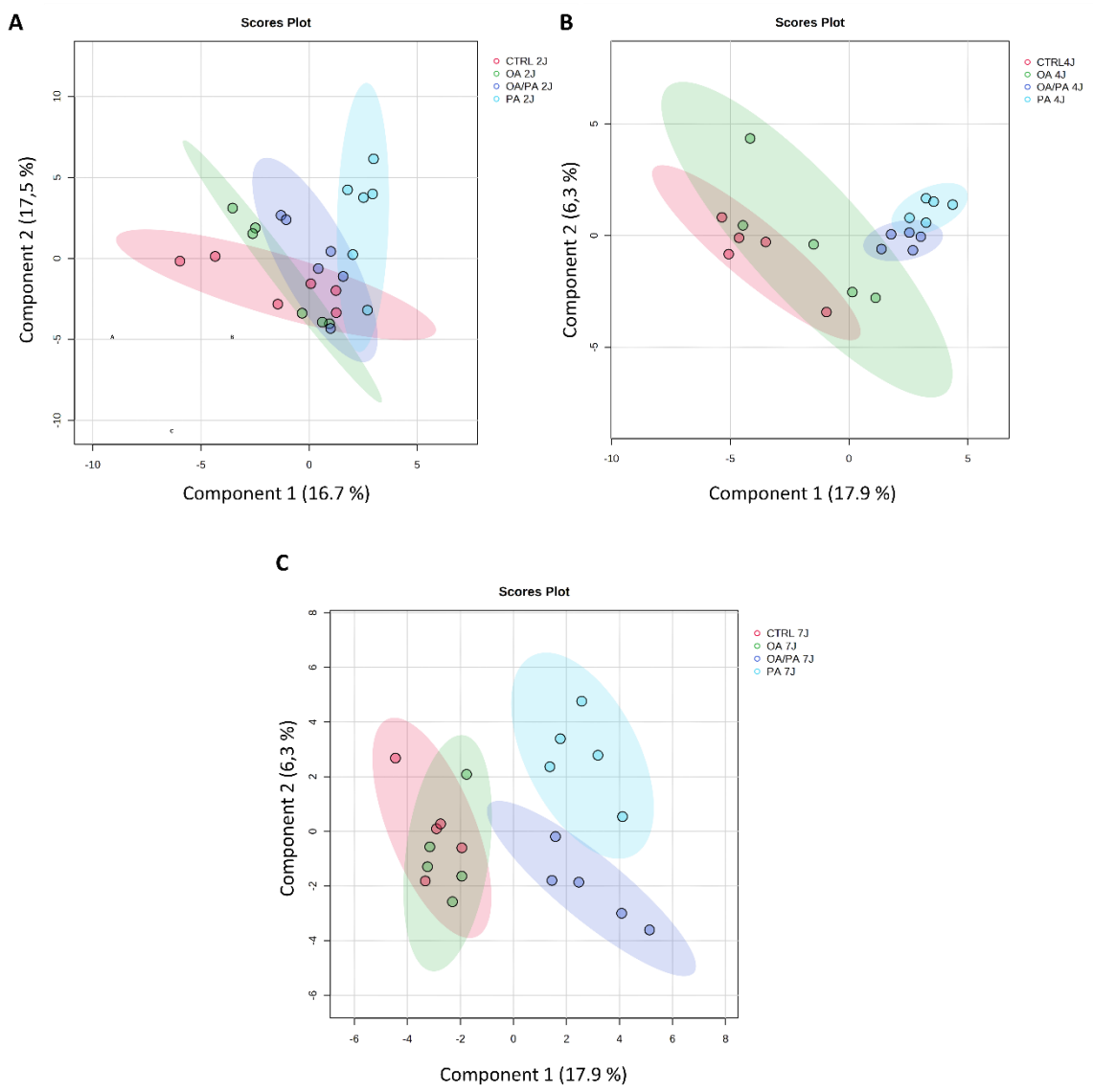

Figure 4. 3: *PLS-DA scores plots of the overall metabolomic profiles at* ***(A)*** *day 2,* ***(B)*** *day 4 and* ***(C)*** *day 7.*

An ANOVA test coupled with the PLS-DA analysis contributed to the extraction of the metabolites significantly modulated for each condition (with a p-value below 0.05 and VIP, Variable Importance for the Projection, scores of above 1.) The heatmaps of the significant metabolites and pathways used to discriminate each treatment according the time point are presented in Figure 4.4. At day 2, we observed a slight modulation of the exo-metabolome with only four metabolites denoted on the heatmap (Figure 4.4A). Indeed, we noticed a consumption of oleic acid for both OA and OA/PA conditions when compared to CTRL condition. We also observed a higher consumption of palmitic acid and higher production of palmitoleic acid for PA condition when compared to CTRL condition. Moreover, we found

varying degrees of lysine consumptions in all treatments although the consumption was higher for PA condition (Figure 4.4A). There were 13 differentially expressed metabolites after 4 days of exposure and the start of a switch in the metabolic signature was observed (Figure 4.4B). The CTRL medium was characterized by the production of proline, trans-4-hydroxy-L-proline, tyrosine and malic acid and the consumption of phosphoric acid. The OA condition also showed a production of tyrosine but, unlike the CTRL condition, we observed a consumption of proline, trans-4-hydroxy-L-proline and malic acid and a production of phosphoric acid. Furthermore, OA/PA and PA conditions demonstrated a similar metabolic pattern. We found a higher consumption of amino acids such as leucine, threonine and aspartic acid. We also observed a higher production of proline and a production of uracil (Figure 4.4B) when compared to CTRL condition. After 7 days of treatment, we extracted 14 differentially expressed metabolites (Figure 4.4C). We still observed similar features between OA/PA and PA conditions. Indeed, we noticed a higher production of proline, beta-alanine, palmitoleic acid, and a higher consumption of threonine and tryptophan for both OA/PA and PA conditions when compared to CTRL condition. However, we observed for PA condition only a production of oleic acid, a higher production of cholesterol (when compared to CTRL and OA/PA conditions) and a lower consumption of nicotinamide when compared to CTRL condition. Concerning the OA condition, we detected a production of tyrosine, a consumption of palmitic acid, trans-4-hydroxy-L-proline, sarcosine, cholesterol, and a higher consumption of oleic acid when compared to CTRL condition. Unlike PA condition, we observed a higher consumption of nicotinamide for OA condition when compared to CTRL condition (Figure 4.4C).

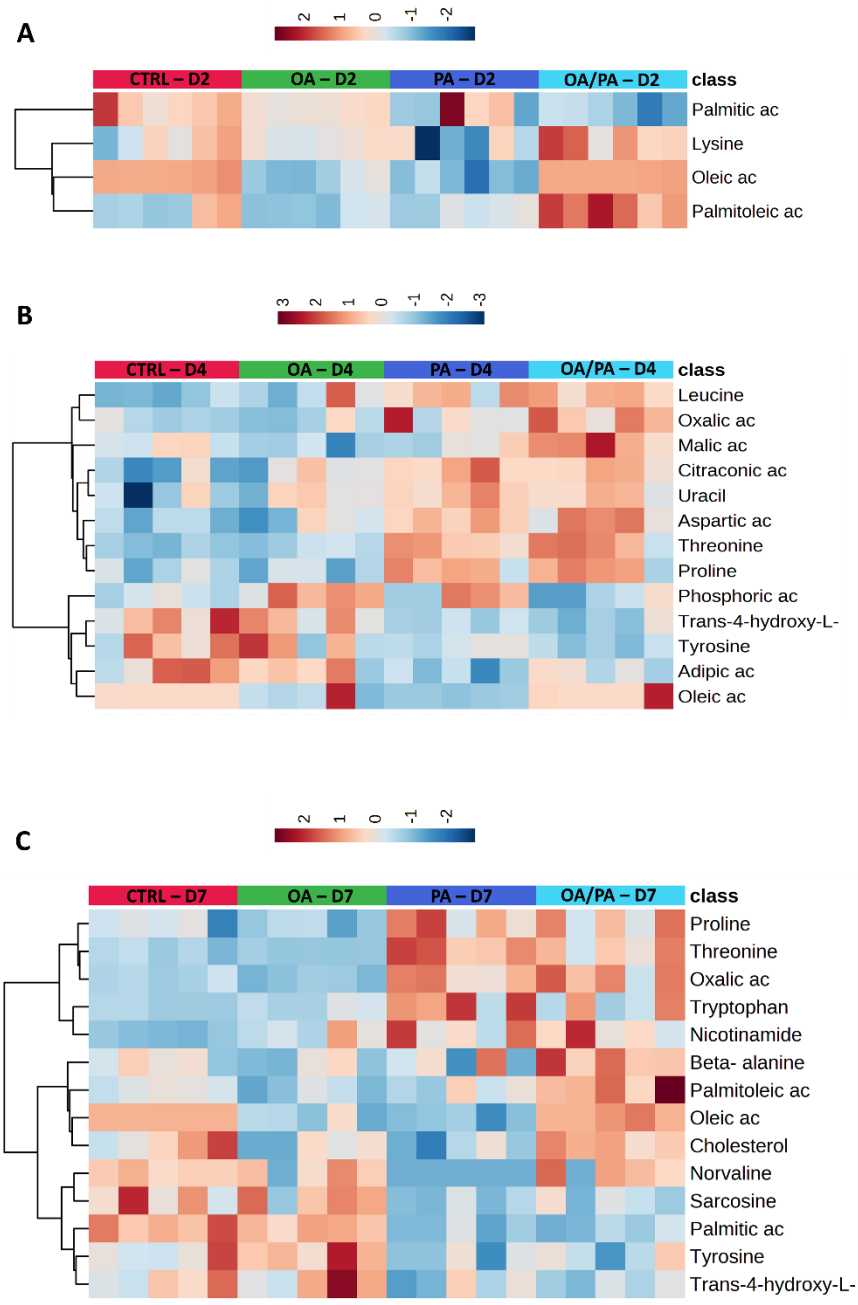

Pathways and metabolites significantly modulated after 2 days of OA, PA and OA/PA	
Pathway name	**Metabolites**
Fatty acid metabolism	Oleic acid, Palmitoleic acid, Palmitic acid
Lysine degradation	Lysine

Pathways and metabolites significantly modulated after 4 days of OA, PA and OA/PA	
Pathway name	**Metabolites**
Fatty acid metabolism	Oleic acid, Palmitoleic acid, Palmitic acid,
Amino acid metabolism	Tyrosine, Threonine, Proline, Trans-4-hydroxy-L-proline
Valine, leucine, isoleucine biosynthesis	Leucine, Citraconic acid
Beta-alanine synthesis	Aspartic acid, Uracil
Citrate cycle and pyruvate metabolism	Malic acid
Oxidative phosphorylation	Phosphoric acid
Purine metabolism	Oxalic acid

Pathways and metabolites significantly modulated after 7 days of OA, PA and OA/PA	
Pathway name	**Metabolites**
Fatty acid metabolism	Oleic acid, Palmitoleic acid, Palmitic acid
Amino acid metabolism	Tyrosine, Threonine, Proline, Trans-4-hydroxy-L-proline, Sarcosine, Norvaline
Pantothenate and CoA biosynthesis	Beta-alanine
NAD biosynthesis	Tryptophan, Nicotinamide
Purine metabolism	Oxalic acid
Cholesterol biosynthesis	Cholesterol

Figure 4. 4: *Heatmaps and tables representing the metabolites significantly modulated and the altered pathways corresponding at* ***(A)*** *day 2,* ***(B)*** *day 4 and* ***(C)*** *day 7.*

4.5 Identification of the specific metabolomic signatures of OA, PA and OA/PA treatment

We compared the exo-metabolomic signature of the CTRL versus the different treatments (OA, PA and OA/PA) at each time point (day 2, 4 and 7). The specific metabolomic for each treatment at day 4 and day 7 are presented in the following paragraphs. As the differential analysis for all treatment at day 2 did not show important variations, we presented the associated PLS-DA dot plots and heatmaps in the Supplementary figures at this end of this chapter (section 4.10).

4.5.1 Differential analysis of CTRL vs OA treatment

First, the PLS-DA plots for day 4 and day 7 showed two groups that were separated although close to each other (Figures 4.5A, B). Moreover, we observed an important variability of samples for the OA conditions regardless the time point (Figures 4.5A, B and Supp. Fig. 1A). At day 2, using ANOVA analysis we extracted only two metabolites that were differentially expressed between CTRL and OA condition (Supp. Fig. 1B). We observed an important consumption of oleic acid for the OA condition while there was a production for CTRL condition. Furthermore, this tendency was also observable for 1-monostearin (also known as 1-stearoyl-rac-glycerol) which is a long chain molecule typically occurring in the body as a by-product of the breakdown of fatty acids. Nevertheless, we observed an important variability in the metabolism of 1-monostearin between the samples of the CTRL condition (Supp. Fig. 1B). After 4 days of exposure these metabolites were not differentially expressed anymore (Figures 4.5C). We extracted four news metabolites which are malic acid, caprylic acid, phosphoric acid and pyroglutamic acid. We noticed that OA condition led to a lower production of malic acid and caprylic acid, and higher production of pyroglutamic acid when compared to CTRL condition (Figure 4.5C). Conversely to the CTRL condition we observed a production of phosphoric acid (Figure 4.5C). At day 7, OA condition presented a lower consumption of glutamine and pyruvic acid and a lower production of oxalic acid and palmitoleic acid. We noted a switch of the metabolic signature of oleic acid and nicotinamide, which, unlike to CTRL condition, were consumed and produced, respectively, in OA condition (Figure 4.5D).

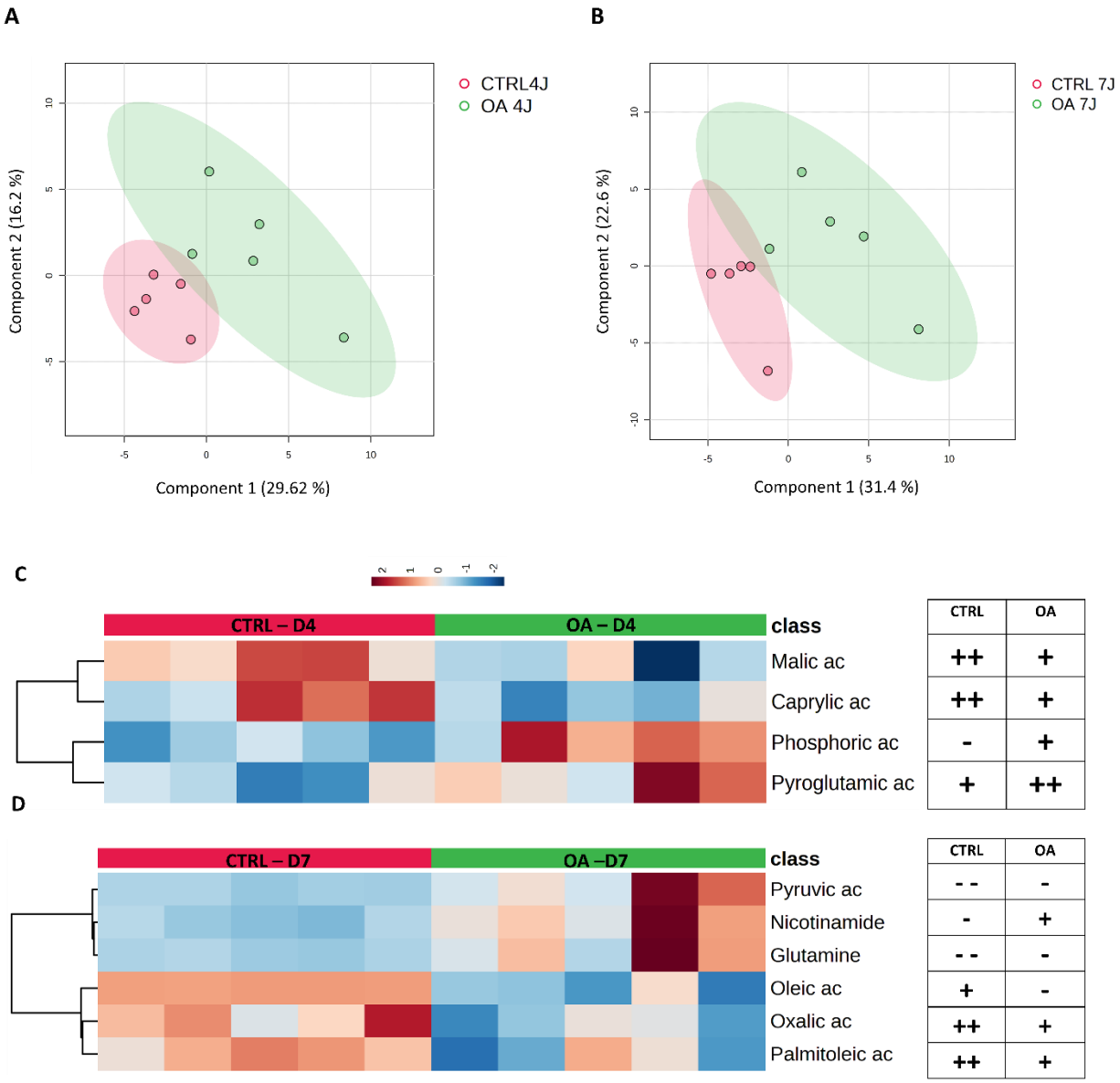

Figure 4. 5: *Comparison of the metabolomic profiles of CTRL and OA condition.* ***(A, B)*** *PLS-DA scores plots at day 4 and day 7, respectively.* ***(C, D)*** *Heatmaps of the metabolites significantly modulated at day 4 and day 7, respectively.* ***+*** *production;* ***++*** *higher production;* ***-*** *consumption;* ***- -*** *higher consumption in comparison with basal culture medium.*

Finally, we highlighted that 4 days of OA treatment contributed to enrich the glutathione metabolism and the malate-aspartate shuttle allowing the regulation of glycolysis and lactate metabolism (Figure 4.6A). At day 7, the top 5 enriched pathways were related to nitrogen metabolism (the urea cycle, ammonia recycling, glutamate metabolism), to amino sugar metabolism and nicotinate and nicotinamide metabolism. Enrichment ratio also

extracted the phenylacetate metabolism (implied in the excretion of nitrogen) and the degradation of the pyruvaldehyde, a toxic metabolite (Figure 4.6B).

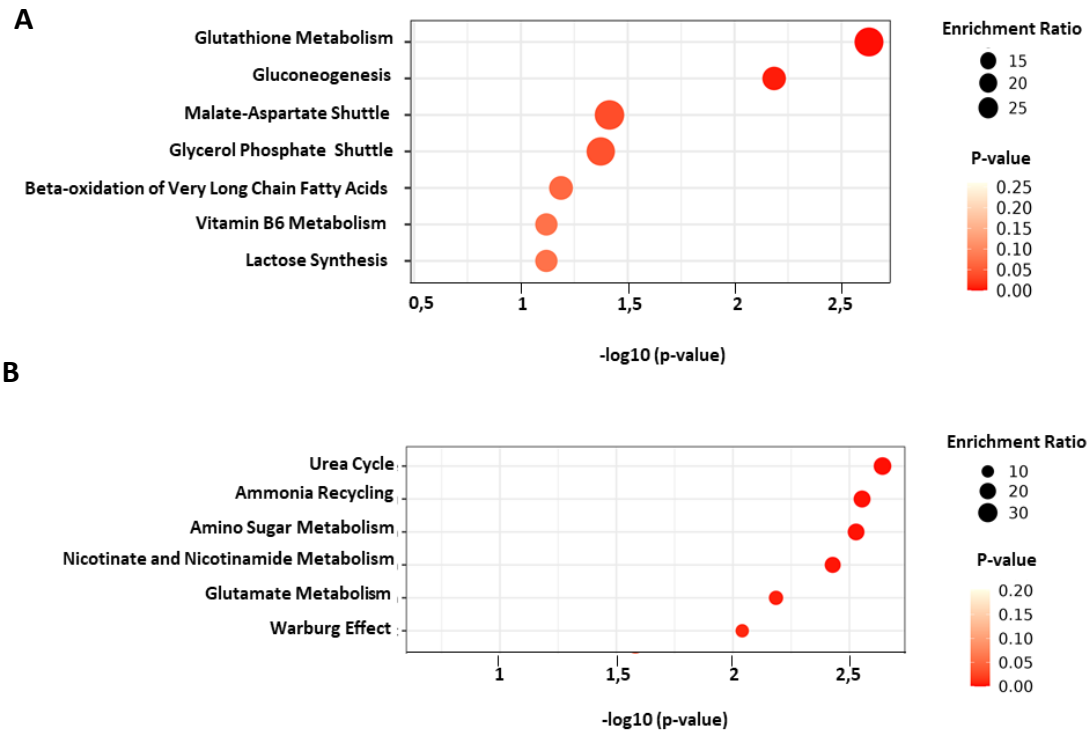

Figure 4. 6: *Extract of the enrichment pathway dot plots for OA condition at* ***(A)*** *day 4 and* ***(B)*** *day 7. The complete dot plots are in Supp. Fig.4 at the end of this chapter.*

4.5.2 Differential analysis of CTRL vs PA treatment

First, after 2 days of treatment with palmitic acid, we noticed a production of palmitoleic acid and benzoquinone when compared to the CTRL condition (Supp. Fig. 2). Then, we observed an intense metabolome perturbation in PA when compared with CTRL particularly after 4 days of exposure (Figure 4.7). Indeed, the PLS-DA plot showed that PA condition is clearly separated from CTRL condition from the fourth days of exposure (Figure 4.7A). We extracted 15 metabolites that were differentially expressed between both conditions. On one hand, we observed a higher production of palmitoleic acid when compared to CTRL condition (Figure 4.7C). In another hand, many metabolites implied in the metabolism of arginine and proline was modulated suggesting a perturbation of the pathway. In fact, we found a decrease

in trans-4-hydroxy-L-proline production associated with a high production of proline and ornithine, and a lower consumption of aspartic acid when compared to CTRL condition. Furthermore, we noticed a lower consumption of asparagine and a production of threonine, leucine and tryptophan (Figure 4.7C). At day 7 of exposure, we observed a lower consumption of palmitic acid but still observed a higher production of palmitoleic acid in PA condition when compared to CTRL condition. In addition, as for 4 days of exposure, we noticed changes in the amino acid's metabolism with a lower production serine and trans-4-hydroxy-L-proline, a lower consumption of leucine and a production of threonine. As in the OA condition, nicotinamide production was detected at this same time point, whereas no production was observed in the CTRL condition. Furthermore, PA treatment was particularly characterized by the production of beta-alanine at day 7 (Figure 4.7D) and oxalic acid at both day 4 and day 7 (Figure 4.7C, D).

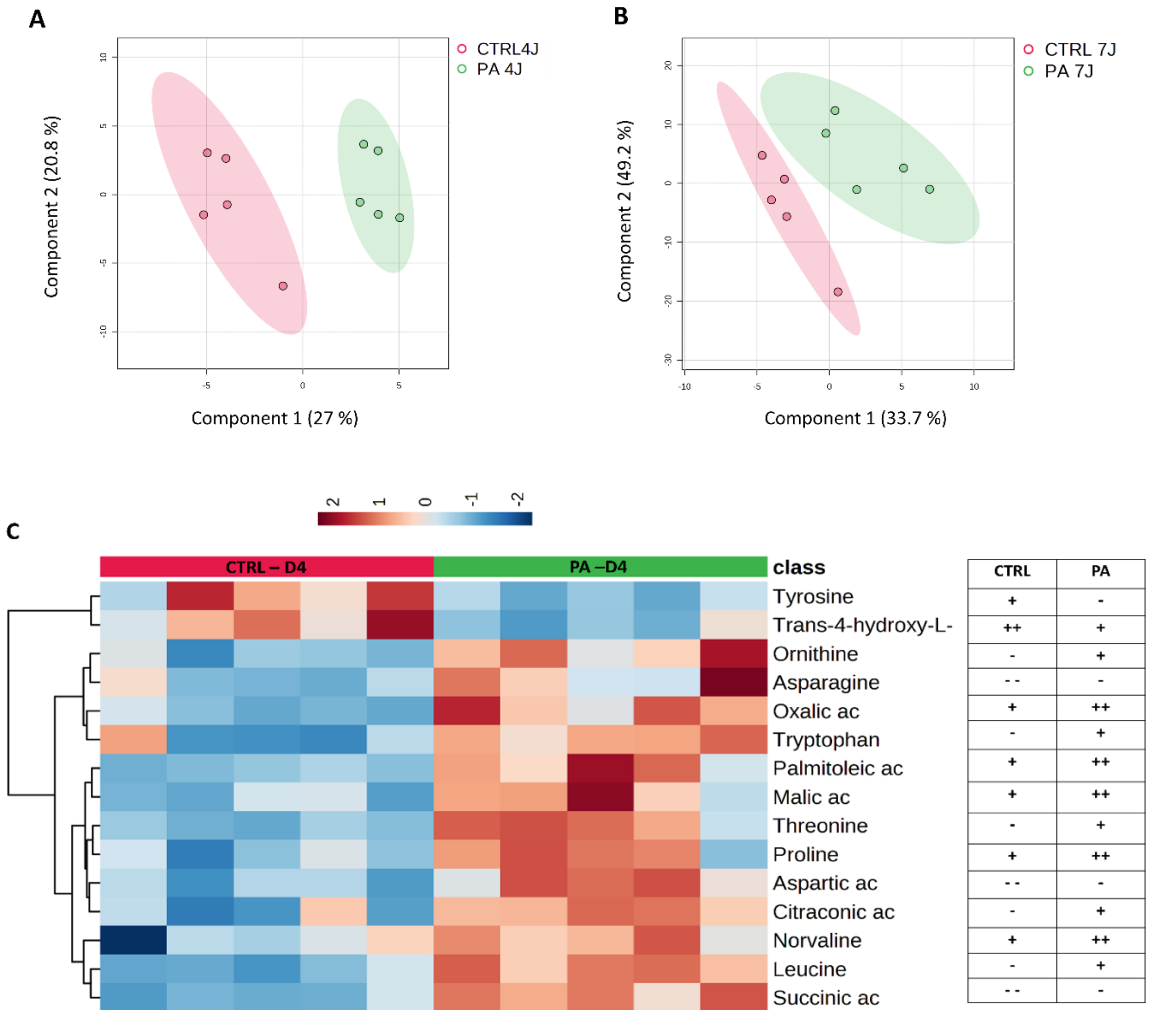

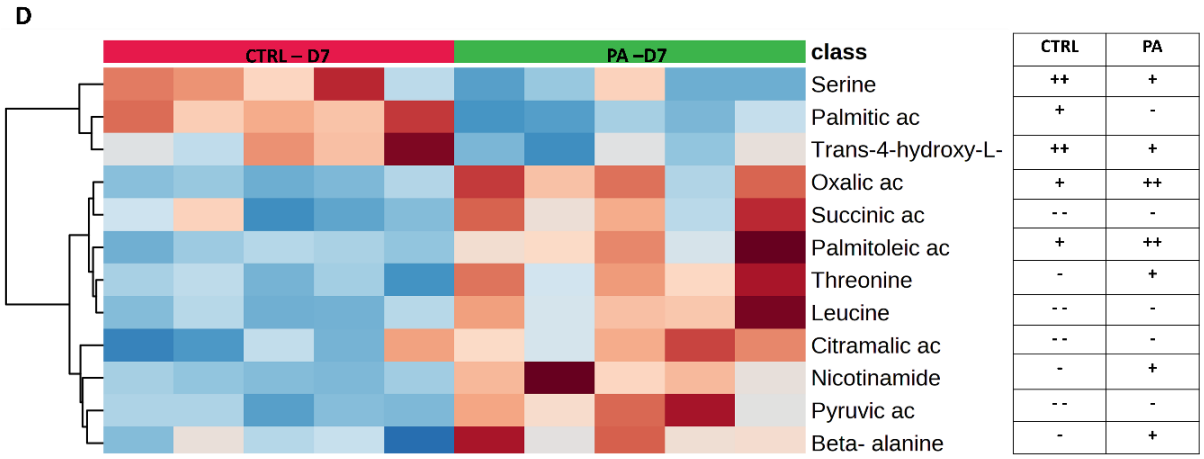

Figure 4. 7: *Comparison of the metabolomic profiles of CTRL and PA condition.* ***(A, B)*** *PLS-DA scores plots at day 4 and day 7, respectively.* ***(C, D)*** *Heatmaps of the metabolites significantly modulated at day 4 and day 7, respectively.* ***+*** *production;* ***++*** *higher production;* ***-*** *consumption;* ***- -*** *higher consumption in comparison with basal culture medium.*

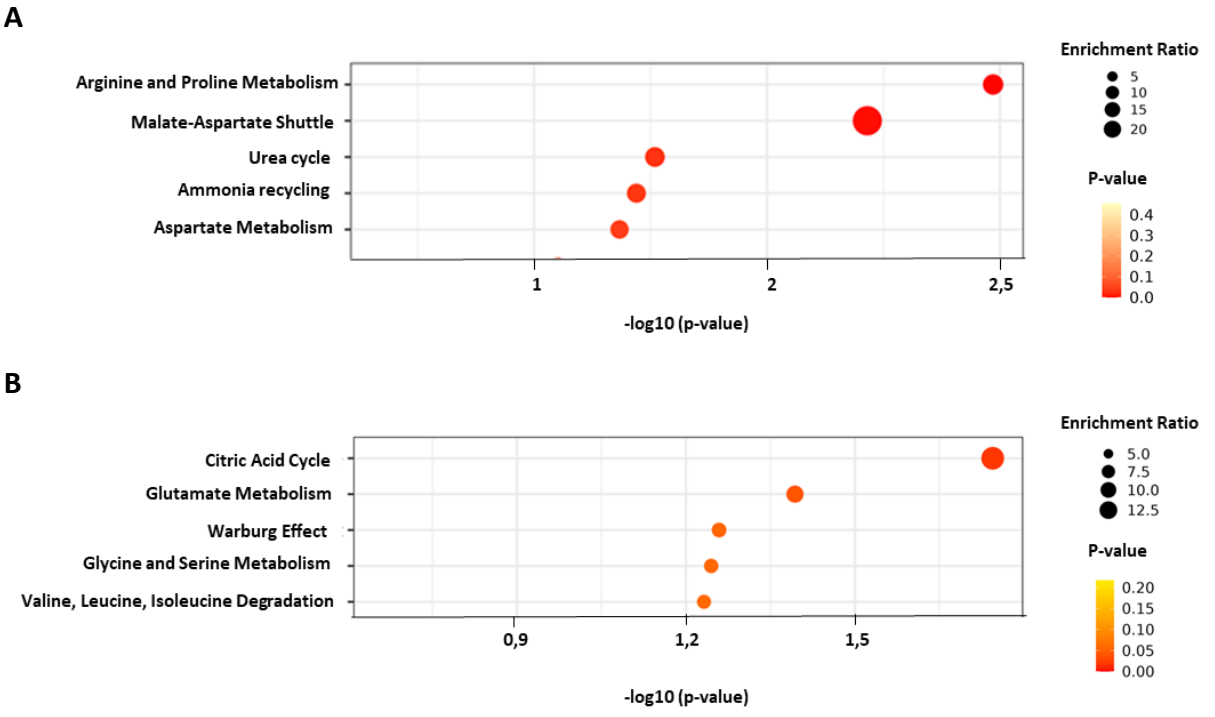

Figure 4. 8: *Extract of the enrichment pathway dot plots for PA condition at* ***(A)*** *day 4 and* ***(B)*** *day 7. The complete dot plots are in Supp. Fig.5 at the end of this chapter.*

The Enrichment ratio highlighted at day 4, five pathways related to nitrogen metabolism (the urea cycle, ammonia recycling, aspartate metabolism,) as the top 5 enriched pathways (Figure 4.8A). At day 7, the top 5 enriched pathways were the citric acid cycle, glutamate metabolism, Warburg effect, glycine/serine metabolism and valine/leucine/isoleucine degradation. The Enrichment ratio also extracted the degradation of the pyruvaldehyde, a toxic metabolite, as for OA treatment for this same time point (Figure 4.8B).

4.5.3 Differential analysis of CTRL and OA/PA mixture treatment

As for the other treatments, we did not observe a specific metabolic signature for the OA/PA treatment after 2 days aside only oleic acid and arginine seemed to have been consumed by the cells (Supp. Fig. 3). At day 4, we identified 13 metabolites that were differentially expressed between when compared to control condition (Figures 4.9A). As for PA condition, we noticed a lower consumption of aspartic acid; a lower production of trans-4-hydroxy-L-proline; a higher production of proline and threonine when compared to CTRL condition. In contrast to PA treatment for the same time point, we observed a consumption of leucine and oleic acid (Figure 4.9C). After 7 days of treatment, we observed a lower production (serine and glycine) and consumption (tryptophan, asparagine and cystine) of amino acids when compared to CTRL condition. We also detected some features of both OA and PA conditions for the same time point, as a higher production of proline and oxalic acid and a production of threonine and nicotinamide when compared to CTRL condition. Nevertheless, we particularly noticed a production of cholesterol in OA/PA treated cells when compared to OA and PA treated cells (Figure 4.9D).

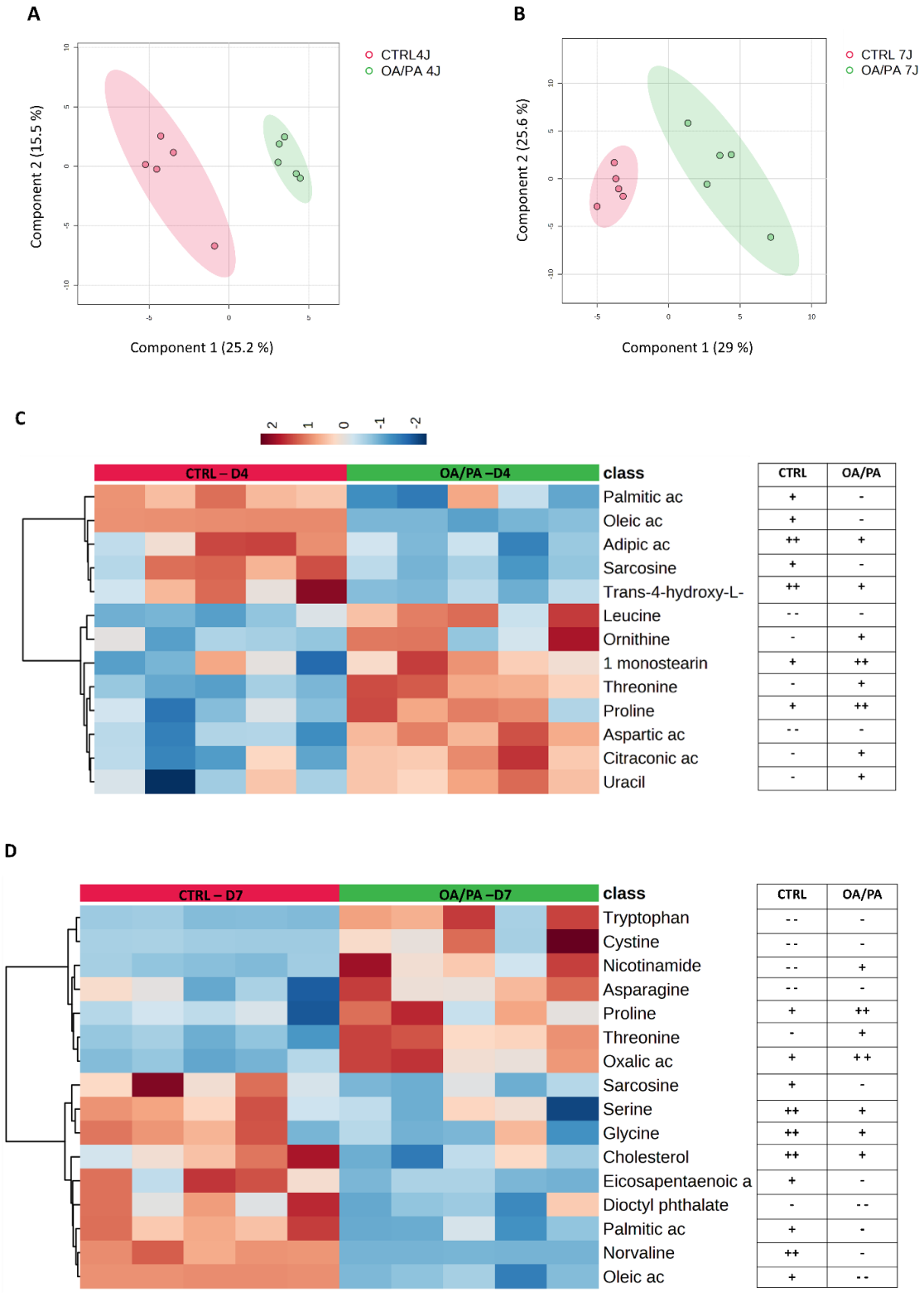

Figure 4. 9: *Comparison of the metabolomic profiles of CTRL and OA/PA mixture condition.* ***(A, B)*** *PLS-DA scores plots at day 4 and day 7, respectively.* ***(C, D)*** *Heatmaps of metabolites significantly modulated at day 4 and day 7, respectively.* ***+*** *production;* ***++*** *higher production;* ***-*** *consumption;* ***- -*** *higher consumption in comparison with basal culture medium.*

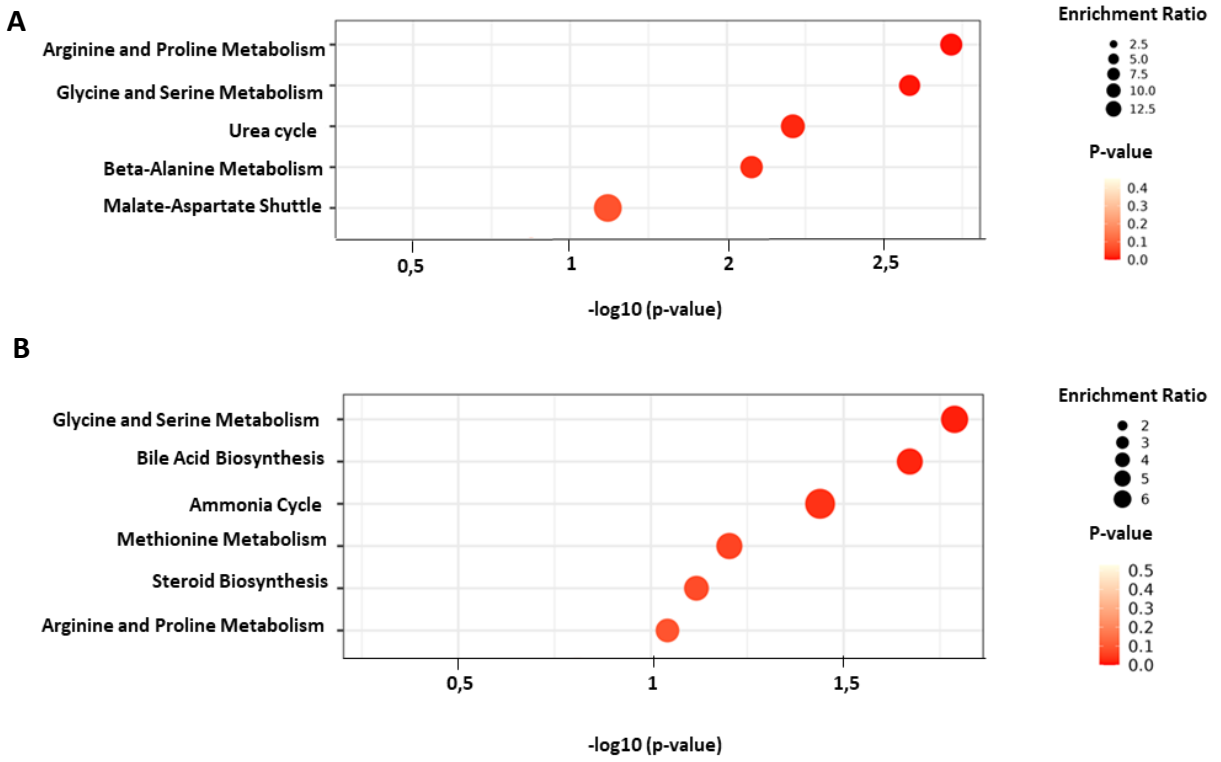

Figure 4. 10: *Extract of the enrichment pathway dot plots for OA/PA condition at* ***(A)*** *day 4 and* ***(B)*** *day 7. The complete dot plots are in Supp. Fig.6 at the end of this chapter.*

The enrichment analysis demonstrated that the top 5 pathways, at day 4, were the arginine/proline metabolism, the glycine/serine metabolism, the urea cycle, the beta-alanine metabolism and the malate-aspartate shuttle (Figure 4.10A). At day 7, the glycine/serine metabolism was the more enriched pathway followed by the bile acid biosynthesis, the ammonia recycling, methionine metabolism and the steroid biosynthesis pathways (Figure 4.10B).

4.6 Common and specific metabolites of the different treatments

We elucidated the common and specific metabolites of each treatment at day 4 and day 7 by designing a Venn's diagram. As shown in Figure 4.11A, at day 4 there were no metabolites common to the three treatments. OA, PA and OA/PA treatments presented three, seven and six specific metabolites, respectively (Figure 4.11A). However, we highlighted that the OA/PA mixture treatment shared seven metabolites in common with the PA treatment while there were no metabolites in common with the OA treatment. Among the metabolites common with the PA treatment, we found a production of trans-4-hydroxy-L-proline, proline, citraconic

acid and consumption of leucine, threonine, aspartic acid and ornithine (Figures 4.7 and 4.9). Interestingly, at day 7 we extracted two metabolites that were common to the three treatments: oxalic acid and nicotinamide (Figures 4.11C, D). Nicotinamide was produced by all treated cells at day 4 and 7 while oxalic acid was consumed by OA-treated cells and highly produced by cells treated with PA and the mixture (Figures 4.5, 4.7 and 4.9). As on day 4, OA/PA condition had more metabolites in common with the PA condition than the OA condition. Indeed, the OA/PA condition shared the consumption of palmitic acid, threonine and serine with the PA treatment whereas it only shared the consumption of oleic acid with the OA treatment (Figure 4.11D). In addition, cells treated with OA/PA for 7 days showed the greatest metabolic change, with 10 specific metabolites differentially expressed including amino acids and lipids (Figure 4.11D).

A

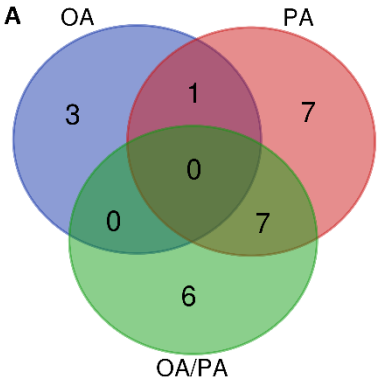

B

Compared treatment	Total	Common metabolites
OA vs PA	1	Malic acid
OA/PA vs PA	7	Trans-4-hydroxy-L-proline, proline, citraconic acid, leucine, threonine, aspartic acid, ornithine
OA	3	Pyroglutamic acid, phosphoric acid, caprylic acid
PA	7	Palmitoleic acid, norvaline, asparagine, oxalic acid, tyrosine, tryptophan, succinic acid
OA/PA	6	Sarcosine, 1-monostearin, uracil, palmitic acid, oleic acid, adipic acid

C

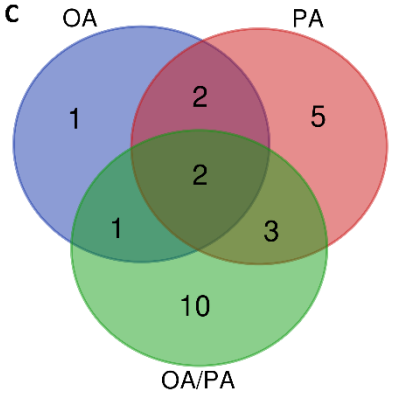

D

Compared treatment	Total	Common metabolites
OA vs OA/PA vs PA	2	Oxalic acid, nicotinamide
OA vs PA	2	Palmitoleic acid, pyruvic acid
OA vs OA/PA	1	Oleic acid
OA/PA vs PA	3	Threonine, pamitic acid, serine
OA	1	Glutamine
PA	5	Trans-4-hydroxy-L-proline, citramalic accid, beta-alanine, leucine, succinic acid
OA/PA	10	Sarcosine, norvaline, asparagine, glycine, proline tryptophan, dioctyl phthalate, cystine eicosapentaenoic acid, cholesterol

Figure 4. 11: (A) *Venn's diagram of OA, PA, OA/PA treatment and* ***(B)*** *table of the common metabolites at day 4.* ***(C)*** *Venn's diagram of OA, PA, OA/PA treatment and* ***(D)*** *table of the common metabolites at day 7.*

4.7 Discussion

A general feature of our metabolome analysis concerned the lipid and fatty acid metabolisms perturbation due to the OA, PA and OA/PA treatments from 2 days of treatments. The perturbation of lipid metabolism is a hallmark of fatty acid exposure on liver cells. Thus, oleic acid is reported to modify the lipidic secretion in hepatocytes (intracellular lipidomic showed the increases of diglycerides, triglycerides and acyl carnitine; the reduction ceramide, cholesterol ester, lysophosphaticylcholine, phosphatidylglycerol)[17]. Although, we did not detect directly those compounds in our extracellular metabolomic analysis, we found in Chapter 3 a lipid accumulation inside of the cells of our OA cultures consistently with the triglycerides lipidomic accumulations. An important feature of the mixture of OA/PA at day 7 is the switch from production of lipids toward their consumption (oleic, palmitic, eicosapenteanic acids), the stop of palmitoleic acid production (when compared PA and OA/PA) in our model. Larger lipidomic analysis on HepG2/C3A spheroids confirmed complex lipidic metabolism switch in OA/PA co-exposures[26]. Furthermore, we noticed that the presence of palmitic acid in the PA exposures contributed to increase the production of palmitoleic acid and to stop the PA production when compared to controls. Palmitoleic acid is synthesized from palmitic acid *via SCD-1* in the endoplasmic reticulum[18]. Although palmitoleic acid effect in NAFLD/NASH is still contradictory[18], palmitoleic acid was reported to reduce the lipid accumulation, to increase the insulin secretion and to improve the glucose homeostasis[19]; in addition to prevent lipo-apoptosis coupled and with anti-inflammatory effects[20–22]. Then, we found a lower production of cholesterol in OA/PA treated condition after 7 days of culture. Interestingly, too high cholesterol level is a pro-steatosis signaling, leading to lipotoxicity including endoplasmic stress and a pro-apoptosis in hepatocytes[23].

After 7 days of exposure, we found that the OA, PA, and OA/PA commonly increased the production of nicotinamide. Nicotinamide is natural molecule that acts as a coenzyme in energy transfer inside the cell[24]. It was involved in the improvement of liver regeneration and liver function[25]. Furthermore, it is known as a protection against liver steatosis and metabolic imbalances in NAFLD[24]. Nicotinamide derivatives are also reported to improve glucose tolerance in mice plasma with elevated FFA[26] and correct the glycolysis and fatty acid beta-oxidation in citrin-KO mice[27]. In addition, serum levels of nicotinamide phosphoribosyl

transferase (NAMPT) are associated with hepatic de novo lipogenesis (DNL) in a sex-dependent manner in NAFLD' patients. Parallelly, we found that PA increased the production of oxalic acid which is an end product derived from glyoxylate metabolism. Changes in glyoxylate metabolism and high release of oxalic acid was correlated with kidney stones formation and kidney damage. Recently, NAFLD was associated with an increased risk of kidney stones. As results, the detection of these compounds appeared consistent with the literature and would be potential biomarkers of fatty acid exposure in our HepG2/C3A-based liver-on-chip model.

When compared to their controls, OA led to lower consumption of glutamine (at day 7), PA and OA/PA led to ornithine and proline productions at day 4, PA led to lower production serine and trans-4-hydroxy-L-proline at day 7 and OA/PA to high proline production at day 7. Those metabolites perturbations showed that an important feature of our data set was the perturbation of the biological processes related to the nitrogen metabolisms (in treated samples, when compared to control, after 4 days and after 7 days of exposure). This interpretation was reinforced by the pathway enrichment analysis. Although the urea was detected in our medium, no particular modulation of this metabolite was measured when we compared the CTRL and the FFA treatments at each time points. However, it is recently reported that NAFLD contribute to downregulate nitrogen genes involved in nitrogen conversion[28]. Furthermore, urea cycle dysregulation leads to ammonia accumulation in the blood of NAFLD' patients. In addition, the disruption of glutamine/glutamate metabolism is a pathway reported to lead to ammonia accumulation in cirrhotic patients after NAFLD[29].

Regarding the specificity of each fatty acid, overall, the OA exposure appeared to induce only a mild modification of the metabolome as far as only few metabolites discriminated the treated conditions and the controls. OA is reported to promote larger lipid droplet accumulation when compared to PA in HepG2 cells and to lead to weaker mitochondrial oxidative metabolism[30]. Furthermore, in the early stage of steatosis, the lipotoxicity is characterized by an intense ROS production *via* the increase of the beta-oxidation of free fatty acid accumulated in the cells[31]. In our culture model, however, we found that OA treated cells displayed an important ROS generation in lipid accumulation dependent manner (reported in Chapter 3). Interestingly, after 4 days of exposure, we

detected a clear production of L-pyroglutamate in OA treated conditions. The 5-oxoproline/pyroglutamate is reported as a typical ROS biomarker[32].

Literature report metabolome perturbation of the phenylalanine, tyrosine, fatty acid metabolism and bile acids when HepG2 are exposed to 400 µM of palmitic acid[33]. Furthermore, tryptophan, kinerusine and carnitine were discriminant to separate NAFLD, NASH to cirrhosis subjects[33]. After 4 days of exposure, we detected a switch from a production in control cells to a consumption of tyrosine in PA treated cells. We also found a switch from a consumption to a production of tryptophan in PA treated cells. Furthermore, after 4 days and 7 days of PA treatment, we detected a modification of the metabolism of TCA intermediates and substrates (such as a lower consumption of pyruvic acid, succinic acid and citramalic acid; a switch from a consumption to a production of beta-alanine at day 7 when compared to control condition). PA is reported to enhance mitochondrial oxidative metabolism in HepG2[30] but to reduce it in some other work[34]. Thus, our signature reflected a modification of the energy and respiration state in PA treated conditions when compared to control, in which we may suspect a lower TCA activation (because of lower consumption of the metabolites) and thus a lower oxidative phosphorylation. Furthermore, it appeared consistent with our Chapter 3 data in which we observed a lower ROS production in PA conditions. Nevertheless, additional experiments are necessary to confirm this hypothesis.

Then, we found a specific glycine/serine pathway signature in OA/PA treatments illustrated by the lower production of glycine and serine. In fact, it is reported that serine, *via* liver folate metabolism, regulate hepatic lipogenesis and NADPH[35]. Then, in parallel, important serine deprivation alters glycerophospholipids and sphingolipids metabolisms and potential mechanism for serine-derived lipids in mitochondrial processes are reported[36]. Furthermore, low serine and glycine are also more and more reported as a disease hallmark (in neuropathy[37]; in alcoholic liver disease[38]). In parallel, serine is also an important metabolite for nucleotide and redox metabolism functions via folate metabolism as well[36]. More particularly, serine is a precursor of glycine and cysteine for glutathione synthesis[36]; glutathione being an important anti-oxidant involved in ROS detoxification. Furthermore, we detected a switch from a production to consumption of sarcosine (sarcosine is a related compound in the serine/glycine/folate pathways), when compared to control. Interestingly,

sarcosine is reported to increase in human and rat bloods in the case of dietary restriction and to reduce with aging[39]. Finally, it is largely reported that OA co-exposure with PA can reduce and attenuate the PA toxicity. Regarding the OA/PA and PA signatures after 7 days of exposure, OA co-exposure to PA seems to reduce the productions of palmitoleic acid and cholesterol when compared to controls, restore the levels of TCA substrates and beta-alanine (when compared to PA condition, Figures 4.7 and 4.9). As cholesterol, palmitoleic acid, TCA, and beta-alanine may have different role in response to fatty acids' overloads, additional investigation would be required to confirm if there is a potential bridge with the serine metabolism.

4.8 Conclusion

In this chapter, we have performed a metabolomic analysis to extract the modification of the exo-metabolome of HepG2/C3A cells when exposed to oleic acid, palmitic acid and oleic/palmitic acid mixture. Due to the microenvironment of the organ-on-chip technology we observed a multilayer cell proliferation that lead to 3D-like tissue. The three fatty acids treatments led in a dependent manner to switch the fatty acid beta-oxidation and the lipogenesis. Furthermore, they commonly led to increase the production of nicotinamide which could appeared as a potential biomarker of FFA exposure in our model as well as oxalic acid.

Then, all treatments led to modify the nitrogen metabolism processes. Specific signatures, illustrating the cell response to each exposure were extracted. The oleic presented a moderate metabolome perturbation in which we detected the production of pyroglutamate as potential ROS detoxification marker. The palmitic acid particularly contributed to modify the TCA intermediates and substrates illustrating a potential cellular respiration adaptation. Finally, the palmitic/oleic acids mixture were characterized by lower production of serine and glycine and consumption of sarcosine highlighting a perturbation of the serine, glycine, folate related pathways. This perturbation was coupled with lower cholesterol synthesis and a more global reduction of the fatty acid and lipid metabolisms. Overall, our data demonstrate the sensibility of our strategy, using organ-on-chip technology coupled with metabolomic profiling, to investigate pro-steatosis cellular response.

4.9 References

1 J. F. Xiao, B. Zhou and H. W. Ressom, *TrAC Trends in Analytical Chemistry*, 2012, **32**, 1–14.

2 K. Burgess, N. Rankin and S. Weidt, in *Handbook of Pharmacogenomics and Stratified Medicine*, 2014, 181–205.

3 A. Artati and J. Tokarz, in *Metabolomics for Biomedical Research*, 2020, 137–157.

4 S. Qiu, Y. Cai, H. Yao, C. Lin, Y. Xie, S. Tang and A. Zhang, *Signal Transduct Target Ther*, 2023, 8.

5 J. M. Prot, A. S. Briffaut, F. Letourneur, P. Chafey, F. Merlier, Y. Grandvalet, C. Legallais and E. Leclerc, *PLoS One*, 2011, **6**, e21268.

6 L. C. Snouber, A. Bunescu, M. Naudot, C. Legallais, C. Brochot, M. E. Dumas, B. Elena-Herrmann and E. Leclerc, *Toxicological Sciences*, 2013, **132**, 8–20.

7 R. Jellali, P. Zeller, F. Gilard, A. Legendre, M. J. Fleury, S. Jacques, G. Tcherkez and E. Leclerc, *Environ Toxicol Pharmacol*, 2018, **59**, 1–12.

8 L. Shintu, R. Baudoin, V. Navratil, J.-M. Prot, C. Pontoizeau, M. Defernez, B. J. Blaise, C. Domange, A. R. Péry, P. Toulhoat, C. Legallais, C. Brochot, E. Leclerc and M.-E. Dumas, *Anal Chem*, 2012, **84**, 1840–1848.

9 T. Messelmani, A. Le Goff, F. Soncin, F. Gilard, Z. Souguir, N. Maubon, B. Gakière, C. Legallais, E. Leclerc and R. Jellali, *Toxicology*, 2023, **492**, 153550.

10 M. Masoodi, A. Gastaldelli, T. Hyötyläinen, E. Arretxe, C. Alonso, M. Gaggini, J. Brosnan, Q. M. Anstee, O. Millet, P. Ortiz, J. M. Mato, J. F. Dufour and M. Orešič, *Nature Reviews Gastroenterology & Hepatology 2021 18:12*, 2021, **18**, 835–856.

11 Y. Zhou, M. Orešič, M. Leivonen, P. Gopalacharyulu, J. Hyysalo, J. Arola, A. Verrijken, S. Francque, L. Van Gaal, T. Hyötyläinen and H. Yki-Järvinen, *Clinical Gastroenterology and Hepatology*, 2016, **14**, 1463-1472.e6.

12 N. Perakakis, S. A. Polyzos, A. Yazdani, A. Sala-Vila, J. Kountouras, A. D. Anastasilakis and C. S. Mantzoros, *Metabolism*, 2019, **101**, 154005.

13 Y. Jung, M. K. Lee, P. Puri, B. K. Koo, S. K. Joo, S. Y. Jang, D. H. Lee, Y. J. Jung, B. G. Kim, K. L. Lee, T. S. Park, K. T. Kang, D. H. Ryu, S. W. Kang, D. Kim, S. Oh, W. Kim and G. S. Hwang, *Aliment Pharmacol Ther*, 2020, **52**, 1603–1614.

14 C. Caussy, J. C. Chuang, A. Billin, T. Hu, Y. Wang, G. M. Subramanian, C. S. Djedjos, R. P. Myers, E. A. Dennis and R. Loomba, *Therap Adv Gastroenterol*, 2020, **13**.

15 H. Y. Kim, *Clin Mol Hepatol*, 2021, **27**, 553–559.

16 R. Mayo, J. Crespo, I. Martínez-Arranz, J. M. Banales, M. Arias, I. Mincholé, R. Aller de la Fuente, R. Jimenez-Agüero, C. Alonso, D. A. de Luis, L. Vitek, J. Stritesky, J. Caballería, M. Romero-Gómez, A. Martín-Duce, J. M. Mugüerza Huguet, J. I. Busteros-Moraza, M. O. Idowu, A. Castro, M. L. Martínez-Chantar, P. Ortiz, R. Bruha, S. C. Lu, P. Bedossa, M. Noureddin, A. J. Sanyal and J. M. Mato, *Hepatol Commun*, 2018, **2**, 807–820.

17 C. Xu, D. Song, A. L. Holck, Y. Zhou and R. Liu, *ACS Omega*, 2020, **5**, 11314–11323.

18 M. A. Bermúdez, L. Pereira, C. Fraile, L. Valerio, M. A. Balboa and J. Balsinde, *Cells*, 2022, **11**, 2146.

19 Z.-H. Yang, H. Miyahara and A. Hatanaka, *Lipids Health Dis*, 2011, **10**, 120.

20 C. O. Souza, A. A. S. Teixeira, E. A. Lima, H. A. P. Batatinha, L. M. Gomes, M. Carvalho-Silva, I. T. Mota, E. L. Streck, S. M. Hirabara and J. C. R. Neto, *Mediators Inflamm*, 2014, **2014**, 1–12.

21 C. O. Souza, A. A. S. Teixeira, L. A. Biondo, L. S. Silveira, C. N. de Souza Breda, T. T. Braga, N. O. S. Camara, T. Belchior, W. T. Festuccia, T. A. Diniz, G. M. Ferreira, M. H. Hirata, A. B. Chaves-Filho, M. Y. Yoshinaga, S. Miyamoto, P. C. Calder, J. K. Sethi and J. C. Rosa Neto, *Biochimica et Biophysica Acta (BBA) - Molecular and Cell Biology of Lipids*, 2020, **1865**, 158776.

22 Y. Akazawa, S. Cazanave, J. L. Mott, N. Elmi, S. F. Bronk, S. Kohno, M. R. Charlton and G. J. Gores, *J Hepatol*, 2010, **52**, 586–593.

23 O. Tirosh, *Oxid Med Cell Longev*, 2018, **2018**, 1–15.

24 R. R. El-Kady, A. K. Ali, L. M. El Wakeel, N. A. Sabri and M. A. Shawki, *Ther Adv Chronic Dis*, 2022 ,**13**.

25 H. Wan, J. Li, H. Liao, M. Liao, L. Luo, L. Xu, K. Yuan and Y. Zeng, *Mol Med Rep*, 2018, **19**, 555–562.

26 A. Nahle, Y. D. Joseph, S. Pereira, Y. Mori, F. Poon, H. E. Ghadieh, A. Ivovic, T. Desai, S. S. Ghanem, S. Asalla, H. T. Muturi, E. M. Jentz, J. W. Joseph, S. M. Najjar and A. Giacca, *Int J Mol Sci*, 2021, **22**, 13224.

27 W. W. Yau, G. Bin Chen, J. Zhou, J. C. Francisco, N. K. Thimmukonda, S. Li, B. K. Singh and P. M. Yen, *Hum Mol Genet*, 2023, **32**, 1922–1931.

28 P. L. Eriksen, H. Vilstrup, K. Rigbolt, M. P. Suppli, M. Sørensen, S. Heebøll, S. S. Veidal, F. K. Knop and K. L. Thomsen, *Liver International*, 2019, **39**, 2094–2101.

29 K. L. Thomsen, P. L. Eriksen, A. JC. Kerbert, F. De Chiara, R. Jalan and H. Vilstrup, *JHEP Reports*, 2023, **5**, 100780.

30 A. Eynaudi, F. Díaz-Castro, J. C. Bórquez, R. Bravo-Sagua, V. Parra and R. Troncoso, *Front Nutr*, 2021, **8**, 775382.

31 R. G. R. Mooli and S. K. Ramakrishnan, *Cell Mol Gastroenterol Hepatol*, 2022, **13**, 1267–1270.

32 W. E. Gall, K. Beebe, K. A. Lawton, K.-P. Adam, M. W. Mitchell, P. J. Nakhle, J. A. Ryals, M. V. Milburn, M. Nannipieri, S. Camastra, A. Natali and E. Ferrannini, *PLoS One*, 2010, **5**, e10883.

33 S. Aggarwal, V. Yadav, R. Maiwall, A. Rastogi, V. Pamecha, O. Bedi, J. S. Maras, N. Trehanpati and G. Ramakrishna, *Biochem Biophys Res Commun*, 2023, **643**, 129–138.

34 I. García-Ruiz, P. Solís-Muñoz, D. Fernández-Moreira, T. Muñoz-Yagüe and J. A. Solís-Herruzo, *DMM Disease Models and Mechanisms*, 2015, **8**, 183–191.

35 L. Zhang Shengli Zhang, T. J. Biol, L. Zhang and S. Zhang, *Turkish Journal of Biology*, 2022, **46**, 298–306.

36 X. Gao, K. Lee, M. A. Reid, S. M. Sanderson, C. Qiu, S. Li, J. Liu and J. W. Locasale, *Cell Rep*, 2018, **22**, 3507–3520.

37 M. K. Handzlik, J. M. Gengatharan, K. E. Frizzi, G. H. McGregor, C. Martino, G. Rahman, A. Gonzalez, A. M. Moreno, C. R. Green, L. S. Guernsey, T. Lin, P. Tseng, Y. Ideguchi, R. J. Fallon, A. Chaix, S. Panda, P. Mali, M. Wallace, R. Knight, M. L. Gantner, N. A. Calcutt and C. M. Metallo, *Nature*, 2023, **614**, 118–124.

38 C. SHI, L. WANG, K. ZHOU, M. SHAO, Y. LU and T. WU, *J Nutr Sci Vitaminol (Tokyo)*, 2020, **66**, 536–544.

39 R. O. Walters, E. Arias, A. Diaz, E. S. Burgos, F. Guan, S. Tiano, K. Mao, C. L. Green, Y. Qiu, H. Shah, D. Wang, A. D. Hudgins, T. Tabrizian, V. Tosti, D. Shechter, L. Fontana, I. J. Kurland, N. Barzilai, A. M. Cuervo, D. E. L. Promislow and D. M. Huffman, *Cell Rep*, 2018, **25**, 663-676.e6.

4.10 Supplementary Figures

Supp. Fig. 1: (A) PLS-DA scores plots and **(B)** Heatmap of the metabolites differentially expressed in OA condition at day 2.

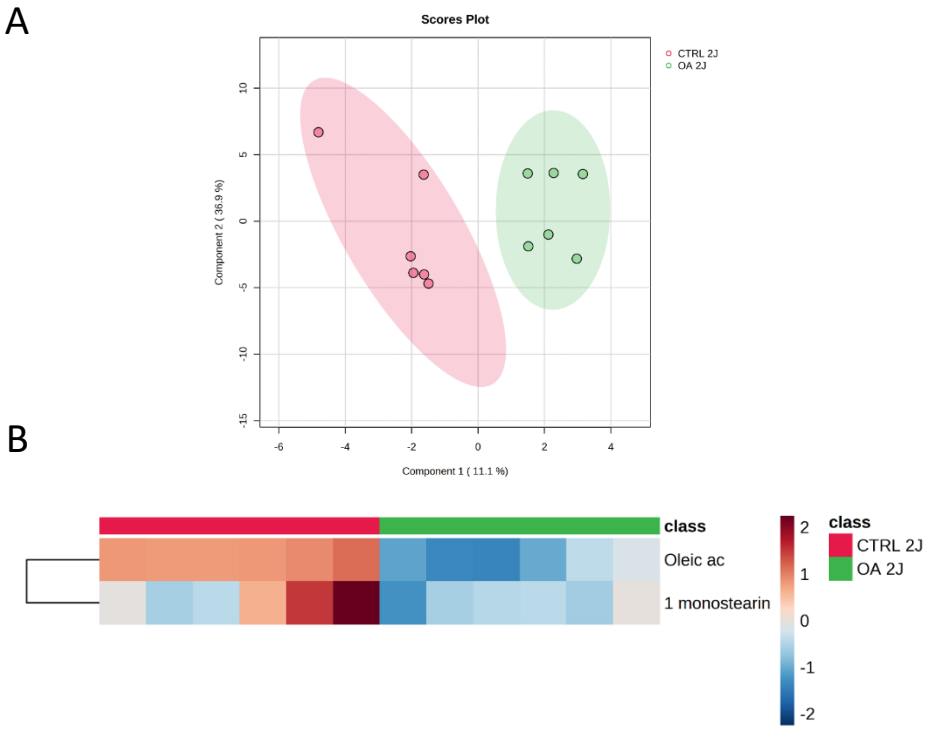

Supp. Fig. 2: (A) PLS-DA scores plots and **(B)** Heatmap of the metabolites differentially expressed in PA condition at day 2.

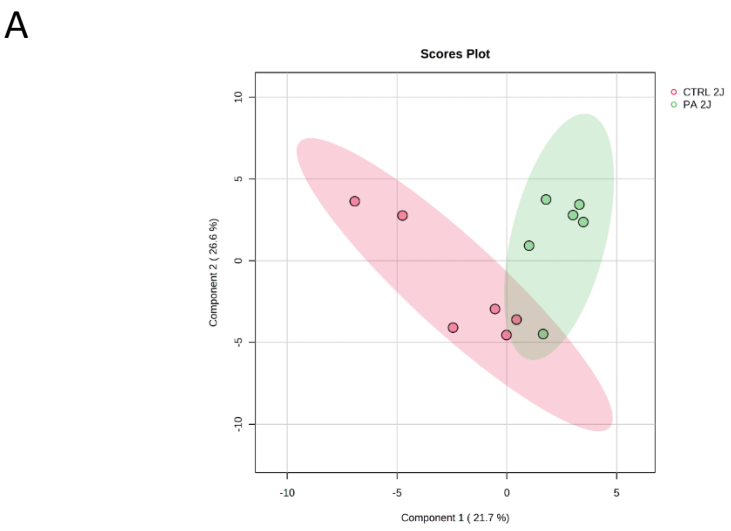

B

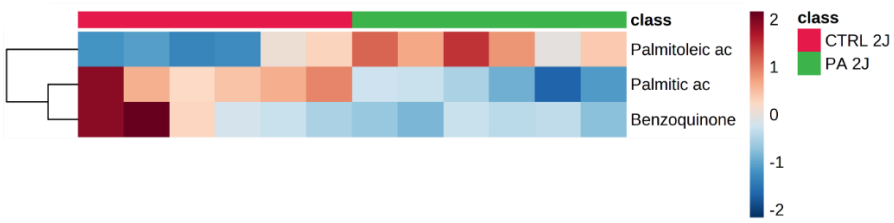

Supp. Fig. 3: (A) PLS-DA scores plots and **(B)** Heatmap of the metabolites differentially expressed in OA/PA condition at day 2.

A

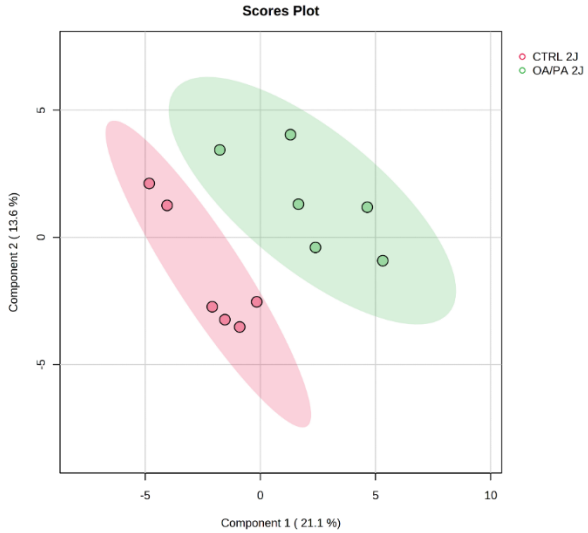

B

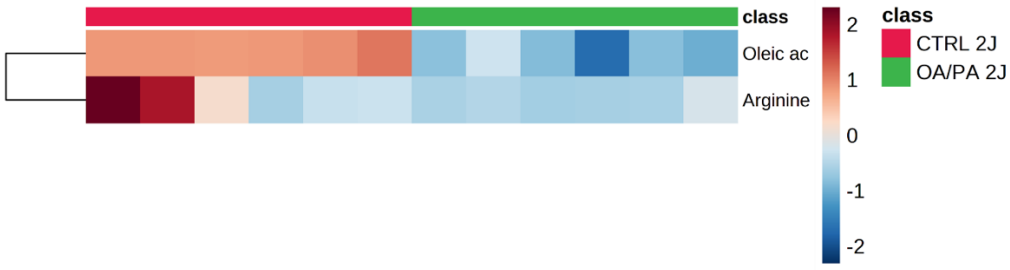

Supp. Fig. 4: Enrichment pathway dot plots for OA condition at **(A)** day 4 and **(B)** day 7.

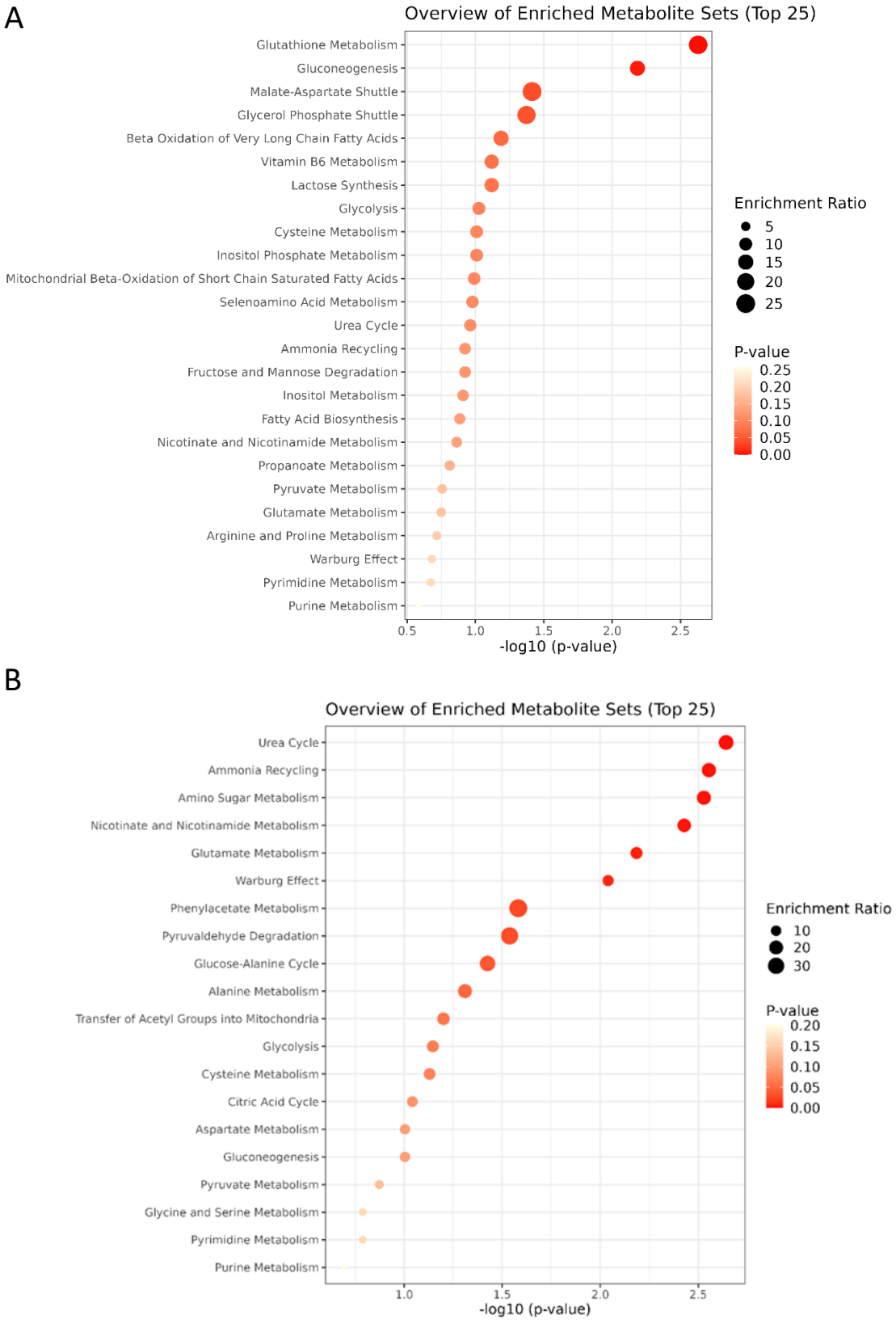

Supp. Fig. 5: Enrichment pathway dot plots for PA condition at **(A)** day 4 and **(B)** day 7.

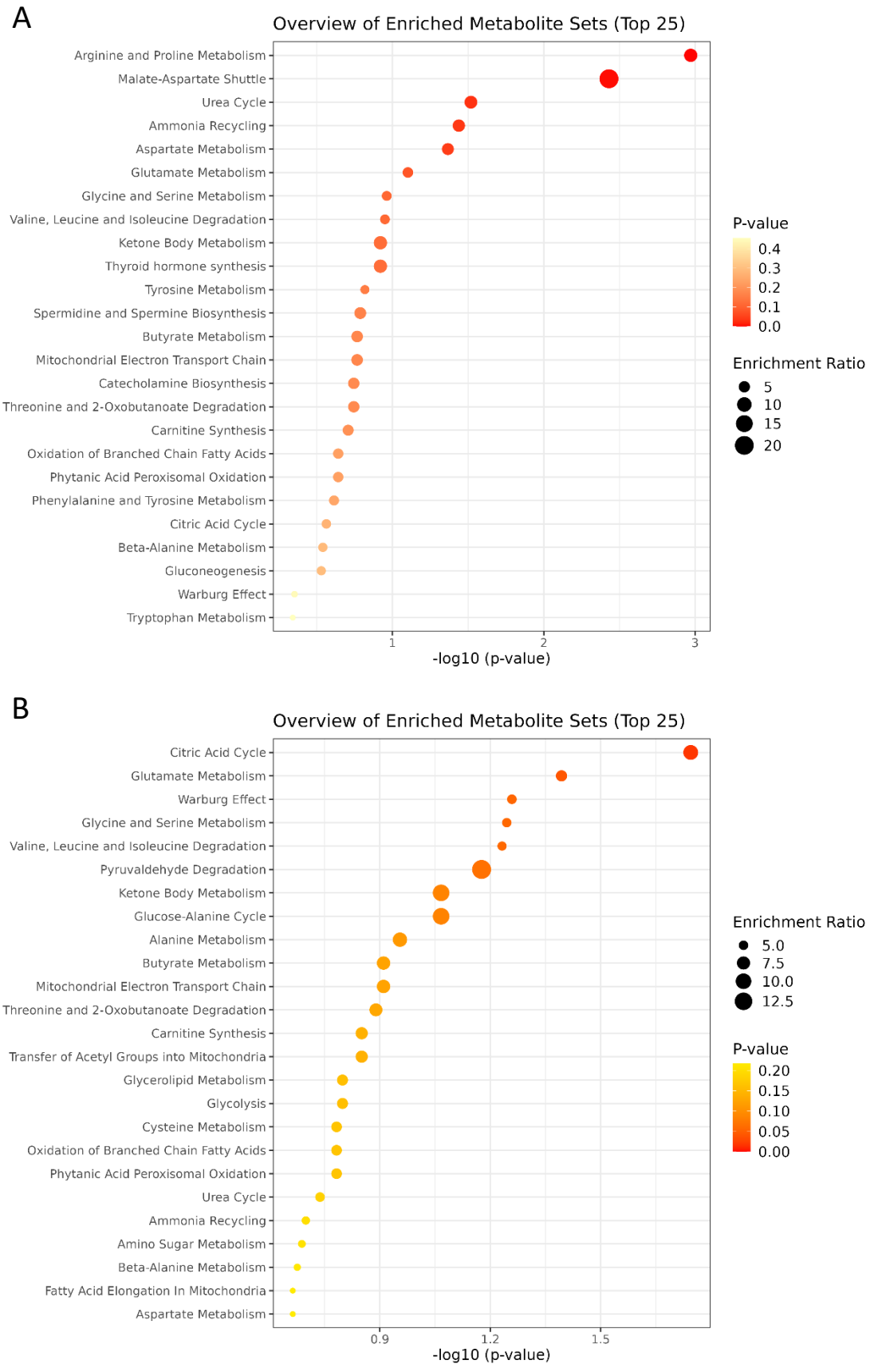

Supp. Fig. 6: Enrichment pathway dot plots for OA/PA condition at **(A)** day 4 and **(B)** day 7.

Chapter V:

Perspectives toward a full NAFL-on-chip model based on human induced pluripotent stem cells – Preliminary results of the cell differentiation process

As enounced in Chapter I, iPSC has emerged as an attractive cell source that can be directly generated from the patients' skin fibroblasts, blood cells and other somatic cell sources. Therefore, patient-specific hiPSCs could serving as an extremely valuable resource for previously inaccessible cell types such as primary hepatocytes. In this chapter, we explored the potential of using human induced pluripotent stem cell to obtained hepatocyte-like cells. Because our final objective is to develop an advanced NAFL-on-chip model and study the crosstalk between liver and pancreas we also explored the differentiation of hiPSC into beta-like cells spheroids.

5.1 Liver-on-chip based on hiPSC: Toward an advanced NAFL-on-chip model

5.1.1 Introduction

Depending on the study aim, the cell type used in hepatic *in vitro* research has to fulfil specific metabolic functions in order to reflect the situation in the native organ. PHH are currently the gold standard for hepatic *in vitro* culture models, since they directly reflect the specific metabolism and functionality of the human liver[1]. However, the difficult logistics to obtain PHH, their cost and their early loss of hepatic functions have driven researchers to explore alternative cell sources. Thus, liver cell lines, such as HepG2/C3A and HepaRG, are widely used due to their good availability and cost. Despite good preservation of certain hepatic functions, cell lines have limitations in the reproduction of the *in vivo* environment and making it difficult to understand the underlying mechanisms of diseases[1,2].

For the past few years, pluripotent stem cells (PSCs) have been attracting scientist's attention, due their ability to proliferate and to differentiate into cells that arise from the 3 germ layers (ectoderm, endoderm, and mesoderm) from which all tissues and organs develop[3]. Since Takahashi and Yamanaka[4] generated pluripotent stem cells by reprogramming somatic cells, human induced pluripotent stem cell (hiPSC) have been widely used. Indeed, hiPSC, as embryonic stem cells, are able to proliferate and differentiate into any cell type. However, these properties are also constraints. hiPSC differentiation requires understanding and mastering cell signaling pathways in order to obtain the desired cell type. Thus, to control cell differentiation pathway into the desired tissue, it is necessary to manipulate culture conditions as composition of the cell culture medium and the atmosphere in the incubator. Despite efforts to control the extracellular environment, it is difficult to achieve a similar effect to *in vivo*. Indeed, the tissues obtained are often heterogeneous with undifferentiated cells and enhanced differentiated cells which are not fully functional. Moreover, a variability between the different existing hiPSC lines has been demonstrated a non-compatibility between some hiPSC cell line and the desired cell types[5].

hiPSC differentiation into hepatocytes-like cells (HLC) have shown some interest since a decade[6]. Numerous hiPSC lines and protocols have been developed by researchers in order to study the physiology of the liver and the associated diseases. Nevertheless, there is a typical protocol, based on Si-Tayeb *et al.,*[7] which consist of four differentiation phases during which

the cells require different growth factors. First, hiPSC differentiate into definitive endoderm cells by 5 days of activin A treatment. Next, differentiation to hepatoblast-like cell is induced by the presence of fibroblast growth factor-2 (FGF2) and bone morphogenetic protein-4 (BMP-4) in the culture medium for 5 days. Then immature hepatocytes are obtained after 5 days of treatment with hepatocyte growth factor (HGF). These two previous steps have to be performed under a 4% O2 atmosphere. For the last step, cells are treated during 5 days with hepatocyte culture medium supplemented with endothelial growth factor (EGF) or oncostatin M (OSM) in order to enhance hepatocytes maturation[1,8]. Many types of medium have been developed to establish a stable maintenance method for hiPSC and their differentiation to HLC. Essential 8 (E8), is a xeno-free medium which is widely used for hiPS cell culture. This culture medium was developed based on TeSR medium, and contain the 8 essential components needed for stem cell culture: insulin, selenium, transferrin, L-ascorbic acid, FGF2, transforming growth factor beta 1 (TGF-β1) in DMEM/F12 (Dulbecco's Modified Eagle Medium/Nutrient Mixture F12) and $NaHCO_3$ for pH adjustment[9,10]. Among the most used media we also find RPMI-1640 which is composed of L-glutamine, HEPES, sodium pyruvate, glucose, and sodium bicarbonate. When used for hiPSC maintenance, RPMI-1640 is usually supplemented with B-27, a serum-free supplement that promote serial generation of stem cells[11]. *In vivo*, the composition and stiffness of liver's extracellular matrix (ECM) cooperatively regulate hepatic phenotype. The ECM is composed of glycoproteins such as collagen, fibrillin, elastin, fibronectin, and laminin. Most of them are commercially available, including fibronectin, different types of collagens, and laminin derivatives and can be used for hiPSC maintenance and differentiation. Other biomaterials are also used such as gelatin, Geltrex and Matrigel® despite its batch-to-batch variability in its protein concentration and composition[12]. Thanks to the combination of all these methods, human ES/iPS cells can be stably cultured for a long time. However, there has been no investigation of the optimal protocol to obtain functional hepatocytes such as human mature primary hepatocytes.

Despite a control of biophysical and biochemical signals the HLC differentiated from hiPSC are immature. The immaturity of these cells can be explained in particular by the absence of a biophysical environment. Indeed, topography, shear stress, and substrate rigidity are factors influencing the phenotype of future cells[13,14]. Considering these characteristics and

based on the typical protocol, Professor Sakai's team propose an optimized protocol for the differentiation of the TkDN4-M hiPSCs line into HLC in a microfluidic system[15]. Indeed, they developed and evaluated different strategies for hepatic differentiation of hiPSCs and highlighted that partial on-chip differentiation promote hepatic maturation when compared to differentiation in Petri dishes[16,17]. Furthermore, in previous works, our group has developed a NAFL liver-on-chip model using HepG2/C3A cell lines to investigate the features of the disease and extract dysregulated metabolic pathways. Nevertheless, this model has limitations in the reproduction of the *in vivo* NAFL physiopathology due to the genetic perturbation of the wnt/β-catenin pathway which is responsible of lipid metabolism dysregulation. Thus, to improve our previous model and to have a better approximation to *in vivo*, we attempted to reproduce our NAFL liver-on-chip model by adapting the partial on-chip protocol to the Cellartis® hiPSC cell line 22 (ChiPSC22, Takara Bio, Europe). We evaluated maturation and steatosis-like state of differentiated hepatocytes by RT-qPCR analysis, immunostaining analysis and several hepatic functional analyses.

5.1.2 Adaptation of the partial on-chip differentiation for Cellartis® cells

To differentiate ChiPSC22, we modified the four-step partial on-chip differentiation protocol developed for hepatic differentiation of hiPSC[16]. First, we performed a cell expansion step, by culturing cells in 6-well plate according to the manufacturer's recommendations. Once their reach 30% confluence, we used CHIR99021 and activin A to induce the definitive endoderm, followed by a bFGF (basic fibroblast growth factor) and BMP-4 treatment to steer them into the hepatic lineage. Immature hepatocytes like-cells obtained after HGF treatment were detached and transferred to Matrigel®-coated biochips for maturation step. In this final step, cells were cultured under a 10 µL/min perfusion flow rate and exposed to HGF, dexamethasone, nicotinamide, ascorbic acid, transforming growth factor beta 1 receptor (TGF-β1R) inhibitor and rock inhibitor. In this adapted protocol, the first two steps (S1 and S2) lasted 5 days, S3 10 days and S4 14 days. RPMI-1640 supplemented with B-27 was used for all steps except the last one for which it was replaced by DMEM/Ham's F-12 (Figure 2.6). At the end of this protocol, the cells were observed and presented much smaller sizes than expected for mature adult hepatocytes. (Figure 5.1A). Moreover, albumin and CYP3A4, specific hepatic markers were moderately expressed by immunostaining (Figure 5.1B).

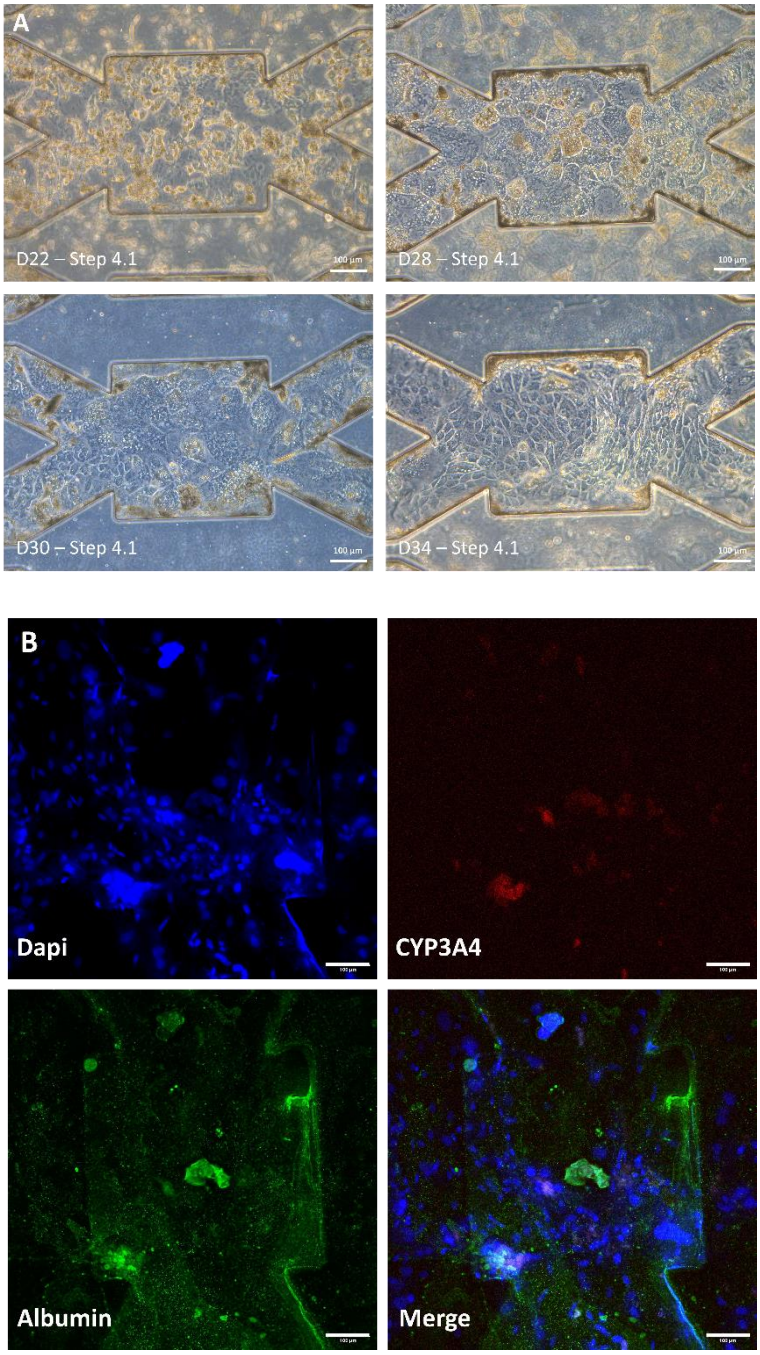

Figure 5. 1: (A) *Cells morphology at day 22, 28, 30 and 34.* ***(B)*** *Albumin (green) and CYP3A4 (red) immunostaining. Scale bar: 100 µm.*

5.1.3 Optimization of the adapted partial on-chip differentiation for Cellartis® cells

To promote hepatocytes maturation, we decided to extend the last step of the differentiation protocol by adding 14 days of culture (Step 4.2). After 48 days through the differentiation procedure, cells formed a confluent tissue layer and displayed hepatocyte-

specific cuboid and bi-nucleated morphology indicating that ChiPSC22 had been differentiated into HLCs (Figure 5.2A). First, cell maturation was assessed by an albumin immunostaining which is a specific hepatic marker. We observed sparse green fluorescent cells indicating albumin secretion (Figure 5.2B). This observation was confirmed with albumin quantification in the culture medium sampled on days 36 and 48 of the Step 4.2. Results shown in Figure 5. 2. C, demonstrated a low production of albumin (69.28±29.5 ng/day) from the first two days of Step 4.2. At day 48, albumin production reached 196.83±42.937 ng/day which is almost 3-fold higher than day 36.

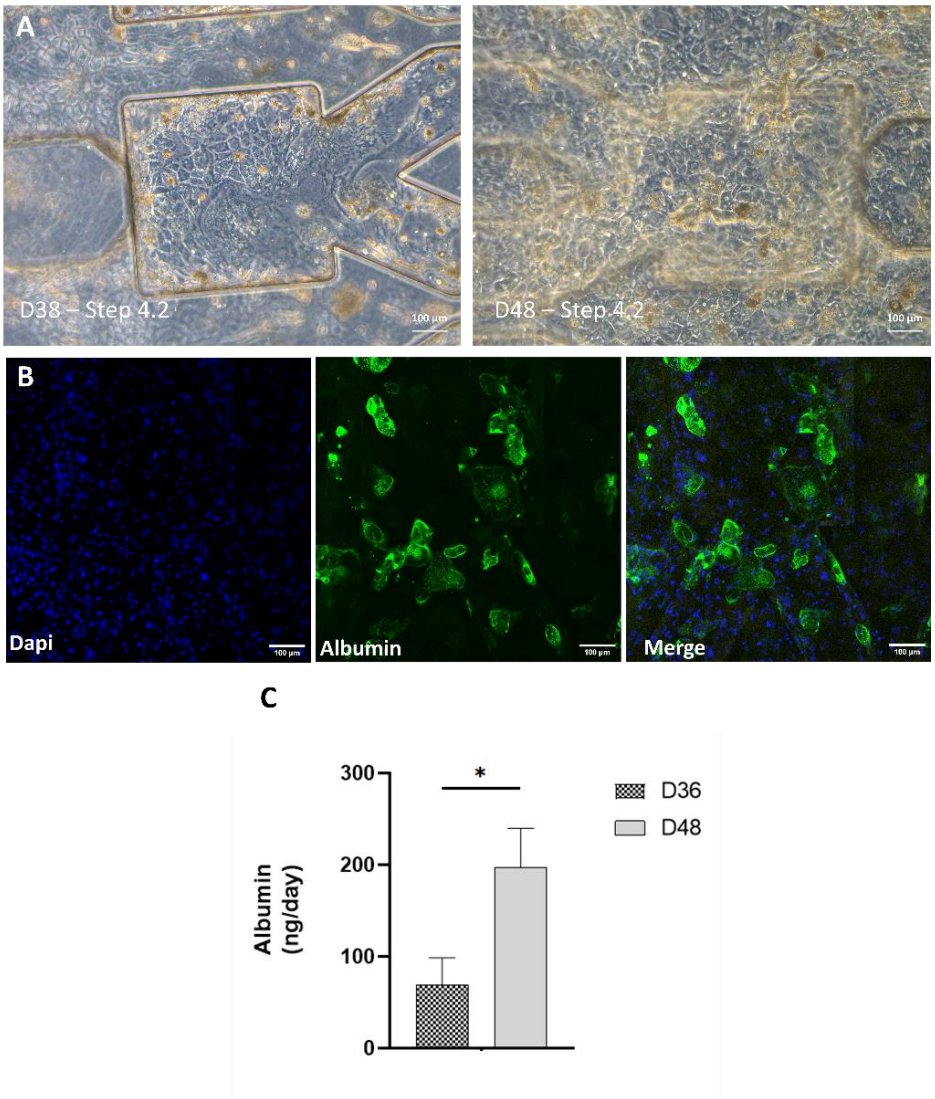

Figure 5. 2: (A) *Cells morphology at day 38 and 48.* ***(B)*** *DAPI (blue) and Albumin (green) immunostaining at the end of differentiation.* ***(C)*** *Albumin production at day 36 and day 48. Statistically analysed by Student t-test. n=3.*

5.1.4 Development of the NAFL liver-on-chip based on Cellartis® cell line

5.1.4.1 Exposure condition and morphological analysis

To develop our NAFL model using HLC from pluripotent stem cell, we exposed the cells to fatty acid. Oleic acid (OA) was chosen because i) it is one of the most abundant fatty acid in the diet ii) it promotes lipid accumulation in the form of lipid droplets in the cytoplasm of hepatocytes iii) it is less toxic than palmitic acid as demonstrated in Chapter 3. Oleic acid was introduced in the culture medium at 0.5mM and cell was exposed for the duration of Step 4.2 i.e. 14 days. The morphological analysis demonstrated the successful cellular adhesion of both control group (non-treated HLC) and treated group (HLC exposed to OA). However, when compared to the control group, the treated group exhibit a less dense cell layer although the population of cells showing a hepatocyte phenotype appears to be larger than those in the control group (Figure 5.3).

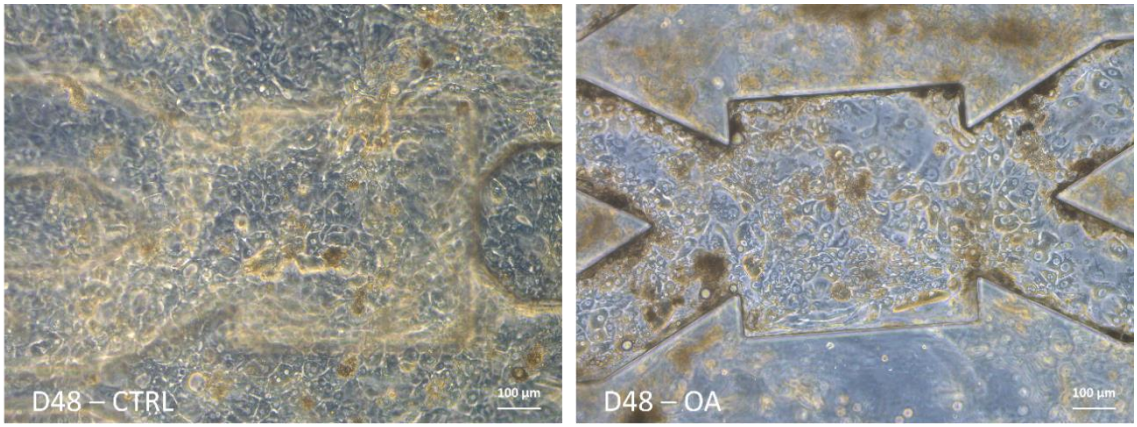

Figure 5. 3: *Cells morphology at the end of the differentiation protocol.*

5.1.4.2 Immunostaining

We performed the immunostaining of the albumin (Figure 5.4), two markers major markers of hepatocytes functionalities. For both control and treated group, cells were positive to albumin, with a higher intensity of the signal in the treated group. E-cadherin (CDH1) a marker of epithelial specification whose expression decreases during hepatic dedifferentiation, was also stained. The intensity signal of CDH1 remained similar for both conditions which indicates that the presence of OA did not alter the differentiation process (Figure 5.5).

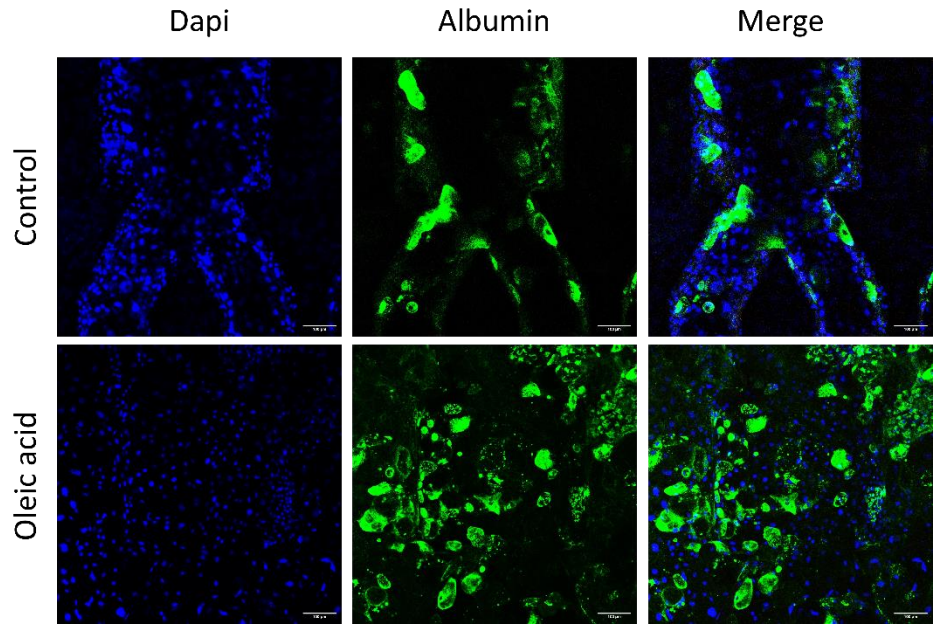

Figure 5. 4: *DAPI (blue) and Albumin (green) immunostaining at the end of the differentiation and exposure protocol for control and treated group. Scale bar: 100 µm.*

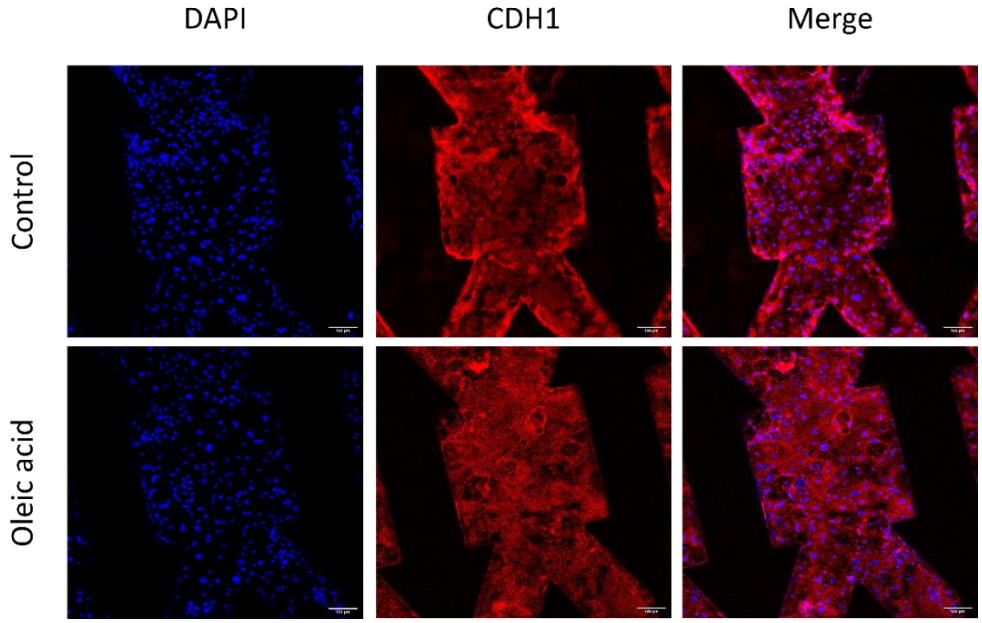

Figure 5. 5: *CDH1 immunostaining on the control and treated group after differentiation and exposure protocol. Scale bar: 100µm.*

5.1.4.3 Functional analysis: albumin and urea production

We assessed HLC functionality by measuring albumin and urea in the culture medium at the end of the differentiation process. Results showed that albumin secretion was not

significantly different between the control group and the treated group, with 263.83±83.9 ng/day and 290.87±125.7 ng/day, respectively (Figure 5.6A). Furthermore, urea production remained in low levels for both control group and treated group. As observed in Figure 5.6B, urea production for the treated group (22.7±5.2 µg/day) was not significantly different than the control group (16.8±2.4 µg/day).

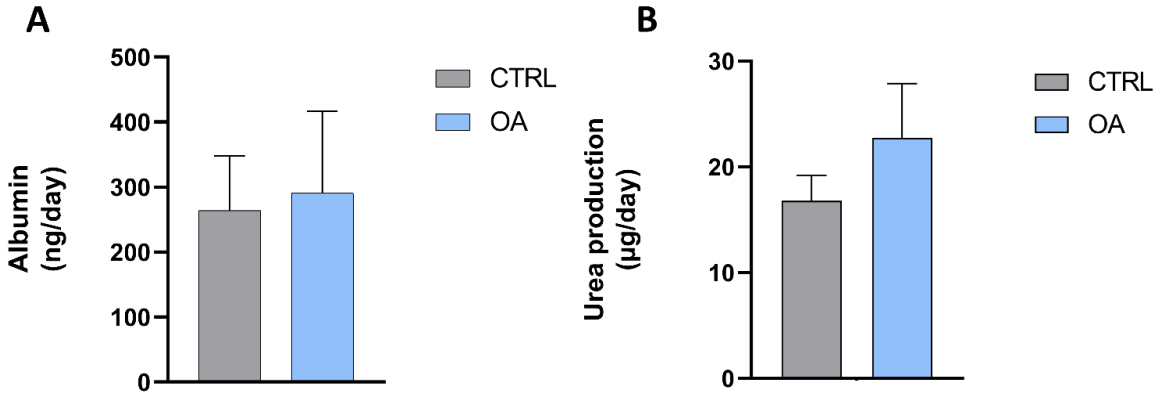

Figure 5. 6: (A) *Albumin production in both control and treated group at day 48.* ***(B)*** *Urea production in both control and treated group at day 48. Statistically analysed by Mann-Whitney test. n=3.*

5.1.4.4 FFA-induced lipid accumulation

We compared the lipid accumulation in the tissue using an oil red staining (Figure 5.7A). We did not observe lipid accumulation in the control group. Conversely, the oil red staining revealed a clear accumulation of lipid in OA treated group. Moreover, we compared the production of collagen and non-collagenous proteins (Figure 5.7B). The control group presented a heterogeneous extra cellular matrix profile with both staining. For the treated group, we observed an intense green network staining suggesting that OA treatment promote non-collagenous proteins expressions.

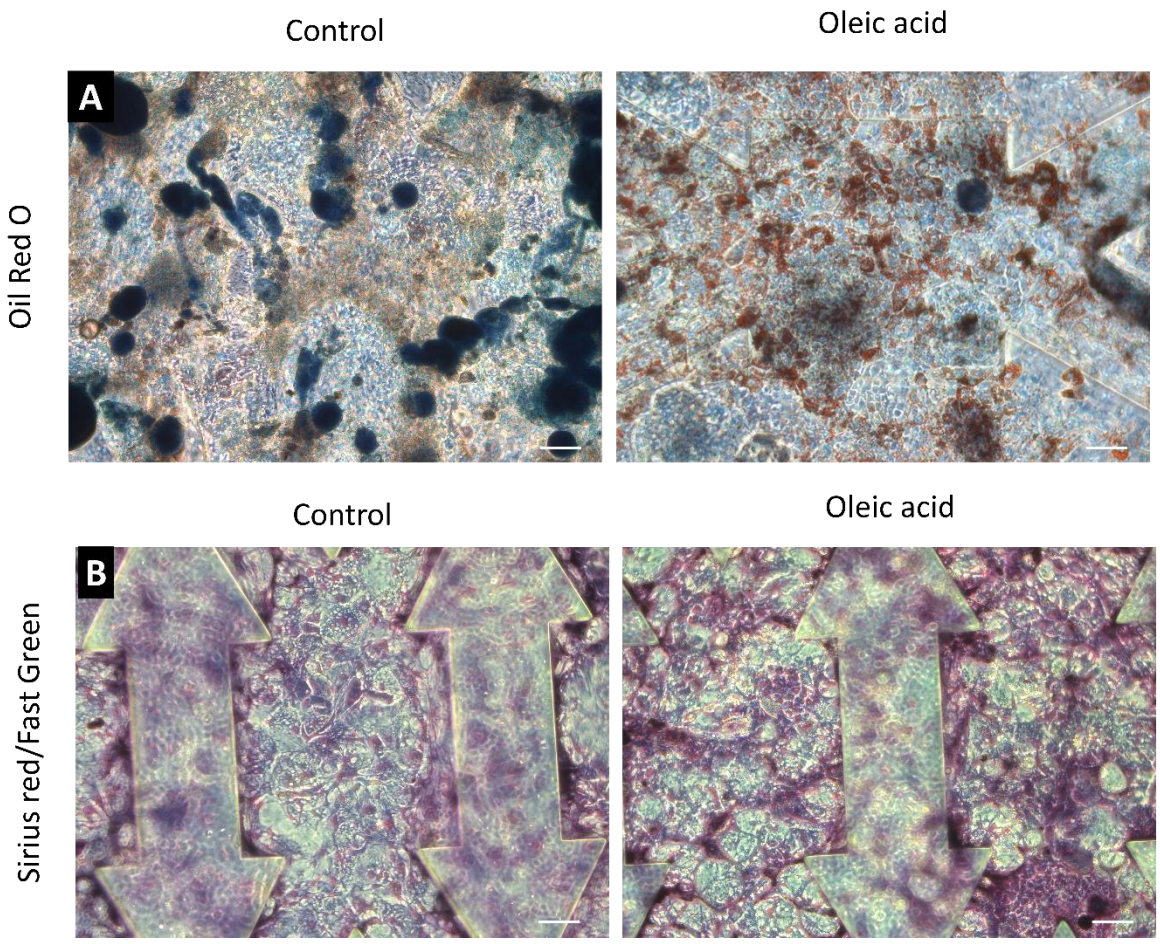

Figure 5. 7: (A) *Lipid droplets staining on control and treated group at day 48.* ***(B)*** *Non-collagenous (green) and total collagen (purple) proteins staining on control and treated group at day 48. Scale bar: 100 µm.*

5.1.4.5 RT-qPCR analysis

The RTqPCR analysis is presented in Figure 5.8. The comparison of the mRNA levels by RTqPCR demonstrated that OA treatment induced an upregulation of the CYP3A4 mRNA levels when compared to control group. Conversely, we observed a downregulation of GLUT2 mRNA levels in treated cells. Nevertheless, the treatment did not modulate the mRNA expression of ALB, CK7, INSRA and INSRB when compared to control group.

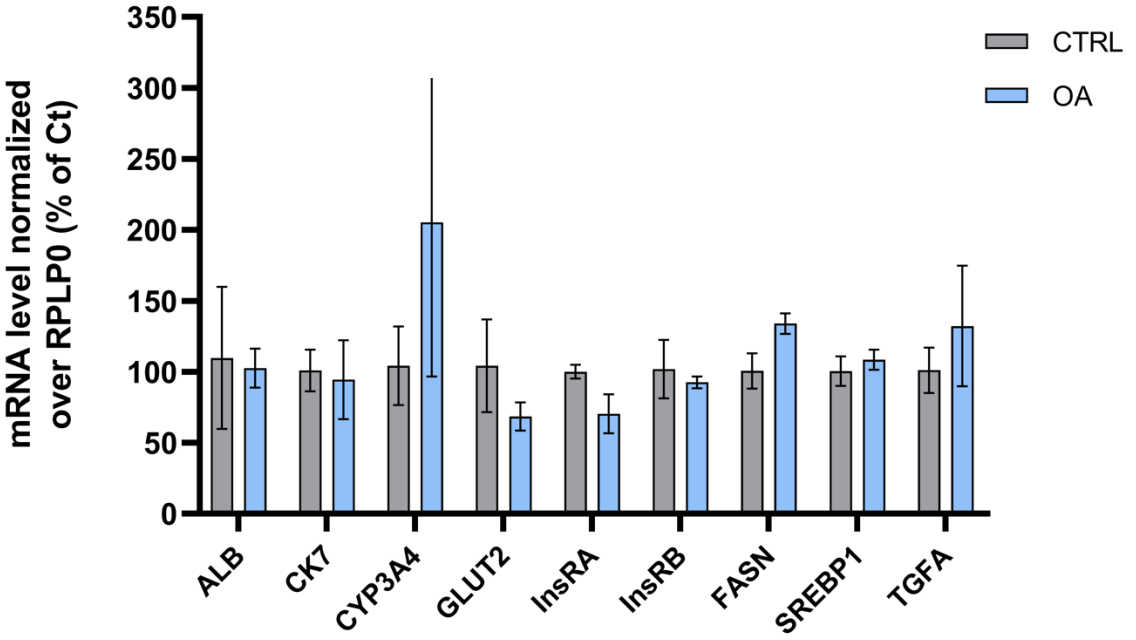

Figure 5. 8: *mRNA expression of selected NAFL genes after differentiation and exposure protocol. n= 2.*

5.1.5 Discussion

In this work we investigated the development of a NAFL liver-on-chip using human pluripotent stem cells. First, we adapted the partial-on-chip protocol, developed by Danoy *et al.*[16] to the Cellartis® ChiPSC22 cells. This adapted protocol is composed of four step whose last step (S4) is performed during 14 days in perfused biochip. We found that cells obtained at the end of the differentiation procedure were not fully matured. Danoy *et al.*[16] improved their protocol by sorting CPM^+ at the end of S3 and added longer maturation in Petri before to inoculate the cells in biochips[18]. Our cells did not exhibit mature hepatocyte phenotype and functions and these results may be explained by the loss of the function of hepatic progenitors during cells transfer in the biochips[16]. Consequently, we investigated the improvement of the maturation into HLC by culturing the cells longer in the microfluidic system in order to promote their adaption to their new environment and further differentiation. By extending the perfused culture to 28 days, we obtained cuboid and bi-nucleated cells corresponding to hepatocyte-specific morphology[19]. Moreover, we detected a secretion of albumin by immunostaining. However, the albumin secretion remained low when

compared to PHH[20,21]. Our preliminary results showed the necessity to extend the development on the Cellartis cells to adapt the protocol to liver on chip cultures, either by practicing the CPM+ sorting, modulating the culture medium with well-known hepatic maturation chemical such as dexamethasone[22,23].

Based on the extended protocol we proposed a first tentative of hepatic steatosis model. For fatty liver simulation, OA, which is an unsaturated fatty acid, was used. Cells were exposed during the second maturation step which last 14 days (Step 4.2). We explored cells morphology and noticed that treated group exhibit more cells with a hepatocyte phenotype supposing that the fatty acids treatment enhanced cellular morphology. Although such results have, to our knowledge, never been demonstrated for HLC, however, it has been proven that fatty acid treatments (oleic or/and palmitic acids) promote the maturation of hiPSC-cardiomyocytes when used in addition or replacing glucose as an energy source[24,25]. RT-qPCR analysis showed an overexpression of CYP3A4 in treated group but comparable albumin expression that confirming partially this hypothesis. In parallel, albumin and CDH1 immunostaining did not highlight any substantial maturation in the treated group. Furthermore, functional analysis confirmed that the production of albumin was comparable in both groups. Similar results were found for urea production that remained low for both groups. Values obtained for both albumin and urea quantification could not be normalized by the number of cells considering the fragility and the value of the samples. As a result, additional experiments would be required to be able to compared with literature data.

Finally, lipid droplets were observed by oil red staining in treated group indicating that oleic acid treatment induced an accumulation of triacylglycerol (TAG). Gene expression analysis showed that fatty acid synthase (FASN) was relatively more expressed in treated group than control group. Although this was not observed in our results, that could be partly explained by an increase of the lipogenic transcription factors sterol regulatory element-binding protein-1 (SREBP-1)[26,27].

5.2 Evaluation of the transfer of pancreatic beta-like cell spheroids protocol

5.2.1 Introduction

As explained throughout the Chapter 1, the pathophysiology of the metabolic syndrome and its progression are not fully elucidated. Nevertheless, it has been shown that NAFLD and T2DM are respectively the hepatic and pancreatic manifestation of Mets, and that the two conditions are linked in complex ways. Indeed, although insulin resistance seems to be at the heart of these metabolic diseases, other mechanisms also seem to play a role. Therefore, in order to study the interdependence of NAFLD and T2DM it is essential to develop *in vitro* models allowing to mimic the liver and pancreas simultaneously. Cellular engineering approach represents the most appropriate approach to mimic and recapitulate the complex biological physiology of the MetS and more specifically the link between NAFLD and T2DM. Nevertheless, only few studies explored the association between NAFLD and TD2M in an *in vitro* model.

Microfluidic platforms have successfully proven their ability to reproduce tissue/organ functions beyond the limits of traditional 2D culture. The most recent innovation is to use organ-on-chip technology to reproduce the behaviour of a group of organs. Most of the time, multi-organ-on-chip tries to faithfully emulate the *in vivo* environment and interactions between organs. The implied signalling pathways create synergic effects on cells which enhance their functions compared to monocultured cells. Nevertheless, the transition to multi-organ-on-chip systems require to have previously enhanced organ-on-chip systems. Each organ type needs individualized system to mimic its micro-environment. For the pancreas, microfluidic platforms are usually design with trapping sites in which human islets are immobilized and cultured under flow as perfusion is essential to maintain their viability and to remove metabolic products[28].

As PHH, human pancreatic islets are difficult to obtain, therefore alternative sources of cells, including the differentiation of stem cells and progenitor cells into insulin-producing beta-cells have been studied over the years. Thus, differentiation of hiPCs toward beta-cells represents a promising process in regenerative medicine and diabetes research. Indeed, several studies were conducted on the use of human beta-cells derived from iPSC to restore endogenous insulin secretion[29–32]. In addition, other studies have demonstrated the value of

using beta-cells derived from iPSC for disease modelling as they provide a better understanding of multiple form of diabetes[33–35]. However, only few experimental studies investigated the correlation between T2DM and NAFL.

In this context, we explored the generation beta-like cell spheroids using iPSC and organ-on-chip technology as a pancreatic model for a liver-pancreas-on-chip. This pancreas-on-chip model, pre-established by Essaouiba,2020 included the combination between static and dynamic culture for iPSC differentiation. Up to now, our beta cells differentiation was performed in collaboration with LIMMS in Tokyo. In order to move a to full harmonise liver-pancreas model at BMBI, using Cellartis® hiPSC cell line and thus similar donors, we investigated the feasibility to transfer to protocol from LIMMS to BMBI. For that purpose, honeycomb technology was sent to Compiegne by our colleagues. Then the pancreas protocol and biochip culture were tested on site.

5.2.2 Generation of beta-like cell spheroids

Cellartis® hiPSC cell line 12 (ChiPSC12, Takara Bio, Europe) were used to derive beta-like cells. As described in Chapter 2.5.1, the cells were seeded in honeycomb microwells at a density of $6x10^5$ cells/wells. We observed formation of aggregate with a rough circumference 24 h after cell seeding and spheroids surrounded with a nudge of cells after 4 days of culture (Figure 5.9A). The formed spheroids were collected from honeycombs well and inoculated into crest biochips (n=1 honeycomb well for 3 biochips) for 11 to 12 days of dynamic culture. At the end of perfusion, we confirmed the presence of spheroids (about 100 spheroids/biochips) illustrating successful dynamic perfusion (Figure 5.9B).

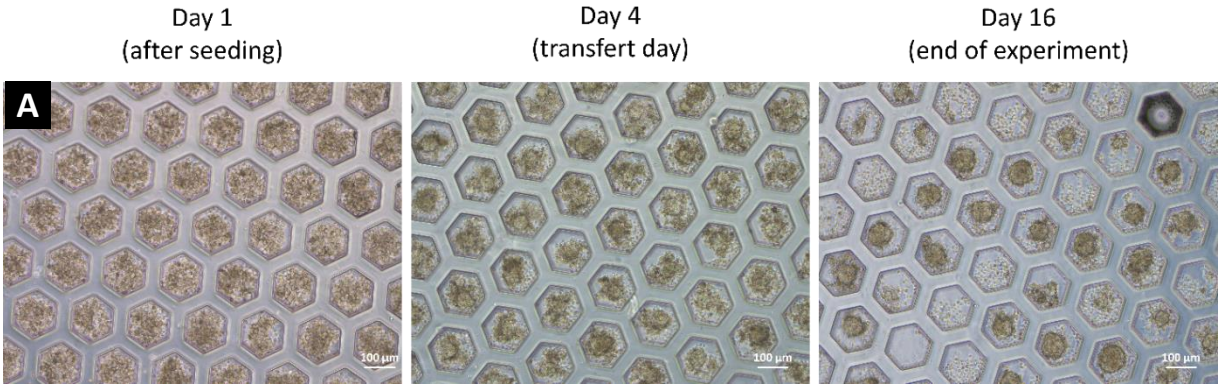

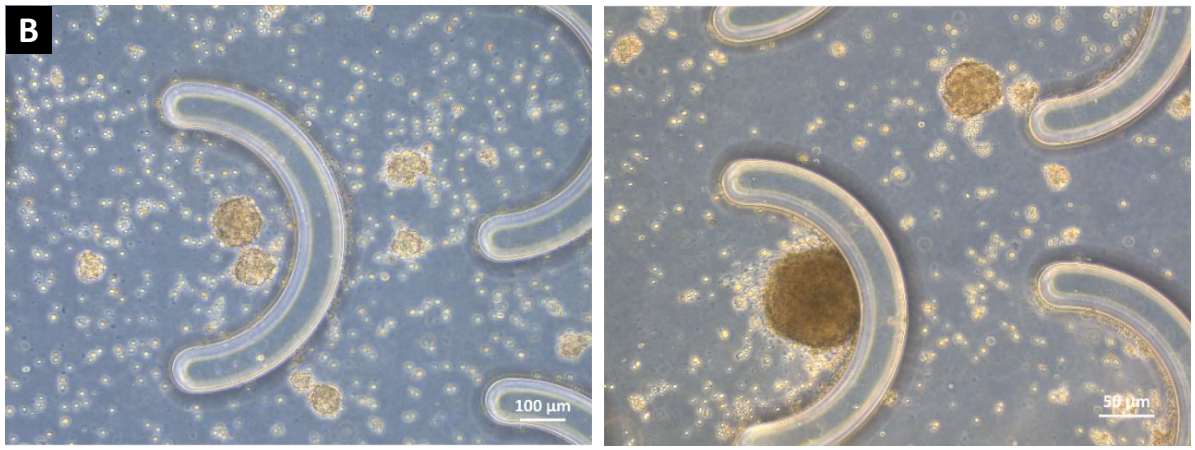

Figure 5. 9: *Morphology of hiPSC derived-β-cells cultivated in honeycombs and biochips.* ***(A)*** *Beta-like cell spheroids formation in honeycomb wells.* ***(B)*** *Beta-like cell spheroids in biochip after 12 days of perfused culture.*

5.2.3 Immunostaining analysis

Immunostaining analysis shown positive spheroids for both glucagon and insulin (Figure 5.11). Glucagon-positive cells appeared to be located at the periphery of the spheroids, while insulin-positive cells seemed to be located in the spheroids core.

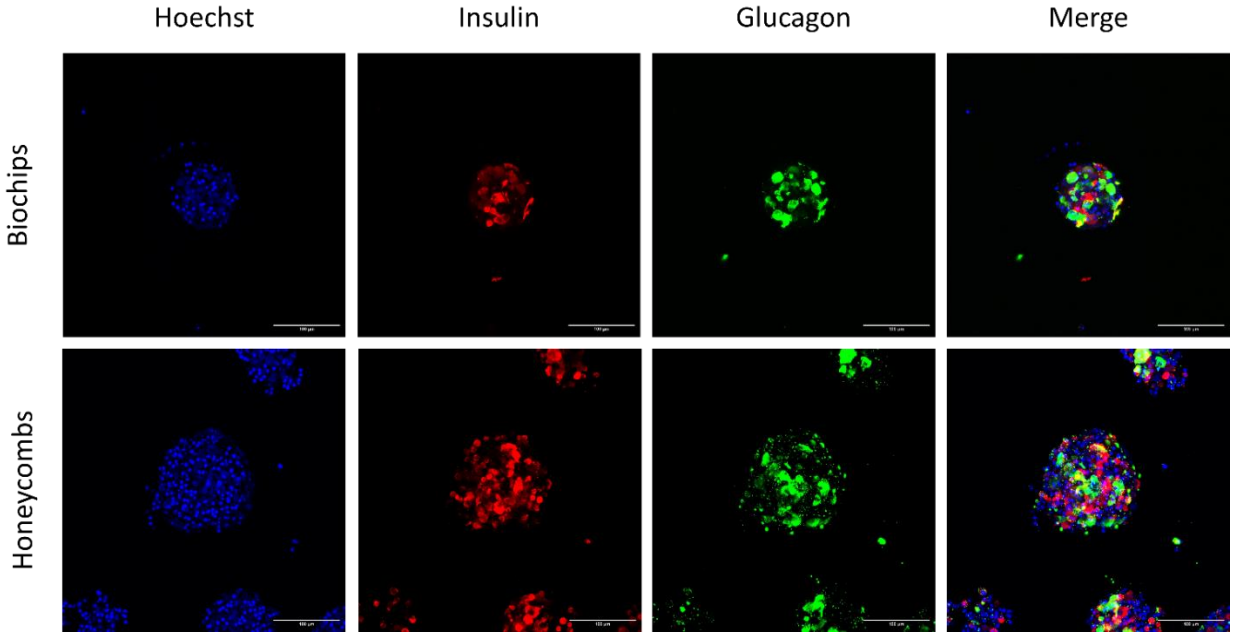

Figure 5. 10: *Insulin (red) and Glucagon (green) immunostaining of beta-like cell spheroids at the end of culture in biochips and honeycombs well. Cell nucleus are stained with DAPI (blue). Scale bar: 100 µm.*

5.2.4 Discussion

We successfully transfer the pancreas-on-chip culture protocol to BMBI. In fact, we perfectly performed spheroids and dynamic culture. Pancreatic spheroids maintained their integrity for both honeycomb and biochip condition until the end of the differentiation process. Interestingly, immunostaining highlighted that the beta-like cell spheroids obtained had a bi-hormonal profile of as they showed glucagon and insulin positive populations.

These promising results lead to a collaboration between BMBI, LIMMS and IEMN in order to the study of the pancreatic subpopulations and their potential role on hormone regulation. This work has been published as an article which is attached in Annex I.

5.3 Conclusion

In this perspectives chapter, we investigated the development of liver-on-chip and pancreas-on-chip by using human induced pluripotent stem cells as the global objective of this project is to develop a multi-organ-on-chip model.

First, we proposed a differentiation protocol of hiPSCs into hepatocytes in a microfluidic system and a primary analysis of its impact on the cells were performed. We highlighted that after seeding, our cells require at least 14 days to stabilize in the biochips to obtain a more functional phenotype. While improvement in our differentiation protocol is still necessary, we used it to propose a model of an hiPSC-based NAFL-on-chip. We observed intracellular TAG accumulation in treated group when compared to control group but no significant difference in the expression of genes involve in NAFL development. Nevertheless, the present results are very encouraging toward the use of our hiPSC-based liver-on-chip for modelling NAFL pathological process.

Parallelly, we successfully reproduced the differentiation protocol of hiPSCs into pancreatic cells by combining static and dynamic culture. The static culture displayed round spheroids able to handle dynamic culture for 12 days. Surprisingly, immunostaining shown the bi-hormonal nature of our pancreatic spheroids opening up exciting new perspectives in the study of cell subpopulation and hormone regulation in the pancreas.

In conclusion both of this hiPSC-based organ-on-chip experiments need to be repeated and enhanced in order to obtain mature cells and significant results. We assumed that co-culture of both liver and pancreas on-chip may have a positive effect on cell maturation, we still need to investigate this hypothesis. Nevertheless, those primary results demonstrated the feasibility of hiPSC-based organ-on-chip for early disease modelling. Indeed, these models can enable the generation of patient specific hiPSC-based liver or/and pancreas-on-chip, allowing disease understanding and treatment testing considering genetic components and interindividual variability.

5.4 References

1 K. Zeilinger, N. Freyer, G. Damm, D. Seehofer and F. Knöspel, *Exp Biol Med*, 2016, **241**, 1684.

2 J. Won Jeon, S. H. Lee, D. Kim and J. H. Sung, *Biotechnol Prog*, 2021, **37(3)**, e3121.

3 S. Yamanaka, *Cell Stem Cell*, 2020, **27**, 523–531.

4 K. Takahashi, K. Tanabe, M. Ohnuki, M. Narita, T. Ichisaka, K. Tomoda and S. Yamanaka, *Cell*, 2007, **131**, 861–872.

5 V. Volpato and C. Webber, *DMM Disease Models and Mechanisms*, 2021, **13(1)**.

6 Y. Shi, H. Inoue, J. C. Wu and S. Yamanaka, *Nat Rev Drug Discov*, 2017, **16**, 115–130.

7 K. Si-Tayeb, F. K. Noto, M. Nagaoka, J. Li, M. A. Battle, C. Duris, P. E. North, S. Dalton and S. A. Duncan, *Hepatology*, 2010, **51**, 297–305.

8 S. K. Mallanna and S. A. Duncan, *Curr Protoc Stem Cell Biol*, 2013, **26**, 1G.4.1.

9 G. Chen, D. R. Gulbranson, Z. Hou, J. M. Bolin, V. Ruotti, M. D. Probasco, K. Smuga-Otto, S. E. Howden, N. R. Diol, N. E. Propson, R. Wagner, G. O. Lee, J. Antosiewicz-Bourget, J. M. C. Teng and J. A. Thomson, *Nat Methods*, 2011, **8**, 424.

10 N. Matoba, T. Yamashita, K. Takayama, F. Sakurai and H. Mizuguchi, *Differentiation*, 2018, **104**, 13–21.

11 Y. Gu, J. Fu, S. Wang and Q. Wang, *Journal of Biotech Research*, 2011, **3**, 7-18.

12 A. Koc, S. Sahoglu Goktas, T. Akgul Caglar and E. Cagavi, *Exp Cell Res*, 2021, **403**, 112599.

13 Kshitiz, J. Park, P. Kim, W. Helen, A. J. Engler, A. Levchenko and D. H. Kim, *Integr Biol (Camb)*, 2012, **4**, 1008.

14 W. Zakrzewski, M. Dobrzyński, M. Szymonowicz and Z. Rybak, *Stem Cell Res Ther*, 2019, **10**, 68.

15 E. Leclerc, K. Kimura, M. Shinohara, M. Danoy, M. Le Gall, T. Kido, A. Miyajima, T. Fujii and Y. Sakai, *Genomics*, 2017, **109**, 16–26.

16 M. Danoy, M. L. Bernier, K. Kimura, S. Poulain, S. Kato, D. Mori, T. Kido, C. Plessy, H. Kusuhara, A. Miyajima, Y. Sakai and E. Leclerc, *Biotechnol Bioeng*, 2019, **116**, 1762–1776.

17 M. Danoy, S. Poulain, R. Jelalli, F. Gilard, S. Kato, C. Plessy, T. Kido, A. Miyajima, Y. Sakai and E. Leclerc, *Biochem Eng J*, 2020, **155**, 107490.

18 D. Mathieu, P. Stéphane, S. Benedikt, J. Rachid, T. Yannick, L. Marjorie, B. Johanna, G. Francoise, G. Bertrand, A. Hiroshi, K. Yukio, K. Soo Hyeon, K. Taketomo, M. Atsushi, S. Yasuyuki and L. Eric, *Biochem Eng J*, 2022, **181**, 108408.

19 W. H. Liu, L. N. Ren, T. Chen, N. You, L. Y. Liu, T. Wang, H. T. Yan, H. Luo and L. J. Tang, *J Cell Mol Med*, 2014, **18**, 1–14.

20 T. Bricks, J. Hamon, M. J. Fleury, R. Jellali, F. Merlier, Y. E. Herpe, A. Seyer, J. M. Regimbeau, F. Bois and E. Leclerc, *Biopharm Drug Dispos*, 2015, **36**, 275–293.

21 R. Jellali, T. Bricks, S. Jacques, M. J. Fleury, P. Paullier, F. Merlier and E. Leclerc, *Biopharm Drug Dispos*, 2016, **37**, 264–275.

22 H. Baribault and N. Marceau, *J Cell Physiol*, 1986, **129**, 77–84.

23 A. Kamiya, N. Kojima, T. Kinoshita, Y. Sakai and A. Miyaijma, *Hepatology*, 2002, **35**, 1351–1359.

24 Y. Horikoshi, Y. Yan, M. Terashvili, C. Wells, H. Horikoshi, S. Fujita, Z. J. Bosnjak and X. Bai, *Cells*,2019, **8(9)**, 1095.

25 W. E. Knight, Y. Cao, Y. H. Lin, C. Chi, B. Bai, G. C. Sparagna, Y. Zhao, Y. Du, P. Londono, J. A. Reisz, B. C. Brown, M. R. G. Taylor, A. V. Ambardekar, J. C. Cleveland, T. A. McKinsey, M. Y. Jeong, L. A. Walker, K. C. Woulfe, A. D'Alessandro, K. C. Chatfield, H. Xu, M. R. Bristow, P. M. Buttrick and K. Song, *Stem Cell Reports*, 2021, **16**, 519–533.

26 F. Ameer, L. Scandiuzzi, S. Hasnain, H. Kalbacher and N. Zaidi, *Metabolism*, 2014, **63**, 895–902.

27 A. Moravcová, Z. Červinková, O. Kučera, V. Mezera, D. Rychtrmoc and H. Lotková, *Physiol Res*, 2015, **64**, S627–S636.

28 S. Abadpour, A. Aizenshtadt, P. A. Olsen, K. Shoji, S. R. Wilson, S. Krauss and H. Scholz, *Curr Diab Rep*, 2020, **20**, 1–13.

29 K. G. Maxwell and J. R. Millman, *Cell Rep Med*, 2021, **2**, 100238.

30 L. Sui, N. Danzl, S. R. Campbell, R. Viola, D. Williams, Y. Xing, Y. Wang, N. Phillips, G. Poffenberger, B. Johannesson, J. Oberholzer, A. C. Powers, R. L. Leibel, X. Chen, M. Sykes and D. Egli, *Diabetes*, 2018, **67**, 26–35.

31 C. Greenhill, *Nature Reviews Endocrinology 2022 18:4*, 2022, **18**, 193–193.

32 Y. Du, Z. Liang, S. Wang, D. Sun, X. Wang, S. Y. Liew, S. Lu, S. Wu, Y. Jiang, Y. Wang, B. Zhang, W. Yu, Z. Lu, Y. Pu, Y. Zhang, H. Long, S. Xiao, R. Liang, Z. Zhang, J. Guan, J. Wang, H. Ren, Y. Wei, J. Zhao, S. Sun, T. Liu, G. Meng, L. Wang, J. Gu, T. Wang, Y. Liu, C. Li, C. Tang, Z. Shen, X. Peng and H. Deng, *Nature Medicine 2022 28:2*, 2022, **28**, 272–282.

33 V. Lithovius, J. Saarimäki-Vire, D. Balboa, H. Ibrahim, H. Montaser, T. Barsby and T. Otonkoski, *Diabetologia*, 2021, **64**, 630–640.

34 X. Wang, M. Sterr, Ansarullah, I. Burtscher, A. Böttcher, J. Beckenbauer, J. Siehler, T. Meitinger, H. U. Häring, H. Staiger, F. M. Cernilogar, G. Schotta, M. Irmler, J. Beckers, C. V. E. Wright, M. Bakhti and H. Lickert, *Mol Metab*, 2019, **24**, 80–97.

35 N. C. Leite, E. Sintov, T. B. Meissner, M. A. Brehm, D. L. Greiner, D. M. Harlan and D. A. Melton, *Cell Rep*, 2020, **32**, 107894.

General conclusion and Perspectives

The harmful impacts of non-alcoholic fatty liver disease (NAFLD) are increasingly posing a significant public health challenge due to the global rise in diabetes and obesity rates. Notably, NAFLD stands as the most prevalent chronic liver disorder in the Western world. It is characterized by hepatic steatosis, wherein no other contributing factors, such as excessive alcohol consumption, can account for the accumulation of fat in the liver. Due to the complexity of this disease, there is still no therapeutic solution although several drugs are under clinical trials. The lack of pertinent model could be a potential bottleneck to identify potential candidate drugs. Recent advancements in microfluidic devices have emerged as a potent tool for preserving cell functionality and extending the lifespan of various cell populations when compared to traditional *in vitro* models. Furthermore, research has shown that cells are highly responsive to the biomechanical stimuli found in living organisms, emphasizing the importance of incorporating such stimuli as a crucial parameter in creating relevant in vitro models. Organ-on-chip is proposed as solution to combine 3D culture and multicellular tissues (even organ-to-organ interaction) by providing a microenvironment allowing biochemical and biomechanical stimulation (through dynamic culture). However, developing liver-on-chip models as viable alternatives to animal testing remains a formidable challenge. While various models have been proposed in scientific literature, to our knowledge, none have been effectively adopted by pharmaceutical companies for drug discovery. Indeed, many of these models lack the capability to faithfully replicate *in vivo* biological processes or consider the intricate microenvironment and physiology of living organisms.

In this work, we try to bring some incremental steps toward the development of liver-on-chip useful to mimic the liver steatosis. In the first part of our work, we investigated if the HepG2/C3A-based liver-on-chip of the laboratory was a pertinent model to reproduce the characteristic of fatty liver disease. Indeed, our technology was previously used to investigate drugs and chemical toxicity but was never applied to reproduce a liver disease. We found that the treatment of oleic acid, palmitic acid and the mixture of oleic and palmitic acid lead to specific HepG2/C3A response. More particularly, we found that the oleic acid and oleic/palmitic acid treatment did not modify the HepG2/C3A proliferation. However, both

treatments led to reactive oxygen species production. In addition, the oleic acid led to the accumulation of lipid. In parallel, the palmitic acid treatment limited the HepG2/C3A proliferation. This limitation was coupled with a low reactive oxygen production and no lipid accumulation. The palmitic treatment led to a lipid metabolism perturbation that was characterized by the important downregulation of glycolic and lipidic genes illustrated by the GLUT2, INSRA, FASN and SREBP1 mRNA levels. Interestingly, the co-exposure of oleic acid with palmitic acid restored the mRNA levels of GLUT2, INSRA, FASN and partially of SREBP1. Although, several patterns of our result appeared consistent with the large literature using HepG2 as liver model for steatosis (either in 2D or 3D spheroids), some physiopathological responses that we observed may include some bias due to the tumoral properties of the HepG2/C3A cell line. Nevertheless, this model was pertinent because it allows to screen easily a large panel of parameters during the establishment of our model and confirmed the sensibility of our organ-on-chip technology to response various free fatty acid stimuli. Then in a second part of our investigation, we have extended the characterization by proposing a metabolomic profiling of the treatments of oleic acid, palmitic acid and the mixture of oleic and palmitic acids. Previously, our laboratory has demonstrated in the past the potential of the organ-on-chip technology to extract hepatoxic signature regarding environmental chemical (pesticides, solvent), drugs (paracetamol, flutamide), but we never confirmed the potential of extracting physiopathological signatures in liver disease-like model. As we established different responses in term of cell growth, lipid accumulation and oxidative stress expression depending on the fatty acid treatments, we were interesting to investigate the cellular secretome modified in our model. The purpose of such analysis was to extract typical metabolic signatures to be able to define potential biomarker and metabolic patterns. Our model has displayed its interest as far as we were able to establish specific metabolic profile for each treatment but also a common response of the three tested treatments. The three different fatty acid treatments induced a shift in the fatty acid beta-oxidation process and lipogenesis in a dependent manner. Additionally, they commonly led to the modulation of the nicotinamide and oxalic acid metabolism, which could potentially serve asbiomarkers. In parallel, all treatments resulted in modifications to nitrogen metabolism processes. Distinctive patterns, reflecting the cellular response to each exposure, were identified. Oleic acid treatment induced a mild perturbation in the metabolome, with the detection of

pyroglutamate production, potentially indicative of reactive oxygen species (ROS) detoxification. Palmitic acid, on the other hand, appeared to significantly alter tricarboxylic acid (TCA) intermediates and substrates, suggesting potential adaptations in cellular respiration. Lastly, the combination of palmitic and oleic acids was characterized by reduced production of serine, glycine, and a consumption of sarcosine, indicating a disruption in this pathway. This disruption was accompanied by decreased cholesterol synthesis and a more comprehensive reduction in fatty acid metabolism. Finally, in a third part of our work, we have move on a more realistic and relevant liver steatosis model by using human induced pluripotent stem cells. The human induced pluripotent stem cells have the interest because they can be directly generated from the patients' cell sources. Therefore, patient-specific iPSCs could serving as an extremely valuable resource to consider patient' medical conditions. Furthermore, they can be an alternative to the lack and the cost of human primary hepatocytes. In the two previous chapter, we found that oleic acid led to the lipid accumulation and to a moderate metabolic perturbation after 7 days of exposure. As lipid accumulation and ballooning was a typical hallmark of the early steatosis, we have selected oleic acid as fatty acid treatment to propose a first tentative of liver steatosis-like model using our organ-on-chip technology with hepatocyte-like cells. Thus, this chapter led to identify a protocol, by adapting the existing one, to allow the hepatocyte-like cells differentiation and culture within our organ-on-chip technology. As a result, we were able to clearly observed the lipid droplet accumulation and some early collagen synthesis in our model. In this chapter, we also studied the complete differentiation of human induced pluripotent stem cells into beta cells. We found a bi-hormonal profile of our cells which led us to the conclusion that we had islet-like spheroids with both beta and alpha cells. Overall, our work has contributed to demonstrate the potential of our organ-on-chip technology for the investigation of steatosis. We have achieved three main milestones: the feasibility study, the metabolic screening potential and the establishment of a stem cell-derived human hepatocytes model. To this end, we have bridged the gap between conventional microtechnology, tissue engineering and molecular biology.

Our multidisciplinary approach is helping to make progress towards an advanced solution that has yet to be characterized. The future perspectives would be to continue to

develop and refine the stem cell-derived hepatocyte model and explore its potential for studying more advanced stages of NAFLD such as NASH and fibrosis (by including stellate cells and Kupffer cells). In addition, integrating the liver-on-chip model with the pancreas-on-chip system to simulate multi-organ interactions, which could provide a more comprehensive understanding of how NAFLD affects the pancreas and how it is linked to insulin resistance and type 2 diabetes mellitus.

Public communications

Review

Messelmani T, Morisseau L, Sakai S, Legallais C, Le Goff A, Leclerc E, Jellali R. **Liver organ-on-chip models for toxicity studies and risk assessment**, Lab on a Chip, 2022, 22, 2423-2450. DOI : 10.1039/D2LC00307D.

Book chapter

Morisseau L, Messelmani T, Essaouiba A, Sakai Y, Legallais C, Leclerc E, Jellali R. in **Nanotechnology for Diabetes Management**, ed. Abderrahmani A, Szunerits S, Boukerroub R, and El Ouaamari A, The Royal Society of Chemistry, 2022, chapter 7, 188-232. DOI: 10.1039/9781839165498-00188.

Articles

Morisseau L, Tokito F, Poulain S, Plaisance V, Pawlowski V, Kim SH, Legallais C, Jellali R, Sakai Y, Abderrahmani A, Leclerc E. **Generation of β-like cell subtypes from differentiated human induced pluripotent stem cells in 3D spheroids**, Molecular Omics, 2023. DOI: 10.1039/d3mo00050h. This article can be consulted in Annex I.

International congress

Morisseau L, Gilard F, Gakière B, Legallais C, Sakai Y, Jellali R, Leclerc E. **Investigation of the metabolomic profiles of HepG2/C3A exposed to oleic acid, palmitic acid and oleic/palmitic acid mixture using organ-on-chip technology** - Oral presentation. Multi-disciplinary approaches of technological sciences for smart society workshop, October 2023, Tokyo, Japan.

Morisseau L, Pawlowski V, Plaisance V, Legallais C, Sakai Y, Abderrahmani A, Jellali R, Leclerc E. **Investigation of oleic acid, palmitic acid and their mixture on the development of hepatic steatosis using liver-on-chip technology** - Oral presentation. 49th ESAO and IFAO Congress, August 2023, Bergamo, Italy.

Morisseau L, Jellali R, Abderrahmani A, Pawlowski V, Legallais C, Sakai Y, Leclerc E. **Modelling NAFLD using human-induced pluripotent stem cell and organ-on-chip technology** – Poster. XLVIII Annual ESAO Congress, September 2022, Krems, Austria.

Morisseau L, Jellali R, Abderrahmani A, Pawlowski V, Legallais C, Sakai Y, Leclerc E. **Modelling NAFLD using human-induced pluripotent stem cell and organ-on-chip technology** – Poster. Microphysiological systems: from organoids to organ-on-chip, February 2022, Cargèse, France.

Morisseau L, Jellali R, Sakai Y, Leclerc E. **Development of a NAFLD model using organ-on-chip technology** – Poster. EUROoCS conference 2021, Online

Award

yESAO Exchange Program Award 2023 – May 2023. The report of this exchange program can be consulted in Annex II.

Morisseau L, Rodriguez-Fernandez J, Gallego-Ferrer G, Tolosa L, Legallais C, Jellali R, Sakai Y, Salmeron-Sanchez M, Leclerc E. **Modelling Non-Alcoholic Fatty Liver Disease by culturing HepG2/C3A cells using a microfluidic biochip combined with a biomimetic hydrogel** – Oral presentation. 49th ESAO and IFAO Congress, August 2023, Bergamo, Italy.

Annexes

Annex I: Published article: “Generation of β-like cell subtypes from differentiated human induced pluripotent stem cells in 3D spheroids”.

We reproduced here the published paper related to Chapter 5 using the journal policy:

"If you are the author of this article, you do not need to request permission to reproduce figures and diagrams provided correct acknowledgement is given. If you want to reproduce the whole article in a third-party publication (excluding your thesis/dissertation for which permission is not required) please go to the Copyright Clearance Center request page."

Molecular Omics

ROYAL SOCIETY OF CHEMISTRY

RESEARCH ARTICLE

View Article Online
View Journal

Cite this: DOI: 10.1039/d3mo00050h

Generation of β-like cell subtypes from differentiated human induced pluripotent stem cells in 3D spheroids†

Lisa Morisseau,‡[a] Fumiya Tokito,‡[b] Stéphane Poulain, ‡[c] Valerie Plaisance,[d] Valerie Pawlowski,[d] Soo Hyeon Kim, [c] Cécile Legallais,[a] Rachid Jellali, [a] Yasuyuki Sakai,[be] Amar Abderrahmani*[d] and Eric Leclerc *[e]

Since the identification of four different pancreatic β-cell subtypes and bi-hormomal cells playing a role in the diabetes pathogenesis, the search for *in vitro* models that mimics such cells heterogeneity became a key priority in experimental and clinical diabetology. We investigated the potential of human induced pluripotent stem cells to lead to the development of the different β-cells subtypes in honeycomb microwell-based 3D spheroids. The glucose-stimulated insulin secretion confirmed the spheroids functionality. Then, we performed a single cell RNA sequencing of the spheroids. Using a knowledge-based analysis with a stringency on the pancreatic markers, we extracted the β-cells INS+/UCN3+ subtype (11%; β1-like cells), the INS+/ST8SIA1+/CD9− subtype (3%, β3-like cells) and INS+/CD9+/ST8SIA1-subtype (1%; β2-like cells) consistently with literature findings. We did not detect the INS+/ST8SIA1+/CD9+ cells (β4-like cells). Then, we also identified four bi-hormonal cells subpopulations including δ-like cells (INS+/SST+, 6%), γ-like cells (INS+/PPY+, 3%), α-like-cells (INS+/GCG+, 6%) and ε-like-cells (INS+/GHRL+, 2%). Using data-driven clustering, we extracted four progenitors' subpopulations (with the lower level of INS gene) that included one population highly expressing inhibin genes (INHBA+/INHBB+), one population highly expressing KCNJ3+/TPH1+, one population expressing hepatocyte-like lineage markers (HNF1A+/AFP+), and one population expressing stem-like cell pancreatic progenitor markers (SOX2+/NEUROG3+). Furthermore, among the cycling population we found a large number of REST+ cells and CD9+ cells (CD9+/SPARC+/REST+). Our data confirm that our differentiation leads to large β-cell heterogeneity, which can be used for investigating β-cells plasticity under physiological and pathophysiological conditions.

Received 9th March 2023,
Accepted 8th August 2023

DOI: 10.1039/d3mo00050h

rsc.li/molomics

1. Introduction

The pancreatic β-cells are the prominent cell type within islets of Langerhans that release insulin, the only hypoglycemic hormone of the body.[1] The number and function of these cells are critical for maintaining blood glucose, as the reduction in their number and function can lead to relative or absolute insulin deficiency and ultimately thereby to diabetes, one of the deadliest diseases worldwide. β-cell population is heterogenous including four distinct subtypes.[2] These subtypes are classified according to the mRNA and protein levels of ST8SIA1 and CD9 genes,[3] INS, GLUT2, GCK,[2] cell adhesion markers,[2,4] and the cells' position within the islets (peripheral *vs.* central).[2] It has been observed that the β-cell subtypes that express the lowest level of ST8SIA1 represent approximately 80% of the cell population.[3] These cells that do express very low level of CD9 are referred as β1-cells, whereas β2-cells harbor abundant CD9.[3] The remaining cells express high levels of ST8SIA1 together with either low (β3) or high expression of CD9 (β4).[3] Glucose competence of β3 and β4-cells is lower than this of β1 and β2-cells.[3] It has been shown that the β3/β4 subpopulation is increased in diabetes, possibly contributing to the drop of

[a] *Biomechanics and Bioengineering UMR 7338, Université de technologie de Compiègne, CNRS, Centre de Recherche Royallieu CS 60319, Compiègne, 60203 Cedex, France*
[b] *Department of Chemical System Engineering, Graduate School of Engineering, University of Tokyo, 7-3-1, Hongo, Bunkyo-ku, Tokyo, 113-8656, Japan*
[c] *Institute of Industrial Science, University of Tokyo, 4-6-1 Komaba; Meguro-ku, Tokyo, 153-8505, Japan*
[d] *Univ. Lille, CNRS, Centrale Lille, Univ. Polytechnique Hauts-de-France, UMR 8520, IEMN, F-59000 Lille, France*
[e] *Laboratory for Integrated Micro Mechatronic Systems, CNRS/IIS IRL 2820, Institute of Industrial Science, University of Tokyo, 4-6-1 Komaba; Meguro-ku, Tokyo, 153-8505, Japan*

† Electronic supplementary information (ESI) available. See DOI: https://doi.org/10.1039/d3mo00050h

‡ Authors with similar contribution.

insulin secretion in diabetes.[3] Beside of the four β-cell types, other possible β-cells expressing other hormones exist as exemplified by the detection of bi-hormonal cells expressing INS and Glucagon (GCG)[5] or Somatostatin (SST)[6] under some circumstances.

The discovery of these new β-cell subtypes and bi-hormonal cells very likely involved in diabetes is now challenging the field in diabetes research. With the lack of available human islets, the number of the cell models available for investigating their physiology and development under normal and diabetes condition is very limited. Therefore, it is required to develop cell models representing these new β-cell subtypes. Toward this objective, human induced pluripotent stem cells (hiPSCs) are very promising for mimicking β-cell plasticity and heterogeneity. In fact, pancreas *in vitro* lineage can be differentiated from hiPSCs into pancreatic β-like cells.[7–11] Although, the maturation and the functionality, similar to those of the primary human β-cells, is still challenging, the hiPSCs sources would provide great insight for investigating the pathogenic mechanisms of pancreas diseases[12,13] and for contributing to cell therapies and drug development.[9,14,15]

In our previous work, we have proposed a protocol to generate C-peptide and insulin secreting β-like cells in spheroids derived from hiPSCs.[16,17] We noticed that our spheroids contained also cells positive to glucagon. A bulk transcriptomic investigation revealed that the spheroids co-expressed mRNA related to several hormones' activities (such as IAPP, INS, INHBB, GCG,[17] and SST[16]) when compared to the control of undifferentiated cells. Those results illustrated a potential cell heterogeneity. The cells also over expressed several genes of the lipids' metabolism (LDLR, SCD, HMGCR, HMGCS1) and various specific transcription factors (HIC2, WRNIP1, SOX8, FOX genes[17]). In order to clarify the composition of our pancreatic model, we proposed in this work an additional investigation consisting of single cell sequencing analysis to extract the β-cell subpopulations.

2. Materials and methods

2.1 Pancreas iPSC protocol

The human pancreatic tissues were based on our previous differentiation protocol from iPSCs[16] (Fig. S1 in Supp. File S1, ESI†). In this protocol, the Cellartis hiPSCs derived β-cells were provided by Takara Bio (Japan). Cellartis hiPSC beta cells were differentiated from ChiPSC12 lines and provided in stage 1 of maturation by the manufacturer.[16] The hiPSCs derived β-cells were differentiated using the hiPSCs β-cell media kit (cat. No. Y10108, Takara Bio, Japan). We created spheroids using the PDMS-based honeycombs microwell technology.[18,19] The array of honeycombs, with a 126 μm diameter, are located at the bottom of a 24-well plate format. The honeycombs were precoated with Pluronic F-127-coated (0.01 g ml^{-1}, Wako). After washing with PBS, the cells were inoculated at a density of 6×10^5 cells per well (corresponding to 3×10^5 cells per cm^2). The culture medium changed was performed following the cell supplier (Takara Bio, Japan). The set of experiments was performed three times leading to 12 independent honeycombs well cultures.

2.2 Biological assays

We measured the level of production of insulin *via* a glucose-stimulated insulin secretion. For that purpose, at the end of the experiments, we first washed 3 times the cells using a low glucose concentration medium (DMEM, 0 mM, Gibco) and exposed them to the low glucose medium (DMEM, 0 mM, Gibco) for 1 h. Then, we exposed the cells to high glucose medium stimulation (DMEM, 25 mM, Gibco) for 2 h 20 min. Finally, the cells were washed 3 times and exposed once more to the low glucose concentration medium (DMEM, 0 mM, Gibco) for 1 h 50 min. The culture medium were sampled and frozen until measurement. The insulin quantification was performed using ELISA assays (human insulin ELISA kit, 10-1113-01, Mercodia), following the manufacturer's protocol.

2.3 Single cell RNA sequencing

The spheroids from several PDMS-bottom 24-well plate were collected by pipetting and dissociated into single cells by Accumax (Inovative Cell technologies, USA) treatment. After being washed 3 times in total DMEM media containing 10% FBS, cells were filtrated with a 40 μm strainer and then resuspended in an appropriate volume of PBS (Mg/Ca-free) containing 0.04% BSA. We recovered prior analysis $4 \pm 0.3 \times 10^6$ cells. Approximately 8000 cells, with 75% cell survival rate, were used for GEM (Gel Bead in emulsion) generation using Chromium Controller (10× Genomics), where RNA molecules contained in each cell are tagged by specific barcode/UMI combinations. The molecular-tagged RNAs were converted into double-stranded cDNA followed by library preparation for next generation sequencing using the Chromium Next GEM Single Cell 3′ Reagent Kit v3.1 (10× Genomics). The resulting libraries were quantified by Qubit dsDNA Assay (ThermoFisher Scientific) and TapeStation D1000 (Agilent). The libraries were sequenced on an Illumina HiSeq platform with the following configuration: read 1 : 28 cycles, read 2 : 91 cycles and i7 index: 8 cycles, yielding approximately 400 M paired-end reads per sample. Image analysis and base calling were conducted by Illumina software on the HiSeq instrument.

Raw FASTQ reads were imported into a Cell Ranger pipeline for mapping and gene expression count analyses (10× Genomics, Cell Ranger version 6.1.2; include introns: false, chemistry: single cell 3′ v3; transcriptome GRCH38-3.0.0). Additional details are given in Supp. File S2 (ESI†). The single cell gene expression study mentioned above were conducted by Azenta Life Sciences (formerly Genewiz), according to the manufactures' instructions. Samples analysis and comparisons were performed using Loupe Browser 6.0.0 (10× Genomics, statistics methods are given in Supp. File S2, ESI†) applying a features per barcode filtration threshold set to 9000 to remove potential multiplets. The percentage of UMIs assigned to mitochondrial RNAs were limited to 20% per barcode to remove cells with high mitochondrial gene expression levels from the analysis.

Gene expression tables for each cell cluster of interest were exported from Loupe Browser and then processed with ShinyGO (**https://bioinformatics.sdstate.edu/go/**) for subsequent pathway analysis (the enrichment analysis is calculated based on hypergeometric distribution followed by false discovery rate, FDR, correction.[20] The FDR was set at 0.05 in our study) and by iDEP96 (**https://bioinformatics.sdstate.edu/idep96/**) for hierarchical clustering and gene representation.[21] Sequencing data supporting the findings presented in this study were deposited at Zenodo (**https://zenodo.org**) with the following Digital Object Identifier: **https://doi.org/10.5281/zenodo.7960673**. All supplementary table data files and supplementary figures prepared for this study are available in ESI† supplementary files provided to the journal.

3. Results

3.1 Morphology and basal functional analysis

We presented the spheroids' morphologies 24 h after seeding (Fig. 1A) and at the end of the culture (16 days, Fig. 1B). The cell suspension aggregated into spheroids within the first 24 h of culture. The spheroids were formed inside the honeycomb and their size was controlled by the microgeometry. They grow up to reach the border of the honeycomb. This led to spheroids with a controlled size driven by the honeycomb geometry of about 130 μm in diameter. The spheroids remained at the bottom of the honeycomb during the cultures and inside the honeycomb. We did not observe particular overgrowth above or outside of the honeycombs. We did not detect differences on the spheroids' morphologies when we compared the honeycombs from the different dishes and experimental campaigns. We also confirmed that the insulin secretion by glucose stimulation was functional as show in Fig. 1C. The results demonstrated a 3.3 ± 1.2 induction in high glucose conditions (n = 3 honeycombs, p_value < 0.05).

3.2 Single-cell sequencing results confirmed the pancreatic differentiation

A knowledge-based data analysis using the pancreatic lineage hallmarks allowed to extract the specific endocrine differentiation patterns. We confirmed the successful differentiation by checking that the cell population largely did not express pluripotent markers (NANOG, POU5F1, Fig. 2A and B) neither mesoderm nor definitive endoderm markers (such as FGF4, SOX17, Fig. 2C and D). The pancreatic progenitor markers NEUROG3, PAX4, NKX6-1, NKX2-2 were expressed in 20%, 13%, 35% and 60% of the populations respectively (Fig. 2E–H). We also confirmed that the cell population expressed the endocrine specification markers (NEUROD1 is expressed in 65% of the population, MAFB is expressed in 73% of the population, Fig. 2I and J). However, the most advanced β-cells markers, such as MAFA, UCN3, were weakly expressed (only in 2% and 11% of the population respectively) illustrating partial β-cells maturation (Fig. 2K and L). Nevertheless, the predominance of the β-cells lineage was illustrated by the overall levels of INS that was expressed in 100% of the sequenced population (Fig. 2M).

3.3 Knowledge based analysis confirmed the presence of seven typical β-cells subtypes

3.3.1 Identification of the typical β-like cells subpopulation based on literature markers. By addressing the knowledge on specific pancreatic markers, we extracted, from the insulin positive cells, seven β-cells subtypes representing 32% of the overall cells' population based on literature data and markers. The plume plots of mRNA levels of the markers used to

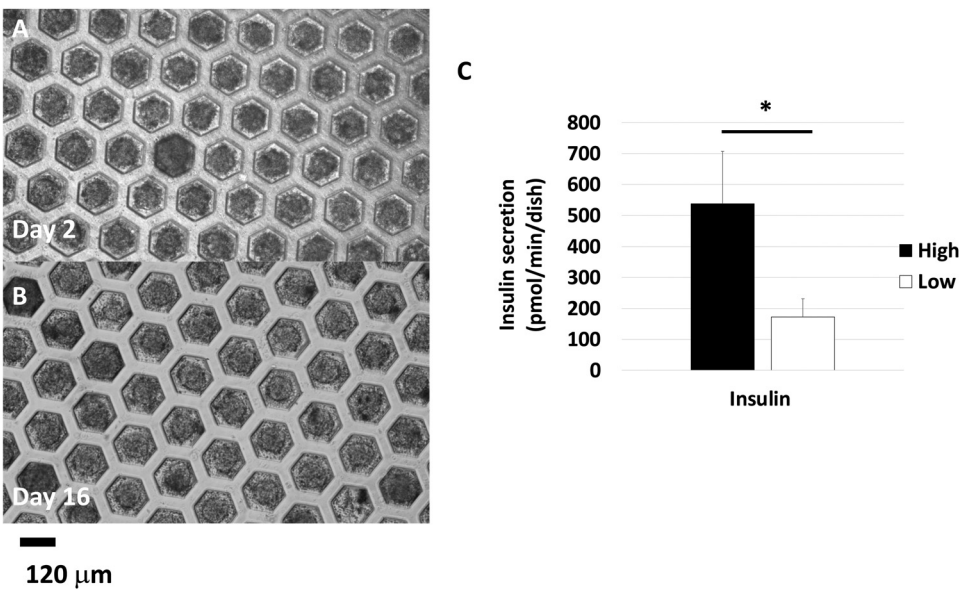

Fig. 1 (A) Morphologies of the spheroids after 24 h of culture; (B) morphologies of the spheroids at the end of the culture (day 16); (C) insulin secretion in glucose stimulation assays: ratio of insulin between low and high glucose (n = 3 honeycombs, p_value < 0.05).

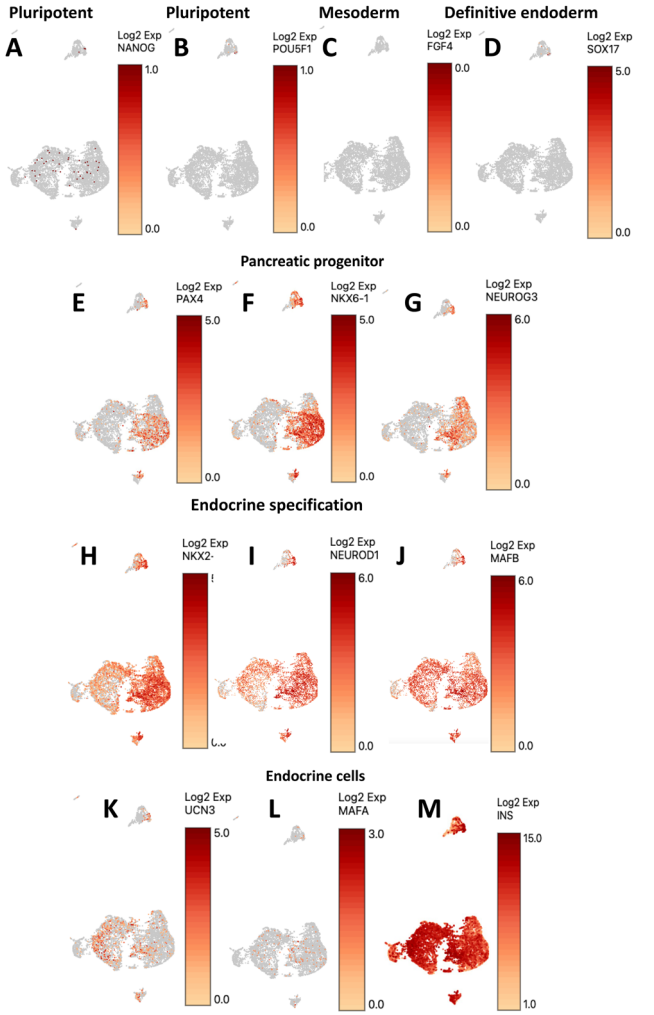

Fig. 2 mRNA expression levels of selected genes based on UMAP low-dimensional space visualization of the sequenced cell populations and illustrating the levels of maturation of the pancreatic spheroids: (A) and (B) pluripotent, (C) mesoderm, (D) definitive endoderm, (E)–(H) pancreatic progenitor; (I) and (J) endocrine specification, (K) and (L) advanced β-cells, (M) insulin markers.

discriminate the populations: GCG, SST, PPY, CD9, ST8SIA1, GHRL and UCN3 (INS), compared to the overall population, is presented in Fig. 3A (Supp. File S3, ESI†). The heatmap of the top 10 discriminating genes is presented in Fig. 3B. The INS+/UCN3+ population showed the highest level of INS and UCN3 (mature β-like cells), 11% of the overall population, upregulating also INS-IGF2 (as reported in the literature[22]). This population was CD9− and ST8SIA1− (representing potentially a β1-cells like subtype[3]). The top upregulated genes of this population enriched the GO_biological processes related to regulation of peptide hormone secretion, neuropeptide pathway, and hormone secretion (Fig. 4A). We also identified an INS+/ST8SIA1+/CD9− population (β3-like cells subpopulation,[3] 3%). This population expressed cell cycle genes (CDK1, CCNB1, CCNB2) and REST. The top upregulated gene of this population enriched the GO_biological processes related to digestive development and extra cellular matrix organization (Fig. 4B). Then, we detected the INS+/CD9+/ST8SIA1− population (β2-like-cell subpopulation,[3] 1%, this population also overexpressed SLC2A5). However, the specificity of the INS+/ST8SIA1+/CD9− cells were very low as far as this population was characterized by only 8 genes differentially expressed (Supp. File S3, ESI†). Using this knowledge-based analysis, we did not extract significant INS+/CD9+/ST8SIA1+ (β4-cells subpopulation, *nb: in fact, there is just one cell in our dataset with this feature*). The specific stratification of the INS+/CD9−/ST8SIA1− (β1-cells), INS+/CD9+/ST8SIA1− (β2-cells) and INS+/CD9−/ST8SIA1+ (β3-cells) populations is given in Fig. 3C (additional stratifications are given in Fig. S2 in Supp. File S1, ESI†).

The other β-cells subtypes selectively co-expressed high levels of INS+/ARX+/GCG+ (β-α-like cells, 6%), INS+/SST+ (β-δ-like cells, 6%, population with also high level of HHEX, ISL1, LEPR, ETV1 consistently with literature[22,23]), INS+/PPY+ (β-γ-like cells, 3%, population with also high level of IAPP, TPH2 and PYY) and INS+/GHRL+ (β-ε-like cells, 2%), illustrating the large pancreatic heterogeneity and the β-cells plasticity of our spheroids. The top upregulated genes of the INS+/GHRL+ subpopulation highly enriched the cholesterol and lipid biological processes (Fig. 4C); the top genes of INS+/SST+ cells enriched nervous system development related biological processes (Fig. 4D); the top genes of INS+/PPY+ cells enriched the angiotensin related processes, the peptide hormone processing, the feeding behavior, endocrine process, and the several inflammation related processes (Fig. 4E); finally the INS+/ARX+/GCG+ upregulated genes enriched the histamine response and heparan sulfate synthesis, the cell mobility and cell migration processes (Fig. 4F).

3.4 Data driven analysis revealed the heterogeneity and new types of β-like cell subpopulations in our spheroids

Then, to identify new potential cell subpopulations, we performed a data driven analysis on our dataset. The analysis contributed to extract 10 typical cell subpopulations (Fig. 5A, Supp. File S4, ESI†). Using a selected list of pancreatic genes including mature, immature, and functional markers (Supp. File S4, ESI†), we observed that the 10 cell subpopulations were classified under three distinct branches according to the hierarchical clustering presented on the heatmap of gene expression shown in Fig. 5B (a second heatmap showing the expression levels of the top 10 genes in each cluster is given in Supp. Fig. S3 in Supp. File S1, ESI†).

3.4.1 A first branch grouped the most mature like β-cells subtypes. The first branch regrouped three cell subpopulations. Among them, we distinguished a subpopulation characterized by the highest level of PPY, IAPP, CGA, NTS genes (PPY+/IAPP+ in Fig. 5A, 9% of the overall population). This subpopulation also co-expressed high levels of GLP1R, GCGR, WNT4 concomitant with low FZD6, INSR. The top 200 genes expressed by this subpopulation enriched the neuropeptide molecular functions and various neuro/synaptic biological functions (Fig. 6A, KEGG enrichment is given in Fig. S4 in Supp. File S1, ESI†).

The second population of this branch was characterized by the high expressions of DPP4, KDR, SPON1, PDK4, CTNND2

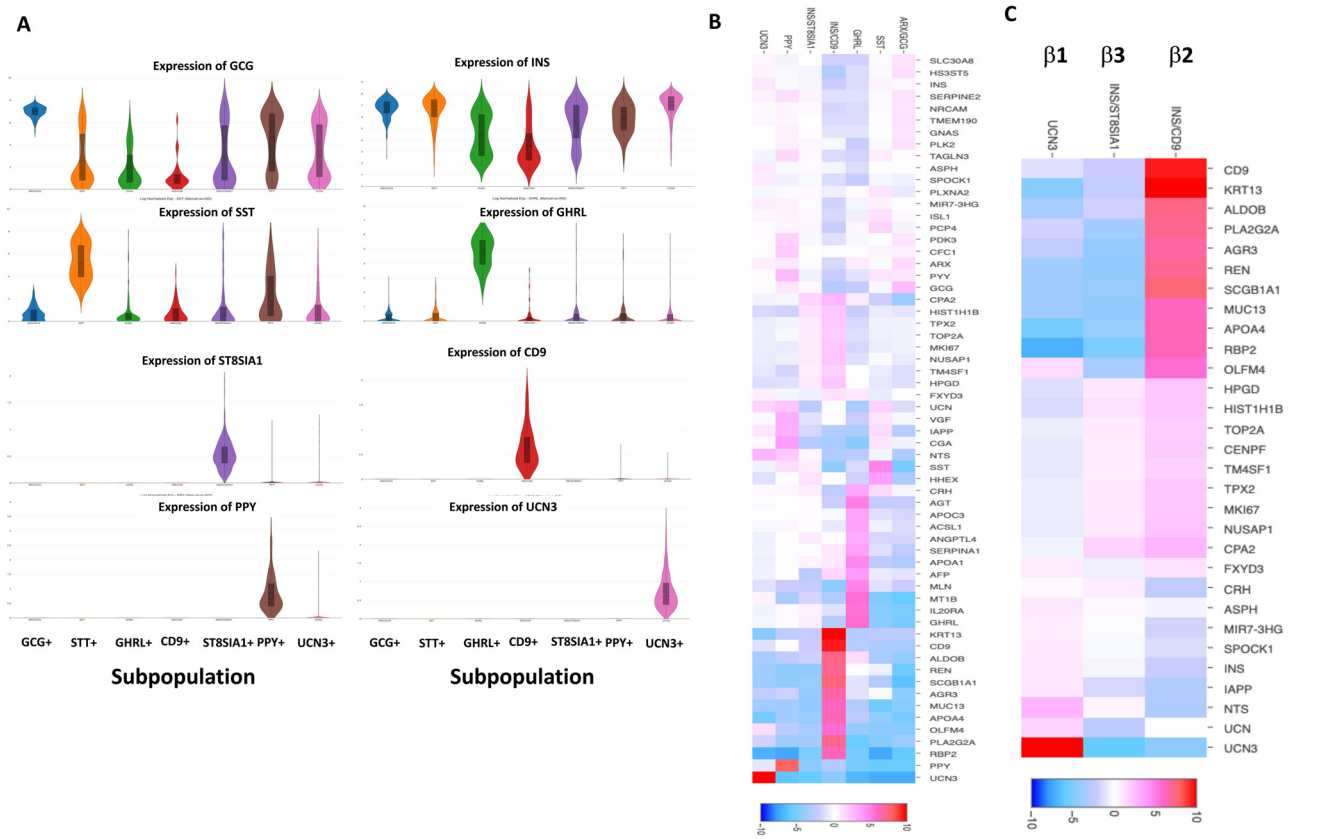

Fig. 3 (A) Plume plots of selected genes used to sort and extract main β-like cells subpopulations: GCG+, SST+, PPY+, CD9+, ST8SIA1+, PPY+, GHRL+ and UCN3+ (INS+); (B) heatmap of expression of the top 10 genes representative of each subpopulation; (C) heatmap of expression of specific genes involved in the stratification of the INS+/CD9−/ST8SIA1− (β1-like-cells), INS+/CD9+/ST8SIA1− (β2-like-cells) and INS+/CD9−/ST8SIA1+ (β3-like-cells) subpopulations.

genes while co-expressing INS, SST and GCG (DPP4+/KDR+ in Fig. 5A; 18%). The top 200 highly expressed genes enriched the reactome pathways related to sodium/calcium exchangers, the synthesis secretion and inactivation (i) of glucose dependent insulinotropic polypeptide, (ii) of incretin, (iii) and GLP1 (Fig. 6B, KEGG enrichment is given in Fig. S5 in Supp. File S1, ESI†).

The third subpopulation was characterized by increased levels of TTR, SST, GCG, UCN, CRH and APOA1 genes expressions (TTR/GCG/SST in Fig. 5A; 14%) It also expressed low levels of ST8SIA1 and CD9 genes. The top 200 genes in this subpopulation enriched the biological processes related to hormones transport, lipid transport, ions and cations homeostasis (Fig. 6C), the reactome of incretin, ghrelin, peptide hormones, fatty acids, and insulin-like growth factors (Fig. 6D). KEGG enrichment is given in Fig. S6 in Supp. File S1 (ESI†).

Those three populations superimposed with most of the cells of the INS+/ARX+/GCG+, INS+/SST+ and INS+/PPY+ subtypes described in Section 3.3.

3.4.2 Identification of three type of cycling cells among the β-cells. The second branch of the heatmap of Fig. 5B grouped three subpopulations of cells highly expressing cell cycle markers such as CDK1, CCNA2, CCNB1, CCNB2.

The "pure cycling" population expressed the highest levels of CDK1, CCNA2, CCNB1, CCNB2 and LDHA (Cycling cells in Fig. 5A) and represented 3% of the overall population. As those cells also presented low level of CD9 and moderate expression of ST8SIA1, it could reflect a proliferative portion of a β3-like cells following one classification of the literature[3] (*nb: this population may reflect a potential source of β3 like-proliferative cells observed in T2DM*[3]). The top genes hallmark the mitotic, microtubule organization as top biological processes (Fig. S7 in Supp. File S1, ESI†).

The second subpopulation of this branch was characterized by the high levels of SLC2A2, SCL2A4, GCGR, GCKR and low INSR (6%). Interestingly, this subpopulation also co-expressed ST8SIA1 while moderately expressing the PPY, SST, and GCG genes and with a low level of INS (SLC2A4+/GCKR+ in Fig. 5A). Nevertheless, this population reflected a very poor specificity when compared to other 9 populations (Supp File S4, ESI†) and no significant enrichment could be detected.

Then, we distinguished in this branch a particular subpopulation expressing immature markers such as REST, PDGFRA, ESRRB, LAMA1, SOX9, SLC2A1 and SPARC genes, but also the highest levels of CD9 (CD9+/SPARC+/REST+ in Fig. 5A, 8%). Furthermore, this population presented low level of ST8SIA1. As such it appeared to include a part of the β2-like-cells described

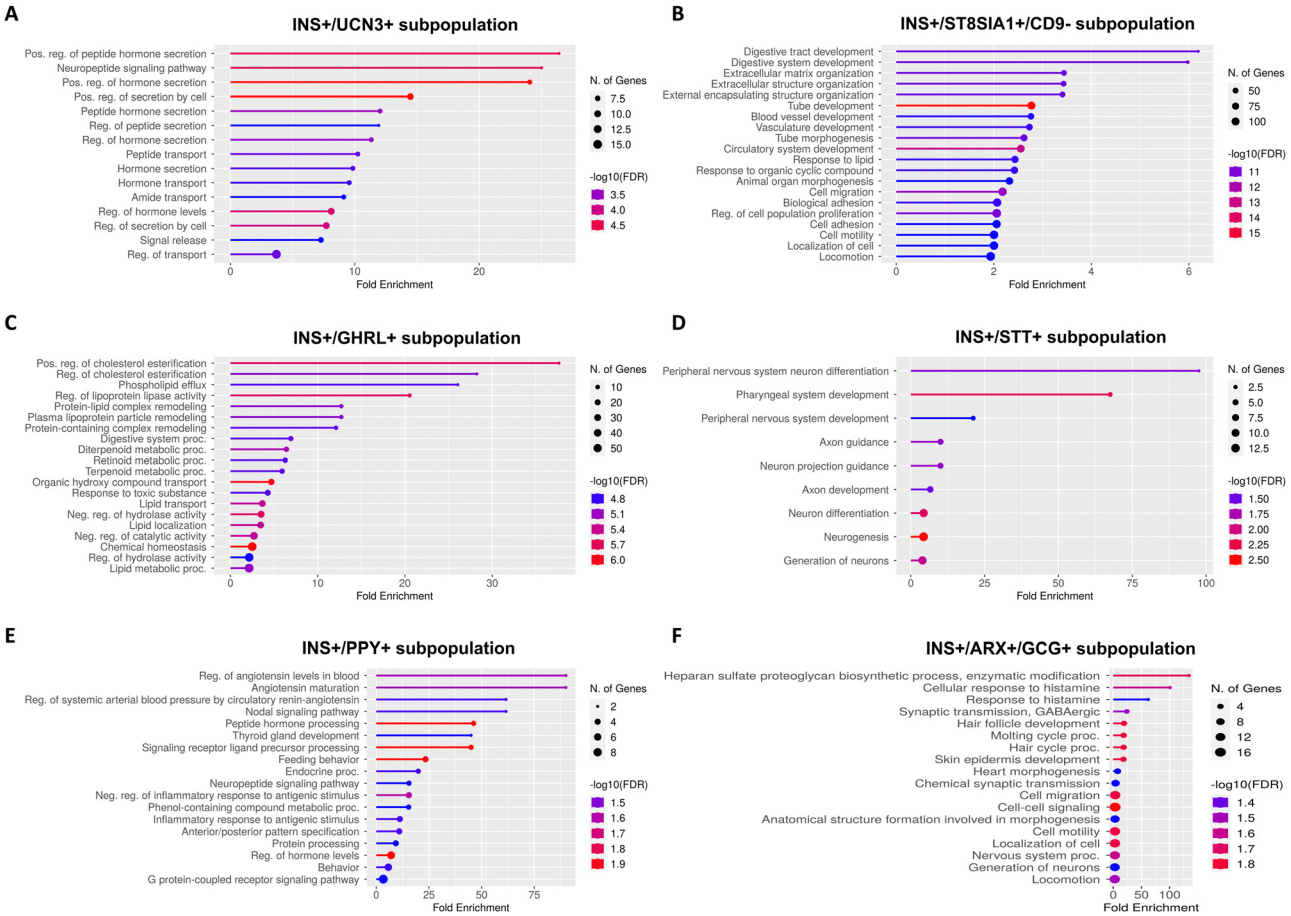

Fig. 4 Enriched GO_biological processes extracted from ShinyGO and highlighted from top expressed genes in (A) INS+/UCN3+ subpopulation, (B) in INS+/ST8SIA1+/CD9− subpopulation, (C) in INS+/GHRL+ subpopulation, (D) in INS+/STT+ subpopulation (E) in INS+/PPY+ subpopulation, (F) in INS+/ARX+/GCG+ subpopulation.

in Section 3.3. This subtype expressed various genes involved in TGF-β and NOTCH signaling pathways. This population also expressed the lowest levels of INS gene and of pancreatic mature markers such as MAFB, NEUROD1 and NEUROG3 genes when compared to other populations. The top 200 genes enriched extracellular matrix biological process, mesenchyme development, the tube and blood vessel formation (Fig. S8A and B in Supp. File S1; KEGG enrichment is given in Fig. S9 in Supp. File S1, ESI†).

Then, we refined the analysis of this CD9+/SPARC+/REST+ subpopulation. We re-clustered those CD9+/SPARC+/REST+ cells, and we extracted four typical subtypes, Fig. 7A (Supp. File S5, ESI†). More particularly, we found a CD9+/BMP4+/SPARC+ positive subpopulation (1% of the overall population and representing about 16% of cells within the CD9+/SPARC+/REST+ cells) expressing the highest levels of TGF-β and NOTCH genes (such as BMP4, SMAD3, TGFB2, and NOTCH3) but also a large panel of ECM genes including LUM, COL6A3, EGFLAM, COL3A1, endothelial membrane markers (VWF, PECAM1) and HGF. The top 200 genes expressed in this subpopulation highlighted the reactome pathways of carbohydrates sulfotransferase (CHST3, CHST4), MET receptor, collagen process and NCAM-1 interactions as well as the biological processes related to the mesenchymal development (Fig. 7B). A second subpopulation co-expressed GHRL+/UCN3+/INS+/SST+, and was positive to KRT20, ISL1, ACSL1, ARX, PAX6, PAX4, FFAR3, ARX, NEUROG3, NKX6-1, NKX2-2 (2% of the overall population and representing about 28% of cells within the CD9+/SPARC+/REST+ cells). The top 200 genes enriched the reactome related to NEUROG3 progenitor, Ghrelin synthesis, serotonin and melatonin biosynthesis and of free fatty acids receptors (Fig. 7C). Altogether, the data converge toward a common root of the endocrine progenitor population expressing typical α,β,γ,δ,ε-like cells marker genes in this subpopulation. This population represented about 2% of the overall population. The third one (2% of the overall population and representing about 28% of cells within the CD9+/SPARC+/REST+ cells) was positive to SOX3, NOG and CTGF (involved in connective tissue in pancreas development), various ECM markers (COL2A1, FN1), cell cycle genes (CDK1, CCNB1, CCNB2, CCNE2) but also REST. The top upregulated genes enriched cell cycle processes (Fig. 7D). Finally, the last one (2% of the overall population and representing about 28% of cells within the CD9+/SPARC+/REST+ cells) not only expressed CDLN4, CDLN6, SCL2A2, IGF2,

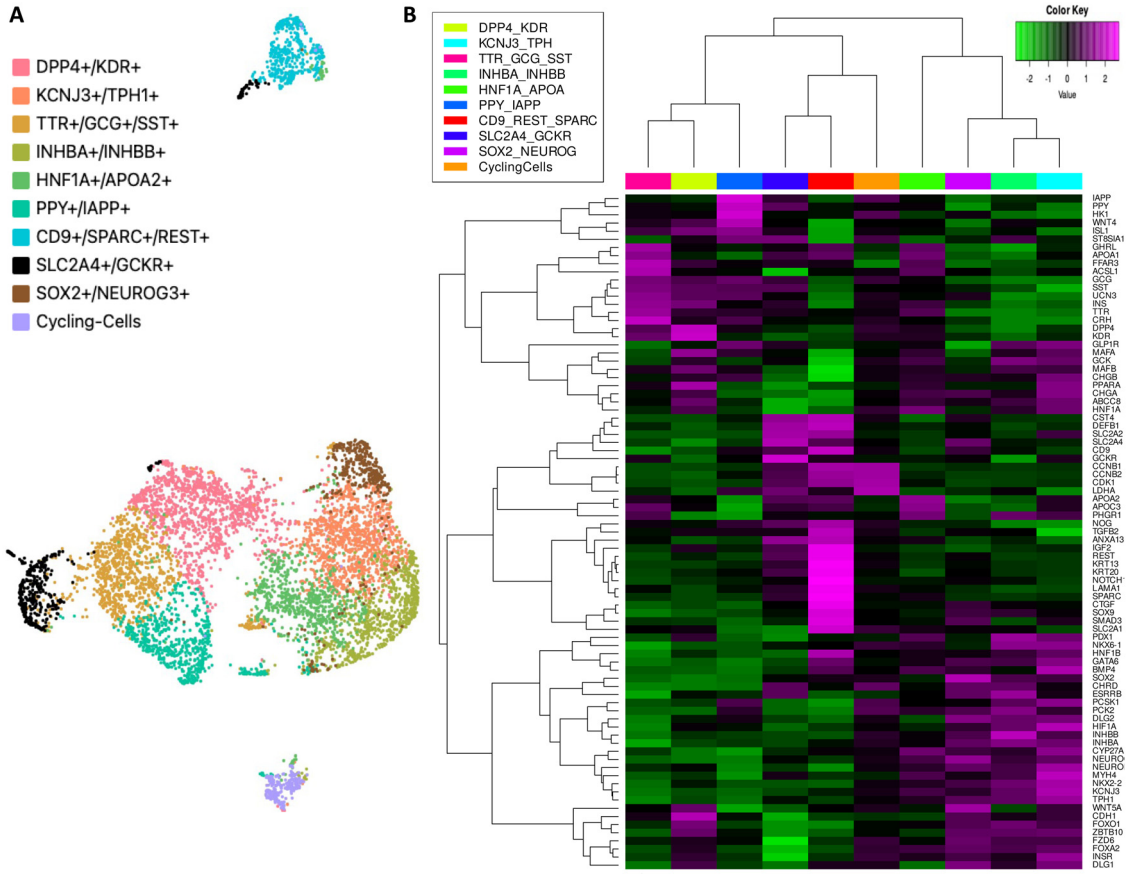

Fig. 5 (A) UMAP plot presenting the 10 cell subpopulations identified by *K*-means clustering; (B) heatmap of expression for selected genes specific of each subpopulation.

and more particularly the genes GP2, LYZ, ANXA4, SPINK1 and SDC4 that are typical pancreatic acinar markers,[24,25] but also the CST4 and SLC4A4 and SPP1 genes (that are pancreas ductal markers[25–27]). This subpopulation was also characterized by low expression levels of INS, GCG, TTR, SQLE and SCD when compared to other four populations. The top upregulated genes of this fourth subpopulation enriched bicarbonate transport, excretion/secretion biological processes (Fig. 7E; *nb:* pancreas ductal cells control bicarbonate secretion[28])

3.4.2.1 Identification of four endocrine progenitors of β-cells subtypes. Finally, the third clustering branch extracted from the heatmap presented in Fig. 5B grouped the four populations co-expressing the typical pancreatic transcription factors representative of immature endocrine cells such as NEUROG3, NKX6-1, PAX4 (endocrine progenitor markers), and NEUROD1, NKX2-2 (more advanced endocrine maturation) but a moderate level of INS.

Among those four subpopulations, one population co-expressed more specifically the SOX2, NEUROG3, CFAP126, MAPK10 genes, reflecting an on-going differentiation, in parallel to the low levels of GLP1R and GCGR (6%, SOX2+/NEUROG3+). The top 200 genes expressed in this population enriched the endocrine system development and MAPK cascade (Fig. 8A; KEGG enrichment is given in Fig. S10 in Supp. File S1, ESI†).

A second subpopulation presented an upregulation of various liver like markers such as HNF1A, FOXA2, APOA1, APOA2, AFP, ALB, NR1H4 and CYP27A1 when compared to other populations (10%, HNF1A+/APOA2+). Most of the GRHL+ cells presented in Section 3.3 were associated with this subpopulation. Consistently, the hallmark of this HNF1A+/APOA2+ population enriched the lipids, sterol, cholesterol metabolic pathways (Fig. 8B; KEGG enrichment is given in Fig. S11 in Supp. File S1, ESI†).

Finally, the two last subpopulations displayed very closed signatures, as far as both expressed INHBA, INHBB, PDX1, MAPK10, MAPK12, NKX6-1, NKX2-2, GCK, GLP1R. Firstly, the labeled INHBA+/INHBB+ expressed more largely those markers (11% of the over cell population). The top 200 genes of this population enriched amylin, calcitonin receptors activities, and hormones activity (Fig. 8C). The biological processes were related to Mast cells degranulation, leucocytes and immune response, or angiogenesis (Fig. 8D; *nb*: the top genes did not contribute to extract significant KEGG pathway enrichment). Secondly, the KCNJ3+/MYH4+ subpopulation (16%) was showing high levels of glycolytic genes (HIF1A, GCK, PCK2, SLC2A2, GLP1R, INSR, PPARA), potassium ion channels (KCNJ3) and serotonin biosynthesis (TPH1). The 200 top expressed genes were related to ions and cations transports (Fig. 8E; KEGG enrichment is given in Fig. S12 in Supp. File S1, ESI†).

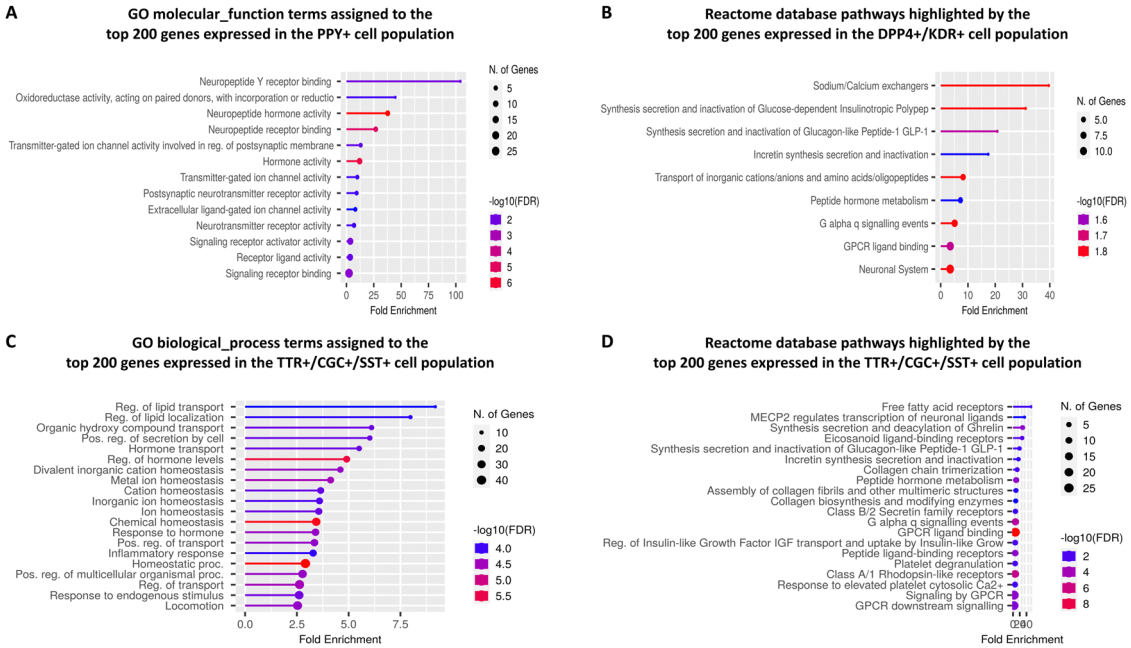

Fig. 6 (A) Enriched GO biological processes characterized by top expressed genes in the PPY+/IAPP+ cell subpopulation; (B) enriched reactome pathways identified in the DPP4+/KDR+ cell subpopulation; (C) enriched GO biological processes characterized by top expressed genes in the TTR+/GCG+/SST+ cell subpopulation; (D) enriched reactome pathways identified in the TTR+/GCG+/SST+ cell subpopulation. Data are extracted from ShinyGO.

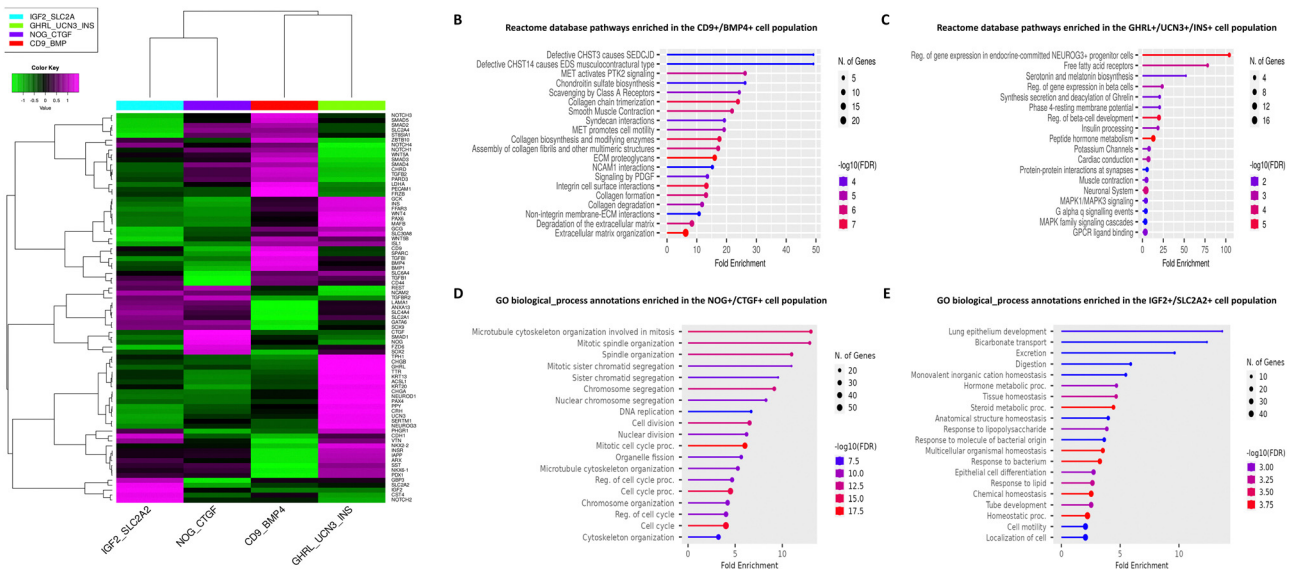

Fig. 7 (A) Heatmap of gene expression levels for selected genes illustrating the expression profiles of the different subtypes of cells identified upon re-clustering of the CD9+/SPARC+/REST+ cell population; enriched pathways identified by the top highly expressed genes in the four subtypes of cells extracted from re-clustering of the CD9+/REST+/SPARC+ population.

4. Discussion

We have performed a characterization of the β-like cell subpopulations derived from induced human pluripotent stem cells in 3D spheroids. The analysis confirmed the endocrine differentiation. We did not achieve a mature β-cells specific tissue as far as we detected immature endocrine like progenitors, endocrine like progenitors and transdifferentiated like β-like cells. Although all cell population expressed INS gene, we observed a graduation of the level of expression of this gene.

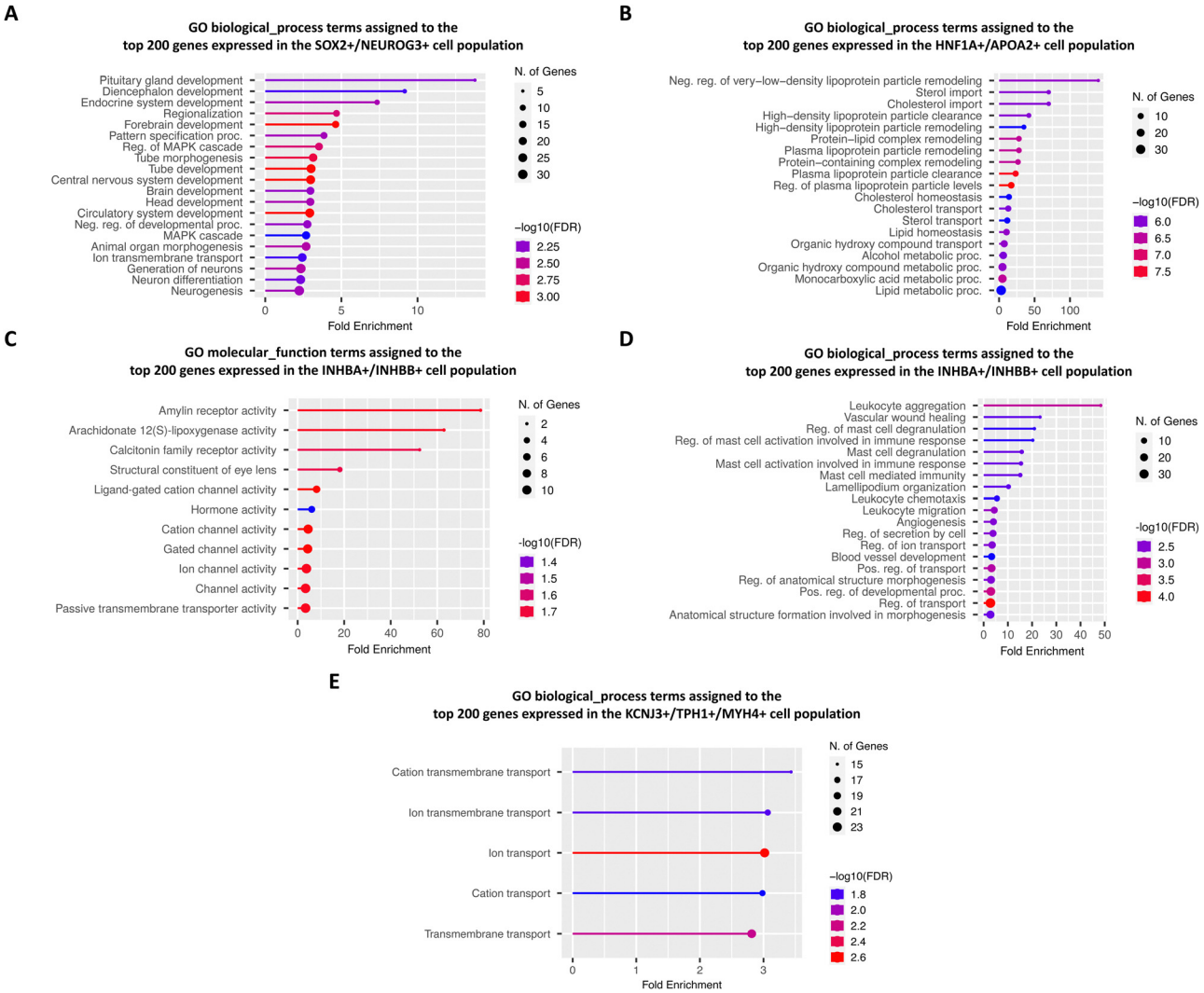

Fig. 8 (A) Enriched GO biological processes identified in the SOX2+/NEUROG3+ cell subpopulation, (B) enriched GO biological processes characterized in the HNF1A+/APOA2+ cell subpopulation, (C) enriched GO molecular functions found in the INHBA+/INHBB+ cell subpopulation, (D) enriched GO biological processes observed in the INHBA+/INHBB+ cell subpopulation, (E) enriched GO biological processes identified in the KCNJ3+/MYH4+ cell subpopulation. Data are extracted from ShinyGO.

Furthermore, our previous studies revealed that not all the islets expressed the INS protein.[16] Nevertheless, we confirmed the advanced maturation by the GSIS assays illustrating functional spheroids.

There are several classifications of the β-cell subtypes in the literatures, including from primary islets or from hiPSCs derived tissues.[29,30] In our study, we detected three types of β-like cells, the INS+/UNC3+/ST8SIA−/CD9−, INS+/CD9+/ST8SIA1−, INS+/ST8SIA1+/CD9−, consistently with the β1, β2, β3 cells classification.[3] We did not find a β4-like cells (INS+/ST8SIA1+/CD9+ subpopulation) conversely to literature.[3,31] Dorell *et al.*, noticed that the proportion of ST8SIA1 cells (β3 and β4 cells) can differ from donors and from healthy to disease patients.[3] They are also less responsive to glucose. Our protocol may also lead to promote a preferential differentiation route which reduced the occurrence of β4 cells. Furthermore, in our analysis, the INS+/ST8SIA1+ cells present a poor transcriptomic specificity as far as they overexpressed only 5 genes (ASB5, CSMD3, CXCL5, DUSP2) and weakly expressed UCN3 when we compared them to other β-like cells subtypes. As the literature displayed more complex ST8SIA1+ profile with its expression in up to 20% of β-cells profile in human primary islets,[31] our results illustrate that our spheroids still not reflect a complete adult pancreatic profile.

Then, the pancreatic markers including somatostatin, ghrelin and pancreatic polypeptide genes were largely expressed in our cells. The graduation of the levels of expression of those pancreatic markers led to extract a large heterogenic cell population. The panel of bi-hormonal profile was previously detected in hiPSCs *in vitro* β-cells differentiation.[29] In addition, several poly-hormonal cells in human islets were classified based on their expression of calcium regulated genes.[32] Interestingly, our data-driven identified TTR+/GCG+/STT+ cells subpopulation have shown that the top genes enriched the calcium signalling pathway (Fig. S6 in Supp. File S1, ESI†). In parallel,

the observation of transdifferentiation of β-cells in other hormones secreting cells is largely observed in the literature.[33–36] We confirmed the presence in our spheroids of a β-like cells (high INS+/UCN3+ 11%), β-δ-like cells (INS+/SST+, 6%), β-γ-like cells (INS+/PPY+, 3%), β-α-cells (INS+/GCG+, 6%) β-ε-like cells (INS+/GHRL+, 2%). The β-cells plasticity is now largely accepted and is illustrated by their capability to dedifferentiate. The dedifferentiation is observed under various metabolic stimulations (such as hyperglycemia) and inflammation process (through cytokines for instance) leading to reactive oxygen species accumulation which in turn conduct to β-cells dysfunction.[1] Dedifferentiation often results either to the conversion from mature phenotype to endocrine progenitors' phenotypes, or to cell apoptosis. The consequences are the β-cells dysfunction and the progression of pathology in the pancreas. Dedifferentiation is largely observed in diabetic patients.[37] The plasticity of the β-cells is also illustrated by their ability to trans-differentiate to other hormones secreting cells.[33–36] It is suspected that this process occurred naturally with aging patients, diabetic patients. *In vitro*, the transdifferentiation was observed in insulin positive cells changing for glucagon positive cells under free serum cultures.[1,35]

In addition to bi-hormonal' profiles and multi-lineage like subtypes, several types of mature like cells (α- and β-like cells), of progenitors (NKX6.1+; PDX1+), and several rare cell subtypes (including ONECUT3+; SST+/HHEX+ cells similar to our INS+/SST+ subpopulation) were reported from *in vitro* hiPSC derived tissues.[29] Our data-driven analysis also revealed several types of advanced pancreatic profiles and progenitors. We found an advanced endocrine profile with 18% of the cells co-expressing INS and GCG and highly co-expressing KDR and DPP4. KDR (VEGFR2) is an endothelial marker found during islet vascularization.[38,39] DPP4 is also involved in GLP1 response and glucose homeostasis.[40] DPP4 is expressed in human pancreatic islets and in both beta cells and alpha cells.[41] Proportion of DPP4 of α and β-cells is reduced in type 2 diabetes. Furthermore, its inhibition improves β-cells function and survival in type 2 diabetes[41] which is consistent with lower expression of this marker in our most advanced endocrine profiles extracted by the data-driven analysis (PPY/IAPP and TTR/SST/GCG profiles in Fig. 5).

Then, we identified four typical endocrine progenitors' populations. Among them, the first one expressed SOX2+/NEUROG3+ that are typical endocrine progenitor markers.[42] NEUROG3+ positive cells were also classified as pancreatic progenitors.[29] Secondly, one population present a liver-like signature with highly expressing HNF1A transcription factor. This result is coherent with the fact that liver and pancreas arise from common multipotent population.[43,44] Furthermore, our results show that this liver-like progenitor population superimposed with the Ghrelin expressing like population (INS+/GHRL+). Interesting, literature report that GHRL stimulates the hepatocyte proliferation[45] and identified it as a key regulator of liver steatosis (*via* the regulation of lipid metabolism[46]).

Then, another progenitors' population was characterized by high levels of INHBA and INHBB (activin A and B ligands). In fact, endocrine differentiation is reported to interact with activins signals.[47] Furthermore, other single cell sequencing identified endocrine maturation *via* INHBA routes from fetal pancreas population in a mesenchymal compartment.[48] Thus, it was predicted that the pancreas endocrine development in humans was dependent on signal input from the mesenchymal niche environment.[48] This population also overexpressed NKX6-3 gene and co-expressed high levels of NKX6-1 and PAX4 genes which are two genes appearing in one progenitor-like population[29] and one rare premature cell population.[29] Then, the target genes of this population enriched the processes related to mast cells. Mast cells are rich in heparan and histamine, that can bridge this population with some of the cells of the INS+/ARX+/GCG+ subtype identified by the knowledge-based analysis in Section 3.3 (as this population also enriched histamine and heparan processes). As INHBA and INHBB are both expressed in normal α-cells, whereas only INHBA is expressed in β-cells,[49] we suspect that INHBA+/INHBB+ is one potential α-cell progenitor source. Finally, we extracted a subpopulation highly expressing TPH1 gene, co-expressing FEV, LMX1A, SCL18A1, with low ISL1 level, which could be consistent with a literature analysis that identified among stem cell-like enterochromaffin cells (TPH1+/FEV+/LMX1A+/SCL18A1+/ISL1−) during β-cell differentiation.[29]

Finally, we identify four INS+/REST+ subpopulations that displayed a potential pancreatic niche profile with an immature progenitor signature prior the endocrine specification. In fact, those cells expressed the lowest level of INS gene in our overall dataset, which is consistent with the role of REST as a repressor of β-cell identity.[50] A first CD9+ subtype co-expressed TGFβ, SPARC, NOTCH3 and ECM genes. The co-expression of SPARC, TGFβ and NOTCH3 genes in this population could reflect a pancreatic-like tumoral population.[51,52] However, the TGF-β signaling is also a key mechanism in β-cell differentiation, in inhibiting the exocrine cell differentiation[53] and repressing pancreatic ductal cell proliferation.[54] TGF-β also promotes p16 cell cycle regulator which controls self-renewal of adult endocrine stem cells[55] (*nb*: which appeared consistent with cell cycle genes expression in this population's heatmap presented on Fig. 5B). This subtype was also characterized by the enrichment of biological process related to the pancreatic mesenchyme. Consistently with our result, several evidence shows that pancreatic mesenchyme is supporting pancreatic epithelial cell growth and differentiation during organogenesis.[56] Furthermore, NOTCH plays an important role in the development of pancreas from immature progenitors.[57] Positive NOTCH blocked endocrine differentiation and led to mesenchymal routes to ductal and acinar cells.[57] More particularly, NOTCH3 is expressed in pancreas mesenchyme.[58] The second subtype of CD9+ cells co-expressed SOX9+/PDX1+/NEUROG3+, the markers of endocrine progenitors such as PAX4 and ARX, the NOTCH1 and NOTCH2 genes. The pancreatic ductal niche is characterized by SOX9+/PDX1+/NEUROG3+ positive cells committed to generate endocrine progenitors. 10% of the pancreatic ductal cells are also reported to produce glucagon and insulin.[59] NOTCH1 and NOTCH2 are the first NOTCH genes

expressed in the pancreatic epithelium development,[58] and need to be repressed for endocrine specification.[57] Therefore, the profile of this subtype is consistent with a profile of a common root of the immature pancreatic progenitor as the one observed in developmental embryology.[57] Our CD9+ like-niche profile was completed by a subpopulation co-expressing CLDN6+ (CLND6 is a tumoral marker;[60] but is also an early marker of the epithelialization during embryogenesis[61]), GP2 (acinar marker,[62] and progenitor pancreatic marker[63]), CST4 and SLC4A4 (pancreas ductal marker) and moderately NOTCH1 and NOTCH2 genes. Finally, the last subtype co-expressed NOTCH1, NOTCH2, NOG (a BMP and TGF-β signaling inhibitor promoting pancreatic development[64]) and CTGF (involved in the pancreatic β-cells replication during embryogenesis[65]) which appeared as another immature progenitor lineage before the endocrine specification.

5. Conclusions

We performed a β-cells like differentiation into pancreas like spheroids. The spheroids were capable to secrete insulin, although 3D differentiation did not lead to fully mature specific pancreatic lineage. We observed an important heterogeneity of the β-like cell populations. The subpopulations included hormone secreting-like cells with α, β, δ, γ, ε profiles. We also extracted four endocrine progenitors' populations. The immature endocrine progenitors were characterized by the expression of CD9. Even if we did not reach fully mature profile, we believe that our model would be a suitable tool to investigate pancreatic development and the pancreatic cells plasticity.

Data availability

Sequencing data supporting the findings presented in this study were deposited at Zenodo (**https://zenodo.org**) with the following Digital Object Identifier: **https://doi.org/10.5281/zenodo.7960673**. All supplementary table data files and supplementary figures prepared for this study are available in the ESI supplementary files provided to the journal.

Author contributions

EL performed the biological experiments, designed the experiments and participated to data analysis and in the writing of the manuscript, LM, FT, VP, VP were involved in biological experiments, AA contributed to the experimental design and participated to the discussion and in the writing of the manuscript, SP and SHK were involved in the sequencing and bioinformatics treatment, processed transcriptomics data and participated in the writing of the manuscript, FT made the honeycomb plates, CL, RJ and YS were involved in the experimental design and LM supervision, EL is the project supervisor, designed the experiments and participated to data analysis and the writing of the manuscript. All authors are involved in the manuscript revision and approval.

Conflicts of interest

The authors declare no conflict of interest.

Acknowledgements

Lisa Morisseau received PhD funding from the French Ministry of Higher Education and Research, mobility grants from CNRS/IIS LIMMS IRL 2820 and from the Université de Technologie de Compiegne. ScRNAseq was funded by the LIMMS internal project 2022 campaign. Stéphane Poulain was supported by the JSPS Grant-in-aid for Scientific Research (S) 16H06328. A part of this work was supported by the JSPS Core-to-Core Program (JPJSCCA20190006) and the Agence Nationale pour la Recherche ANR-22-CE09-0016-01. This work was carried out in the framework of the Research Training Innovation Chair, DOT project – Disruptive Organoids Technologies, an action funded by the Research Direction of the Université de Technologie de Compiègne.

References

1 N. Honzawa and K. Fujimoto, The Plasticity of Pancreatic β-Cells, *Metabolites*, 2021, **11**(4), 218.
2 M. Miranda, J. Macias-Velasco and H. Lawson, Pancreatic β-cell heterogeneity in health and diabetes: classes, sources, and subtypes, *Am. J. Physiol.: Endocrinol. Metab.*, 2021, **320**(4), E716.
3 C. Dorrell, J. Schug, P. S. Canaday, H. A. Russ, B. D. Tarlow, M. T. Grompe, T. Horton, M. Hebrok, P. R. Streeter, K. H. Kaestner and M. Grompe, Human islets contain four distinct subtypes of β cells, *Nat. Commun.*, 2016, **11**(7), 11756.
4 F. Esni, I. B. Täljedal, A. K. Perl, H. Cremer, G. Christofori and H. Semb, Neural cell adhesion molecule (N-CAM) is required for cell type segregation and normal ultrastructure in pancreatic islets, *J. Cell Biol.*, 1999, **144**, 325.
5 H. Chakravarthy, X. Gu, M. Enge, X. Dai, Y. Wang and N. Damond, *et al.*, Converting Adult Pancreatic Islet α Cells into β Cells by Targeting Both Dnmt1 and Arx, *Cell Metab.*, 2017, **25**(3), 622.
6 S. Chera, D. Baronnier, L. Ghila, V. Cigliola, J. N. Jensen and G. Gu, *et al.*, Diabetes recovery by age-dependent conversion of pancreatic δ-cells into insulin producers, *Nature*, 2014, **514**(7523), 503.
7 M. Hosoya, Preparation of pancreatic β-cells from human iPS cells with small molecules, *Islets*, 2012, **4**, 249.
8 S. Zhu, H. A. Russ, X. Wang, M. Zhang, T. Ma, T. Xu, S. Tang, M. Hebrok and S. Ding, Human pancreatic beta-like cells converted from fibroblasts, *Nat. Commun.*, 2016, **7**, 10080.
9 S. Kahraman, E. R. Okawa and R. N. Kulkarni, Is transforming stem cells to pancreatic beta cells still the holy grail for type 2 diabetes?, *Curr. Diab. Rep.*, 2016, **2016**(16), 70.
10 M. Hohwieler, M. Müller, P. O. Frappart and S. Heller, Pancreatic progenitors and organoids as a prerequisite to model pancreatic diseases and cancer, *Stem Cells Int.*, 2019, 9301382.

11 J. R. Millman, C. Xie, A. Van Dervort, M. Gürtler, F. W. Pagliuca and D. A. Melton, Generation of stem cell-derived β-cells from patients with type 1 diabetes, *Nat. Commun.*, 2016, **7**, 11463.
12 D. Balboa, J. Saarimäki-Vire and T. Otonkoski, Concise Review: Human Pluripotent Stem Cells for the Modeling of Pancreatic β-Cell Pathology, *Stem Cells*, 2019, **37**, 33.
13 N. S. Amirruddin, B. S. J. Low, K. O. Lee, E. S. Tai and A. K. K. Teo, New insights into human beta cell biology using human pluripotent stem cells, *Semin. Cell Dev. Biol.*, 2020, **103**, 31.
14 T. Boettler, D. Schneider, Y. Cheng, K. Kadoya, E. P. Brandon, L. Martinson and M. von Herrath, Pancreatic tissue transplanted in TheraCyte encapsulation devices is protected and prevents hyperglycemia in a mouse model of immune-mediated diabetes, *Cell Transplant.*, 2016, **25**, 609.
15 J. R. Millman and F. W. Pagliuca, Autologous pluripotent stem cell–derived b-like cells for diabetes cellular therapy, *Diabetes*, 2017, **66**, 11111120.
16 A. Essaouiba, R. Jellali, M. Shinohara, B. Scheidecker, C. Legallais, Y. Sakai and E. Leclerc, Analysis of the behavior of 2D monolayers and 3D spheroid human pancreatic beta cells derived from induced pluripotent stem cells in a microfluidic environment, *J. Biotechnol.*, 2021, **330**, 45.
17 A. Essaouiba, R. Jellali, S. Poulain, F. Tokito, F. Gilard, B. Gakière, S. H. Kim, C. Legallais, Y. Sakai and E. Leclerc, Analysis of the transcriptome and metabolome of pancreatic spheroids derived from human induced pluripotent stem cells in 3D static micro honeycombs and in dynamic organ on chips, *Moelcular omics*, 2022, **18**, 791.
18 M. Shinohara, H. Kimura, K. Montagne, K. Komori, T. Fujii and Y. Sakai, Combination of microwell structures and direct oxygenation enables efficient and size-regulated aggregate formation of an insulin-secreting pancreatic beta-cell line, *Biotechnol. Prog.*, 2014, **30**, 178.
19 M. Shinohara, K. Komori, T. Fujii and Y. Sakai, Enhanced self-organization of size-controlled hepatocytes aggregates on oxygen permeable honeycomb microwell sheets, *Biomed. Phys. Eng. Express.*, 2017, **3**, 045016.
20 S. X. Ge, *et al.*, ShinyGO: a graphical gene-set enrichment tool for animals and plants, *Bioinformatics*, 2020, **36**(8), 2628.
21 S. X. Ge, E. W. Son and R. Yao, iDEP: an integrated web application for differential expression and pathway analysis of RNA-Seq data, *BMC Bioinf.*, 2018, **19**(1), 534.
22 L. van Gurp, L. Fodoulian, D. Oropeza, K. Furuyama, E. Bru-Tari, A. N. Vu, J. S. Kaddis, I. Rodríguez, F. Thorel and P. L. Herrera, Generation of human islet cell type-specific identity genesets, *Nat. Commun.*, 2022, **13**(1), 2020.
23 J. Zhang, L. B. McKenna, C. W. Bogue and K. H. Kaestner, The diabetes gene Hhex maintains δ-cell differentiation and islet function, *Genes Dev.*, 2014, **28**(8), 829.
24 Y. Kurashima, T. Kigoshi and S. Murasaki, *et al.*, Pancreatic glycoprotein 2 is a first line of defense for mucosal protection in intestinal inflammation, *Nat. Commun.*, 2021, **12**, 1067.
25 Å. Segerstolpe, A. Palasantza, P. Eliasson, E. M. Andersson, A. C. Andréasson, X. Sun, S. Picelli, A. Sabirsh, M. Clausen, M. K. Bjursell, D. M. Smith, M. Kasper, C. Ämmälä and R. Sandberg, Single-Cell Transcriptome Profiling of Human Pancreatic Islets in Health and Type 2 Diabetes, *Cell Metab.*, 2016, **24**(4), 593.
26 C. Yang, T. Yu, Z. Liu, X. Ye, X. Liao, X. Wang, C. Han, G. Zhu, W. Qin, T. Peng and T. Peng, *et al.*, Cystatin F as a key family 2 cystatin subunit and prognostic biomarker for early-stage pancreatic ductal adenocarcinoma, *Oncol. Rep.*, 2019, **42**, 79.
27 Z. Wu, J. Xu, C. Liang, Q. Meng, J. Hua, W. Wang, B. Zhang, J. Liu, X. Yu and S. Shi, Emerging roles of the solute carrier family in pancreatic cancer, *Clin. Transl. Med.*, 2021, **11**(3), e356.
28 P. Hegyi, J. Maléth, V. Venglovecz and Z. Rakonczay, Pancreatic Ductal Bicarbonate Secretion: Challenge of the Acinar Acid Load, *Front. Physiol.*, 2011, **2**, 1–3.
29 A. Veres, A. L. Faust, H. L. Bushnell, E. N. Engquist, J. H. Kenty, G. Harb, Y. C. Poh, E. Sintov, M. Gürtler, F. W. Pagliuca, Q. P. Peterson and D. A. Melton, Charting cellular identity during human *in vitro* β-cell differentiation, *Nature*, 2019, **569**(7756), 368.
30 G. Dominguez-Gutierrez, Y. Xin and J. Gromada, Heterogeneity of human pancreatic β-cells, *Mol Metab.*, 2019, **27S**(Suppl), S7.
31 J. S. Liu and M. Hebrok, All mixed up: defining roles for β-cell subtypes in mature islets, *Genes Dev.*, 2017, **31**(3), 228.
32 J. S. Yoon, S. Sasaki, J. Velghe, M. Y. Y. Lee, H. Winata, C. Nian and F. C. Lynn, Calcium-dependent transcriptional changes in human pancreatic islet cells reveal functional diversity in islet cell subtypes, *Diabetologia*, 2022, **65**(9), 1519.
33 N. Weinberg, L. Ouziel-Yahalom, S. Knoller, S. Efrat and Y. Dor, Lineage tracing evidence for the in vitro dedifferentiation but rare proliferation of mouse pancreatic β-cells, *Diabetes*, 2007, **56**, 1299.
34 H. S. Spijker, H. Song, J. H. Ellenbroek, M. M. Roefs, M. A. Engelse, E. Bos, A. J. Koster, T. J. Rabelink, B. C. Hansen, A. Clark and F. Carlotti, Loss of β-cell identity occurs in type 2 diabetes and is associated with islet amyloid deposits, *Diabetes*, 2015, **64**(8), 2928.
35 M. C. Gershengorn, A. A. Hardikar, C. Wei, E. Geras-Raaka, B. Marcus-Samuels and B. M. Raaka, Epithelial-to-Mesenchymal Transition Generates Proliferative Human Islet Precursor Cells, *Science*, 2004, **306**, 2261.
36 M. Diedisheim, M. Oshima, O. Albagli, C. W. Huldt, I. Ahlstedt, M. Clausen, S. Menon, A. Aivazidis, A. C. Andreasson, W. G. Haynes and P. Marchetti, Modeling human pancreatic beta cell dedifferentiation, *Mol. Metab.*, 2018, **10**, 74.
37 W. Wang and C. Zhang, Targeting β-cell dedifferentiation and transdifferentiation: opportunities and challenges, *Endocr. Connect.*, 2021, **10**(8), R213.
38 W. Staels, Y. Heremans and H. Heimberg, *et al.*, VEGF-A and blood vessels: a beta cell perspective, *Diabetologia*, 2019, **62**, 1961.

39 C. M. Toselli, B. M. Wilkinson and J. Paterson, *et al.*, Vegfa/vegfr2 signaling is necessary for zebrafish islet vessel development, but is dispensable for beta-cell and alpha-cell formation, *Sci. Rep.*, 2019, **9**, 3594.
40 C. Daecon, Physiology and Pharmacology of DPP-4 in Glucose Homeostasis and the Treatment of Type 2 Diabetes, *Front. Endocrinol.*, 2019, **10**, 1–14.
41 M. Bugliani, F. Syed, F. M. M. Paula, B. A. Omar, M. Suleiman, S. Mossuto, F. Grano, F. Cardarelli, U. Boggi, F. Vistoli, F. Filipponi, P. De Simone, L. Marselli, V. De Tata, B. Ahren, D. L. Eizirik and P. Marchetti, DPP-4 is expressed in human pancreatic beta cells and its direct inhibition improves beta cell function and survival in type 2 diabetes, *Mol. Cell. Endocrinol.*, 2018, **473**, 186.
42 K. A. D'Amour, A. G. Bang, S. Eliazer, O. G. Kelly, A. D. Agulnick, N. G. Smart, M. A. Moorman, E. Kroon, M. K. Carpenter and E. E. Baetge, Production of pancreatic hormone-expressing endocrine cells from human embryonic stem cells, *Nat. Biotechnol.*, 2006, **24**(11), 1392.
43 K. Zaret, Genetic programming of liver and pancreas progenitors: lessons for stem-cell differentiation, *Nat. Rev. Genet.*, 2008, **9**, 329.
44 N. Cerdá-Esteban, H. Naumann, S. Ruzittu, N. Mah, I. M. Pongrac, C. Cozzitorto, A. Hommel, M. A. Andrade-Navarro, E. Bonifacio and F. M. Spagnoli, Stepwise reprogramming of liver cells to a pancreas progenitor state by the transcriptional regulator Tgif2, *Nat. Commun.*, 2017, **8**, 14127.
45 Q. Wang, M. Zheng, Y. Yin and W. Zhang, Ghrelin Stimulates Hepatocyte Proliferation via Regulating Cell Cycle Through GSK3β/B-Catenin Signaling Pathway, *Cell. Physiol. Biochem.*, 2018, **50**(5), 1698.
46 M. Quiñones, J. Fernø and O. Al-Massadi, Ghrelin and liver disease, *Rev. Endocr. Metab. Disord.*, 2020, **21**(1), 45.
47 Y. Q. Zhang, H. Zhang, A. Maeshima, H. Kurihara, J. Miyagawa, T. Takeuchi and I. Kojima, Up-regulation of the expression of activins in the pancreatic duct by reduction of the beta-cell mass, *Endocrinology*, 2002, **143**(9), 3540.
48 O. S. de la, Z. Liu, H. Sun, S. Yu, D. Wong, E. Chu, S. Rao, N. Eng, G. Peixoto, J. Bouza, Y. Shen, S. Knox, A. Tward, A. Gloyn and J. Sneddon, Single-Cell Multi-Omic Roadmap of Human Fetal Pancreatic Development, *bioRxiv*, 2022, preprint, DOI: 10.1101/2022.02.17.480942.
49 M. L. Brown, N. Ungerleider, L. Bonomi, D. Andrzejewski, A. Burnside and A. Schneyer, Effects of activin A on survival, function and gene expression of pancreatic islets from non-diabetic and diabetic human donors, *Islets*, 2014, **6**(5–6), e1017226.
50 D. Martin and A. Grapin-Botton, The Importance of REST for Development and Function of Beta Cells, *Front. Cell Dev. Biol., Sec. Epigenom. Epigenetics*, 2017, **5**, 12.
51 J. Liu, N. Akanuma and C. Liu, *et al.*, TGF-β1 promotes acinar to ductal metaplasia of human pancreatic acinar cells, *Sci. Rep.*, 2016, **6**, 30904.
52 C. Hartley, D. Rowan, X. Chen, L. Gomez-Arellano, A. M. West, K. Oshima and A. C. Mackinnon, Increased SPARC expression is associated with neoadjuvant therapy in resectable pancreatic ductal adenocarcinoma, *Pract. Lab. Med.*, 2020, **29**(21), e00171.
53 F. Sanvito, P. L. Herrera and J. Huarte, *et al.*, TGF-beta 1 influences the relative development of the exocrine and endocrine pancreas in vitro, *Development*, 1994, **120**(12), 3451.
54 J. A. Shin, O. K. Hong, H. J. Lee, S. Y. Jeon, J. W. Kim, S. H. Lee, J. H. Cho, J. M. Lee, Y. H. Choi, S. A. Chang, H. Y. Son, J. H. Kim and K. H. Yoon, Transforming growth factor-β induces epithelial to mesenchymal transition and suppresses the proliferation and transdifferentiation of cultured human pancreatic duct cells, *J. Cell. Biochem.*, 2011, **112**(1), 179.
55 S. Dhawan, E. Dirice, R. N. Kulkarni and A. Bhushan, Inhibition of TGF-b signaling promotes human pancreatic b-cell replication, *Diabetes*, 2016, **65**, 1208.
56 D. Hibsher, A. Epshtein and N. Oren, *et al.*, Pancreatic Mesenchyme Regulates Islet Cellular Composition in a Patched/Hedgehog-Dependent Manner, *Sci. Rep.*, 2016, **6**, 38008.
57 X. Y. Li, W. J. Zhai and C. B. Teng, Notch Signaling in Pancreatic Development, *Int. J. Mol. Sci.*, 2015, **17**(1), 48.
58 E. Lammert, J. Brown and D. A. Melton, Notch gene expression during pancreatic organogenesis, *Mech. Dev.*, 2000, **94**(1–2), 199.
59 G. Carpino, A. Renzi, V. Cardinale, A. Franchitto, P. Onori, D. Overi, M. Rossi, P. B. Berloco, D. Alvaro, L. M. Reid and E. Gaudio, Progenitor cell niches in the human pancreatic duct system and associated pancreatic duct glands: an anatomical and immunophenotyping study, *J. Anat.*, 2016, **228**(3), 474.
60 H. Qu, Q. Jin and C. Quan, CLDN6: From Traditional Barrier Function to Emerging Roles in Cancers, *Int. J. Mol. Sci.*, 2021, **22**(24), 13416.
61 K. Turksen and T.-C. Troy, Claudin-6: A novel tight junction molecule is developmentally regulated in mouse embryonic epithelium, *Dev. Dyn.*, 2001, **222**, 292.
62 G. A. Scheele, S. I. Fukuoka and S. D. Freedman, Role of the GP2/THP family of GPI-anchored proteins in membrane trafficking during regulated exocrine secretion, *Pancreas*, 1994, **9**, 139.
63 K. F. Cogger, A. Sinha and F. Sarangi, *et al.*, Glycoprotein 2 is a specific cell surface marker of human pancreatic progenitors, *Nat. Commun.*, 2017, **8**, 331.
64 C. Nostro, F. Sarangi, S. Ogawa, A. Holtzinger and B. Corneo, *et al.*, Stage-specific signaling through TGFβ family members and WNT regulates patterning and pancreatic specification of human pluripotent stem cells, *Development*, 2011, **138**(5), 861.
65 A. Charrier and D. R. Brigstock, Regulation of pancreatic function by connective tissue growth factor (CTGF, CCN2), *Cytokine Growth Factor Rev.*, 2013, **24**(1), 59.

Annex II: yESAO exchange program report

The yESAO exchange programme award is an exchange program set up by the European Society for Artificial Organs (ESAO). The aim is to establish international and interdisciplinary collaboration between young researchers in order to improve our scientific knowledge and gain experience of research in a new environment. The two collaborators

My colleague Julio Rodriguez-Fernandez from the Center for Biomaterials and Tissue Engineering (CBIT) at the Universitat Politecnica de Valencia (UPV) and I were awarded a grant to carry out our collaborative project entitled **"Modelling Non-Alcoholic Fatty Liver Disease by culturing HepG2C3A cells using a microfluidic biochip combined with a biomimetic hydrogel".** The report on this one-month project is reproduced on the following pages.

Modelling Non-Alcoholic Fatty Liver Disease by culturing HepG2C3A cells using a microfluidic biochip combined with a biomimetic hydrogel.

Lisa Morisseau[1, *], Julio Rodriguez-Fernandez[2, *], Gloria Gallego-Ferrer[2,6], Laia Tolosa [5,6], Cécile Legallais[1], Rachid Jellali[1], Yasuyuki Sakai[3], Manuel Salmeron-Sanchez[2,7], Eric Leclerc[1,4]

[1] UMR 7338 - CNRS - Laboratoire BioMécanique et BioIngénierie (BMBI), Université de Technologies de Compiègne, Compiègne, France

[2] Center for Biomaterials and Tissue Engineering (CBIT), Universitat Politècnica de València, 46022, Spain

[3] Department of chemical System Engineering, University of Tokyo, Japan

[4] IRL 2820 LIMMS/CNRS, Institute of Industrial Science, University of Tokyo, Japan

[5] Experimental Hepatology Unit, Health Research Institute La Fe (IISLAFE), Valencia, 46026, Spain

[6] Biomedical Research Networking Center on Bioengineering, Biomaterials and Nanomedicine (CIBER-BBN), Valencia, Spain

[7] Centre for the Cellular Microenvironment, Division of Biomedical Engineering, School of Engineering, University of Glasgow, G12 8LT, Glasgow, United Kingdom

* Equal contributions of the authors

Introduction and objectives:

To understand the molecular mechanisms implicated in Non-Alcoholic Fatty Liver Disease (NAFLD), hepatic steatosis has been mimicked in 2D *in vitro* models supplemented with high concentrations of oleic and/or palmitic acids [1]. Nevertheless, to better elucidate the cellular mechanisms under hepatic steatosis it is needed to represent the complex architecture of the liver tissue by using 3D *in vitro* models and recreate its key features such as shear stress, zonation, nutrient/gas exchange and waste/toxins removal [2]. Hydrogels have been widely used as 3D *in vitro* models because of their tunable composition and ability to reproduce the native tissue structure and composition of the hepatic extracellular matrix which is mainly composed by collagen (type I, type IV, and type V) and glycosaminoglycans such as hyaluronic acid (HA) [3]. The aim of this project will be to develop a steatosis liver-on-chip under dynamic conditions with hepatic cells embedded inside a 3D hydrogel to mimic liver architecture and steatosis environment.

Materials and Methods:

1. Microsystem design

The biochip consists of a large cell culture chamber which is manufactured with two polydimethylsiloxane (PDMS) layers. The bottom PDMS layer, used as a support for cell attachment, consists of a series of microchambers interconnected by microchannels and its specific geometry makes a uniform flow field possible above the microstructures. The upper PDMS layer is composed of a reservoir with a depth of 100 µm for culture medium perfusion. After sealing the two layers, the total resulting depth and volume of the assembled cell culture

chamber are 200 µm and 40 µL respectively, with a cell growth surface area of 2 cm^2 [4]. The biochips are sterilised by autoclaving before use.

2. Gelatin-Hyaluronic acid (Gel-HA) hydrogel preparation

Tyramine conjugates of gelatin (Gel) and hyaluronic acid (HA) are crosslinked enzymatically by horseradish peroxidase (HRP) and H_2O_2. Volumetric ratio between polymers and crosslinker is 80% either Gel and/or HA, 10% HRP and 10% H_2O_2. Hydrogel is prepared by mixing first the polymers (2-4% w/v) with HRP and then at the last step the addition of H_2O_2 starts the crosslinking process with the desired volume [5]. Polymers are sterilised by filtering with 0.22µm filters previous a sterile process of freeze-dry.

3. Mechanical and stability assays

Mechanical properties of the selected hydrogels are analysed by different measurements based on oscillatory rheology. Firstly, a time sweep (1Hz and 1%), frequency sweep (1%) from 0.01Hz to 10Hz and an amplitude sweep (1Hz) from 0.1% to 20%. Geometry selected is a 20 mm flat plate heated at 37ºC. Hydrogel stability inside the biochip under dynamic conditions is tested using syringe pumps for perfusion of a blue solution then manually assessing the integrity.

4. Hydro-chip: Gel-HA hydrogel integration in biochip

Gel-HA hydrogel is put into the PDMS biochip through the connectors by two different syringes. Thus, one syringe contained Gel-HA 20-80 (2%) precursor solution and HRP (12.5 U/mL), while on the other the content was H_2O_2 (20 mM). The crosslinking started when both solutions were pushed back and forth through the PDMS biochip, 4-5 complete syringe cycles are enough to ensure a proper crosslink. Then, chips along the syringes are left for 15-20 min at 37ºC to ensure a proper crosslink.

5. HepG2/C3A cell culture in hydro-chip and static hydrogel

The HepG2/C3A cell line (ATCC HB-8065) is a human hepatocyte cell line coming from a hepatocellular carcinoma. HepG2/C3A cells are cultured in T75 culture flask with supplemented Minimal Essential Medium (MEM) with phenol red and maintained at 37°C in a 5% CO_2 supplied incubator. At a confluence of 80%, cells are detached with 0.25% trypsin-EDTA for 5 min in order to be seeded in biochips.

The steps in order to fill the biochips with Gel-HA hydrogel are similar to what is described previously in section 4, but this time, cells are included in the precursor solutions of Gel-HA along with the HRP. A total of 200000 HepG2/C3a cells/biochip is thoroughly homogenized and embedded within the hydrogel before an incubation step at 37ºC for 30-45 min to ensure a proper crosslink. Then, the hydro-chip are connected to the bubble trap (containing 2 mL of fresh medium), and the perfusion is started using a peristaltic pump with a flux rate of 10 µL/min. The whole system is placed in an incubator at 37°C and 5% CO_2.

For static hydrogel condition HepG2/C3A cells are added to Gel-HA mixture (200,000 cells/hydrogel). Finally, 90 µL of the Gel-HA cell suspension is crosslinked with 10 µL of H_2O_2 (20 mM) on 24-well plate, resulting hydrogels of 100 µL.

For both hydro-chip and static hydrogel conditions culture medium are sampling after 4 and 6 days of culture.

6. Exposure to free fatty acids

After 4 days of culture, cells in hydro-chip and static hydrogel are exposed to oleic acid (0.66 mM for 2 days. An oleic acid (OA, Sigma-Aldrich) stock solution, is first prepared in EtOH 99% at a concentration of 500 mM. Then, as a vehicle, we used a 10% BSA solution prepared in sterile water. Oleic acid solution at 0.66mM is obtained according to the following percentages: 0.13% of OA stock solution, 4.4% of 10% BSA solution and 95.47% of MEM. Medium sampling for biological assays is performed after exposure (day 6).

7. Biological assays

Albumin concentration was determined on the culture media using the Human Serum Albumin DuoSet ELISA kit (R&D Systems, Minneapolis, MN) according to the manufacturer's guidelines. Ureogenic capacity is measured directly from the culture medium by an improved Jung method using the Urea Assay Kit (QuantiChrom DIUR100; BioAssay Systems, Hayward, CA). F-actin staining with phalloidin is performed to observe the cells structure. Finally, steatosis is evaluated by staining cytoplasmic lipid droplets with Oil red O.

Results

1. Gel-HA hydrogels exhibit liver-like mechanical properties and long-term stability in dynamic and non-dynamic systems.

The Gel-HA 20-80 hydrogels exhibit a storage modulus (G') of 400 Pa (Figure 1A). Gel-HA hydrogels inside biochip under dynamic conditions retained integrity for 5 days (Figure 1B).

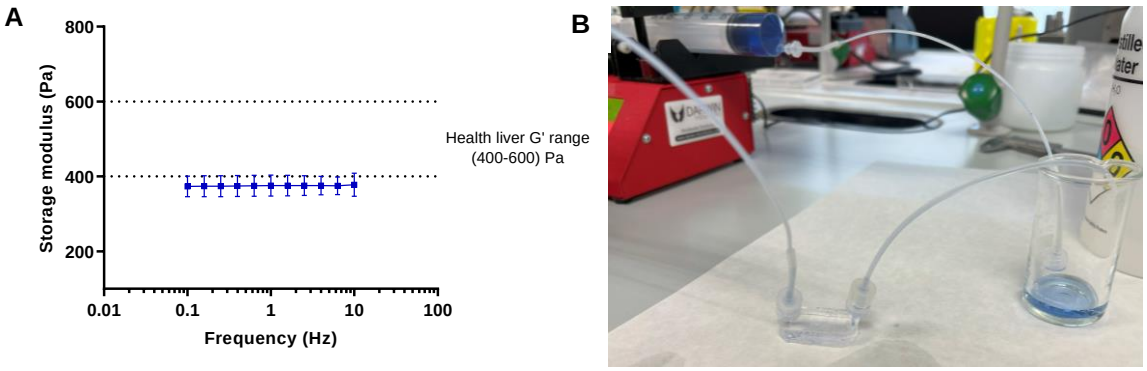

Figure 1. Mechanical properties of hydro-chip. ***(A)*** *Storage modulus (G') of Gel-HA 20-80 hydrogels by oscillatory rheology.* ***(B)*** *Stability test of biochip fill with Gel-HA hydrogel after 5 days of perfusion at 10 µL/min.*

2. HepG2 cells embedded in Gel-HA hydrogels confined in PDMS biochips: morphological and functional analysis

24 hours after seeding, the cells started to aggregate and create spheroids both in hydro-chips and static hydrogels (Figure 2A). After 6 days of culture, large size spheroids were observed in both hydro-chip and static hydrogel. To analyze the actin cytoskeleton of the spheroids, F-actin staining with phalloidin was performed. The actin cytoskeleton of the cells was perfectly observable with the microscope's binoculars but slightly visible in the confocal images as shown in the Figure 2B. We can assume that there is a network of actin throughout the spheroids.

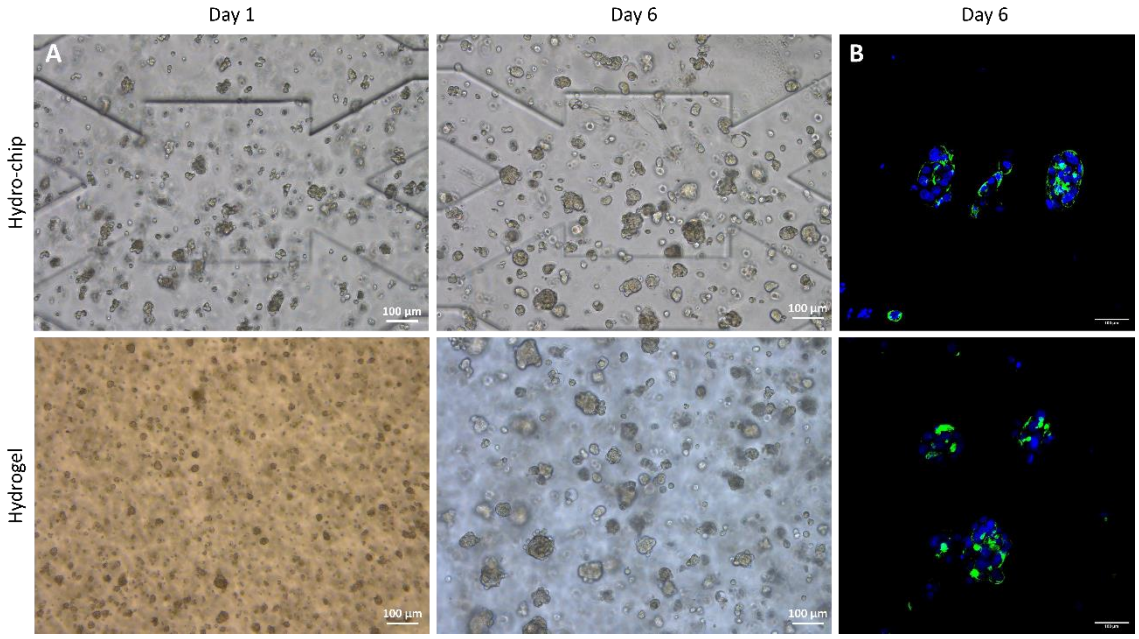

Figure 2. Morphological analysis of HepG2/C3A cells in hydro-chip and static hydrogel. ***(A)*** *Contrast-phase image at day 1 and 6 of culture in hydro-chip and static hydrogel.* ***(B)*** *Confocal images of cells embedded in hydro-chip and static hydrogel after 6 days of culture. Nuclei are stained in blue and F-actin are stained in green. Scale bar 100 um.*

Assessment of albumin secretion is commonly used as a liver function test to indicate potential liver injury and functionality. We found a similar albumin secretion in both hydro-chip and static hydrogel after 4 days of culture. At day 6, we also observed no significant differences between hydro-chips and static hydrogels regarding albumin secretion. Nevertheless, a significant increase in albumin secretion in static hydrogel condition between day 4 and day 6 (Figure 3A) was observed. Urea quantification revealed significantly higher levels in hydro-chip than in static hydrogels (0.92±0.012 and 0.77±0.036 µg/h, respectively) at day 4. After 6 days of culture, although we observed a significant increase of urea levels for both hydro-chip and static hydrogel when compared to day 4; urea levels in hydro-chip remained higher than those in static hydrogel (1.73±0.077 and 1.57±0.076 µg/h, respectively) (Figure 3B).

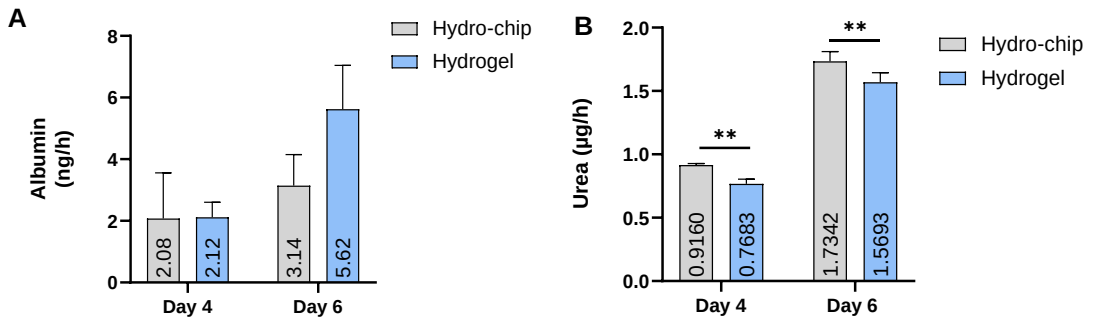

Figure 3. Functional analysis of Hepg2/C3A cultured in hydro-chip and static hydrogel for 4 and 6 days. (A) *Albumin secretion quantification.* ***(B)*** *Urea secretion quantification. *At least p≤0.05 and ** at least p≤0.01; T-test statistic was performed for comparison between conditions.*

3. *In vitro* disease modelling of NAFLD using hydro-chip and HepG2/C3a cells

We observed intracellular lipid droplets in cells for both hydro-chip or static hydrogel after treatment with OA for 2 days as shown in Figure 4A. Lipid accumulation seemed to be more important in treated static hydrogels to hydro-chip. However, urea quantification did not show significant changes after2 days of fatty acid exposure (Figure 4B).

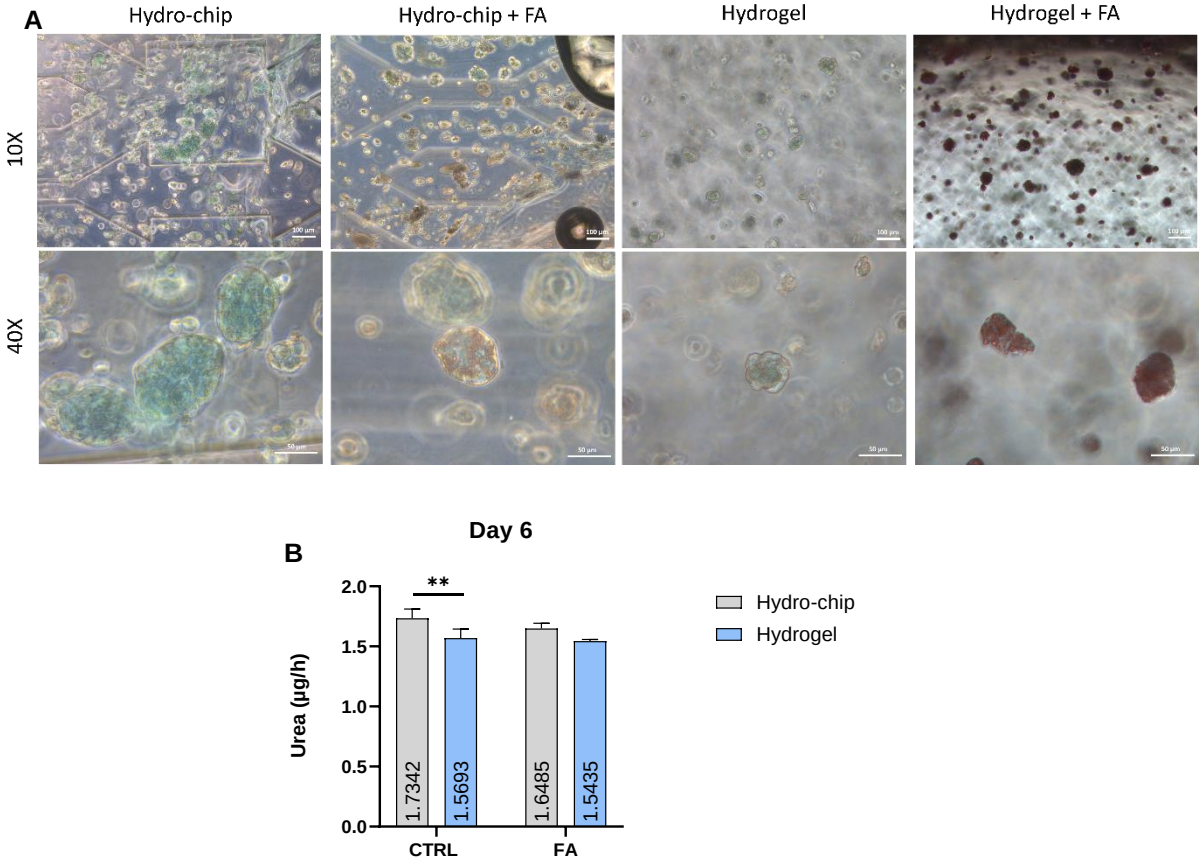

Figure 4. Hydro-chip and static hydrogel as model for steatosis. (A) *Intracellular lipid droplet staining on control and treated samples.* ***(B)*** *Urea secretion quantification of control and treated samples at day 6.*

4. Discussion & Conclusion

The present work combines the advantages of a hydrogel based on Gel-HA and microfluidic culture. Literature has widely shown that 3D configuration (spheroids) enhances cellular morphology reorganization, metabolic capability but also regulates the development of liver disorders[6], [7]. Furthermore, microfluidic culture allows to reproduce zonation-like patterns, shear stress and reduces the accumulation of toxic compounds [4], [8].

Liver tissue is described as a soft tissue with a high ratio between cells/ECM. However, despite this ratio liver ECM displays relatively high mechanical properties. In fact, it has been described that a healthy liver exhibits a storage modulus (G') between 400-600 Pa [3], [5]. Therefore, the chosen Gel-HA 20-80 ratio hydrogels reproduce a healthy liver-like mechanical properties and can sustain flow at 10µL/min for at least 5 days.

The HepG2/C3a cells proliferated in hydro-chip and static hydrogels and formed spheroids after 24hours. After 6 days of culture, spheroids in perfusion culture (hydro-chip) and in static hydrogels seemed to reach a similar size. The present study demonstrated non-significant differences in albumin secretion in hydro-chip and static hydrogels after 4 and 6 days of perfused culture. While higher levels of urea were observed in hydro-chips when compared to static hydrogels at day 4 and 6. We hypothesized that the dynamic environment promoted metabolic capability as demonstrated in Messelmani *et al*., 2022.

Regarding NAFLD modelling, we found intracellular lipid accumulation for both hydro-chips and static hydrogels. Although, hydrogels showed a higher lipid accumulation than hydro-chips, urea levels in control and treated conditions were similar. This phenomenon may suggest that hydrogel along the dynamic flow potentially allow to better mimic physiological features in the liver tissue.

5. Conclusion and outlook

We have developed a hydro-chip by combining a Gel-HA hydrogel and a microfluidic biochip to investigate steatosis development in HepG2/C3a cells. The preliminary results described in this report show the potential of this combination to better mimic liver disease. We believe this work must be taken further.

References:

[1] F. A. Müller and S. J. Sturla, “Human in vitro models of nonalcoholic fatty liver disease,” *Curr Opin Toxicol*, vol. 16, pp. 9–16, Aug. 2019, doi: 10.1016/J.COTOX.2019.03.001.

[2] T. Messelmani *et al.*, “Development of Liver-on-Chip Integrating a Hydroscaffold Mimicking the Liver’s Extracellular Matrix,” *Bioengineering*, vol. 9, no. 9, p. 443, Sep. 2022, doi: 10.3390/BIOENGINEERING9090443/S1.

[3] J. Rodriguez-Fernandez *et al.*, “Primary human hepatocytes-laden scaffolds for the treatment of acute liver failure,” *Biomaterials Advances*, vol. 153, p. 213576, Oct. 2023, doi: 10.1016/J.BIOADV.2023.213576.

[4] R. Baudoin, L. Griscom, J. M. Prot, C. Legallais, and E. Leclerc, “Behavior of HepG2/C3A cell cultures in a microfluidic bioreactor,” *Biochem Eng J*, vol. 53, no. 2, pp. 172–181, 2011, doi: 10.1016/j.bej.2010.10.007.

[5] E. Sanmartín-Masiá, S. Poveda-Reyes, and G. Gallego Ferrer, “Extracellular matrix–inspired gelatin/hyaluronic acid injectable hydrogels,” *http://dx.doi.org/10.1080/00914037.2016.1201828*, vol. 66, no. 6, pp. 280–288, Apr. 2016, doi: 10.1080/00914037.2016.1201828.

[6] H. Gaskell, P. Sharma, H. E. Colley, C. Murdoch, D. P. Williams, and S. D. Webb, “Characterization of a functional C3A liver spheroid model,” *Toxicol Res (Camb)*, vol. 5, no. 4, pp. 1053–1065, 2016, doi: 10.1039/C6TX00101G.

[7] S. Moscato, F. Ronca, D. Campani, and S. Danti, “Poly(vinyl alcohol)/gelatin Hydrogels Cultured with HepG2 Cells as a 3D Model of Hepatocellular Carcinoma: A Morphological Study,” *Journal of Functional Biomaterials 2015, Vol. 6, Pages 16-32*, vol. 6, no. 1, pp. 16–32, Jan. 2015, doi: 10.3390/JFB6010016.

[8] J. W. Allen, S. R. Khetani, and S. N. Bhatia, “In Vitro Zonation and Toxicity in a Hepatocyte Bioreactor,” *Toxicological Sciences*, vol. 84, no. 1, pp. 110–119, Mar. 2005, doi: 10.1093/TOXSCI/KFI052.